INLAND WATER AUTHORITY OF INDIA (IWAI)

SUBMERGED VANES FOR RIVER TRAINING AND SEDIMENT MANAGEMENT IN STREAMS AND THEIR FIELD APPLICATION

Prof. Z. Ahmad, Prof. P. K. Sharma, Dr. H. Sharma, Mr. A. Mandal

Department of Civil Engineering
Indian Institute of Technology Roorkee
Roorkee – 247667, Uttarakhand

July 2025

EXECUTIVE SUMMARY

Submerged vanes are small flow training structures designed to redistribute flow and sediment within the channel cross-section. The structural stability and economic feasibility of submerged vanes, which distinguish them from conventional methods such as dikes and groins, have inspired many researchers to study their use and efficiency in river management over many decades. The shape of a submerged vane has widely been recognized as a crucial factor influencing its performance as noted by several researchers. Previous studies predominantly focused on rectangular shape of the vanes due to their simplicity, ease of fabrication and construction processes. One significant drawback of using rectangular submerged vanes is the potential risk of structural failure due to excessive local scour occurring near their tips. Previous studies confirmed that bevel shape of submerged vane can reduce local scour occurring near their tips. The task of optimizing the size and shape of the submerged vanes and their testing for field applications was awarded to IIT Roorkee with the following scope of works:

(i) To study analytically and experimentally the flow pattern generated due to submerged vanes for their different bevel shapes and sizes in the flow for varying discharges.

(ii) To study analytically and experimentally the bed form changes of an alluvial channel due to submerged vanes of different bevel shape and sizes.

(iii) To identify the geometrical parameters of the vanes and flow parameters affecting the generation of secondary currents in the flow.

(iv) To fix the optimal size and shape of the submerged vanes which would cause maximum generation of secondary current and bed form changes on the basis of studies carried out in the present study.

(v) The optimal size and shape of the submerged vanes shall be tested for two field applications i.e., a) Inducing siltation towards right side and to shift the main course of the Ganga river towards the left side at Bhagalpur, Bihar and

b) Removal of sediment from the mouth of the spill channel of Padma/Ganga river near Jangipur, West Bengal.

The laboratory and numerical studies were conducted to evaluate the efficiency of vanes in generating vortices and the resulting changes in bed morphology for various vane shapes and sizes under open channel flow conditions. The optimal size and shape of the submerged vanes is tested for two field applications i.e., to control right bank erosion and to shift the main course of the Ganga river towards the left side at Bhagalpur, Bihar and to removal of sediment from the mouth of the spill channel of Padma/Ganga river near Jangipur, West Bengal for revival of the spill channel.

Both experiments were carried out under different discharge conditions and with both without and with submerged vanes situations. On the basis of physical model study, the following conclusions are made:

(i) Experimental study was carried out for different bevelled angle, angle of attack and submergence of the vanes along with its curved shape. Characteristics of flow field and bed morphology for all the tested vanes and for different discharges were measured.

(ii) Curved vanes indicate excessive scour in the vicinity of the vanes. Considering the stability of the curved vanes under severe scour conditions, this shape was not adopted for the further study.

(iii) Both experimental and numerical study show that rectangular vane with bevel angle of 45^{0} reduces the local scour in the vicinity of the vanes without compromising the generation of vortex when compared to rectangular vanes without bevel. Based on these findings, rectangular vanes with 45-degree bevel angle vanes are recommended their applications.

(iv) Flow characteristics reveal that the velocity distribution is logarithmic with a S-type variation over the vertical for all the bevel angles. This indicates presence of point of inflexions in the velocity profiles and it confirms the presence of strong vortices at the transect due to submerged vanes.

(v) Experimental study on bed morphology reveals that cutting the leading-edge w.r.t vertical axis or bevel shape of the submerged vane decreases the horseshoe vortex significantly, which reduces the local scour depth at the leading edge compared to the rectangular vane.

(vi) The present study reveals that the tip vortex increases with increase of angle of attack. However, for higher angle of attach scour around the submerged vanes is higher which will pose a problem of stability of the vanes. In view of this, it is recommended to adopt angle of attack equal to 20 degree.

(vii) Developed bevelled submerged vanes have been used to control right bank erosion of the Ganga river downstream of the Vikramshilla bridge at Bhagalpur through a physical model study to a scale of 1/700 (horizontal) and 1/70 (vertical). With the use of the submerged vanes, the percentage reduction in bank erosion is ranging from 63.4% to 100%, from 30% to 100%, and from 15.6% to 79.8% for 0 km, 0.14 km, and 0.28 km offsets from the right bank. Results shows that submerged vanes can effectively reduce the bend erosion along the outer bank of the river by diverting the main course of the river towards the inner side from the outer side of the bank.

(viii) Developed bevelled submerged vanes have been used to activate a spill channel by removal of sediment at its mouth of Padma/Ganga river near Jangipur, West Bengal. Results indicate that installation of submerged vanes at the mouth of the spill channel increases discharge passing through it. The percentage increases in discharge in the spill channel with the installation of submerged vanes compared to existing conditions are 2.27%, 4.93%, 5.88%, 4.54%, and 7.6% for river discharges of 19,445 m^3/s, 24,218 m^3/s, 30,052 m^3/s, 35,355 m^3/s, and 41,500 m^3/s, respectively in the river. Thus, the bevelled vanes can be used to desilt the mouth of a spill channel or water intake for passing the flow through it.

(ix) It is recommended that rectangular submerged vanes with bevelled angle of 45 degree and angle of attack of 20 degree shall be adopted for effective use

of the submerged vanes. Other dimensions and configuration shall be fixed on the basis of Odgaard recommendations.

Date: 25th August 2025 **(Z. Ahmad)**

Place: Roorkee Prof. of Civil Engineering

TABLE OF CONTENTS

1. INTRODUCTION

1.1 BACKGROUND

Sediment management in alluvial channels, acting on sediment transport, erosion and deposition, presents a significant challenge for river engineers. Scouring in river bends frequently results in bank destabilization and land loss (see Fig. 1.1), whereas sediment deposition on the riverbed often reduces flood conveyance capacity and obstructs channel navigation. River bends are generally the most unstable segments of the river stretch, where bank erosion is frequently observed. This erosion is primarily influenced by curvature-induced secondary currents induced by centrifugal forces in the bend section. It is also referred to as transverse circulation or helical motion (Kalkwijk & Booij, 1986; Blanckaert & Graf, 2004). These currents arise due to variations in centrifugal acceleration along the vertical profile of the flow, contributing to the progressive instability of the riverbanks. High-velocity surface currents are driven toward the outer bend of the river, while lower-velocity near-bed currents shift toward the inner bank of the channel (Dey, 2014; Kadia et al., 2024; Stoesser et al., 2010). This dynamic flow pattern leads to increased flow depths and velocities near the outer banks, contributing to channel instability and erosion. Sediment concentration is relatively high in near bed region. This flow pattern transport sediment inward, leading to its deposition near the inner side of the bend. Conversely, the concave bank experiences erosion due to the impact of sediment-deficient fluid originating from the upper layers of the flow (Odgaard & Mosconi, 1987).

Sediment deposition is a persistent challenge at numerous water intakes and diversion structures (see Fig. 1.2). Intake canals are designed to extract water from rivers for multiple uses, including irrigation, navigation, potable water supply, cooling in thermal power stations, and various industrial applications (Nakato et al. 1990). Sediment entry and deposition in intakes damage systems and raises maintenance expenses for them. Different structures have been used to control diverted discharge and sediment entrance into the basin, but Submerged vanes have been used most widely for reducing sediment entry into intake canals for the last three decades (Nakato et al. 1990; Barkdoll et al. 1999). A major obstacle in addressing this issue lies

in the lack of effective and economically feasible methods for regulating sediment transport.

Fig. 1.1 Stream bank erosion in East Nishnabotna River, Iowa. Source: Odgaard (1987)

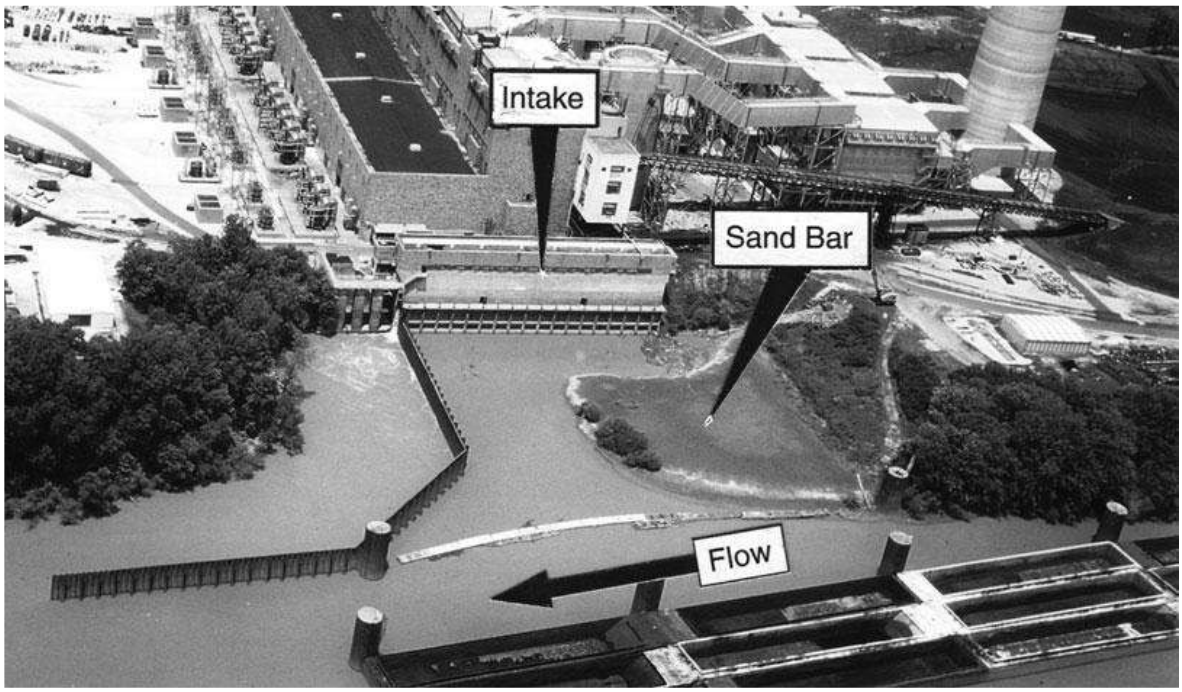

Fig. 1.2 Sedimentation in forebay of intake adjoining Ohio River, U.S.A. Source: Neary et al. (1999), ASCE

At the Iowa Institute of Hydraulic Research, low-height, high-length structures known as Iowa vanes, or submerged vanes, were designed by Odgaard and colleagues (Odgaard and Spoljaric 1986; Odgaard and Mosconi 1987; Odgaard and Wang 1991a) to modify near-bed flow patterns and bed sediment movement across rivers. Recent research has shown that submerged vanes are effective in increasing flow depth, reducing sediment diversion at water intakes (Barkdoll et al. 1999; Baltazar et al. 2021; Bor 2022; Gumgum and Cardoso 2022), protecting bridge piers and foundations (Zarei et al. 2019; Safaripour et al. 2020; Vaghefi et al. 2023; Hamidi et al. 2024), and preventing streambank erosion (Odgaard & Kennedy 1983; Bhuiyan et al. 2010; Tasar et al. 2023). Submerged vanes offer a distinct advantage over traditional structures such as dikes, spurs, and groins due to their capacity to redistribute flow with reduced resistance, facilitating easier installation and greater economic feasibility. In contrast to groins and dikes, which function by redirecting flow through basic continuity, submerged vanes employ vorticity aligned with the flow, leading to diminished drag forces (Wang and Odgaard 1993). Odgaard and Wang (1991a) explain that the angled orientation of the vane results in a pressure differential across its sides, causing an upward flow on the pressure side and a downward flow on the suction side. This configuration generates a tip vortex that moves downstream, modifying the shear stress field. The resulting longitudinal, helical flow pattern effectively redirects sediment downstream, thus preventing sediment from entering intake canals (Barkdoll et al. 1999). Recent field experiments (Rodriguez 2020) have highlighted the considerable effectiveness of submerged vanes in reducing erosion at river bends, including in the East Nishnabotna River, Iowa (Odgaard and Mosconi 1987), as shown in Fig. 1.3. In Fig. 1.4, submerged vanes are shown being installed at the water intake of the Kosi River, Nepal, to reduce sediment entrainment.

Fig. 1.3 Submerged vanes in East Nishnabotna River, Iowa, protecting stream bank against erosion (Odgaard 2009)

Fig. 1.4 Submerged vanes being installed at water intake on Kosi River, Nepal

1.2 BRIEF REVIEW OF LITERATURE

The primary objective in designing submerged vanes is to induce secondary circulation within the primary flow, alter flow patterns near the riverbed, and divert sediment within the channel cross-section. The author has discussed the theory related to submerged vanes and examined the critical findings and challenges identified by various researchers. Over the past few decades, numerous studies (Odgaard & Kennedy 1983; Odgaard & Spoljaric 1986; Odgaard & Wang 1991a; Ouyang 2009; Gupta et al. 2010; Odgaard 2015; and Solanki et al. 2020) on submerged vanes have been conducted, leading to the development of design guidelines for vane systems based on their outcomes. Van Zwol (2004) argue that the Odgaard theory falls short of accurately predicting the lift and drag forces applied to vanes because the existing model fails to fully consider the underlying flow physics associated with the passage of water flow over submerged vanes. The theory of Odgaard is based on the lifting line theory for finite wings, known as Prandtl's lifting theory, which is unsuitable for low aspect ratio wings as well. At a greater angle of attack, the main vortex becomes stronger. The primary vortex appears to originate from the suction side of the vane surface away from the leading edge, which decreases as the angle of attack increases and increases as the initial vane height decreases (Odgaard & Spoljaric 1986). In summary, the angle of attack and aspect ratio are critical factors that must be carefully considered when designing a submerged vane to ensure optimal performance. As lift decreases for lower angles of attack and the drag becomes more noticeable with increasing angle of attack, the ideal range is described as 15° to 30°, suggested by many researchers (Odgaard & Kennedy 1983; Odgaard & Spoljaric 1986; Odgaard & Wang 1991a). According to Odgaard & Spoljaric (1986), the occurrence of flow separation results in a decrease in the lift coefficient when the angle of attack increases above 15°. At a greater angle of attack, the higher stream-wise velocities are more effectively redistributed towards the bed via vortex motion. According to Odgaard & Mosconi (1987) research, fluctuations in the H/d ratio over the range $0.2 < H/d < 0.5$ have little impact on how much torque a vane generates when submerged. At the design stage, a study by Odgaard & Spoljaric (1986) proposed $0.4 < H/d < 0.5$, whereas Odgaard & Mosconi (1987) suggested $0.2 < H/d < 0.5$ for all flow stages that induce erosion.

The orientation of the flow significantly impacts the local scour depths at submerged vanes. The intensity of the horseshoe vortex along the pressure side is such that it effectively carries material away from the scour hole at angles of attack of 30° and above. As the angle of attack increases, the region of maximum scour migrates along the pressure side of the vane towards the trailing edge (Marelius & Sinha 1998). However, a notable increase in scour depth is observed at an angle of attack of more than 20°, which is not practical for field application (Gupta et al. 2010). The primary disadvantage of utilizing submerged vanes is the potential for structural disintegration due to local scour near their tips. Therefore, there is a need for more research on reducing the local scour depth around the vane's tip, as very few researchers (Bejestan & Azizi 2012; Teronpi & Misra 2015; and Azizipour et al. 2020) have attempted to address this aspect. The experimental investigation conducted by Bejestan and Azizi (2012) demonstrated that cutting the leading edge (called bevel shape) of the vanes reduces the local scour around the vanes; however, though the extent of the reduction remains uncertain. Also, grabion submerged vane can be also the alternative use of the scour reduction around the vane (Sarlak et al. 2023). The horseshoe vortex and potentially additional vortices may introduce unfavorable forces in the system, influencing the transverse movement of sediment. However, this aspect has not yet been thoroughly investigated (Marelius & Sinha 1998). In the case of a vane array, the equilibrium strength of horseshoe vortices may be lower compared to that of a single vane, as the scour holes of nearby vanes might overlap. Additionally, the presence of scour holes could lead to some vortex stretching in the transverse direction, effectively increasing the width of each vane (Odgaard 2009).

Most investigations have prioritized rectangular vanes, primarily due to the simplicity of the underlying theory and in consideration of previous research conducted on submerged vanes. Anderson Jr. (2007) and Bertin & Smith (1979) have established that wings with non-rectangular geometries, such as tapered or delta wings, offer greater lift capabilities compared to wings with a rectangular shape. Some researchers, such as Gupta et al. (2007), Ouyang (2009), and Solanki et al. (2020), have suggested that tapered vanes are more efficient in sediment management than rectangular vanes

because tapered vanes introduce a more gradual adverse pressure into the flow. However, there is still a lack of extensive experimental research on the potential flow lift generated by non-rectangular vanes. Hence, further research is imperative to optimize the geometric vane parameters, specifically in terms of their taper angle. Despite significant advancements in submerged vanes over the years, there are still unexplored applications. Only a limited number of studies have delved into the potential of submerged vanes for excavation purposes (Odgaard 2009, 2015), indicating the need for further research in this area. Consequently, the potential of submerged vanes to enhance inland navigation has been partially explored, and the impact of a vane system on induced changes in energy slope remains unclear and requires further research.

1.3 NEED FOR THE STUDY

Previous studies predominantly focused on rectangular vanes due to their simplicity per existing theories and ease of fabrication and construction processes. As a result, only a limited number of laboratory investigations were conducted beyond the use of rectangular vanes, such as camber, curve, swept, triangular, and bevel vanes. The shape of a submerged vane has been widely recognized as a crucial factor influencing its performance improvement, as noted by several researchers. The non-rectangular vane also used in some of the field application. The installation of bevel-submerged vanes at a water intake on the Kosi River in Nepal serves as a notable example of their application in mitigating sediment ingress, shown in Fig. 1.5. In recent times, the use of submerged vanes for various field applications has significantly increased, owing to their ease of installation and cost-effectiveness. One significant drawback of using rectangular submerged vanes is the potential risk of structural failure due to local scour occurring near their tips. It is known that a bevel shape can reduce the local scour, though the extent of the reduction remains uncertain. No calculation methods are currently available to quantify this effect. And, no comprehensive study on scour around vane are available to find the most efficient bevel angle. Therefore, further research is needed to explore strategies for reducing the local scour near the submerged vanes without compromising their efficiency on various field applications.

Also, utilizing a beveled leading edge on submerged vanes can assist in deflecting floating debris that comes into contact with the vane and reducing the construction material.

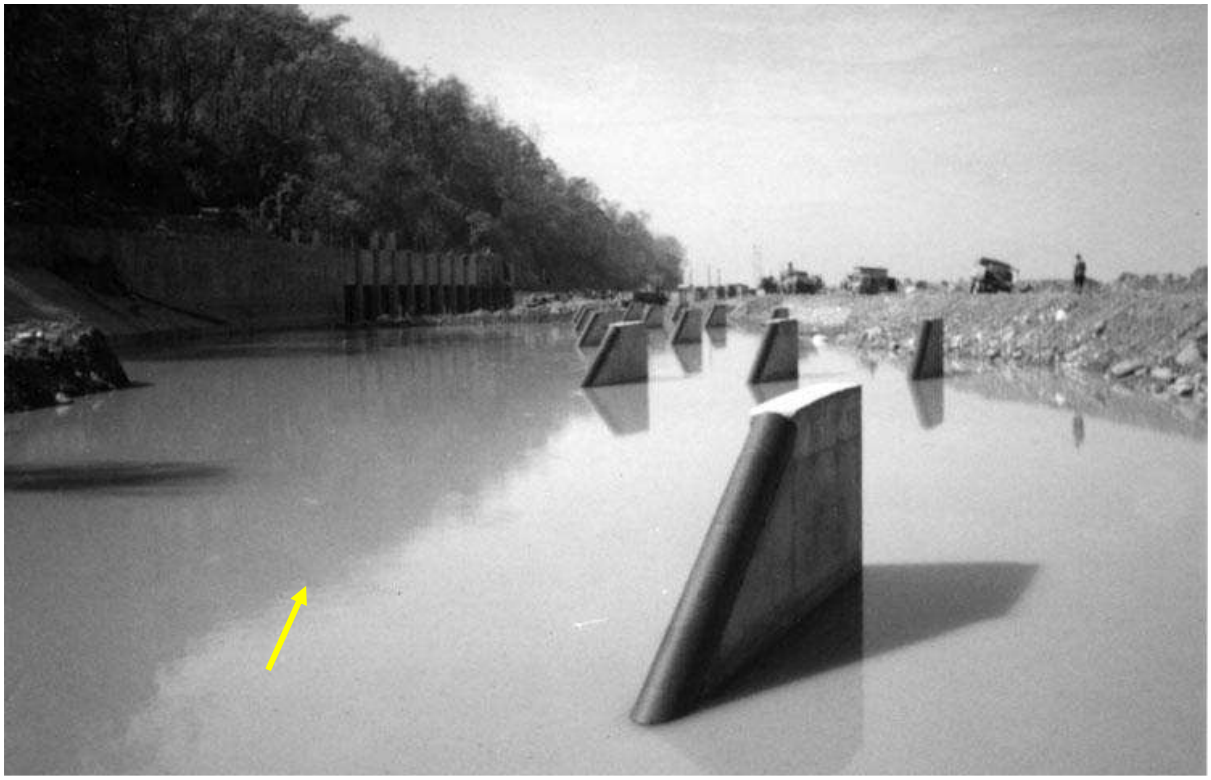

Fig. 1.5 Submerged vanes being installed at water intake on Kosi River, Nepal (Odgaard 2009)

1.4 OBJECTIVES OF THE STUDY

Based on the present state of the art of river training, channel stabilisation and management of sediments in streams, the following objectives have been fixed:

(a) To study analytically and experimentally the flow pattern generated due to submerged vanes for their different shapes and sizes in the flow for varying discharges.

(b) To study analytically and experimentally the bed form changes of an alluvial channel due to submerged vanes of different shape and sizes.

(c) To identify the geometrical parameters of the vanes and flow parameters affecting the generation of secondary currents in the flow.

(d) To fix the optimal size and shape of the submerged vanes which would cause maximum generation of secondary current and bed form changes on the basis of studies carried out in the present study.

(e) The optimal size and shape of the submerged vanes shall be tested for two field applications i.e., a) Inducing siltation towards right side and to shift the main course of the Ganga river towards the left side at Bhagalpur, Bihar and b) Removal of sediment from the mouth of the spill channel of Padma/Ganga river near Jangipur, West Bengal.

1.5 METHODOLOGY

The present work adopted both experimental and numerical approaches for studying the above objectives. The optimized size and shape of bevel submerged vane also study in two field application. A thorough literature review was carried out to understand the current state of research in the field of hydrodynamics efficiency of submerged vane. Experiments were performed in a rectangular flume 28 m long, 1.0 m wide and 0.4 m deep. Three Dimensional velocities downstream of submerged vane were collected using Acoustic Doppler Velocimeter (ADV), and the live scour and scour pattern around the vane was measured with the help of a 5 MHz ultrasonic bed profiler. Data obtained from these experiments was carefully analyzed to study the flow field, scour morphology and maximum scour depth near the submerged vane. An empirical relationship for the computation of maximum scour depth in the local scour hole and extension of scour hole downstream of the vane was developed using the data collected in the experimental study. Computational Fluid Dynamics (CFD) based numerical modelling was done for simulating the flow field around the vane vorticity downstream of the vane. The results of numerical simulations were validated with the experimental observations and were found to be in good agreement.

1.6 ORGANIZATION OF REPORT

Present thesis makes up of seven chapters, in each chapter detailed description of the whole methodology adopted for the fulfilment of objectives is given. The contents of chapters are as follows:

Chapter 1: Introduction - general background of the research problem with a concise literature review, also the need and objectives of present study has been discussed. The methodology adopted for the present work is also given in this chapter.

Chapter 2: Literature Review - provides a comprehensive review on hydrodynamics phenomenon of submerged vanes. It also includes discussion on the various parameters of submerged vane and effect on flow characteristics and bed morphology.

Chapter 3: Experimental Programme - details of the experimental program conducted for the present study is given in this chapter. It gives a complete picture of the set-up used and experimental methodology adopted for the present work. This chapter also includes detailing on the various instruments used for the experimental program and some observations made during experimentation.

Chapter 4: Flow Characteristics: Experimental Study - contains analyses of velocity fields, turbulence kinetic energy and Reynolds stress downstream of submerged vane.

Chapter 5: Morphological Changes: Experimental study - provides complete analyses of data obtained in the experimental programme. The effect of various parameters on scour pattern and maximum scour depth near the submerged vane are explained. An empirical relationship to predict maximum scour depth near the vane and extended scour depth downstream of the vane.

Chapter 6: CFD Simulation of Flow - describes the CFD based numerical modelling done for investigation of the flow field around the submerged vane. It includes detailing on the geometry, meshing, boundary conditions, turbulence models adopted, and the results obtained.

Chapter 7: Case Study – I –physical model study was conducted to evaluate the effectiveness of submerged vanes in promoting siltation along the right bank and in redirecting the main flow of the Ganga River toward the left bank at Bhagalpur, Bihar.

Chapter 8: Case Study – II –physical model study was conducted to removal of sediment from the mouth of the spill channel of padma/ganga river near Jangipur.

Chapter 9: Conclusions and Recommendations - summarizes the major conclusions obtained from the present study on hydrodynamics efficiency of bevel submerged vane.

2. LITERATURE REVIEW

2.1 INTRODUCTION

Sediment diversion structures on the riverbed are widely utilized in river engineering projects, aiming to prevent bank erosion along the river curves, intake choking, shoaling of the channel bed, and river meandering. Additionally, vanes contribute to protecting the bridge pier and foundation. Despite the employment of various sediment control structures, such as groins and dikes, their usage has been limited due to structural instability and economic unfeasibility. At the Iowa Institute of Hydraulic Research in Iowa, (Odgaard & Spoljaric 1986; Odgaard & Mosconi 1987; Odgaard & Wang 1991a; Wang & Odgaard 1993) designed low-height, high-length structures known as Iowa vanes or submerged vanes. These structures were intended to modify the near-bed flow pattern and bed-sediment motion in the transverse direction of rivers. Recent studies on submerged vanes have demonstrated their successful use in increasing flow depth and reducing sediment diversion at water intakes (Nakato et al. 1990; Wang et al. 1996; Barkdoll et al. 1999; Moghadam & Keshavarzi 2010; Kalathil et al. 2018), protecting bridge pier and foundations (Zarei et al. 2019; Fathi & Zomorodian 2017; Johnson et al. 2001; Ghorbani & Kells 2008), and preventing stream bank erosion (Odgaard & Kennedy 1983; Odgaard & Mosconi 1987; Wang 1989; Wang & Odgaard 1993; Bhuiyan et al. 2010; Dey et al. 2017). The advantage of submerged vanes over traditional sediment diversion structures, such as dikes, spurs, and groins, lies in their efficient flow redistribution with lower resistance, facilitating easy installation and economic viability. Unlike groins and dikes, which redirect flow perpendicularly through basic continuity, submerged vanes achieve redistribution through vorticity by aligning with the flow, leading to comparatively lower drag forces (Wang & Odgaard 1993). As per Odgaard & Wang (1991a), the oblique orientation of the vane angle results in a pressure differential between its two sides, inducing an upward flow component on the pressure side and a downward flow component on the suction side. The vane produces a tip vortex that propagates downstream, consequently altering the shear-stress field. The longitudinal, horizontally helical flow pattern effectively diverts sediment

downstream, preventing sediment ingress into the intake canal (Barkdoll et al. 1999). Recent field tests (Rodriguez 2020) have demonstrated the remarkable potential of submerged vanes in effectively mitigating erosion at river curves and providing erosion protection in a bend of the East Nishnabotna River, Iowa (Odgaard & Mosconi 1987). In modern river engineering projects, submerged vanes are widely employed for sediment control. Submerged vanes are being installed at the water intake to mitigate the entrainment of sediment from the intake on Kosi River, Nepal. Another study by Lake et al. (2021) aimed to divert sediment away from existing infiltration routes and enhance riverbed depth within the matrices by implementing submerged vanes in an Australian river.

2.2 HYDRODYNAMICS PHENOMENA OF SUBMERGED VANES

Submerged vane is a river training structure designed to manage sediment and control water flow in a river channel. Many researchers (Odgaard & Kennedy 1983; Odgaard & Spoljaric 1986; Odgaard & Mosconi 1987; Odgaard & Wang 1991a) investigated the physics of fluid flow and sediment motion around the submerged vane and provided theorem on it. Figure 2 illustrates the alignment of the submerged vane with the incoming flow and types of vortex by the submerged vane. Wang & Odgaard (1993) referred to submerged vanes as vortex generators as they are known for inducing vorticity. Here, two different types of vortex are created by the submerged. They are mainly the horseshoe vortex (its axis perpendicular to the submerged vane) and primary vortex (its axis parallel to the submerged vane, also called as tip vortex). The vane's leading edge is the primary factor contributing to the horseshoe vortex, which created an intense scour hole near the origin point of the vortex and was dismissed after some distance. Due to the pressure difference between the two sides of the vane, the primary vortex is generated. The primary vortex is the main reason for a scour channel downstream of the submerged vane (Fig. 2.1).

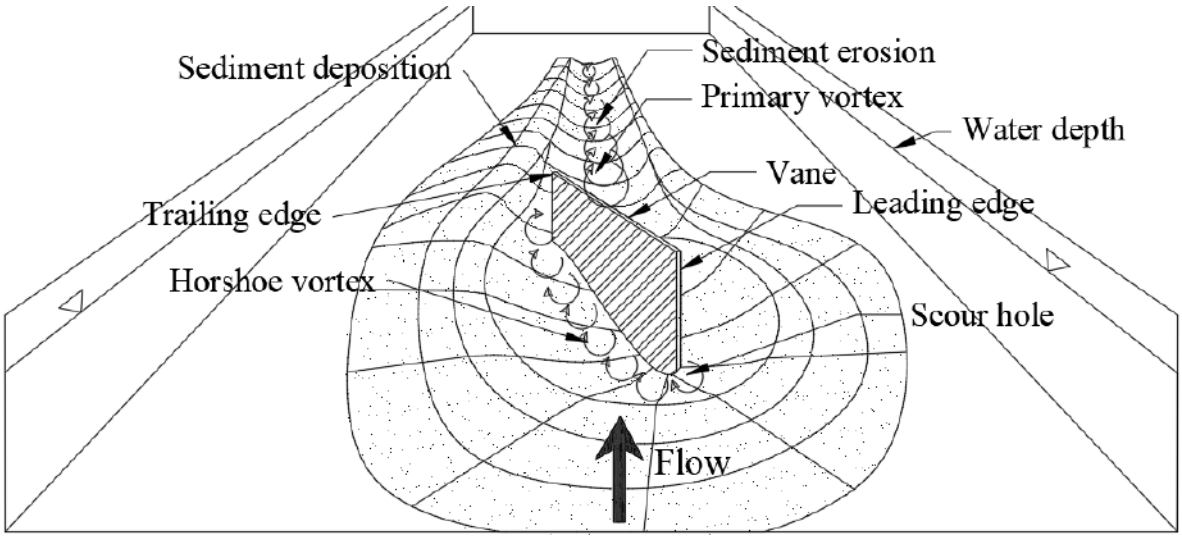

Fig. 2.1 A schematic diagram showing the vortex flow and bed morphology around the vane

2.2.1 Forces Around the Vane

The flow structure around a submerged vane can vary depending on various factors, such as the forces around the vane, flow characteristics, and vane properties. Researchers have experimentally and analytically studied the effects of these characteristics on a submerged vane (Odgaard & Kennedy 1983; Odgaard & Spoljaric 1986; Odgaard & Wang 1991a; Tan et al. 2005). The bends of a river are typically its most unstable sections, where bank erosion commonly occurs. This erosion is often driven by centrifugally generated secondary currents, known as transverse circulations or helical motion, which emerge due to variations in centrifugal acceleration along a vertical line in the flow. This phenomenon arises from the non-uniformity of the vertical velocity profile and the interaction between vertical velocity gradients. Fast-moving surface currents are compelled to migrate towards the curved bend, while slow-moving near-bed currents are compelled to move towards the center of the river, resulting in large depths and velocities near the outer banks. The difference in centrifugal force between the faster-moving fluid near the free surface and the slower-moving near-bed fluid leads to the erosion of the river bend. By applying a torque on the flow that counterbalances the centrifugally induced torque, a submerged vane can effectively suppress the secondary flow and its associated effects, which are responsible for the erosion of the river bend (Odgaard & Mosconi,

1987), as shown in Fig. 2.2. In Fig. 2.2, T_c represents the centrifugal force torque, T_v denotes the vane-induced torque, F_L indicates the vane-induced lift force, r is the radius of curvature, r_i and r_o are the innermost and outermost section radius, b is the width of the section, α is the angle of attack, d is the flow depth, L is the vane length, U is the average velocity, and ρ is the mass density of water. Odgaard & Mosconi (1987) derived the formula for centrifugal torque about the centroid of the vane acting on a volume element with the included angle ∅, given as follows:

$$T_c = \frac{1}{2}\rho\bar{u}^2 \frac{m+1}{m(m+2)} b\emptyset d^2 \tag{2.1}$$

Here, $\bar{u}$ is the depth-averaged mean velocity. The velocity profile exponent, m, is related to the Darcy-Weisbach friction factor, f, as $m = \kappa\sqrt{8/f}$, where κ is the von Karman constant (approximately 0.40 for clear water). The friction factor f is given by $f = 8(u_*/\bar{u})^2$, where u_* is the shear velocity. Since the radial-pressure-gradient force remains relatively constant across the depth and does not produce any moment around the centroid, T_c is primarily responsible for the secondary flow (Odgaard & Mosconi, 1987). Submerged vanes are installed to counter the secondary currents generated by T_c. F_L exerted by each vane on the flow generates the T_v. The equation for T_v produced by N independent vanes about the section centroid is given by (Odgaard & Mosconi 1987).

$$T_v = \frac{1}{4} C_L \rho \bar{u}^2 L d^2 \left(\frac{H}{d}\right)^{(2+m)/m} \left[\frac{(m+1)^2}{m(m+2)} - \frac{m+1}{m}\frac{H}{d}\right] N \tag{2.2}$$

Here, H represents the height of the vane, and C_L is the lift coefficient. In order to neutralize the secondary flow, the torque exerted by the vane, denoted as T_v, must balance with the T_c (Odgaard & Mosconi 1987). To calculate the vane, lift force (F_L) and drag force (F_D), Odgaard & Wang (1991a) derived the following equations:

$$F_L = \frac{1}{2}\rho C_L H L \bar{u}^2 \frac{(m+1)^2}{m(m+2)} \left(\frac{H}{d}\right)^{2/m} \tag{2.3}$$

And,

$$F_D = \frac{C_D}{C_L} F_L \tag{2.4}$$

Here, C_D is the drag coefficient. Based on the assumption that the distribution of the vertical circulation around the vane follows an elliptical pattern, with maximum values at the bed and zero at the top of the vane. The lift drag coefficient can be calculated using Eqs. 2.5 and 2.6, respectively (Odgaard & Mosconi 1987).

$$C_L = \frac{2\pi\alpha}{1 + \frac{L}{H}} \tag{2.5}$$

And,

$$C_D = \frac{1}{2\pi}\frac{L}{H}C_L^2 \tag{2.6}$$

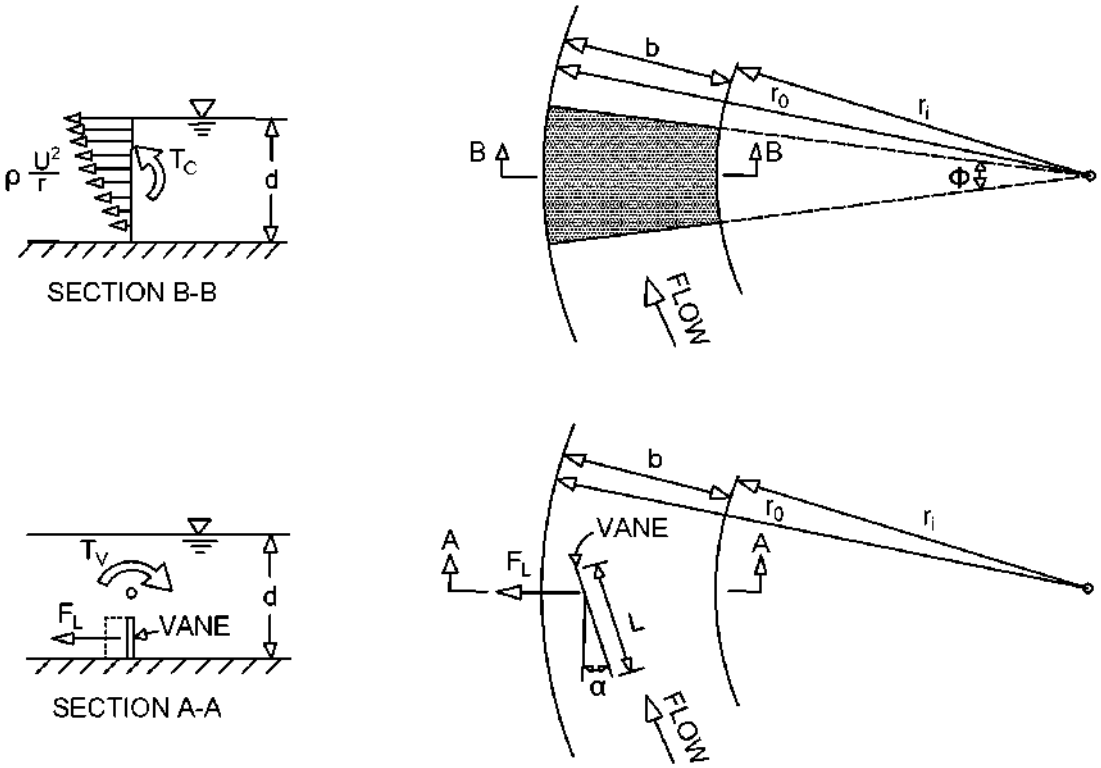

Fig. 2.2 A schematic representation of the torque induced by centrifugal acceleration (Section B-B) and the secondary flow caused by vanes (Section A-A), (Odgaard & Mosconi 1987)

2.2.2 Sediment Diversion

Odgaard & Spoljaric (1986, 1989) proposed an analytical technique for designing a system of submerged vanes to regulate depth in alluvial rivers. They concluded that flow separation becomes significant and causes excessive scour around the vane when angles exceed 15°. The employment of vanes alters the secondary flow at bends, which causes the sediment to be redistributed within the channel cross-section and reduces scour at river bends (Odgaard & Mosconi 1987). On a mobile bed, higher shear stresses on the suction side will increase sediment movement in that location, whereas lower shear stresses on the pressure side will decrease sediment movement (Wang & Odgaard 1993). In order to quantify the transverse bed shear stress (τ_{vn}) necessary to mitigate the presence of secondary currents in fully developed bend flows, Odgaard & Wang (1991a) derived the equation, which is given as follows:

$$\tau_{vn} = \frac{\rho\, k(2m+1)(m+1)}{m^2[2m^2 + k(m+1)]}\,\bar{u}^2\,\frac{d}{r} \tag{2.7}$$

Tan et al. (2005) conducted an extensive investigation into the flow structures and bed load particle motion within the four distinct zones surrounding the submerged vane. They identified four distinct spatial zones around the vane: the left and right head zones, the immediate frontal zone, and the lee zone. Each zone exhibited a different flow structure. The flow skewed towards the center top of the vane due to lateral diffusion of flow, with a helical vortex generated at a location on the frontal face of the vane. Near-bed fluid flowed around the vane at the left head zone and then along the vane's lee zone toward the center. The study observed that upper fluid dived over the vane and into the bed, increasing near-bed velocity and the rate of bed scour, resulting in a significant scour hole in the vane's lee zone. Their results indicated that the submerged vane offered the best sediment diversion when the vane height was one-fifth of the approach flow depth. Aware et al. (2005) experimentally observed that sediment gets deposited towards the outer bank due to the vortex leaving the trailing edge of the vane. Because of the vane alignment, the vortex travels towards the outer bank in the direction of the flow, and sediment deposition at the outer bend mitigates

scour and leads to a more uniform flow depth, contrasting with the condition where no vanes are present.

2.2.3 Flow Interaction

Multiples vanes are installed to generate a strong coherent vortex that propagates the flow structure over a wider area of the river cross-section. Each vane creates a unique vortex, and the resulting circulation is roughly equivalent to that caused by a single isolated vane. However, the aim of using several vanes is not achieved if the vortices do not mix to produce a combined vortex. When the transverse vane spacing (δ_n) is very small, the contact between the vanes increases, and the vortex created by one vane interacts with the vortex created by another. As the flow traverses the vane system, the circulation induced by each vane generates a velocity field that interacts with the vortex generated by the others. Consequently, the effective circulation induced by each vane within the system is smaller than that of an individual vane under identical flow conditions. The optimal spacing between vanes, ensuring the formation of a coherent vortex without compromising the effectiveness of individual vanes, has been determined by previous studies conducted by Wang and Odgaard (1993), Ouyang et al. (2008), and Odgaard and Wang (1991a).

Milne-Thomson (1966) proposed the following equation to determined effective circulation induced by each vane.

$$\Gamma_i = \pi L u_a \left(\alpha - \frac{v_i}{u_a}\right) \tag{2.8}$$

Where, subscript i is 1,....., N, and N denotes the number of the vane, u_a is the approach flow velocity, v_i is the transverse velocity components at vane i.

Milne-Thomson (1966) provided the following equation for the induced circulation of a single vane.

$$\Gamma_0 = \frac{\pi L u_a \alpha}{1 + \pi L/4H} \tag{2.9}$$

Odgaard and Mosconi (1987) also derived the same finding for a single vane. To investigate the effectiveness of the vanes, an interaction coefficient λ_i is defined as the ratio of the effective circulation to the undisturbed circulation and is given as:

$$\lambda_i = \frac{\Gamma_i}{(\Gamma_0)_i} \tag{2.10}$$

Where, Γ_i is the effective circulation for i^{th} no of vane under the effect of vane interactions, $(\Gamma_0)_i$ is the undisturbed circulation for i^{th} no of the vane. Odgaard & Wang (1991a) observed that having more than one vane in an array increases the width of the affected area of the flow field but reduces the effectiveness of circulations due to the interaction of their vortices. Wang & Odgaard (1993) found that an effective coherent structure can be generated with an interaction coefficient (λ) of approximately 0.9 by maintaining the vane spacing within 2-3 times the vane height. They also observed that if the vane spacing exceeds 2-3 times the vane height, the vane array will generate individual vortices and be less efficient. Furthermore, they concluded that vortices generated by neighboring vanes interfere, resulting in a circulation per vane that is less than that generated by an isolated vane, along with downwash along the flow. Figure 2.3 shows the values of the vane-interaction coefficient λ for various aspect ratios, showing an increase in this coefficient as the aspect ratio decreases (Odgaard & Wang 1991a). To maintain a specifically induced circulation and induced bed shear stress downstream, the vane array must be repeated at regular intervals. In a vane array characterized by vanes of uniform size and spacing, the area-averaged induced bed shear stresses are as follows:

$$\tau_{vn} = \lambda \beta_n \frac{F_L}{A_v} \tag{2.11}$$

And,

$$\tau_{vs} = \lambda \beta_s \frac{F_D}{A_v} \tag{2.12}$$

Where, τ_{vs} is the longitudal bed shear stress, Av is equal to (δn. δs), δs is the longitudinal vane spacing and β_n and β_s are the factors arising from the area-averaging process (Wang 1990).

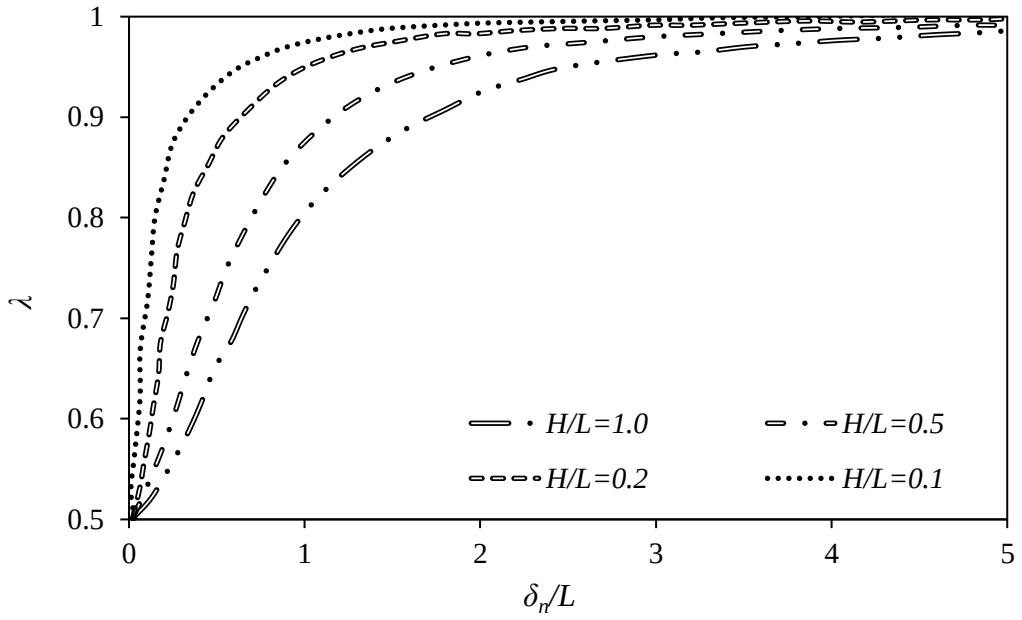

Fig. 2.3 Calculated values of interaction coefficient λ, with different aspect ratios (Odgaard & Wang 1991a)

Ouyang et al. (2008) modeled the vane-induced flow field by considering each vane inducing a bound vortex and a tip vortex. They investigated a row of three vanes constituting the vane system and showed that if the vane spacing is smaller than the inner vane within the three-vane system, it serves no purpose and may be removed without significantly affecting the vane system. According to the λ calculated by Ouyang et al. (2008), the acceptable working range for the lateral spacing between the vanes is approximately 0.6 to 1.5 times the vane lengths. If the spacing exceeds 1.5 times the vane length, all interaction coefficients of the vanes tend to unity. In a three-vane arrangement, Ouyang & Lu (2016) found that the ratio of interaction parameters between the second and first vanes was less than 1 for small values of relative lateral spacing (ratio of lateral spacing with a depth of water) and the value exceeds 1 as the relative lateral spacing increases, indicating that the first tapered vane influenced the flow for smaller relative lateral spacing and the second one dominated the flow for larger relative lateral spacing.

2.3 OPTIMUM VANE DIMENSIONS AND ORIENTATION

This chapter focuses on how the effectiveness of submerged vanes is influenced by their dimensions and orientation. In this context, the focus is limited to vane structures that aim to achieve design goals related to inducing bed shear stresses by creating a secondary circulation in the flow downstream rather than using alternatives such as deflecting walls. The efficiency of a submerged vane is determined by vane parameters such as vane angle, height, length, and spacing, among others.

2.3.1 Angle of Attack and Aspect Ratio of Vanes

Adjusting the angle of attack makes it possible to control the lift and drag forces generated by the vane. At low angles of attack, the lift force is generally small, and the drag force is relatively low, while at higher angles of attack, the lift force increases, but so does the drag force. At first, Odgaard & Kennedy (1983) examined the effectiveness of vanes in diminishing near-bank velocity and near-bank depth by adjusting the angles of attack of the vanes. Their findings indicated that when the vanes were positioned at angles of attack greater than 20°, the scour holes were generated at the upstream edges of each vane due to separation of flow. The study further revealed that reducing the angle of attack decreased the size of the scour holes. According to Odgaard & Spoljaric (1986), the flow separation causes the lift coefficient to drop when the angle of attack increases above 20°. As the angle of attack increases, lift decreases while flow separation and resulting drag become more pronounced. Therefore, the optimal range is typically between 15° to 20°.

The aspect ratio, defined as the ratio of the vane height to vane length, significantly influences vane efficiency by affecting the generation and distribution of vortices in the fluid flow. Generally, a higher aspect ratio leads to a more efficient vane, promoting the formation of longer and narrower vortices that produce less drag. Conversely, as the aspect ratio decreases, the flow at the suction side becomes increasingly dominated by tip flow, resulting in the enlargement of the primary vortex. Odgaard & Spoljaric (1986) recommend an aspect ratio in the range of 0.1 to 0.5. During the design stage, they suggest a vane height to flow depth (H/d) ratio of

approximately 0.4 to 0.5, while Odgaard & Mosconi (1987) propose a range of 0.2 to 0.5 suitable for all flow stages that can cause erosion. Summary of the experimental setup and range of different parameters used by various investigators provide in Table 2.1.

Table 2.1 Summary of the experimental setup and range of different parameters used by various investigators

SL .No.	Author (s)	Discharge (cumecs)	Depth of flow (m)	Sediment size (mm)	Vane parameters			
					Height (m)	Length (m)	No. of vanes (Nos)	Angle of attack
1.	Odgaard & Kennedy (1983)	0.154	0.064-0.253	0.30	0.048	0.12	36-52	15^{o}
2.	Odgaard & Spoljaric (1986)	0.021	0.152	0.3-1.5	0.076	0.213	1	5^{o}-20^{o}
3.	Nakato et al. (1990)	0.029	0.047-0.152	0.33	0.076	0.152	2 vanes in 13 rows	19.5^{o}
4.	Odgaard & Wang (1991 a)	0.088-0.15	0.178-0.182	0.41	0.074	0.152	4 vanes in 3-4 rows	15-25°
5.	Wang & Odgaard (1993)	0.033-0.133	0.152-0.16	0.41,4	0.076	0.152	Single and multiple rows	15°-30°
6.	Marelius & Sinha (1998)	-	0.4	0.9	0.12	0.24	1	25-57^{o}
7.	Barkdoll et al. (1999)	0.104	0.152	0.9	0.032	0.10	3 vanes in each 7 rows	20^{o}
8.	Johnson et al. (2001)	0.017-0.084	0.09-0.28	1	0.16-0.29	0.5	-	20^{o}-30^{o}
9.	Voisin & Townsend (2002)	0.0085	0.10	0.7	0.05-0.15	0.015 -0.065	-	-4^{o}-16^{o}
10.	Gupta et al. (2005-2012)	-	0.14-0.18	0.225-0.405	0.06	0.18	1	30^{o}-50^{o}
11.	Tan et al. (2005)	0.4	0.2-0.6	10–20	0.05-0.15	1-4	1	30º

12.	Aware et al. (2005)	-	-	0.3	0.03-0.10	0.07-0.17	Single and double array	30^o
13.	Ranjan et al. (2006)	0.005	0.06	0.3	0.04	0.1	Multiple vanes arrangement	30^o
14.	Allahyonesi et al. (2008)	0.05-0.09	0.056-0.084	3.4	0.075	0.025	2 vanes in 12 rows	20^o
15.	Ghorbani & Kells (2008)	0.018-0.094	0.10-0.30	0.57	0.00-0.057	0.114	Single and multiple vanes	8.5^o-28.5^o
16.	Moghadam & Keshavarzi (2010)	0.011-0.251	0.15	0.63	0.03	-	2 and 3 vanes in 5 rows	10^o-40^o
17.	Bejestan & Azizi (2012)	-	0.25	0.5	0.25	0.075	1	20^o
18.	Barani and Sardo (2013)	0.35	-	1.6	0.15	0.135	3-vanes in a row	-
19.	Bejestan et al. (2015)	0.048	0.17	0.5	0.10	0.05	1	15^o
20.	Karami et al. (2017)	0.058	-	0.8	0.09	0.03	6 vanes in two rows	15^o-30^o
21.	Maatooq & Adhab (2017)	0.004	0.03	0.327	0.009	0.03	8-12	10^o-20^o
23.	Fathi & Zomorodian (2017)	0.045	0.14	0.78	0.056	0.225	one vane in each row	20^o
24.	Kalathil et al. (2018)	0.030	0.08	0.28	0.03-0.06	0.016	7 vanes in single row	15^o-75^o
25.	Biswas & Barbhuiya (2018)	0.05	0.288	0.28	0.075	0.27	18-36	15^o
26.	Sharma & Ahmad (2020)	0.024-0.052	0.09-0.1241	-	0.05-0.12	0.02-0.06	28-76 vanes in four rows	30^o
27.	Azizipour et al. (2020)	-	0.14	1.5	0.14	-	1	23^o-60^o
28.	Sarlak et al. (2023)	0.024, 0.05	0.16	0.48	0.08	0.16	4	10^o-35^o

2.3.2 Shape of the Vanes

Most of the investigations have focused on rectangular vanes due to the simplicity of the theory, building upon earlier research on submerged vanes. While Spoljaric (1988) and Ouyang (2009) delved into the connection between vane form and flow training effects, their findings only pertain to single vane. According to Bertin & Smith (1979), wings with non-rectangular geometries, such as tapered or delta wings, can provide more significant lift than rectangular shapes. The shape of a submerged vane has been widely recognized as a crucial factor influencing its performance improvement, as noted by several researchers (Ouyang 2009; Gupta et al. 2006a, 2007; Ouyang & Lin 2016). Thus, investigating the flow pattern around non-rectangular submerged vanes is essential to produce stronger secondary currents. The leading edge of a submerged vane significantly influences the vortex, with non-linear effects being more significant for vanes with sharp edges due to flow separation and vortex creation. Therefore, the shape of the leading edge is crucial, while the shape of the top edge may be less significant.

To explain the non-linear lift behavior of delta wings at high angles of attack, Polhamus (1966) introduced the leading-edge suction analogy, which provided rise to the concept of vortex lift. According to this analogy, if flow reattachment occurs on the top surface, the total lift can be estimated as the sum of potential-flow lift and the lift associated with separated leading-edge spiral vortices. The lift coefficient (C_L) combines both vortex lift, which depends on flow, and lift from potential flow, which depends on the form or shape of the aerofoil. Polhamus assumed that the total lift coefficient could be determined as the sum of potential flow lift ($C_{L,p}$) and lift from separated leading-edge spiral vortices ($C_{L,v}$). The potential-flow lift coefficient for the zero-leading-edge-suction condition is given as:

$$C_{L,P} = K_p \sin\alpha\cos^2\alpha \tag{2.13}$$

Here, K_p ($\partial C_L/\partial\alpha$) represents the slope of the normal force, as derived from the small disturbance potential flow lifting surface theory. Additionally, the derived equation of vortex lift is given as follows:

$$C_{L,V} = K_V \cos\alpha \sin^2\alpha \quad (2.14)$$

Where,

$$K_V = (K_P - K_P{}^2 K_i)\frac{1}{\cos\theta} \quad (2.15)$$

Here, θ represents the sweep angle at the leading edge, and K_i is defined as the derivative of drag coefficient with respect to the square of lift coefficient, i.e., $K_i = \frac{\partial C_{Di}}{\partial C_L^2}$. Equations (14) and (15) suggest that as the θ increases, K_V will also increase, consequently leading to an increase in C_L. According to Gupta et al. (2007), a delta wing with a greater θ is capable of generating higher axial vorticity values at the same angle of attack compared to a wing with a smaller sweep. With the aim of producing secondary currents with the greatest possible strength, Gupta et al. (2006a) conducted an experimental study to determine the ideal characteristics of double curve and J-type vanes. While regulating sediment erosion in fluvial channels, the results shows that double curve and J-type vanes performed less effectively than rectangular vanes with the same aspect ratio. In another experiment, Gupta et al. (2007) investigated the ideal tapering angle of a tapered vane to produce the strongest secondary currents possible. They calculated the ideal tapering angle using the moment of momentum approach and found it to fall between 33º and 45º. Ouyang (2009) measured the performance of the vane by $(d_0-dv)/d_0$ with different α where d_0 is the initial pre-vane water depth; d_v is the water depth at the river bank after installation of the vane, λ_t is the taper ratio, and Λ is the swept ratio (η/L, is defined to measure the degree that the top of the vane is swept; where η = displacement of the vane's quarter-length line on the top of the vane) shown in Fig. 2.4 (a-b). The finding explored the use of tapering vanes to regulate silt in alluvial channels and observed that a lower tapering ratio (defined as the ratio of a tapered vane's top width, L_T, to its base width, L_b) improved the vane's efficacy as a sediment-managing device for a given constant surface area and height (Fig. 2.4a). Additionally, results for the swept vane indicate that it performs better than the baseline rectangular vane when its top is swept forward ($\Lambda < 0$) only to the oncoming flow. Ouyang & Lin (2016) conducted a numerical analysis of the performance of a row of rectangular, swept, and tapered

vanes. They discovered that rectangular and sweeping vanes both elevated the bank bed level by 16% and 17%, respectively, while tapered vanes increased the bed level by 19%. Shafai Bejestan & Azizi (2012) analyzed the effectiveness of rectangular and triangular vanes and found that the triangular vane outperforms rectangular vanes in reducing local scour at the leading edge of the submerged vane. They also concluded that the largest chamfer at the leading edge of the vanes resulted in the highest reduction in scour depth. Teronpi & Misra (2015) suggested that among rectangular, curved, and trapezoidal submerged vanes, the maximum scour depth occurs specifically with rectangular vanes. Therefore, further investigations are needed to explore approaches aimed at minimizing local scour depth around the tip of submerged vanes by utilizing non-rectangular vane shapes, as this particular region has received limited attention in previous research.

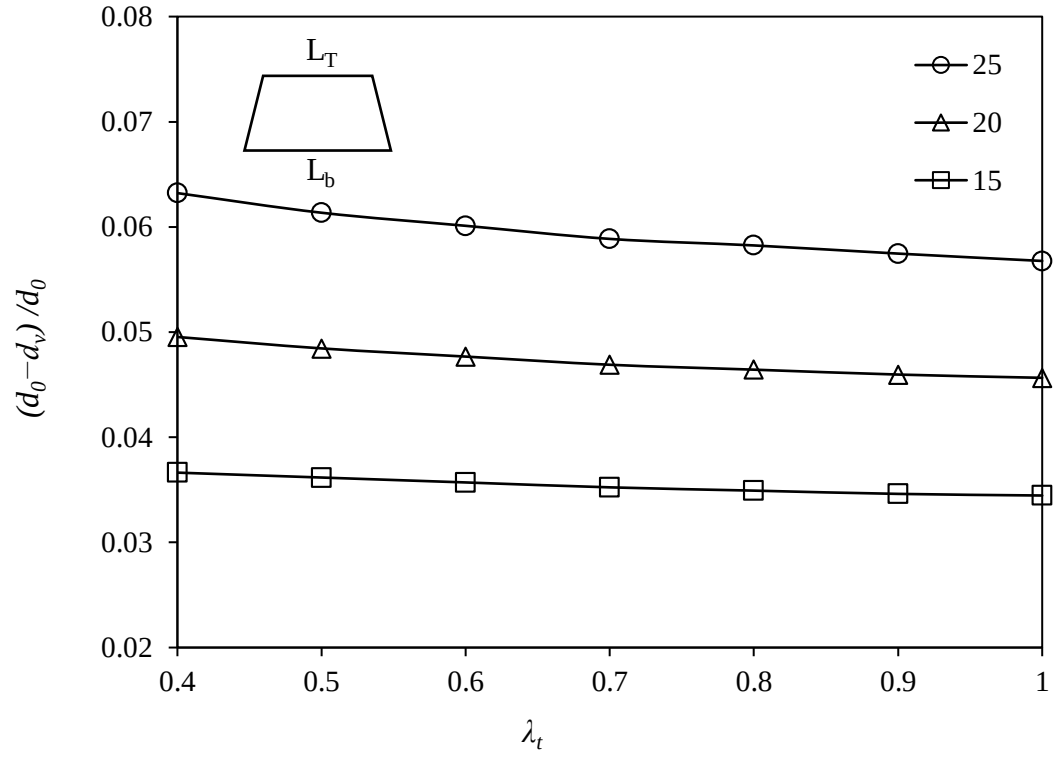

Fig. 2.4a Near-bank bed level change induced by a taper vane (Ouyang 2009)

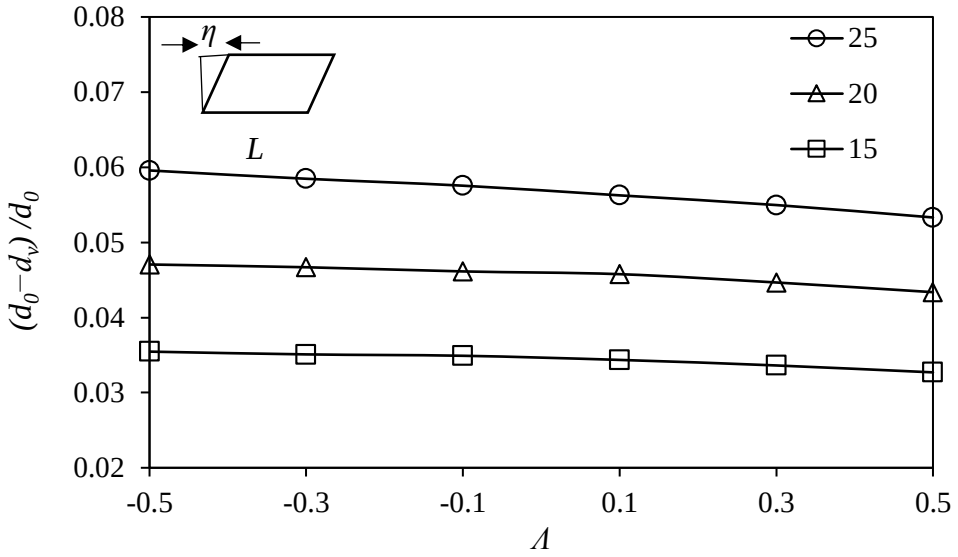

Fig. 2.4b Near-bank bed level change induced by a swept vane (Ouyang 2009)

2.4 EFFECT OF SUBMERGED VANES ON VARIOUS FLOW PARAMETERS

The use of submerged vanes for river training and sediment deflection can be formulated empirically by incorporating kinetic parameters, as outlined in the following sections. This section provides a review of how previous researchers have expressed various flow parameters, including vorticity, velocity distribution, bed shear stress, and moment of momentum, in their studies.

2.4.1 Vane-Induced Vorticity

Vorticity holds significance in fluid dynamics, where it plays a crucial role in comprehending the behavior of turbulence, boundary layers, and other intricate flows. When a fluid flows past a submerged vane, it can generate vorticity due to changes in flow direction caused by the vane's orientation with the flow. Vorticity emerges at the edges of the vane and moves downstream with the fluid flow. Essentially, the angle of attack of the vanes significantly influences the vorticity. Marelius & Sinha (1998) identified that continuously evolving flow fields and topographical features in the field may result in vanes at higher angles of attack. They observed that at a 40º angle of attack, a horseshoe vortex was present on the pressure side of the vane. However, there has been a lack of experimental studies focusing on developing a dimensionless parameter for assessing the strength of secondary

circulation induced by submerged vanes. The development of such a dimensionless parameter necessitates experimental research to establish an empirical correlation between the damping function of vortex strength (Gupta et al. 2006a, b). It noted that the decay of vane-induced strength does not follow a consistent trend and appears to be influenced by factors such as the location of the vortex center, Froude number, and other variables.

2.4.2 Velocity Distribution and Vane-Induced Bed Shear Stresses

When a fluid flows over a submerged vane, it undergoes changes in velocity distribution, leading to the generation of bed shear stresses. The velocity profile for a submerged vane can be modeled using different equations, such as the logarithmic law or the power law. The power-law velocity distribution is given as:

$$\frac{u}{\bar{u}} = \frac{m+1}{m}\left(\frac{z}{d}\right)^{\frac{1}{m}} \tag{2.16}$$

Here, u is the point velocity at height z. As the velocity profile changes, the submerged vane also generates bed shear stresses, whose magnitude depends on the velocity of the fluid and the roughness of the bed surface. The tip vortex exhibits similarities to a Rankine vortex but degrades with distance downstream of the vane due to viscous diffusion. The tangential velocity (v_θ) perpendicular to the core axis in an unbounded flow field is defined as (Odgaard & Wang 1991a):

$$v_\theta = \frac{\Gamma_0}{2\pi r}\left[1 - e^{-\frac{K}{4\varepsilon s}r^2}\right] \tag{2.17}$$

Where, Γ_0 is the strength of circulation, r is the radius of local curvature, K is the equivalent sand roughness, ε is eddy viscosity, and s is the stream-wise component. In the open channel, the presence of the channel bed and the free surface distorts the vortex. The method of images can be employed to incorporate the influence of boundaries on tangential velocity analytically. Here, the transverse component of the tangential velocity (v_{vn}) near the bed is given as:

$$v_{vn} = \frac{F_L}{\pi\rho u H_v}\sum_{j=1}^{\infty}\frac{(-1)^{j+1}}{r_j}\left[1 - e^{-\frac{k}{4\varepsilon s}r_j^2}\right]\frac{z_j}{r_j} \tag{2.18}$$

Where r_i and r_o are the innermost and outermost radius of curvature of depth-averaged turbulence, respectively, i and j are the influence functions, and z is the vertical coordinate. Calculations and experimental data by Wang & Odgaard (1993) have shown that the core of the vortex is located approximately 0.2 times the vane height below the top elevation of the vane.

2.4.3 Moment of Momentum

The moment of momentum (MOM) is non-dimensional parameter, also known as angular momentum. It is a physical quantity that describes the amount of rotational motion of an object around an axis. At first, Marelius & Sinha (1998) and Sinha & Marelius (2000) used this non-dimensional parameter (moment of momentum or MOM) to present the physics of the flow past a submerged vane at higher angles of attack. Using the MOM concept, Marelius & Sinha (1998) discovered that the angle of attack for generating optimal strength of vortical currents from a submerged vane must be 40° (Fig. 2.5). Furthermore, Gupta et al. (2007) investigate the maximum level of secondary circulation strength generated by vanes of different shapes and determined that maintaining a taper angle of 33.7^o could further enhance the MOM for a given optimal angle of attack of 40^o.

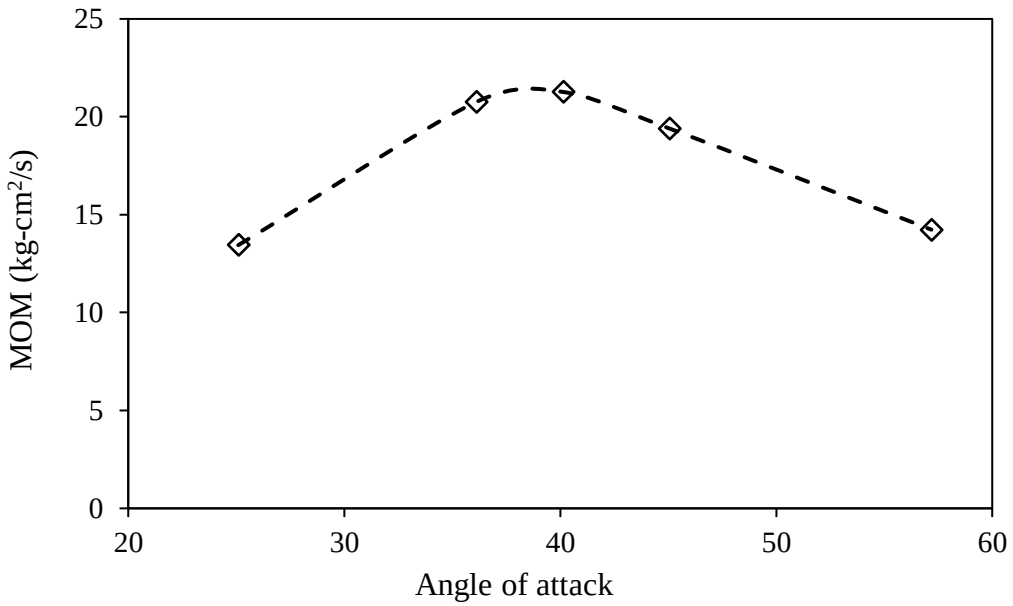

Fig. 2.5 Moment of Momentum (MOM) with an angle of attack (Marelius & Sinha 1998)

2.5 CONCLUDING REMARKS

In view of the above literature survey, it has been observed that

- The majority of investigations have prioritized rectangular vanes, primarily due to the simplicity of the underlying theory and in consideration of previous research conducted on submerged vanes; however, limited attention has been given to submerged vanes featuring non-rectangular shapes of submerged vane.

- The principal drawback associated with the utilization of submerged vanes lies in the susceptibility to structural deterioration caused by localized scour in the vicinity of their tips. Because, the vane's leading edge is the primary factor contributing to the horseshoe vortex, which created an intense scour hole near the origin point of the vortex and was dismissed away from the hole. A lack of investigation still exists to minimize the depth of local scour around the submerged vanes. In the future, further study is required to assess the viability of utilizing non-rectangular-shaped vanes in safeguarding against local scour around submerged vanes.

- The horseshoe vortex and potentially additional vortices may constitute unfavorable forces in the system regulating the transverse movement of sediment, although this has not yet been properly investigated. In the future, the experiments should concentrate on vanes at the higher ranges of angle of attack, despite enlarged scour holes, increased resistance to flow and the presence of additional vortical structures.

- Only a limited number of studies have investigated the potential of submerged vanes for desilting purposes, indicating the need for further research in this area. Because of this, the potential of submerged vanes to enhance inland navigation should be explored.

3. EXPERIMENTAL PROGRAMME

3.1 INTRODUCTION

The experimental study was conducted to investigate the flow characteristics around the submerged vane and the associated changes in bed morphology under open channel flow conditions. Various parameters influence the flow characteristics and local scour patterns around the vane; therefore, a comprehensive examination of these parameters is essential for developing a sustainable and effective design of submerged vanes. The present chapter aims to describe the experimental setup, bed materials, instruments used, procedures followed during the experimental study, and the observations made. All the experiments were performed in a masonry flume of the Hydraulics Laboratory of Civil Engineering Department at Indian Institute of Technology Roorkee, India.

3.2 EXPERIMENTAL WORK

3.2.1 Details of Experimental Setup

(a) Laboratory Flume

A fixed bed masonry flume of 28.0 m length, 1.0 m width and 0.4 m depth were used for conducting the experiment. A constant head tank is used for the supply of water in the flume. The inlet pipe is equipped with a valve for the regulation of discharge. The discharge in the flume was regulated with the help of valves provided in the inlet pipes coming from an overhead tank. In the experimental flume, a test section measuring 6.0 m in length and 0.25 m depth in sediment bed was prepared 12.0 m from the inlet. The location of the test section was made in such a way that the flow became fully developed before it reaches the test sections followed by Nikora et al. (1998). Figure 3.1 shows the schematic section and plan view of the experimental setup.

To reduce the effects of the sudden entrance of the extremely turbulent flow into the flume a temporary water storage tank of 2.0 m in length, 1.0 m in height, and 1.0 m

wide is provided at the inlet. Following the tank, a honeycomb masonry grid constructed from small bricks, along with a flow straightener, was installed to minimize turbulence dissipation and to align the flow parallel to the flume walls. At the experimental channel entrance, the 1st two meter of the flume bed will be filled with gravel to smoothen the flow transition and turbulence and a wooden floater was placed to maintain the uniformity of the flow depth. An adjustable slotted wooden gate was provided at the downstream end of the flume to adjust the depth of the flow in the flume. Ragulating trolleys and rails were installed on the flume walls to convey measuring devices such as pointer gauge, Ultrasonic bed profiler and Acoustic Doppler Velocimeter (ADV) to measure the flow depth, velocity profile, and scour profile. The arrangement of instruments without and with flow.

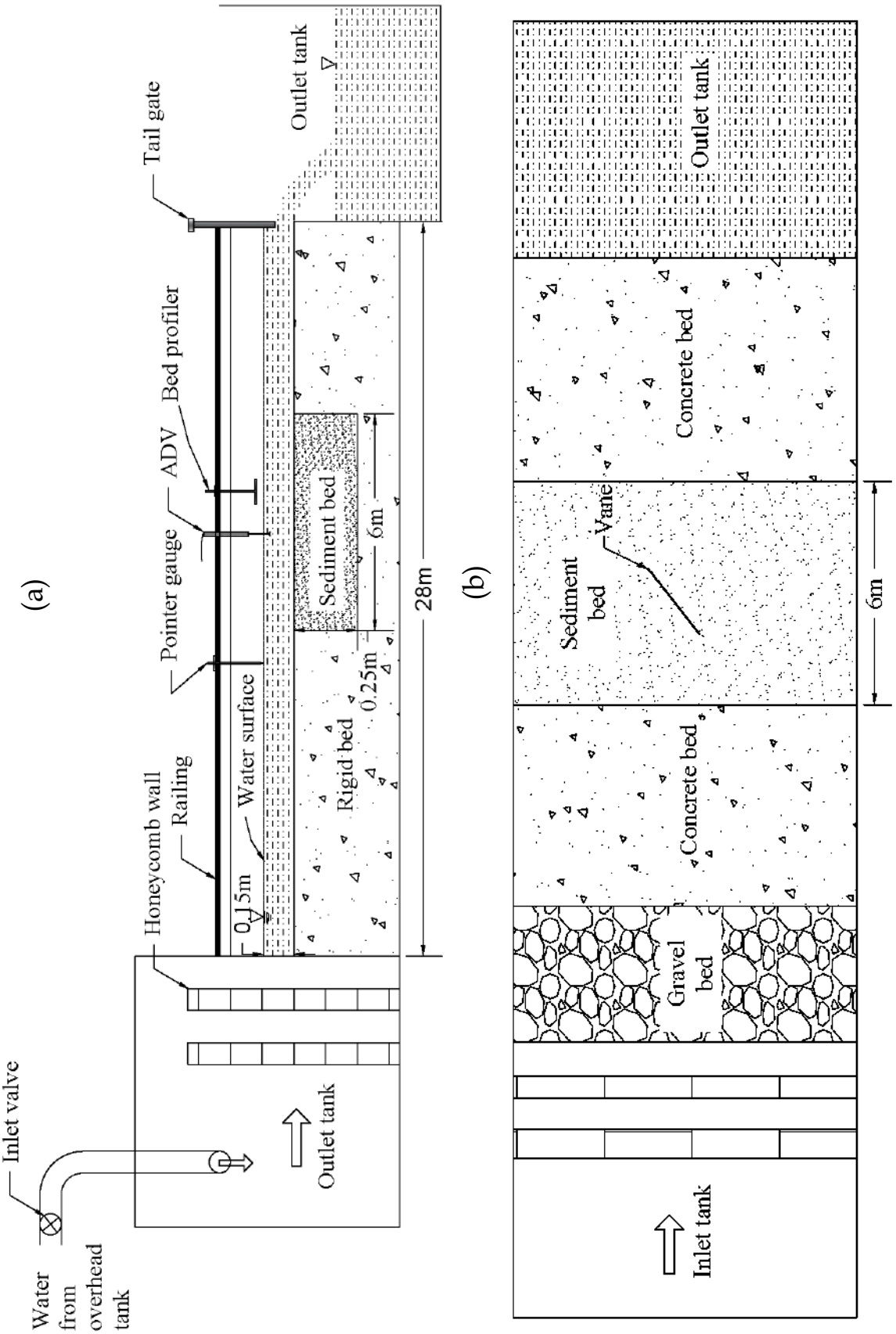

Fig. 3.1 Schematic diagram of the flume with a experimental setup (a) Section and (b) Plan view

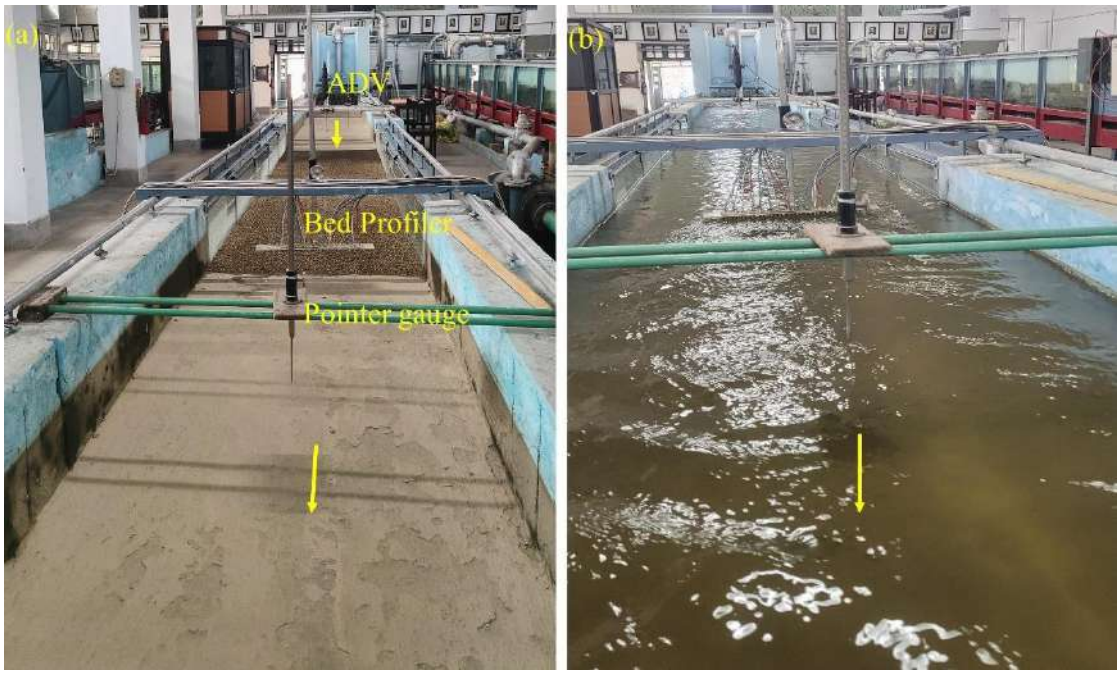

Fig. 3.2 Photographic view of the flume (a) without flow, and (b) with flow

(b) Bed Material and Preparation

Sieve analysis was done at the Hydraulics Laboratory of Civil Engineering Department, Indian Institute of Technology Roorkee. The sediment was sieving within 1.18 mm to 3.5 mm diameter of sieve shown in Fig. 3.3 (a). The sediment bed was prepared with coarse sand having a median diameter (d_{mm}) of 2.36 mm and having a geometric standard deviation ($\sigma_g = \sqrt{d_{84}/d_{16}}$) less than 1.4, confirming the uniformity of the grain (Marsh et al. 2004) where, where d_{84} and d_{16} are grain sizes for which 84% and 16% of the sample are finer than that size by weight. The relative density of sand was 2.65. Spirit level was used to level the sediment bed of the flume. The depth of the sediment bed layer of the test section was fixed at 0.25 m. After every experimental run, the sediment bed was prepared, shown in Fig. 3.3 (b).

Fig. 3.3 Photography shows a) sediment sieve and b) sediment bed preparation

(c) Specifications of Vane

Prior investigations have focused on implementing submerged vanes with rectangular geometries; however, limited attention has been given to submerged vanes featuring non-rectangular shapes like bevel submerged vane. In present studies, different type of non-rectangular shape were investigated. The vane size of length = 0.15 m; height = 0.045 m; and thickness = 0.002 m were used. Here in this experimental and numerical study, the author investigated five shapes of vanes, a simple rectangular vane and four beveled at the leading edge at 30, 45, 60, and 70 degrees with respect to the base, respectively shown in Fig. 3.4.

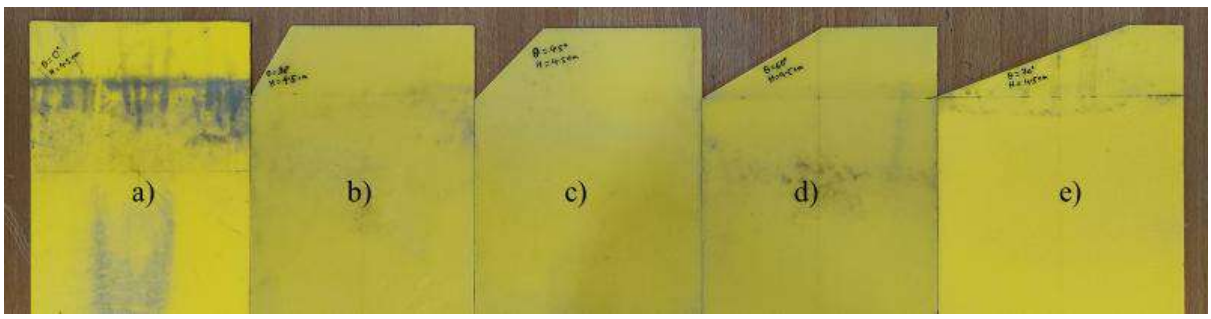

Fig. 3.4 Vane specification of different bevel angles (a) Simple rectangular vane (θ = 0°); (b) θ = 30°; (c) θ = 45°; (d) θ = 60°; and (e) θ = 70°

3.2.2 Measuring Instruments

(a) Bed Slope Measurement

The slope of the flume was measured by two independent methods. In first method, two containers connected at their bottom by a long plastic tube were placed on the bed of the flume, one each at two pre-determined locations along the length of the flume. Care was taken to remove air bubbles in the connecting tube. Enough time was allowed for equalization of water level in the containers to occur. The water levels in both the containers were read by means of pointer gauge mounted on rails. The difference in the readings gives the vertical drop of the flume over the selected length and hence the slope. In the second method, an Auto Level was used to take levels, at 2.0 m interval along the bed of the flume. A mean line passing through these points gives the slope of the flume. Both these methods gave results very close to each other. The slope so obtained was found to be $1 * 10^{-03}$.

(b) Electromagnetic Flowmeter

The diverted discharge from the intakes was measured using an electromagnetic flow meter made by Siemens Inc. The volumetric flow measurement instrument known as an electromagnetic flow meter is frequently used to gauge pipeline system flow. The induction of voltage resulting from the movement of an electrical conductor in a magnetic field is the fundamental idea behind an electromagnetic flow meter (USBR, 2001). This is regarded as one of the most extensively used flow measurement tools for pipelines, typically found in industrial fluid application systems, municipal water supply systems, and pipeline oil transport systems. This flow meter had two parts: a transmitter and a sensor. The transmitter is branded as SITRANS FM MAG 5000 which is a microprocessor based having a measuring accuracy range of 0.4% ±1 mm/s. SITRANS F M MAGFLO MAG 5100 W is the brand name of the sensor which is having an accuracy of 0.2% ± 2.5 mm/s which can measure velocity from 0 to 10 m/s that can give good results at a maximum pressure condition up to 16×10^5 Pa. Figure. 3.5 shows the image of the electromagnetic flow meter used in the present study.

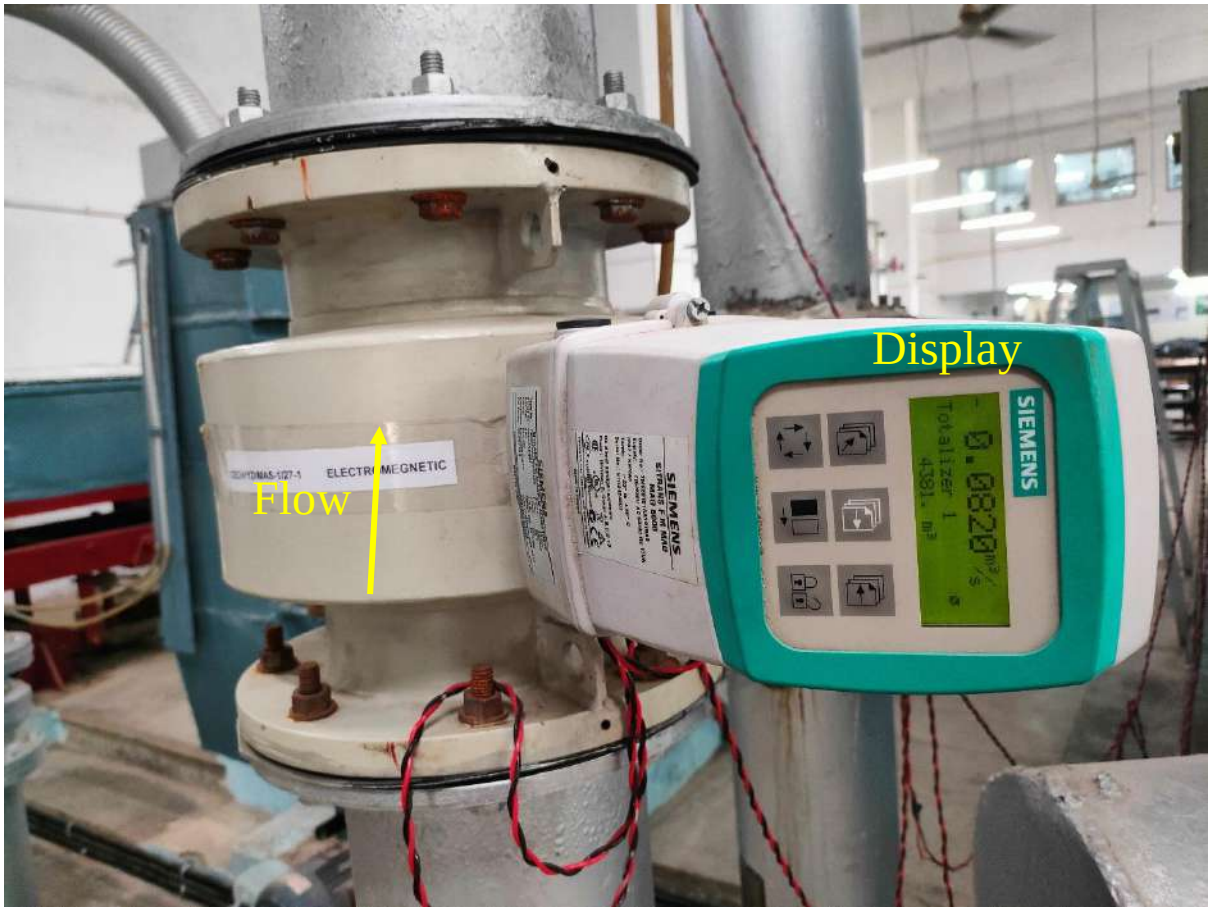

Fig. 3.5 Measurement of discharge using Ultrasonic floe meter

(c) Acoustic Doppler Velocimeters

Acoustic Doppler Velocimeters (ADV) is used for measurement of 3D velocity fields in turbulent flows (Fig. 3.6a). The acoustic Doppler velocimeter is a relatively simple to use device which registers instantaneous velocity components at a single-point.The instantaneous data recordedwith an ADV is generally used to compute mean flow statistics such as the 3D mean velocity, the turbulent kinetic energy and the Reynolds stresses.In this study, a Vectrino, Nortek ADV (serial no. VNO. 0006), equipped with a downlooking sensor mounted on a fixed stem was deployed.Vectrino has four receivers symmetrically spaced around the central emitter. It has a much smaller probe head, includes one transmitter and four receivers instead of three found in other systems (Fig. 3.6b). The fourth receiver provides redundant information in one velocity component, typically the vertical, depending on orientation. The distance between the control volume and probe was large enough to avoid considering its

effect in the measurement. The sampling volume was located 5.0 cm from the tip of the probe. In a standard configuration, the sampling volume is about a cylinder of water with a diameter of 6 mm and a height of 9 mm. A typical ADV system equipped with N receivers records simultaneously 4×N values with each sample. In the present study, the ADV system records simultaneously sixteen values with each sample. Hence, for each receiver, velocity components, signal strength, a signal-to-noise ratio (SNR) and a correlation value are recorded. The Vectrino model measures 4 velocity components u, v, w1 and w2, where w1 and w2 are independent and redundant measurements of the vertical velocity. The velocity components are measured along the line connecting the sampling volume to the receiver ranging from 0.3 to 1.0 m/s. Measurements are averaged over a small representative volume. The time series of velocity at each sampling point is used to produce a time-averaged velocity.

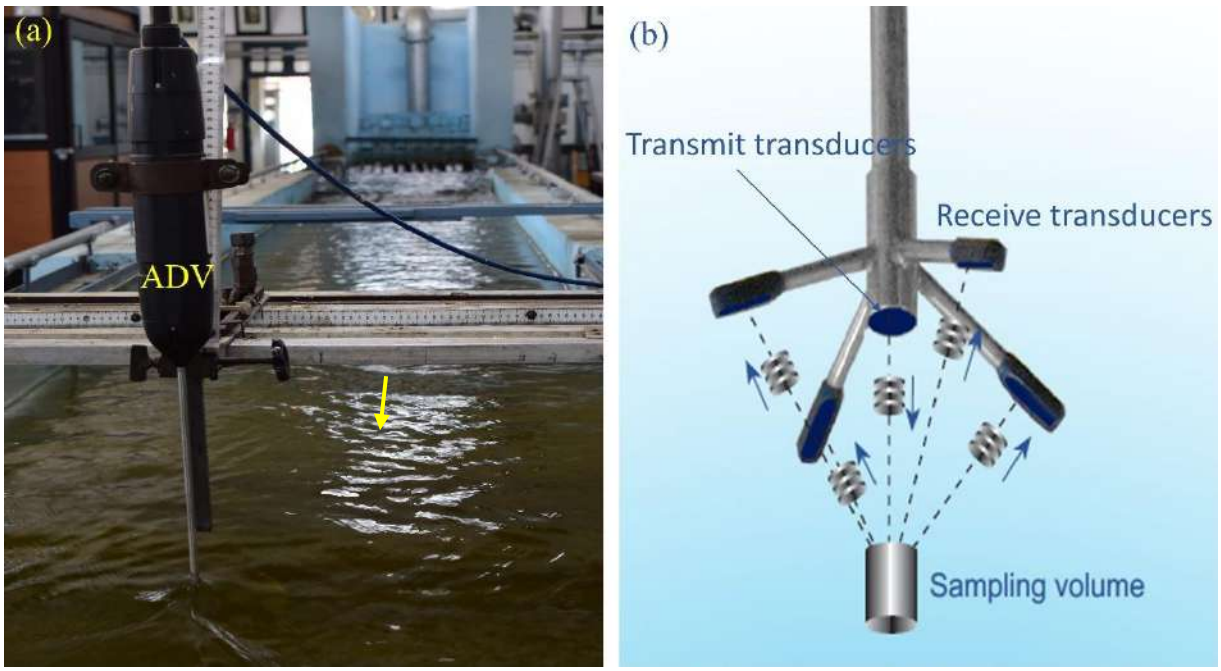

Fig. 3.6 Velocity measurement instruments (a) Acoustic Doppler Velocimeters (ADV), (b) Transmitter and four receiving proves with remote sampling volume (Source: Vectrino manual)

(d) Ultrasonic Bed Profiler

The scour pattern was measured with the help of a 5 MHz ultrasonic bed profiler. This SeaTek ranging system was composed of 32 transducers and an electronics package. The acoustic operating frequency of this system was 5 MHz, sample rate was 1 s, and no of samples was 1000. The electronics package communicates with a PC via a USB communications port. The electronics were set up to accept AC power ranging from 110 to 240 Volts at 50 to 60 Hz. The electronics package was capable of running up to 32 transducers and sampling up to 4 external analog channels, have a half beam angle of 0.9 degrees. The closest range measurement of this system is 3.5 cm; the furthest range was 0.1 m. In the present study, the sample rate was kept at 1 s, and 100 samples were taken. The ultrasonic bed profiler was installed to take the bed to scour reading, as shown in Fig. 3.7.

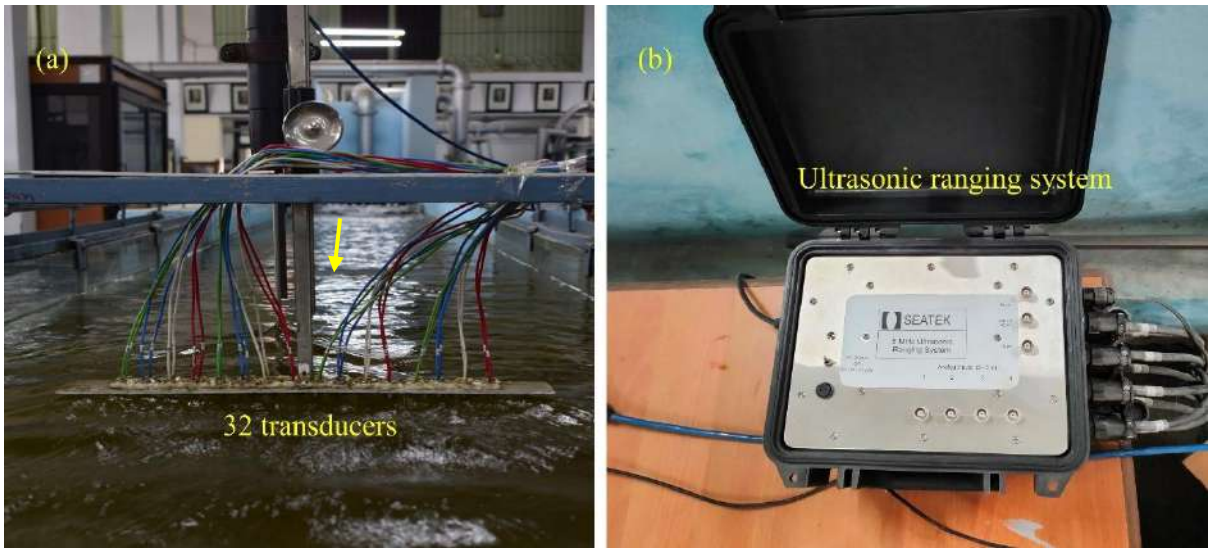

Fig. 3.7 Photography shows the taking reading with an a) 32 transducers and b) ultrasonic ranging system

3.2.3 Experimental Procedures

(a) Flow Characteristics Study

Flow field and turbulence characteristics downstream of the vane were studied on the equilibrium scoured bed condition for five bevel angles (θ = 0º, 30º, 45º, 60º and 70º), three vane heights (H = 0.045 m, 0.06 m, and 0.075 m), and four angles of attack (α) of

15º, 20º, 30º and 40º. Once the equilibrium scoured conditions developed, water allowed to drain out from the flume. Once the bed had sufficiently dried, a mixture of synthetic resin and water (in a volume ratio of 1:3) was uniformly sprayed over the scoured bed and left to set for 24h. This operation was necessary to facilitate the measurement of instantaneous velocities using the ADV without risking further alteration of the equilibrium bed. 3D velocity components were taken with a 5.0 cm side-looking acoustic Doppler velocimeter (ADV) manufactured by Nortek with an acoustic frequency of 16 MHz and a sampling frequency of up to 200 Hz. In all the experiments; the velocity range setting was ±100 cm/s with frequency of 50 Hz. The minimum signal-to-noise ratio (SNR) was kept higher than 15, and the minimum signal correlation was kept higher than 70% (Nortek mannul). It is necessary to filter the velocity data collected using an Acoustic Doppler Velocimeter using the signal-to-noise ratio (SNR) and the correlation parameters since most of the collected data contains spikes. So in post-processing, the measured data were filtered using WinADV (Wahl, 2000), which incorporated a phase space threshold despiking filter developed as described by Goring and Nikora (2002). Instantaneous velocities were measured in three cross-sections along the downstream of the channel, x = 3H, 8H, and 20H from the middle of the vane, where H is the height of the vane. At each cross-section, velocity measurements were made at nine lateral positions at stabilized scoured bed with a single vane which was 10 cm right and left from the middle of the vane (-10.0, -7.5, -5.0, -2.5, 0, 2.5, 5.0, 7.5, 10.0 cm from middle of the vane) across the channel, here, zero point was denoted as middle of the vane. And at each lateral position, instantaneous velocities were taken at 18 points in the vertical direction from the bed to the water surface. Flow characteristics were investigated for all run at three cross-sections planes as 3H, 8H, and 20H plane from the middle of the vane, where H is the height of the vane along the downstream of the vane area. For some of the experiments, velocity measurements were taken at mid point of each section. Figure 3.8 shows the coordinate systems of arrangement of vane and ADV location. The x, y, and z axes were in the stream-wise, vertical and transverse directions, respectively, and the associated velocity components are u, v, and w.

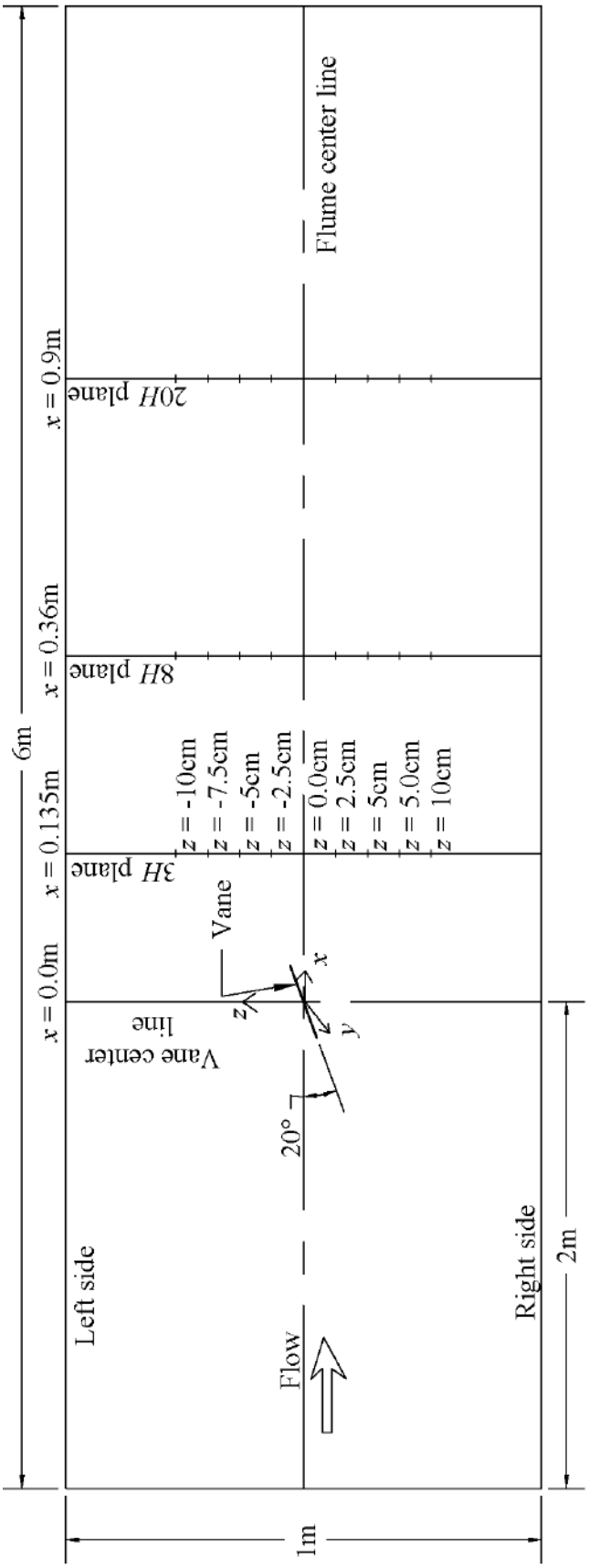

Fig.3.8 Coordinate systems and arrangement of vane for measuring velocity

The raw ADV data needs to filter to eliminate spikes and noise from the data before using it for further analysis. Filtering is used to remove samples with low correlation scores or low signal-to-noise ratios. Filtering may be based either on the 3-beam averages or the 3-beam minimums (2-beam averages and minimums for 2D probes). Spikes and outliers are produced in the ADV data due to a weak signal-to-noise ratio because of insufficient scattering particles in the flow to reflect the sound signals. The raw ADV data was filtered for Low SNR and correlation. In post-processing, the experimental data were filtered using WinADV (Wahl, 2000), which incorporated a phase space threshold despiking filter developed as described by Goring and Nikora (2002). This software program was designed for the post-processing of the real time data files (.adv files) recorded by nortek ADV. The output from Win ADV was taken in the excel format for further flow characteristics analysis. The output file contains various information such as average SNR, boundary distance, 3-D velocity, root mean square of the velocity, correlations, and covariance.

(b) Scour Pattern and Maximum Scour Depth

Experiments were conducted to investigate the scour pattern downstream of the vane and maximum scour depth around submerged vanes under varying conditions of discharge (Q = 0.07 m^3/s, 0.082 m^3/s, and 0.09 m^3/s), five bevel angles (θ = 0°, 30°, 45°, 60°, and 70°), three vane heights (H = 0.045 m, 0.06 m, and 0.075 m), and four angles of attack (α = 15°, 20°, 30°, and 40°). Prior to initiating each experimental run, the sediment bed was carefully prepared with the help of sprite level. After the preparation of sediment bed and installation of submerged vane, the flow was initiated through the flume's inlet. At first, to prevent undesired scour caused by sheet flow with insufficient flow depth, the flume was initially filled with water at a low rate by closing the tailgate until the desired flow depth was attained. Subsequently, the discharge in the flume was gradually increased to the desired value, corresponding to the condition of clear-water scour. After achieving the certain water depth in the flume, the tailgate was gradually opened, and the discharge was increased to the target value while maintaining the flow depth using the downstream tailgate. This process was carried out with utmost care to ensure that no unintended

scouring occurred during the operation. After the experiment over, the pump was stopped and the water was drained slowly without disturbing the scoured bed by slowly opening the tailgate.

To ensure the clear water conditions, the flow was increased gradually and the sediment movement was observed visually. Once the sediment starts moving, the discharge and the flow depth were measured and the critical shear stress was computed using $\tau_c = \rho gRS$ and critical shear velocity of the sediment was computed using $u_{*c} = \sqrt{\tau_c/\rho}$, Where ρ is the mass density of flowing fluid, g is acceleration due to gravity, *R* is hydraulic radius and S is the bed slope.The clear water condition ($u_*/u_{*_c} < 1$, where u_* is the approaching flow shear velocity and u_{*_c} is the critical shear velocity of the bed sediment) was maintained for all experimental runs, meaning that no sediments travelled from the upstream part of the flume.

3.2.4 Observation During Experimentation

(a) Flow Visualization

In present study, Fluorescent dye namely Rhodamine WT (Molecular Formula: C29H29CIN2Na2O5) was used to visualization the flow pattern downstream of the submerged vane as shown in Fig. 3.9. The dye was injected at the upstream of the vane in middle position of the vane. Observations revealed that the leading edge of the vane deflects the approaching flow and generates a helical flow structure downstream of the vane.

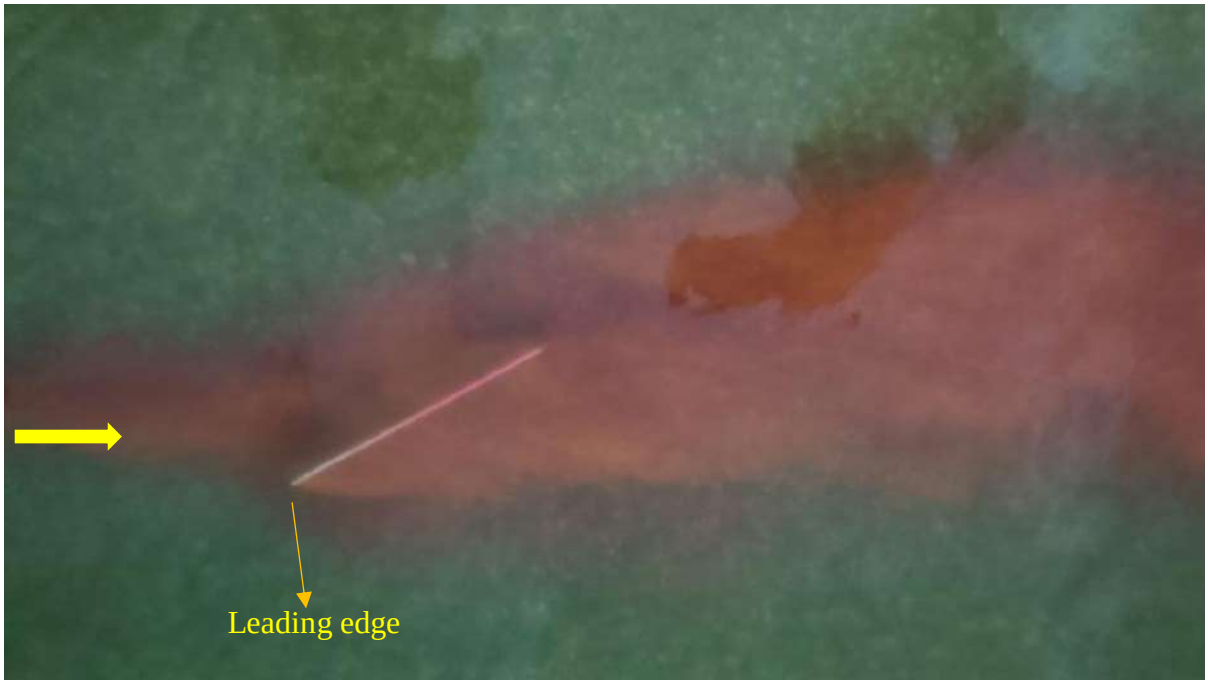

Fig. 3.9 Visualization of the helical flow with dye for Q = 0.058 m^3/s, H = 0.045 m, α = 20º, θ = 0º

(b) Temporal Variation of Scour Depth

This investigation aimed to study the scour profile at equilibrium, so it was important to determine the saturation time so that the setup attained its equilibrium within that time frame. An equilibrium is expected to be attained when there is no more sediment movement can be identified. Temporal variation of the scour was measured using an ultrasonic bed profiler under three different experimental conditions to determine the time required to reach equilibrium. The maximum scour depths at a temporal resolution of 10 min to 12 hr , as shown in Fig. 3.10. A steep increment of scour depth within a few minutes suggest that the most of the scour was occoured within the first 2 hours of start of experiment. The temporal variation of the scour depth showed that the maximum scouring occurs in the early 5 hours of testing, as shown in Fig. 3.10. After this, only minor scour was occoured to reached the equilibrium scour condition. Considering this, the experiments were conducted for 12 hours on the safer side to achieve equilibrium conditions. At last, the pump was stopped, and the water was drained out slowly without disturbing the scoured bed by slowly opening the tailgate.

A certain scour also occoured due to the displacement of materials from the side slope of the scour hole.

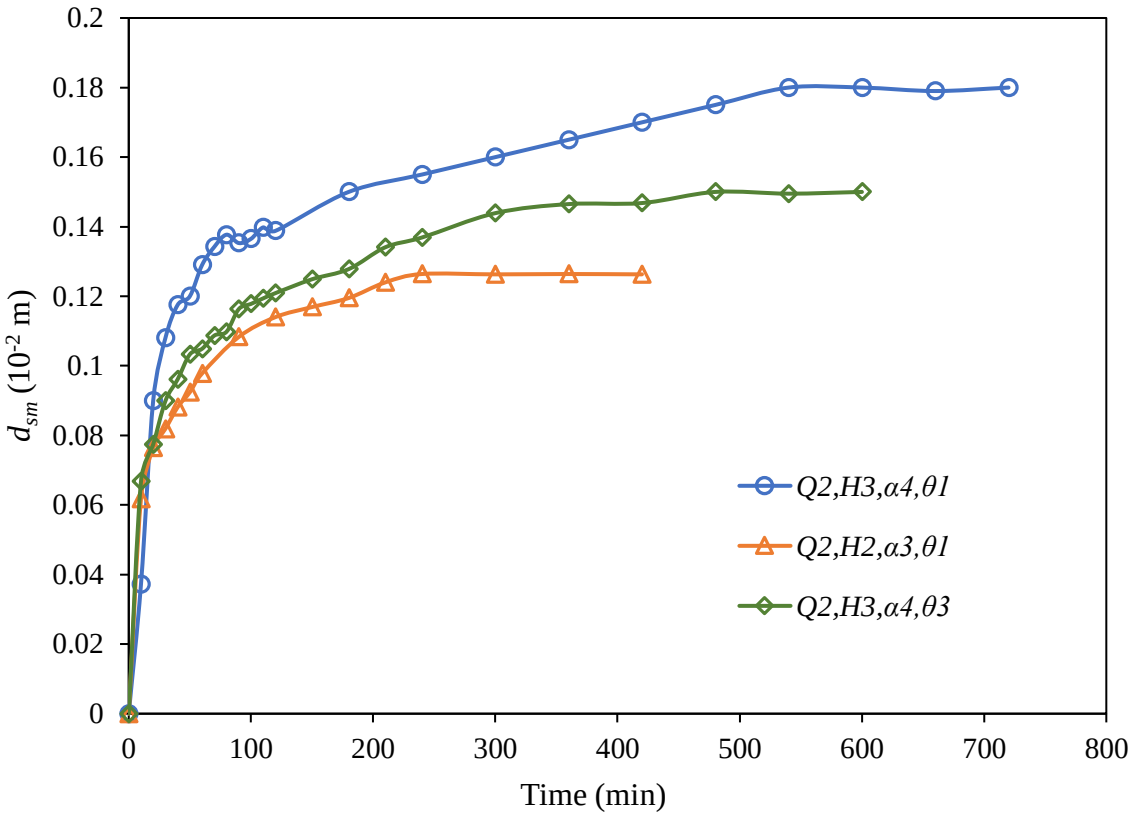

Fig. 3.10 Temporal variation of scour depth (d_{sm})

(c) Bed Morphology

In none of the experiment sediment movement occurred upstream of the vane, in accordance with the intended clear-water conditions. Fig. 3.11 (a) illustrates the initial sediment bed configuration with a rectangular submerged vane before the experimental run, and Fig. 3.11 (b) shows the equilibrium scour bed after 12 h of the experimental run. After the water was drained, two scour holes became visible due to the vane's orientation angle: one formed locally around the vane, while the other extended downstream after the trailing edge of the vane, as shown in Fig. 3.11 (b). Due to the angle of attack along the flow, the horseshoe vortex along the pressure side of the vane becomes significant enough to transport material away from the scour hole effectively. Observations indicate that more significant scour occurred on the pressure

side of the vane, whereas some deposition is noted on the suction side at low angles of attack. Eroded sediment particles from the vicinity of the vane primarily begin to accumulate after a certain distance and continue to spread over a longer distance downstream. The vane's angle orientation creates a pressure difference, leading to an upward flow on the higher part of the pressure side and a downward flow on the suction side. This interaction generates a primary vortex that propagates downstream of the vane, eroding material from the right side and depositing it on the left side along the flow, as illustrated in Fig. 3.11 (b). Another observation reveals that changes made to the bed topography gradually diminish as they move downstream. This phenomenon occurred because the strength of the vortex responsible for generating scour weakened as it moved downstream from the trailing edge of the vane. Experiments observation shows the scour hole at leading edge of the submerged vane with various bevel shape under Q = 0.082 m^3/s, H = 0.045 m, α = 20º, as shown in Fig. 3.12. It can be observed that the scour depth is reducing with increasing the bevel angle of submerged vane. Figure 3.13 shows the scour bed due to the curved vane for Q=0.082 m3/s, H = 0.045 m, α = 0º. The curved vane was installed with its leading edge aligned parallel to the flow. The vane represented one-quarter of a circular arc and had a length of 15 cm. It was observed that the curved vane induced the maximum local scour compared to the other vane configurations, shown in Fig. 3.13. Such excessive local scour poses a risk to the structural stability of the vane. Consequently, the curved vane was excluded from further consideration in the present study, considering both structural stability and economic feasibility.

Fig. 3.11a Photographic image of the rectangular vane before experiment run

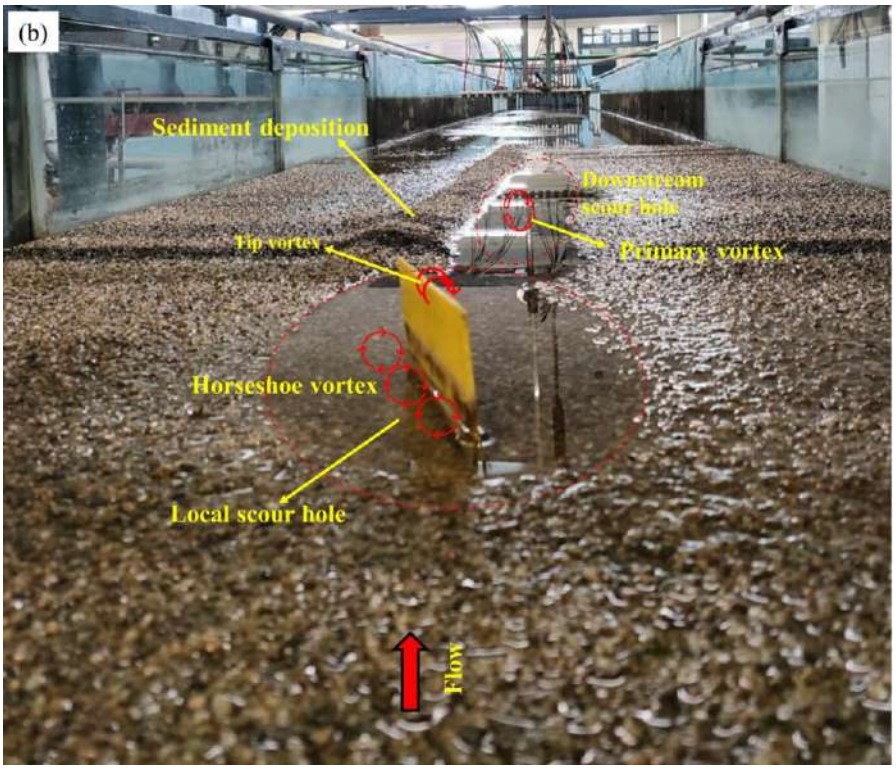

Fig. 3.11b Photographic image of equilibrium scour bed condition after the experimental run for Q = 0.082 m^3/s, H = 0.045 m, $\alpha = 20^0$, $\theta = 0^0$

Fig. 3.12 Scour hole geometry as observed during experimentation for various shape of bevel submerged vane under Q = 0.082 m^3/s, H = 0.045 m, α = 20°

Fig. 3.13a Photographic image of the curved vane before experiment run

Fig. 3.13b Photographic image of equilibrium scour bed condition after the experimental run for Q = 0.082 m^3/s, H = 0.045 m, $\alpha = 0^o$

3.2.5 Range of Collected Data

Experiments were conducted on a cohesionless sediment bed using submerged vanes of various sizes and shapes under different flow conditions, with the aim of collecting data on flow and bed morphological characteristics over the broadest possible range for the present study. The current study used a wide range of discharge rates (Q), angles of attack (α), different bevel angles (θ), and vane heights (H), with the specific ranges summarized in Table 3.1. The dimensions of the vanes are determined using the Odgaard and Wang (1993), and Odgaard and Wang (1991a) design criteria: vane height to water depth ratio of H/d = 0.2-0.5, and aspect ratio of H/L = 0.3-0.5. A table outlining the experimental scheme is included in Appendix I and Table 1.

Table 3.1 Parameter range used for experimental test

Parameter	Unit	Value	Notation
Discharge (Q)	m^3/s	0.058	Q1
		0.082	Q2
		0.092	Q3
Angle of attack (α)	degree	15	α1
		20	α2
		30	α3
		40	α4
Bevel angle (θ)	degree	0	θ1
		30	θ2
		45	θ3
		60	θ4
		70	θ5
Vane height (H)	m	0.045	H1
		0.06	H2
		0.075	H3

3.3 CONCLUDING REMARKS

A detailed description of the experimental work conducted to study the flow characteristics and bed morphology induced around the submerged vanes in open channel flow is presented. All salient fetures of the experimental setup and the instruments used are discussed. The methodology adopted for the experimentation on flow characteristics and bed morphology near the submerged vane under uniform flow conditiond is also explained. The comprehensive detailing of the setup, instrumentation, and measurement procedures adopted provides a solid foundation for the subsequent analyses and insights in the following chapters.

- The experimental study were performed in open channel flume uner clear water condition to understand the flow pattern, flow characteristics and bed morphology downstream of the submerged vane.
- The design and execution of the experimental setup used in this study are provided with the detailing and precision with which this study was conducted. The selected sediment bed materials, calibrated instruments, and controlled environmental conditions collectively ensured that the obtained dataset was robust and representative of real-world scenarios.
- This chapter employing state-of-the-art measuring equipments, including an ultrasonic flowmeter for discharge measurement, a pointer gauge with vernier caliper for depth measurement, ultrasonic bed profiler for scour measurements and ADV for velocity measurements.
- The ovservation after draining revealed that a scour hole formed locally around the vane, while the other extended scour downstream after the trailing edge of the vane.

4. FLOW CHARACTERISTICS: EXPERIMENTAL STUDY

4.1 INTRODUCTION

A submerged vane is essentially an aerofoil-shaped structure that induces enhanced turbulence in the form of a helical flow pattern. This helical motion arises due to the pressure differential between the approaching flow side and the opposite side, and propagates downstream, thereby modifying the near-bed flow characteristics and altering the shear stress distribution (Odgaard and Spoljaric, 1986; Odgaard and Mosconi, 1987; Odgaard and Wang, 1991; Wang and Odgaard, 1993). In this present chapter, the flow characteristics such as velocity field, turbulence parameters and Reynolds shear stress were studies downstream of the submerged vane. Three dimensional velocities were measured with the help of ADV in the equilibrium scoured condition.

4.2 RESULTS AND DISCUSSION

4.2.1 Velocity Distribution

Instantaneous 3D velocities were measured in three cross-sections along the downstream of the channel, x = 3H, 8H, and 20H from the middle of the vane, where H is the height of the vane. At each cross-section, velocity measurements were made at nine lateral positions at stabilized scoured bed with a single vane which was 10 cm right and left from the middle of the vane (-10.0, -7.5, -5.0, -2.5, 0, 2.5, 5.0, 7.5, 10.0 cm from middle of the vane) across the channel, here, zero point was denoted as middle of the vane. And at each lateral position, instantaneous velocities were taken at 18 points in the vertical direction from the bed to the water surface. For some of the experiments, velocity measurements were taken at mid point of each section. Figure 4.1 shows the coordinate systems of arrangement of vane and ADV location. The x, y, and z axes were in the stream-wise, vertical and transverse directions, respectively, and the associated velocity components are u, v, and w. The velocity data were collected for five bevel angles ($\theta = 0^{o}$, 30^{o}, 45^{o}, 60^{o} and 70^{o}), and four angles of attack of 15^{o}, 20^{o}, 30^{o} and 40^{o} under Q = 0.082 m^3/s, H = 0.045 m. Time averaging method was

applied to analysing data. The avarage velocities were further analysed for compare turbulent intensity (TI) and tirbulent kinetic energy (TKE).

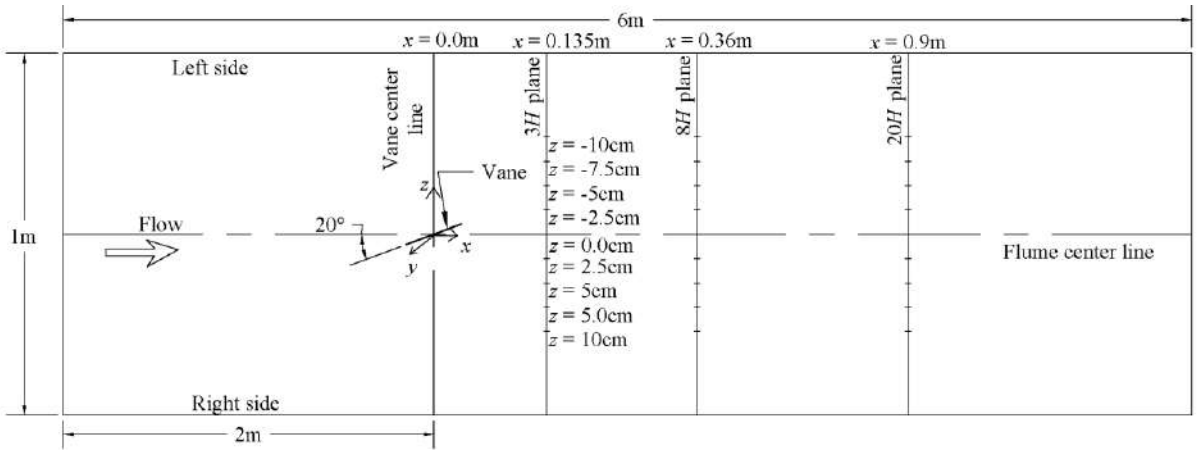

Fig. 4.1 Coordinate systems for measuring 3d velocity by using ADV

The computation of average velocity in three directions at a point over the bed has been done using the following equations:

$$\bar{u} = \frac{1}{N}\sum_{i=1}^{N} u_i \tag{4.1}$$

$$\bar{v} = \frac{1}{N}\sum_{i=1}^{N} v_i \tag{4.2}$$

$$\bar{w} = \frac{1}{N}\sum_{i=1}^{N} w_i \tag{4.3}$$

Where; $\bar{u}$, $\bar{v}$ and $\bar{w}$ are the average velocity at any point in x, y, and z-directions, respectively. u_i, v_i and w_i represents the instantaneous velocity in respective directions. N is the number of data samples collected at that point. The instantaneous velocity fluctuations in the longitudinal, lateral, and vertical directions (u_i', v_i', w_i') of the respective recorded instantaneous velocities (u_i, v_i, w_i) was computed from the time average velocities ($\bar{u}$, $\bar{v}$ and $\bar{w}$) as per equations:

$$u' = u - \bar{u} \tag{4.4}$$

$$v' = v - \bar{v} \tag{4.5}$$

$$w' = w - \bar{w} \tag{4.6}$$

The stream-wise velocity profile in vertical direction at x = 3H, 8H, and 20H from the middle of the vane for all bevel shape of vane were shown in Fig. 4.2 for 15º angle of attack, Fig. 4.3 for 20º angle of attack, Fig. 4.4 for 30º angle of attack and Fig. 4.5 for 40º angle of attack. At x = 3H, the velocity distribution is observed to lose its logarithmic nature but it shows a S-type variation over the vertical direction for all bevel angle which suggests the presence of point of inflexions in the velocity profiles and it confirms the presence of strong vortices at the transect due to submerged vane upto 8H plane. At x = 20H, the flow has reached an appreciable distance from the submerged vane and it is observed that velocity distribution has become nearly logarithmic in comparison with velocity profiles at x = 3H and 8H which suggested the dampening of vortices in the flow by viscosity. we can observed that vorticity is not decreasing due to introducing the bevel angles upto 60º but decreasing drastically at 70º bevel angle for different angle of attack. At 40º angle of attack, rectangular vane generate the maximum circulation than bevel submerged vane.

Figures 4.6 to 4.8 show the contour profile of observed streamwise velocity distribution across all the planes for various shape of bevel vane, where z/d = 0 denotes the center of the vane. The generation of the vane-induced tip vortex can be represented by contour plots of streamwise velocity, as reported by Wang (1990) and Wang and Odgaard (1993). The combination in upward flow and opposite side downward flow indicates the location of vortex in the contour plot. The upward velocity component of the vortex lifts up the low velocity fluid near the bed on pressure side, while downward velocity component of the vortex directed the high velocity fluid near core region towards the bed on suction side. A similar flow distribution has been reported by Wang (1990), Sharma and Ahmad (2019), and Solanki et al. (2020). The pressure difference between the pressure and suction side generates a primary clockwise vortex that propagates downstream the vane, which is briefly described in the following section. The streamwise velocity distribution further demonstrates that the generated vorticity remained discernible for a considerable distance downstream of the vane, although its intensity progressively diminished, as shown in Figs. 4.6, 4.7 and 4.8. Further observation indicates that the vortex is more

concentrated at 3h plane (Fig. 4.6), but the maximum velocity of the vortex in the lower part remains close to the bed, the location of the maximum velocity in the upper pan shifts toward the water surface as the vortex moves downstream. The reason is that the vortex spreads out as a result of viscous diffusion (Wang, 1990). The weakening of the vortex can be noted as it moves downstream from the center of the vane; viscosity is the primary factor influencing this phenomenon, shown in Fig. 4.8.

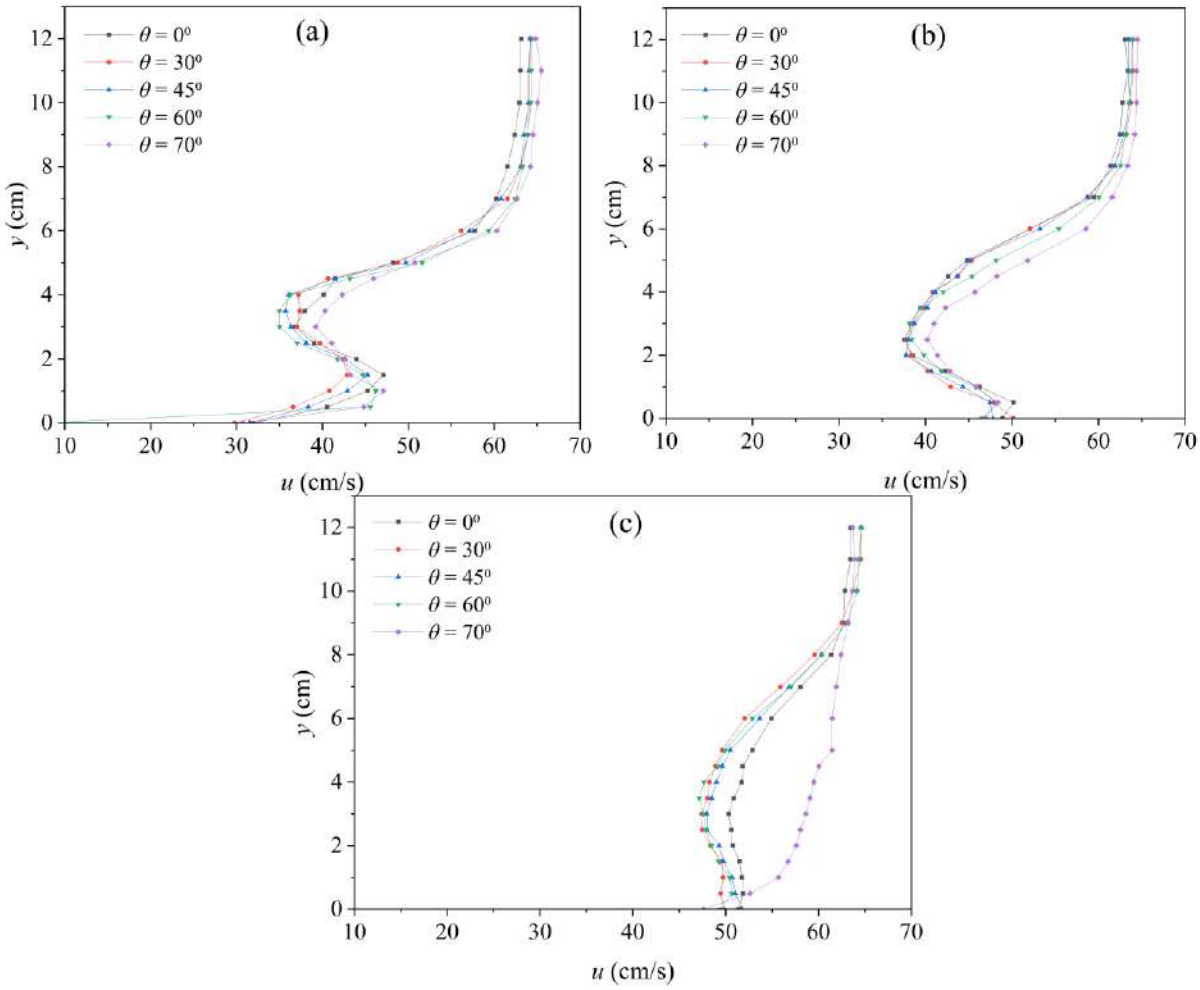

Fig. 4.2 Streamwise velocity profile at (a) 3H plane, (b) 8H plane, and (c) 20H plane for all vanes with different bevel angle under Q = 0.082 m^3/s, H = 0.045 m, α = 15°

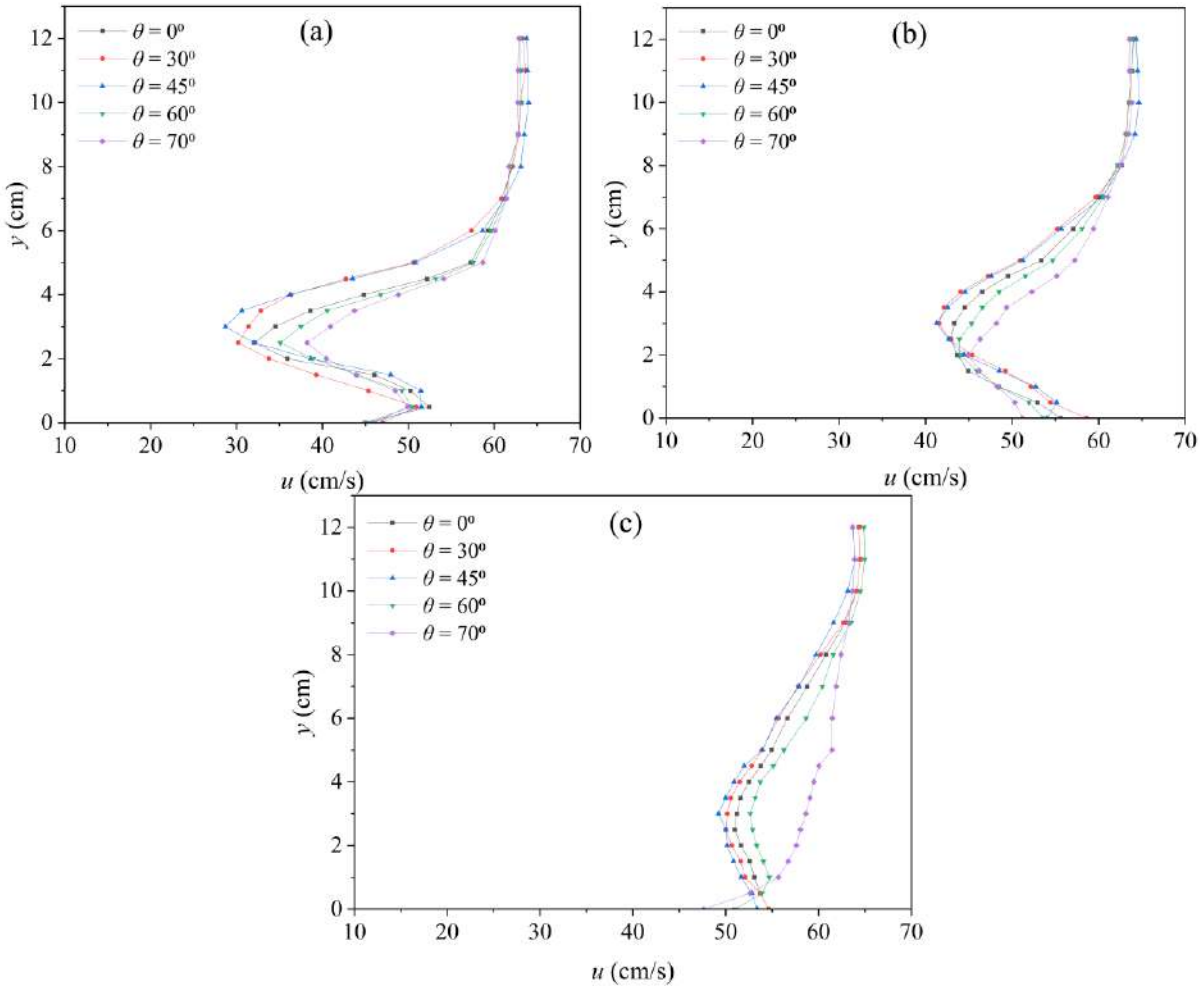

Fig. 4.3 Streamwise velocity profile at (a) 3H plane, (b) 8H plane, and (c) 20H plane for all vanes with different bevel angle under Q = 0.082 m^3/s, H = 0.045 m, α = 20°

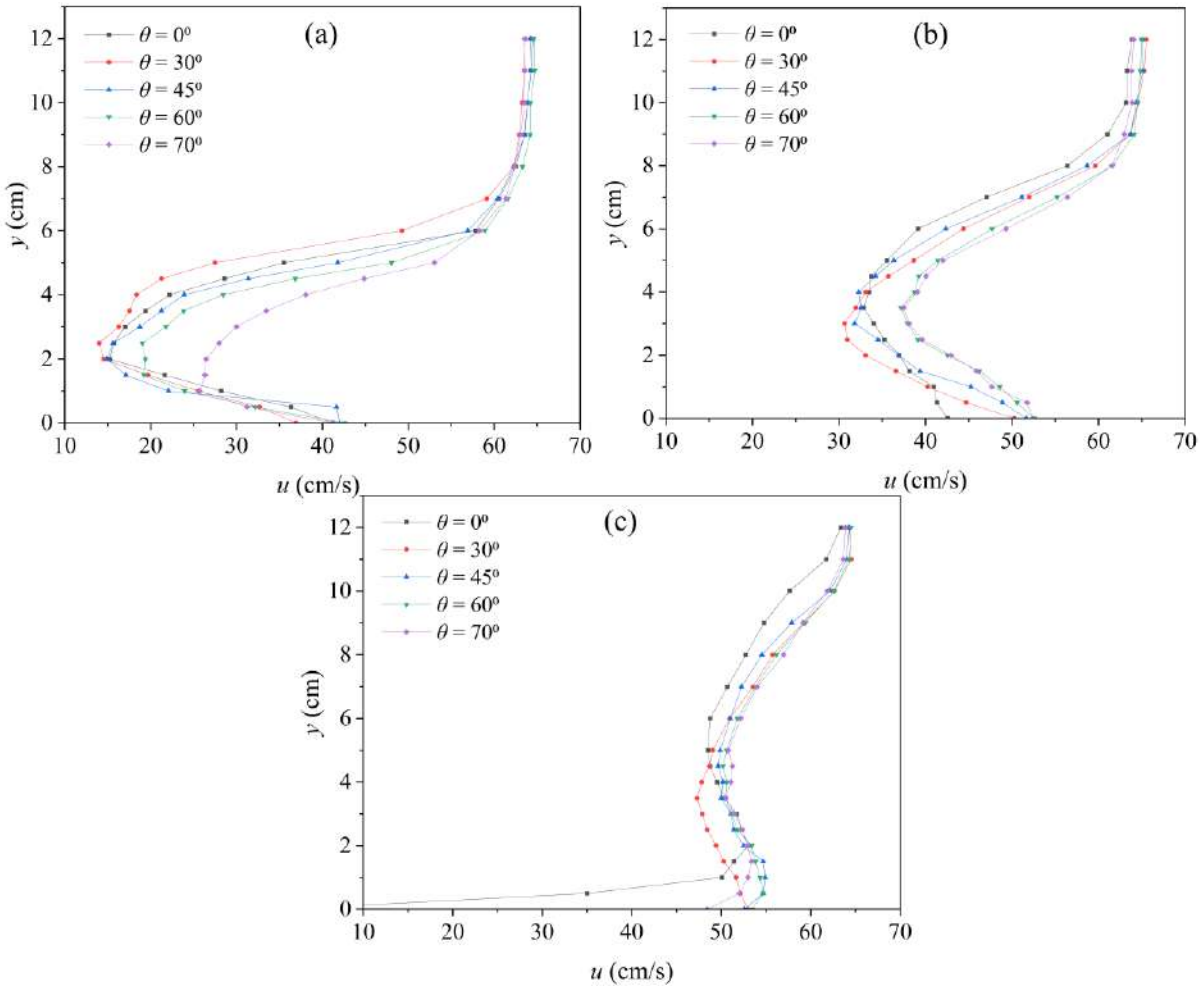

Fig. 4.4 Streamwise velocity profile at (a) 3H plane, (b) 8H plane, and (c) 20H plane for all vanes with different bevel angle under Q = 0.082 m^3/s, H = 0.045 m, α = 30°

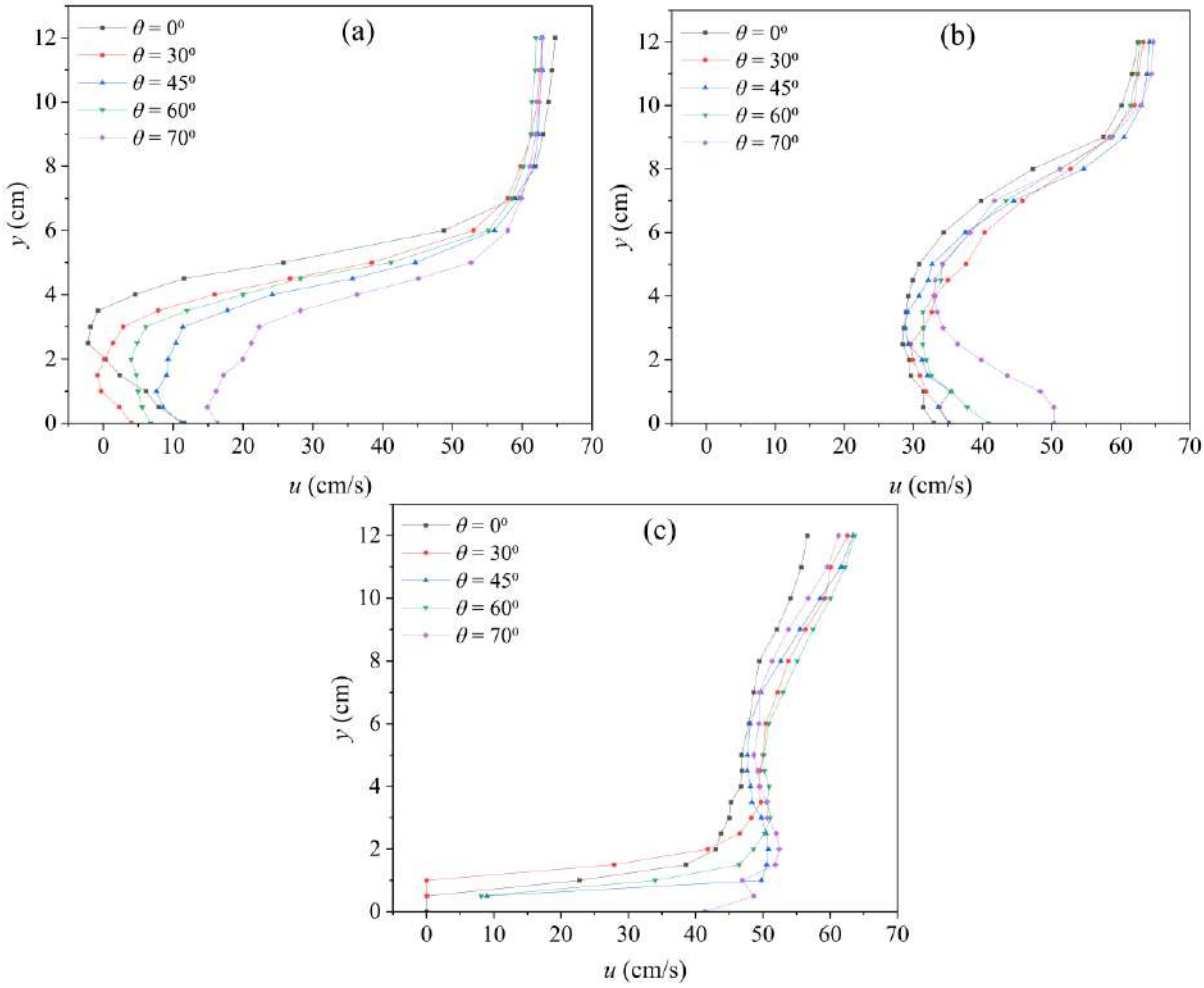

Fig. 4.5 Streamwise velocity profile at (a) 3H plane, (b) 8H plane, and (c) 20H plane for all vanes with different bevel angle under Q = 0.082 m^3/s, H = 0.045 m, α = 40°

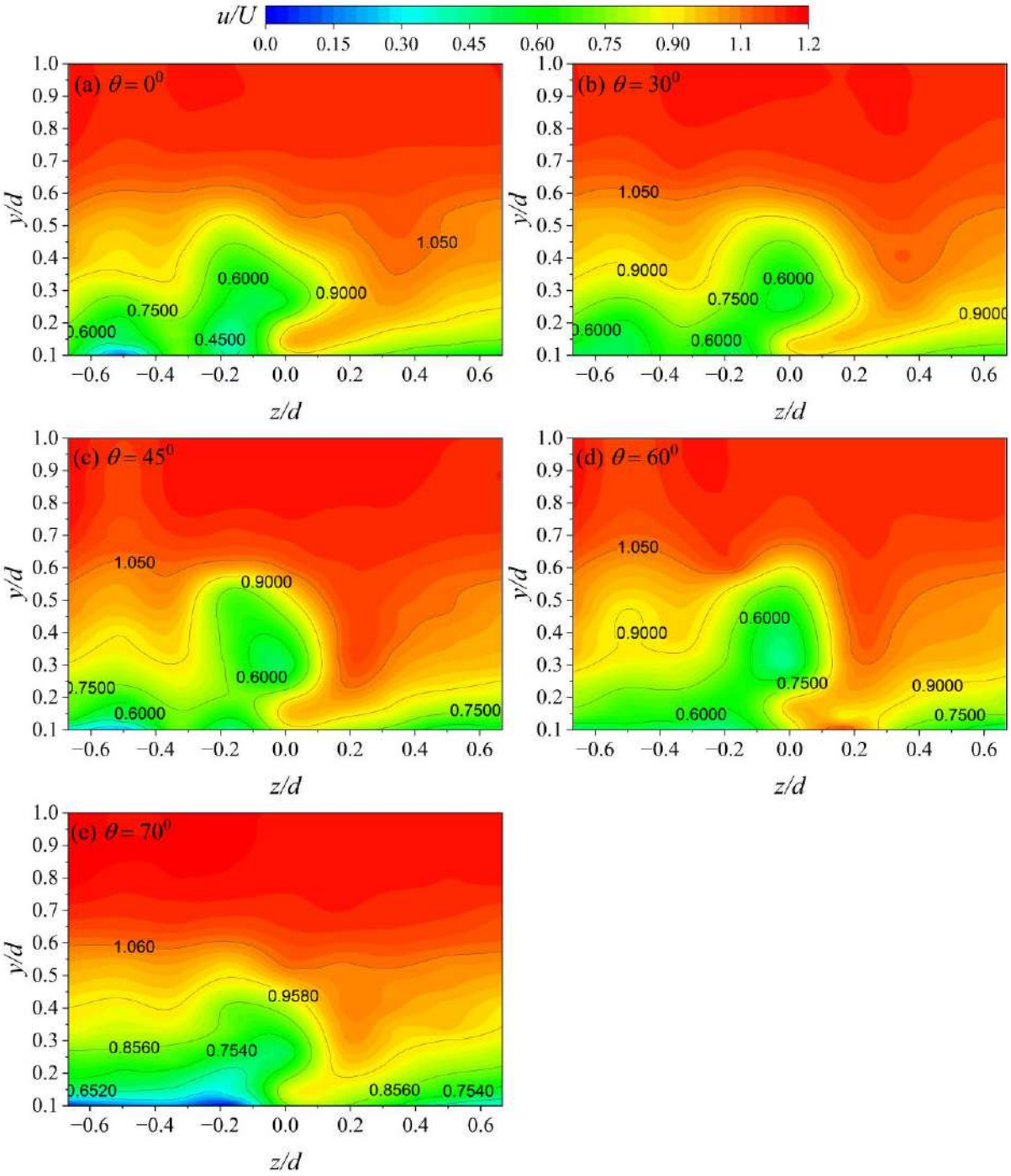

Fig. 4.6 Cross-sectional stream-wise velocity contour profile for all vane with different bevel angles at 3H plane for Q = 0.082 m^3/s, H = 0.045 m, α = 20º

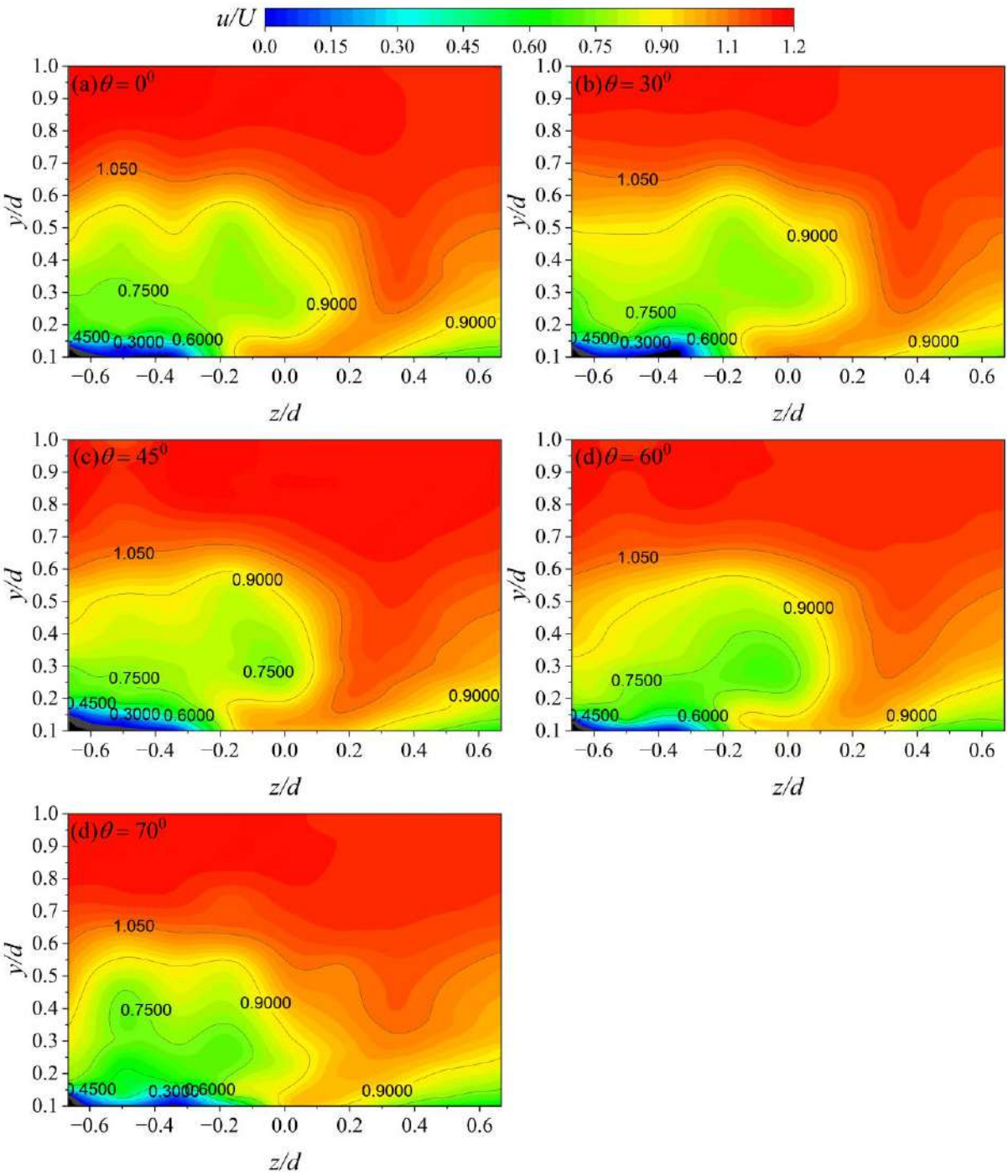

Fig. 4.7 Cross-sectional stream-wise velocity contour profile for all vane with different bevel angles at 8H plane for Q =0.082 m^3/s, H = 0.045 m, α = 20º

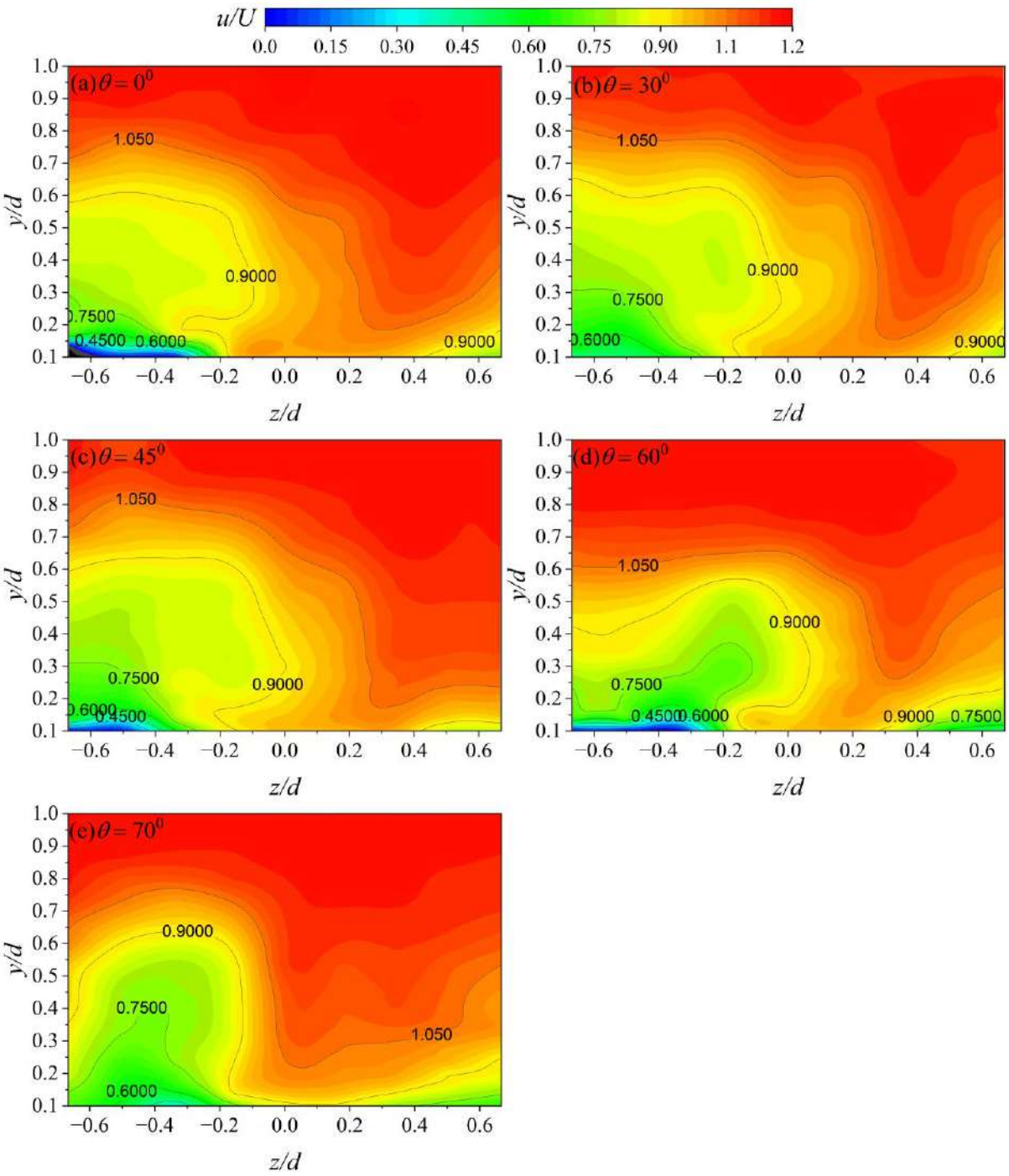

Fig. 4.8 Cross-sectional stream-wise velocity contour profile for all vane with different bevel angles at 20H plane for Q = 0.082 m^3/s, H = 0.045 m, α = 20º

In the present study, the stream-wise velocity contour was utilized to understand the flow pattern downstream of the submerged vane. In each cross-section total nine vertical section were taken, and each vertical section instantaneous stream-wise velocity were measured at 18 points in the vertical direction to introduce the contour profile. Here, one velocity contour profile in the 8H plane and the final topography of

the sediment bed after the experimental run of the rectangular submerged vane at 20º angle of attack were compared to describe the flow and bed conditions due to the presence of submerged vane in Fig. 4.9a & 4.9b. Due to the orientation of the vane angle, the pressure difference between the two sides causes the flow on the pressure side to attain an upward component and the flow on the suction side a downward motion. It generates a primary vortex that travels downstream with the flow and changes the shear-stress field (Wang and Odgaard,1993). One more vortex also generated from the leading edge and decayed quickly, which was the main reason for local scour at the pressure side of the vane known as horseshoe vortex. The downward pressure gradient occurred rise to downflow at the face of the submerged vane, which eroded sediment in front and along the pressure side of the submerged vane. From the velocity contour profile at the 8H plane, it can also be observed that the maximum sediment deposited at the left side of the 8H plane as can be seen in Fig. 4.9b. Basically, the sediment particle eroded from the local area around the vane which deposited after the 3H plane and became maximum at 8H plane. Due to the clockwise rotation of the vortex, the sediment bed scoured from the right side and deposited on the left side of the channel.

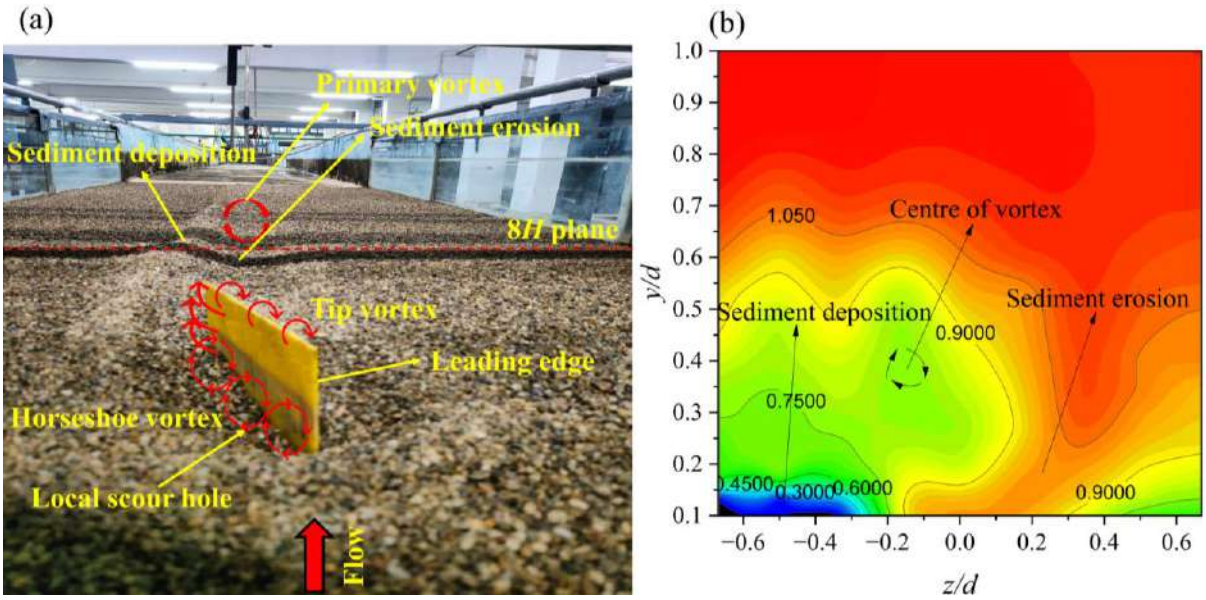

Fig. 4.9 a) Final topography b) Velocity contour profile at rectangular submerged vane in 8H plane for Q = 0.082 m^3/s, H = 0.045 m, α = 20º

4.2.2 Turbulent Intensities

According to the studies conducted by Nezu and Rodi (1986), and Nezu and Nakagawa (1993), the flow near the bed experiences higher shear stress due to the steeper velocity gradient in this region compared to the core flow. This increased gradient arises primarily from the influence of fluid viscosity. This viscosity starts breaking these large-scale eddies to smaller eddies and by a cascading process, turbulent kinetic energy of larger eddies is transferred to bed (Nezu & Nakagawa, 1993). Due to cascading of turbulent kinetic energy from the core flow region to the near bed region and the velocity gradient diminishing, the turbulence intensities decrease along the vertical. The fluctuations near the bed are responsible for the transportation of sediment as they start hoping and eventually become suspended and bed load (Garde & Ranga Raju, 2001). Submerged vanes are designed to generate a circulation of fast-moving fluid towards the bed and slow-moving fluid towards the core region. Figures 4.10 to 4.12 shows the variation of the normalised turbulence intensities, $\sigma_u^+ = u'/u_*$, $\sigma_v^+ = v'/u_*$, and $\sigma_w^+ = w'/u_*$ along the depth downstream of submerged vanes for various bevel angle. The profile of turbulence intensities over the verticals degenerated near the submerged vane rows due to distortion of the homogeneity of flow turbulence by secondary circulation generated by the submerged vanes. For x = 3H, it is seen that the turbulence intensities are less near the bed and then the turbulence intensities increase and reach the maximum at the 0.85 times the vane height and then again, they reduce when the water surface is approached. It is close to observation of Odgaard and Wang (1991a) who suggested that at 0.8H the tip vortices separated the submerged vane from its trailing edge. For x = 8H and 20H, the viscosity regains its dominance which leads to dissipation of the tip vortices. Thus, the turbulence in the flow starts to regain its homogeneous and isotropic structure.

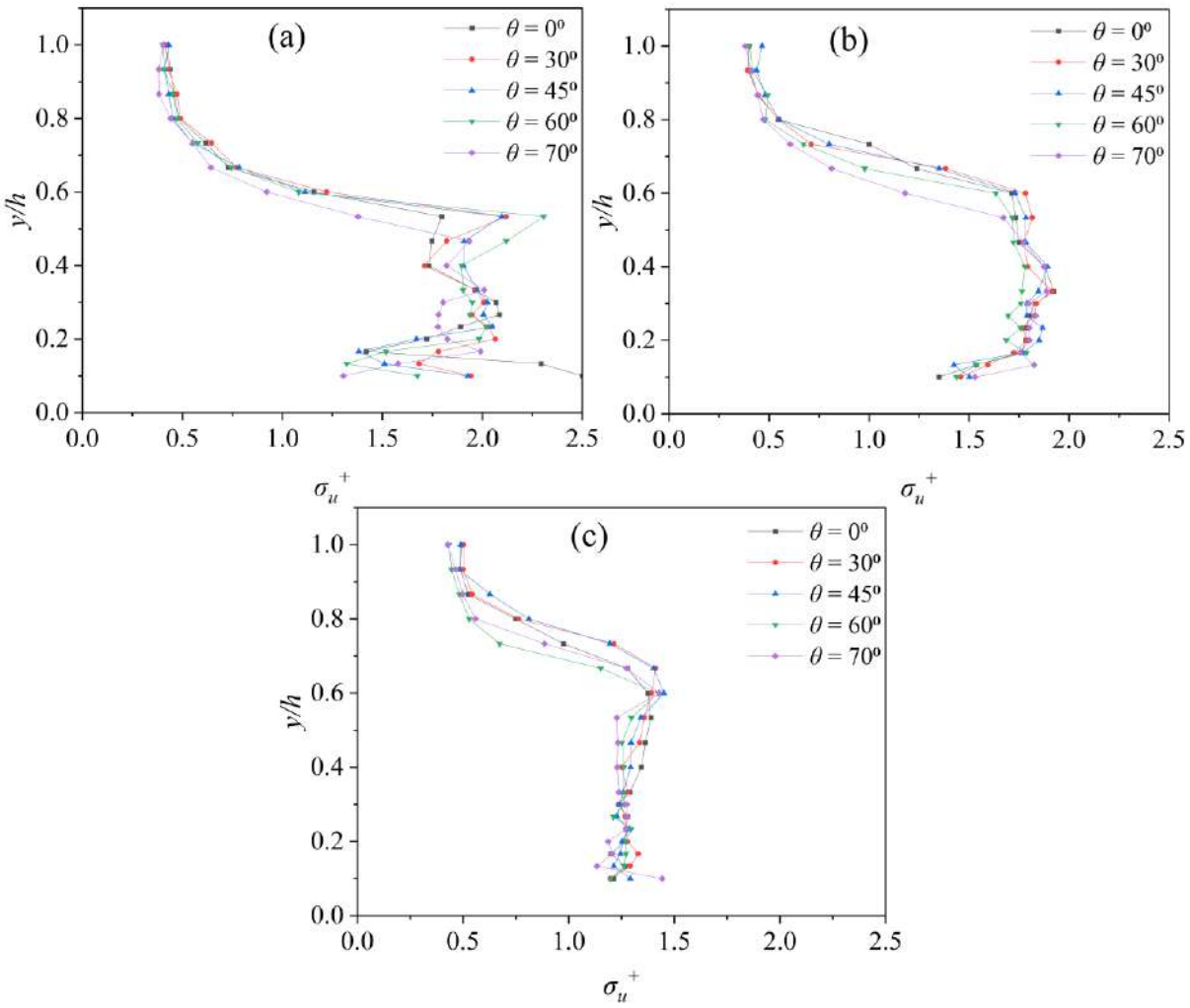

Fig. 4.10 Variation of σ_u^+ downstream along the depth at (a) 3H plane, (b) 8H plane, and (c) 20H plane for all vane with different bevel angle for Q = 0.082 m^3/s, H = 0.045 m, α = 20°

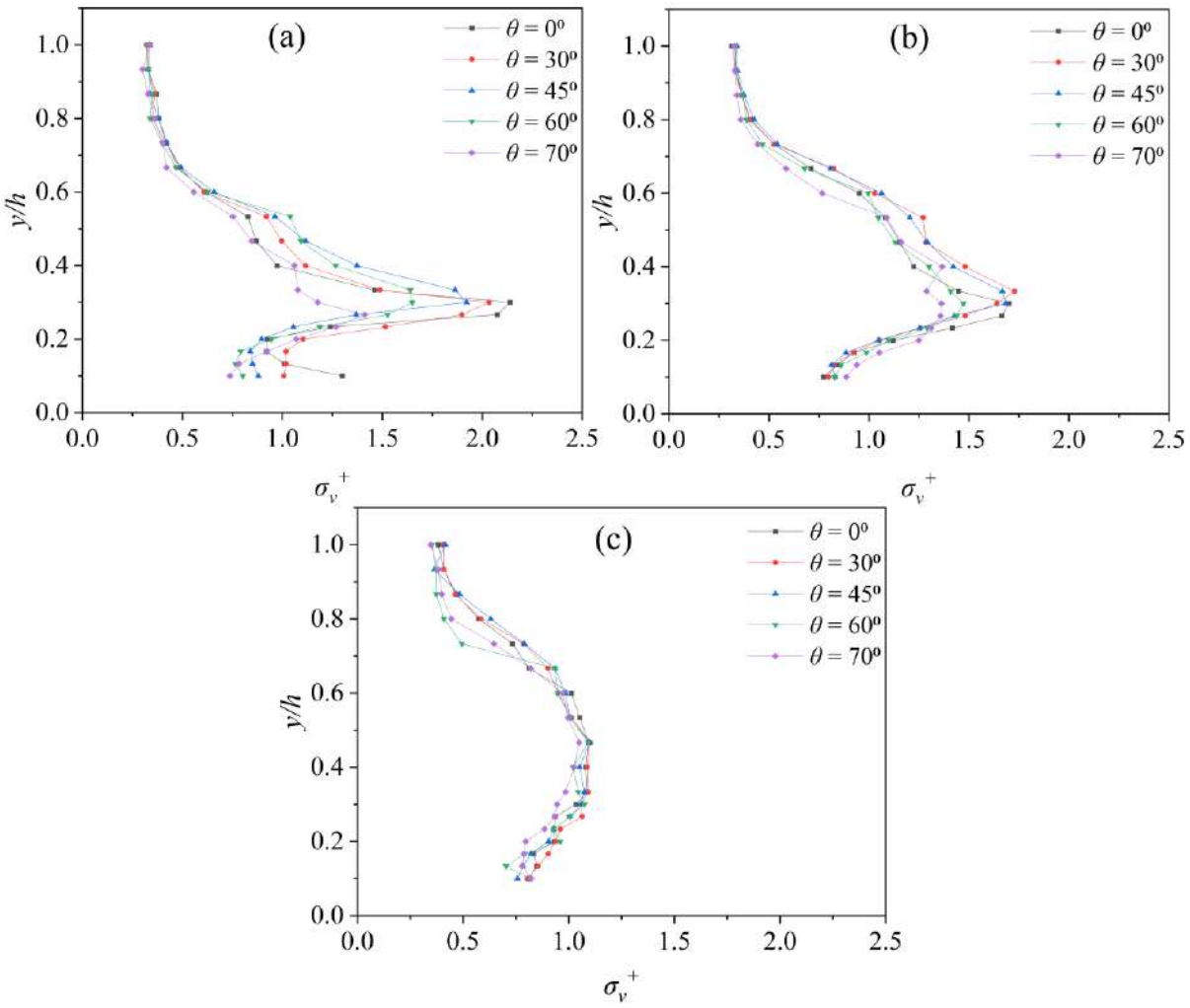

Fig. 4.11 Variation of σ_v^+ downstream along the depth at (a) 3H plane, (b) 8H plane, and (c) 20H plane for all vane with different bevel angle for Q = 0.082 m^3/s, H = 0.045 m, α = 30°

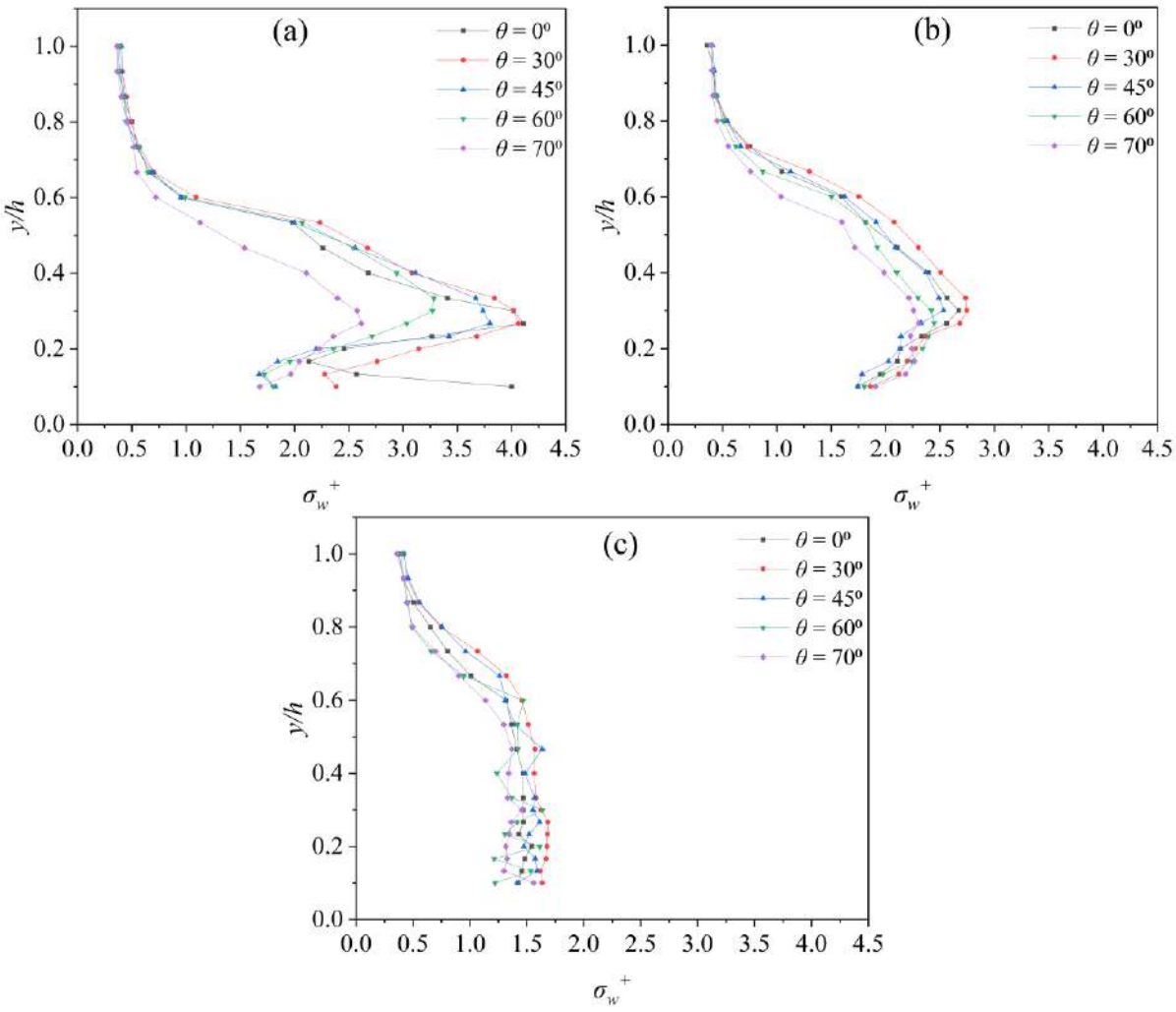

Fig. 4.12 Variation of σ_w^+ downstream along the depth at (a) 3H plane, (b) 8H plane, and (c) 20H plane for various bevel angle for Q = 0.082 m^3/s, H = 0.045 m, α = 40°

4.2.3 Turbulent Kinetic Energy (TKE)

Turbulent kinetic energy (TKE) quantifies the kinetic energy associated with turbulent fluctuations as they are transferred across the flow domain through the fluid layers, expressed as $1/2\left(\overline{u'^2} + \overline{v'^2} + \overline{w'^2}\right)$ (Sharma and Ahmad, 2020). Figure 4.12 represents the variation of the normalized TKE along the vertical mid line up to water surface for Q=0.082 m^3/s, H = 0.045 m, α = 20°. The submerged vane generates vortices downstream of the vane, which transport the fast-moving upper fluid towards the bed and near bed fluid redirected towards the core flow regions as the vortices propagate through the fluid layers. The generation of significant fluctuations within the fluid layers of the core flow region enhances the transport of turbulent kinetic energy (TKE),

resulting in a pronounced peak in the profile. The maximum turbulent kinetic energy (TKE) was observed at 0.85 to 0.9 times the height of the submerged vane, which is consistent with the findings of Sharma and Ahmad (2020), who identified 0.85H as the location of vortex emanation. For 3H plane, the magnitude of TKE profile is maximum for all different shape of bevel submerged vane (Fig. 4.12a) and the rectangular submerged vane creates maximum peak of TKE profile. At 8H plane, the bevel shape up to 45º angle dominance on the TKE fluctuation away from the trailing edge of the vane, shown in Fig. 4.12(b). Figure 4.12(c) shows that at the 20H plane, the TKE profiles of all bevel vanes converging towards each other and the magnitude of the peak is reduced. When the turbulence travel towards downstream of the vane, the viscosity regains its dominance which leads to dissipation of the tip vortices.

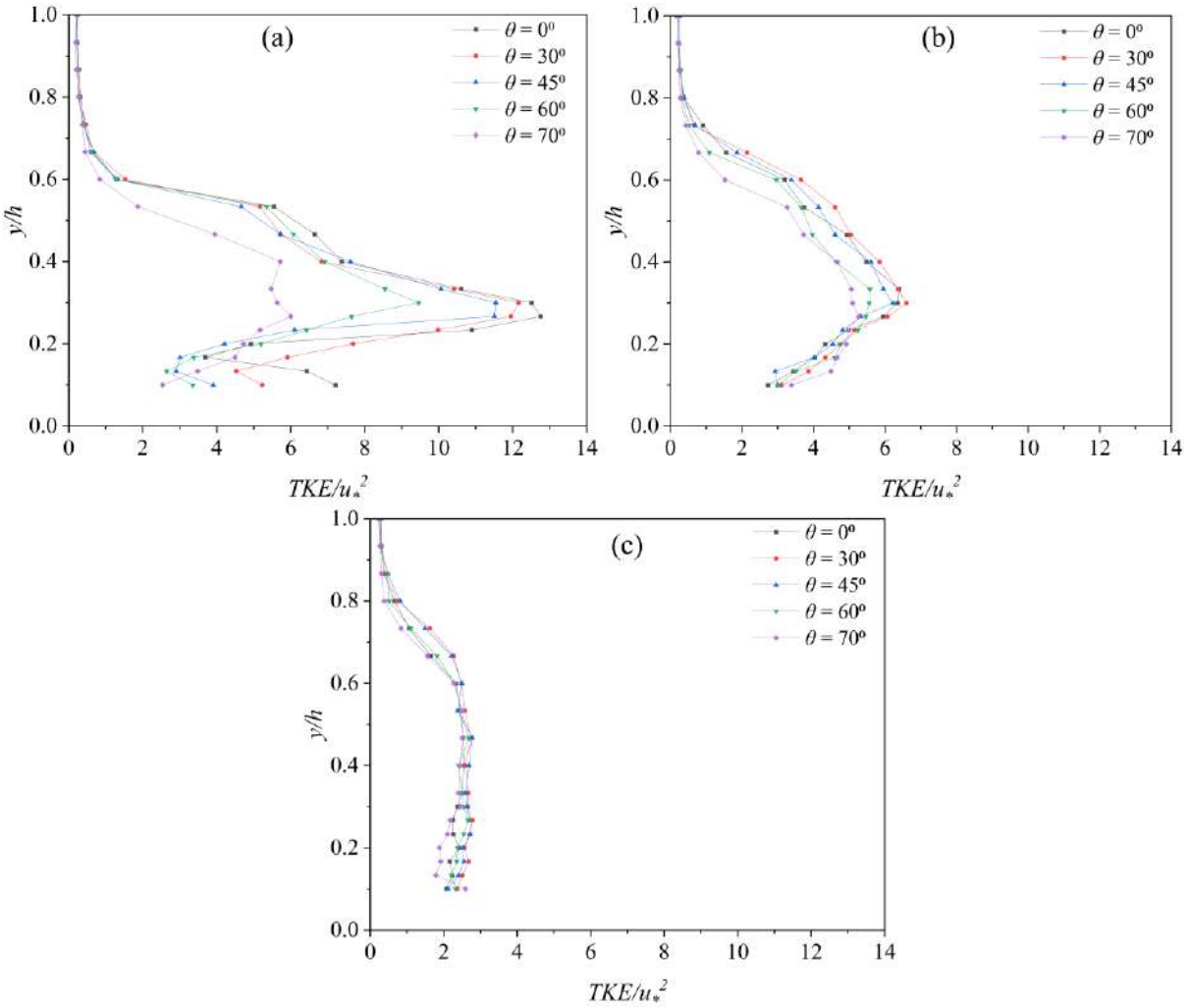

Fig. 4.12 Variation of normalized TKE downstream along the depth at (a) 3H plane, (b) 8H plane, and (c) 20H plane for all vane with different bevel angle

4.3 CONCLUDING REMARKS

The flow characteristics and velocity fields were calculated from the experimental data. Three dimensional velocities were measured with the help of ADV and were processed for further analysis. The velocity field at x-y plane shows strong formation of vortex downstream of the vane, which is responsible for the changes the bed shear stress downstream of the vane.

- At x = 3H, the velocity distribution is observed to lose its logarithmic nature but it shows a S-type variation over the vertical direction for all bevel angle which suggests the presence of point of inflexions in the velocity profiles and it confirms the presence of strong vortices at the transect due to submerged vane up to 8H plane. At x = 20H, it is observed that velocity distribution regains its original logarithmic velocity profiles as the dampening of vortices in the flow by viscosity.
- It is observed that the turbulence intensities are less near the bed and then the turbulence intensities increase and reach the maximum at the 0.85 times the vane height and then again, they reduce when the water surface is approached. Beyond 45º bevel angle its significantly reduced. At 20H plane, the normalized TI profiles of all bevel vanes converging towards each other and the magnitude of the peak is reduced.
- The generation of significant fluctuations within the fluid layers of the core flow region enhances the transport of turbulent kinetic energy (TKE), resulting in a pronounced peak in the profile. The maximum turbulent kinetic energy (TKE) was observed at 0.85 to 0.9 times the height of the submerged vane. At 3H and 8H plane, the TKE is maximum up to 45º bevel angle than it reduces significantly. At 20H plane, the TKE profiles of all bevel vanes converging towards each other and the magnitude of the peak is reduced as the viscosity regains its dominance which leads to dissipation of the tip vortices.

5. MORPHOLOGICAL CHANGES: EXPERIMENTAL STUDY

5.1 INTRODUCTION

In the present chapter, the data collected from the experimental programme have been analysed. The observations made during the experiment were further used to investigate the effect of the various parameters on the temporal variation of scour depth, scour pattern, maximum scour depths and extension of the scour hole in downstream channel. The reduction of scour depth due to introducing bevel shape of submerged vane also evaluated in this chapter. A dimensional analysis was performed to determine the key parameters affecting the maximum scour depths and extension of the scour hole. Using present experimental data, empirical equations were proposed for determining maximum scour depths at local area and downstream of the vane. Sensitivity analysis was carried out to determine the relative importance of the various parameters.

5.2 ANALYSIS OF DATA

5.2.1 Scour Pattern

Present studies were conducted to examine how to reduce the impact of the submerged vane on the riverbed morphology. Because the local scour is the most dangerous threat to the stability of the hydraulic structure. An ultrasonic bed profiler was used to measure the scour profile within 2.0 m test sections of the sediment bed for Q=0.082 m3/s, H = 0.045 m, α = 20º, 30º and 40º. The effect of all submerged vanes with a different bevel angle for different angle of attacks on the scour bed morphology represents by the contour graph shown in Figs. 5.1, 5.2, and 5.3. It can clearly be observed that the scour hole is shifted from the leading edge to the downstream of the vane due to the increasing bevel angle. The local scour around the vane enormously decreased due to the increasing bevel angle. Also, it can be observed that the local scour hole was sifted from the left side to the right side of vane. Main reasons behind this, the two separate vorticity were generated from the leading edge and trailing edge of the vane, and the leading edge's vorticity was responsible for the local scour around

the vane. Because the leading edge is the main reason for creating the horseshoe vortex. Due to cutting the leading edge, the vorticity was moved from the local area of the vane to the downstream of the vane and decreased the strength of the horseshoe vortex. Here cutting the leading edge with an angle is highly efficient for controlling the local scour around the vane. Further quantitate comparison of the effectiveness of bevel submerged vanes to reduction of local scour is provided next.

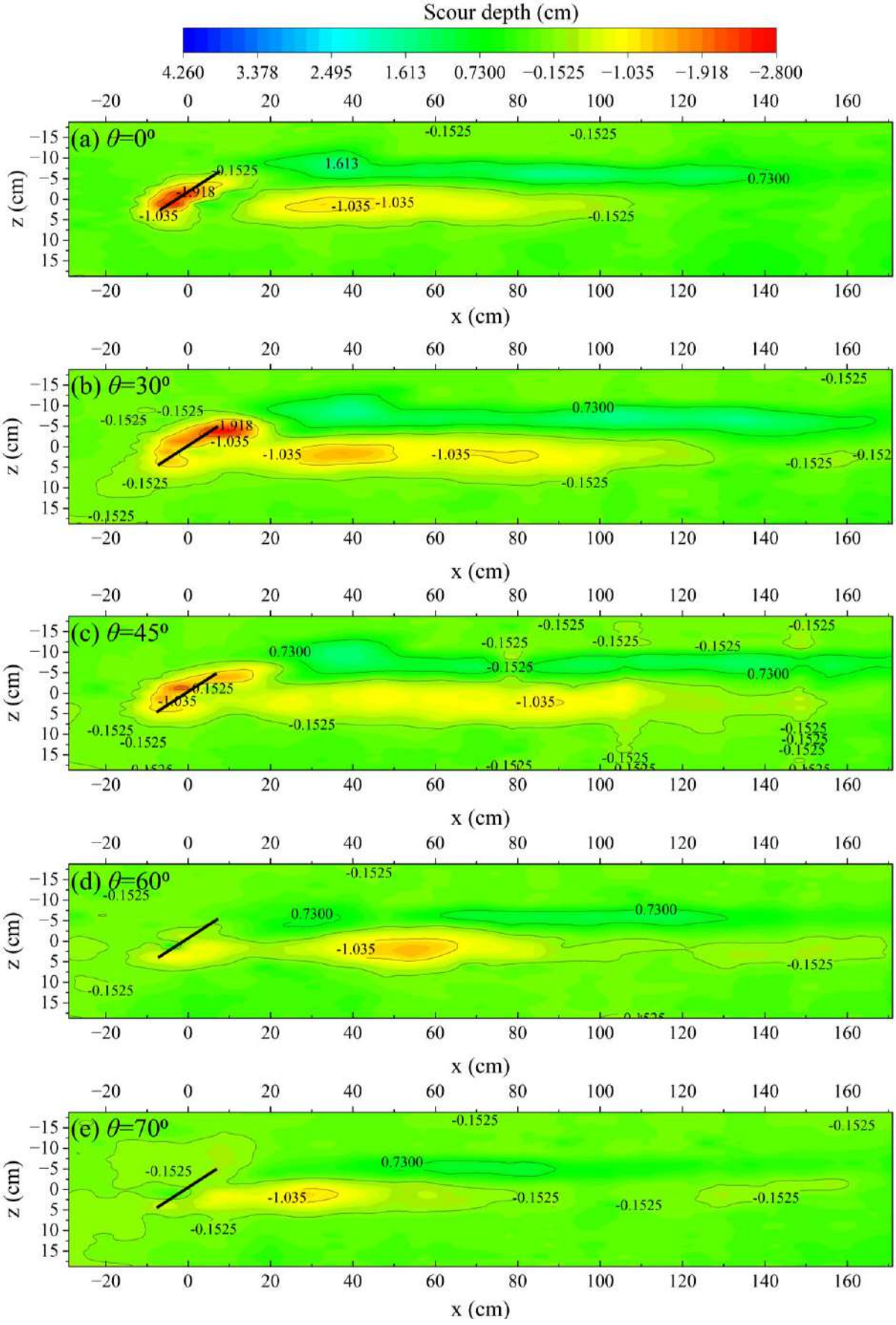

Fig. 5.1 Scour profile in 2.0 m long reach for Q = 0.082 m^3/s, H = 0.045 m, α = 20°

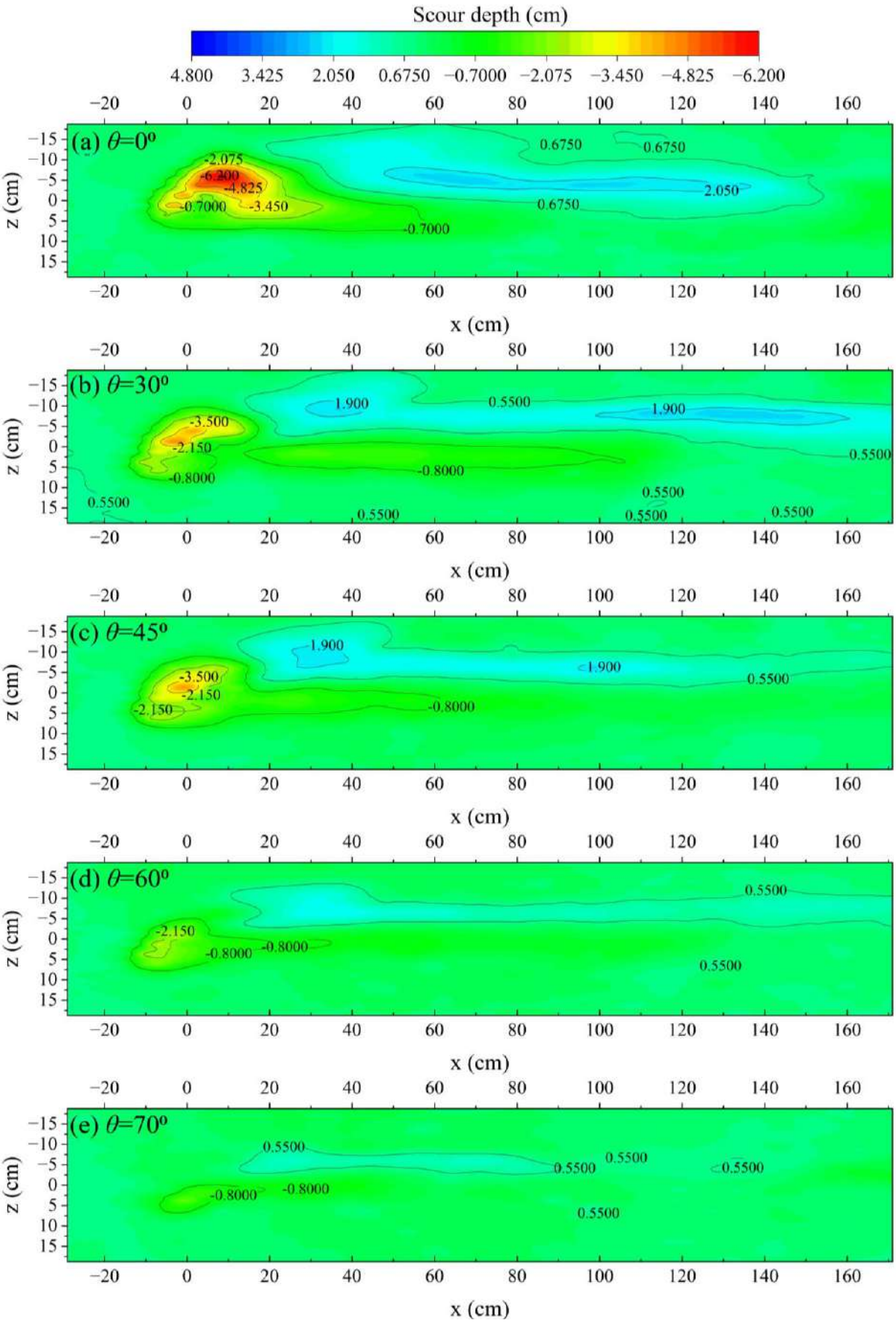

Fig. 5.2 Scour profile in 2.0 m long reach for Q = 0.082 m^3/s, H = 0.045 m, α = 30°

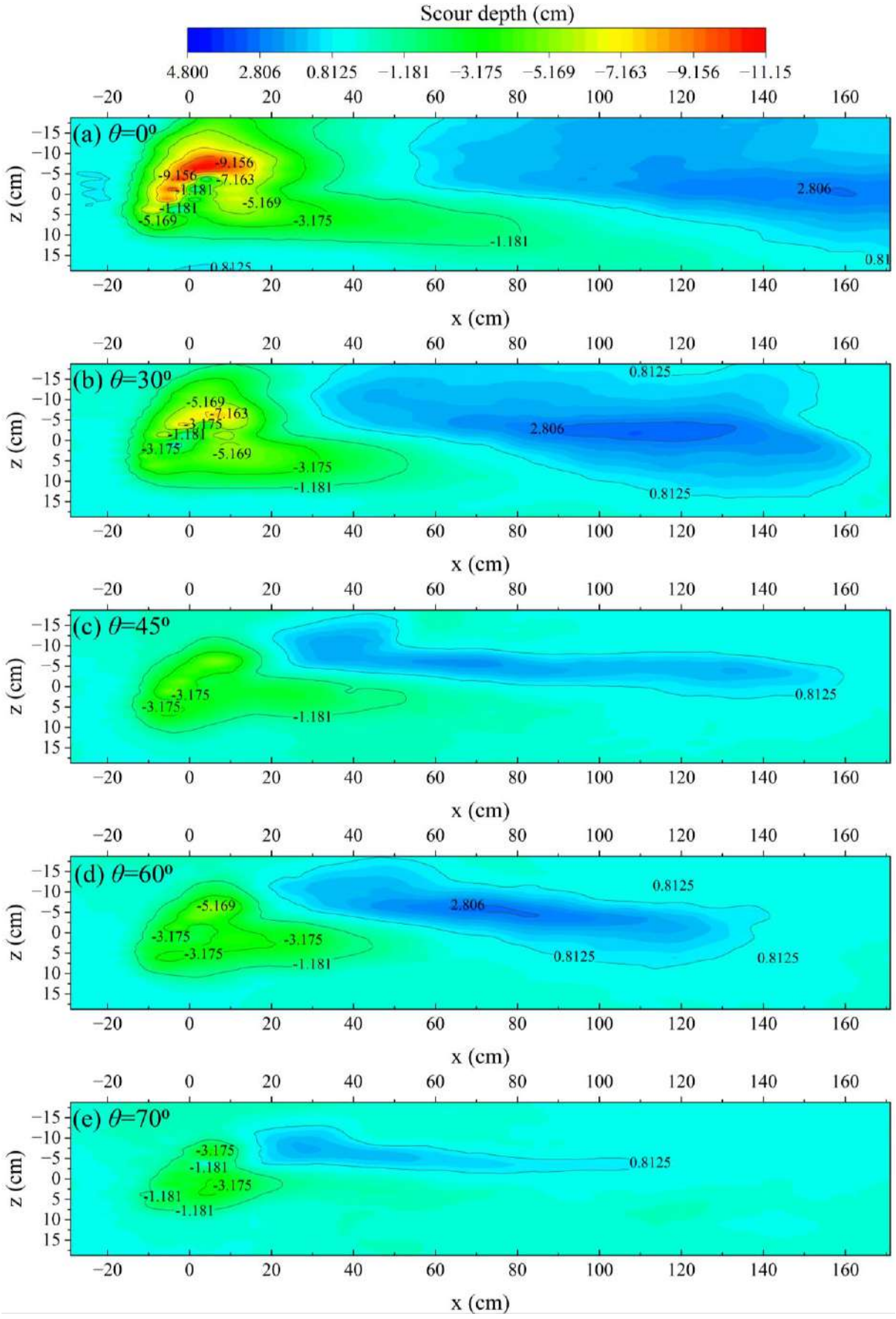

Fig. 5.3 Scour profile in 2.0 m long reach for Q = 0.082 m^3/s, H = 0.045 m, α = 40º

5.2.2 Transverse Scour Profiles

The transverse scour bed profiles were measured by ultrasonic bed profiler for Q = 0.082 m^3/s at the leading edge and downstream of the vanes. Figures 5.4 (a-c) shows the transverse scour profile along the leading edge for five bevel angles (θ = 0º, 30º, 45º, 60º and 70º), three vane heights (H = 0.045 m, 0.06 m, and 0.075 m), and four angles of attack of 15º, 20º, 30º and 40º. In all graphs, the zero point (z/d = 0) in the transverse direction indicates the center of the vane. As the angle of attack and vane height increased, the scour hole at the leading edge became more pronounced. The leading edge of the rectangular vane creates the strong horseshoe vortex at leading edge, which generates the intense scour on the pressure side and decay quickly. The vertical horseshoe vortex on the pressure side drives particles downward along the vane and upstream along the bed of the scour hole. The horseshoe vortex plays a significant role in generating local scour on the pressure side of the vane, while the primary vortex originating from the trailing edge persists over a longer distance. A similar observation was reported by Marelius and Sinha (1998); Odgaard and Spoljaric (1989); and Wang and Odgaard (1993). Cutting the leading edge at various bevel angles with respect to the vertical axis reduced the strength of the horseshoe vortex near the leading edge. The local scour at the leading edge decreased substantially with an increase in bevel angle. as shown in Figs. 5.4 (a-c). The observation shows that the bevel shape effectively reduces local scour at higher angles of attack and vane heights compared to the rectangular vane. Figures 5.5 (a-c) shows the transverse scour profile at a distance downstream corresponding to five bevel angles (0º, 30º, 45º, 60º and 70º), three vane heights (0.045 m, 0.06 m, and 0.075 m), and four angles of attack (15º, 20º, 30º and 40º). The scour hole downstream of the vane increases with the increasing the angle of attack and the vane height. The primary vortex is responsible for generating scour downstream of the vane, which extends over a considerable distance beyond the trailing edge. The scour and deposition observed downstream of the vane, are shown in Figs. 5.5 (a-c). The reduction in local scour became more pronounced compared to the downstream scour as the bevel angle of the vane increased. The downstream scour decreased more significantly for bevel vanes at greater vane

heights, as the bevel angle results in a greater reduction in the vane's surface area at increased heights, observed in Fig. 5.5 (c).

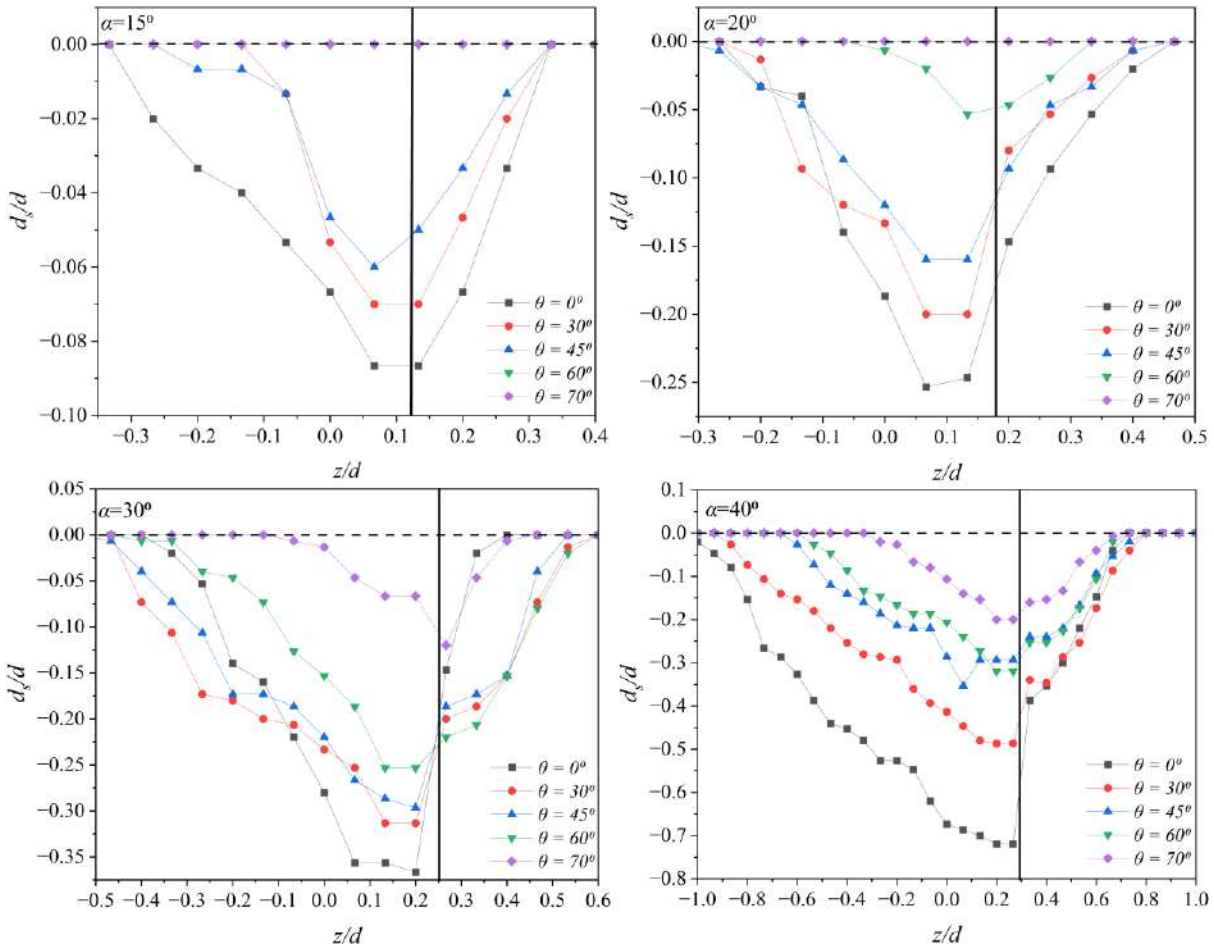

Fig. 5.4a Transverse scour profiles for θ = 0º, 30º, 45º, 60º and 70º at leading edge, with different angles of attack for Q = 0.082 m^3/s, H = 0.045 m. The dashed line and solid line denote the initial bed level and the position of leading edge of the vane, respectively

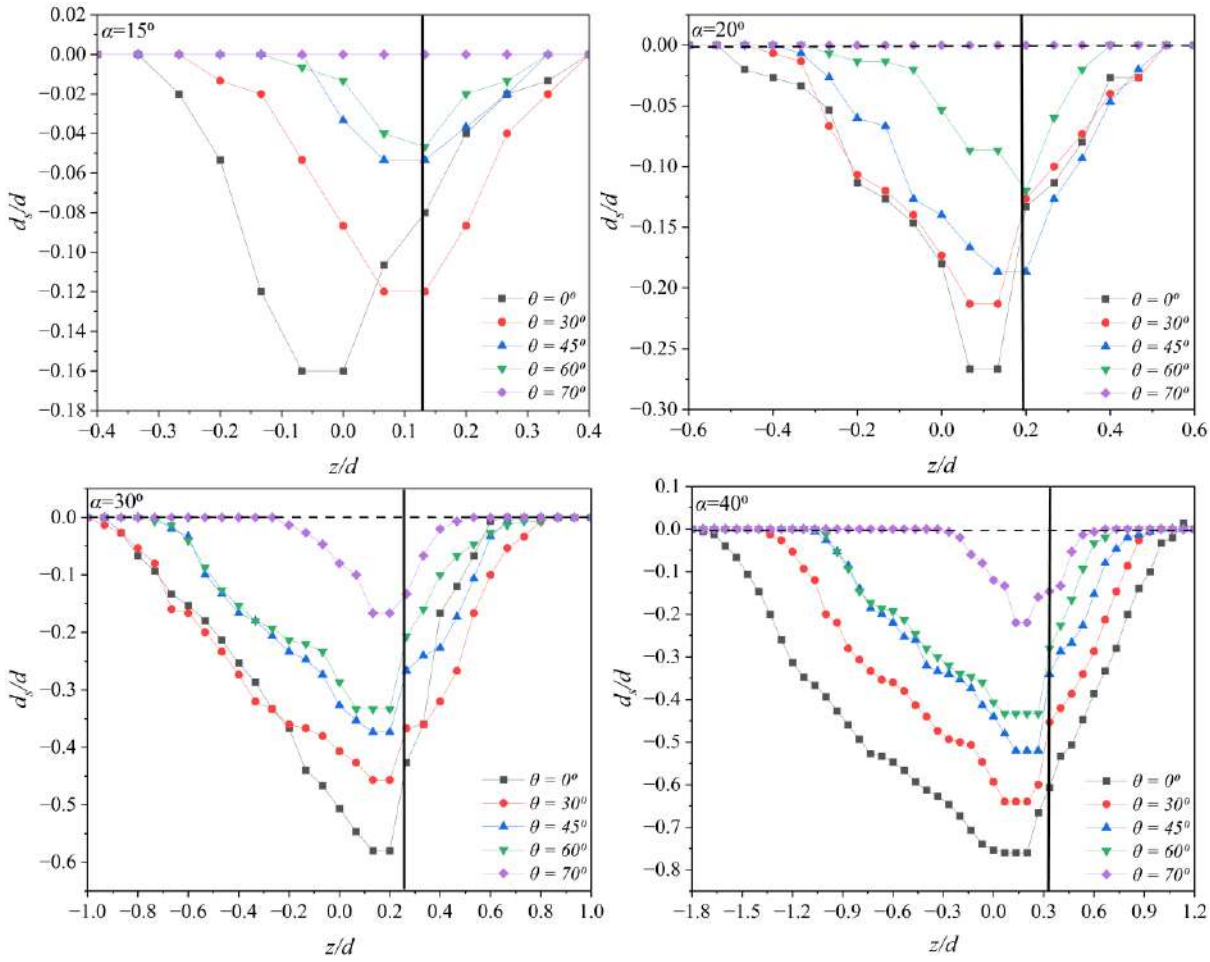

Fig. 5.4b Transverse scour profiles for θ = 0º, 30º, 45º, 60º and 70º at leading edge, with different angles of attack for Q = 0.082 m^3/s, H = 0.06 m. The dashed line and solid line denote the initial bed level and the position of leading edge of the vane, respectively

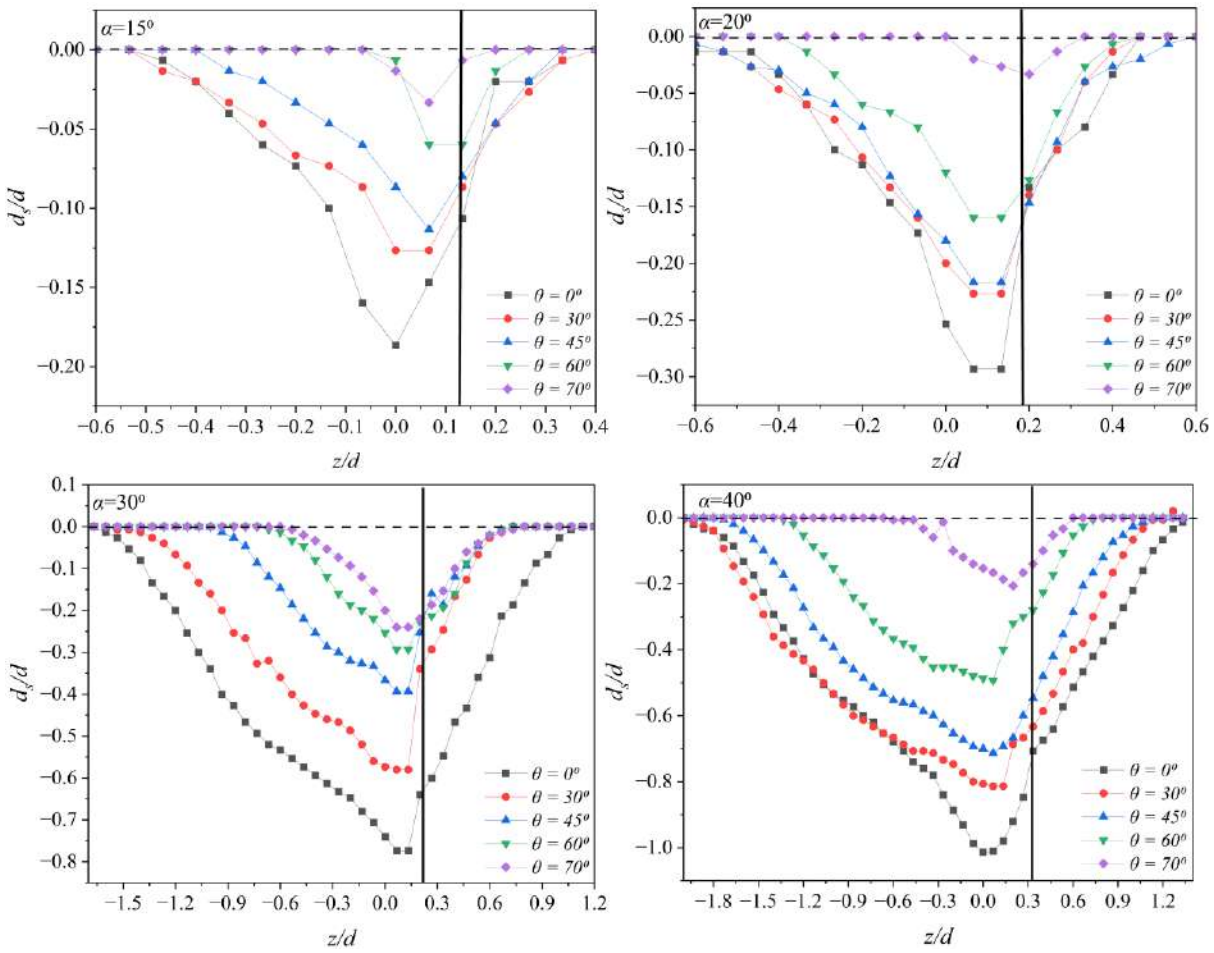

Fig. 5.4c Transverse scour profiles for θ = 0º, 30º, 45º, 60º and 70º at leading edge, with different angles of attack for Q = 0.082 m^3/s, H = 0.075 m. The dashed line and solid line denote the initial bed level and the position of leading edge of the vane, respectively

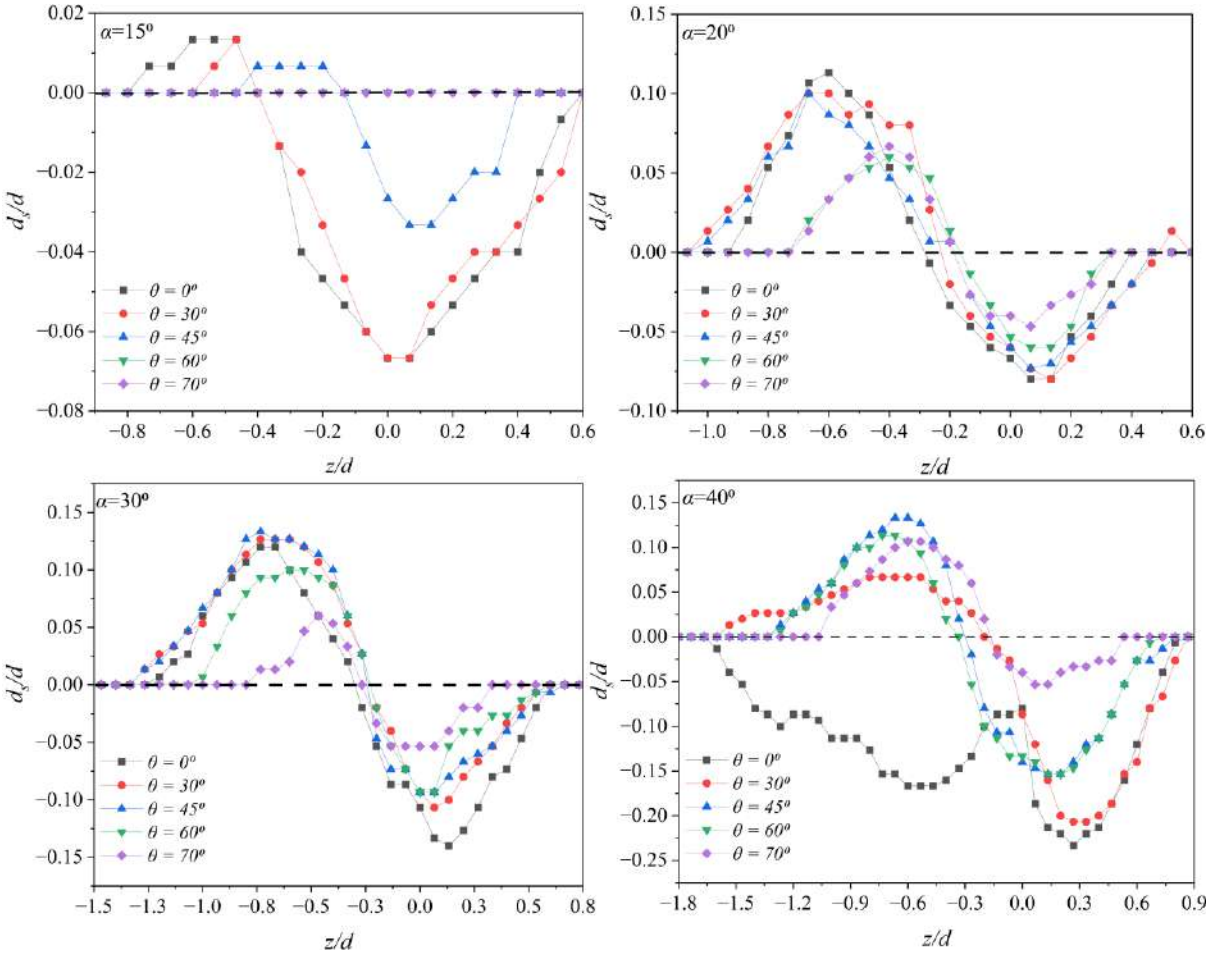

Fig. 5.5a Transverse scour profiles for θ = 0º, 30º, 45º, 60º and 70º at downstream, with different angles of attack for Q = 0.082 m^3/s, H = 0.045 m. The dashed line denotes the initial bed level

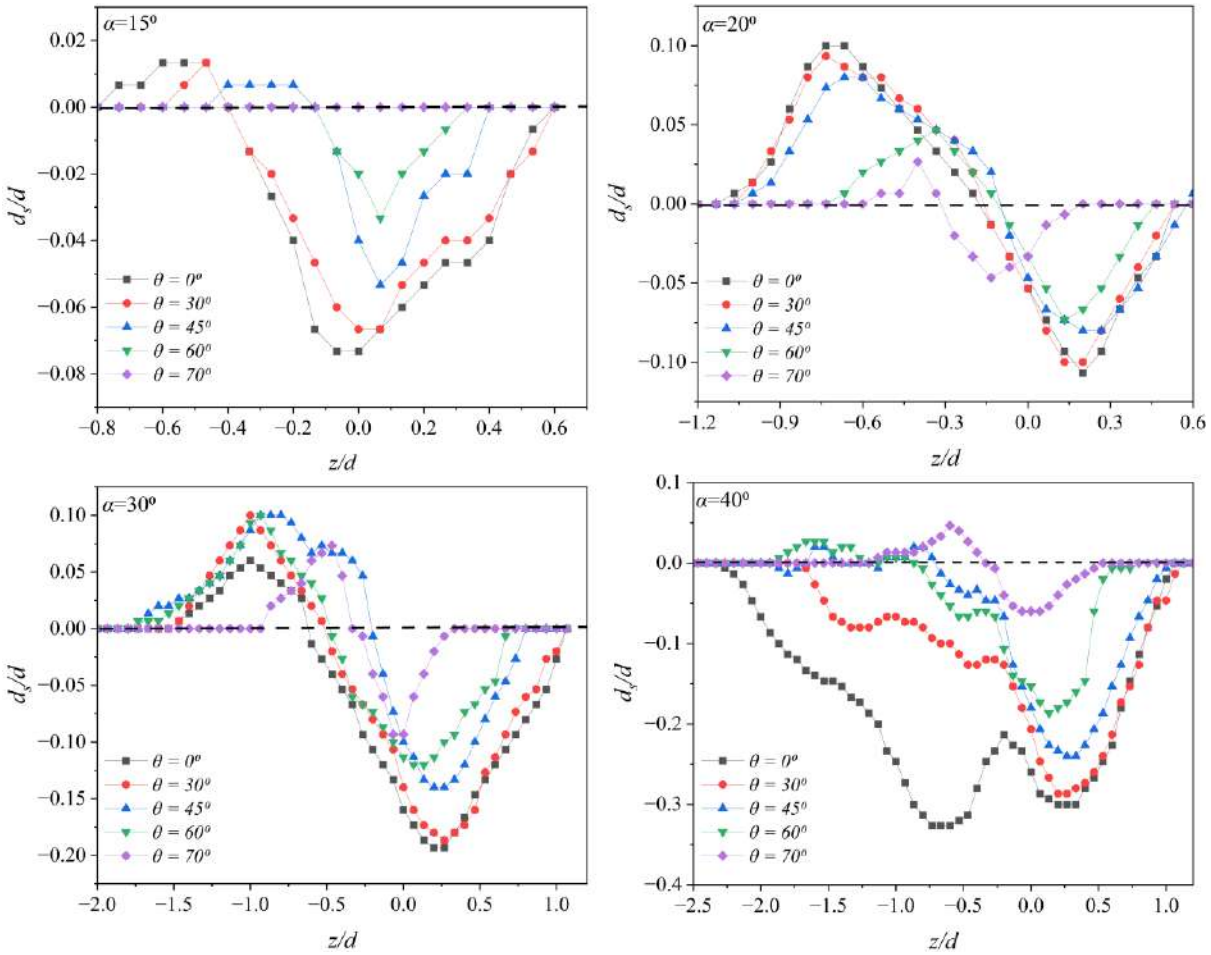

Fig. 5.5b Transverse scour profiles for θ = 0º, 30º, 45º, 60º and 70º at downstream, with different angles of attack for Q = 0.082 m^3/s, H = 0.06 m. The dashed line denotes the initial bed level

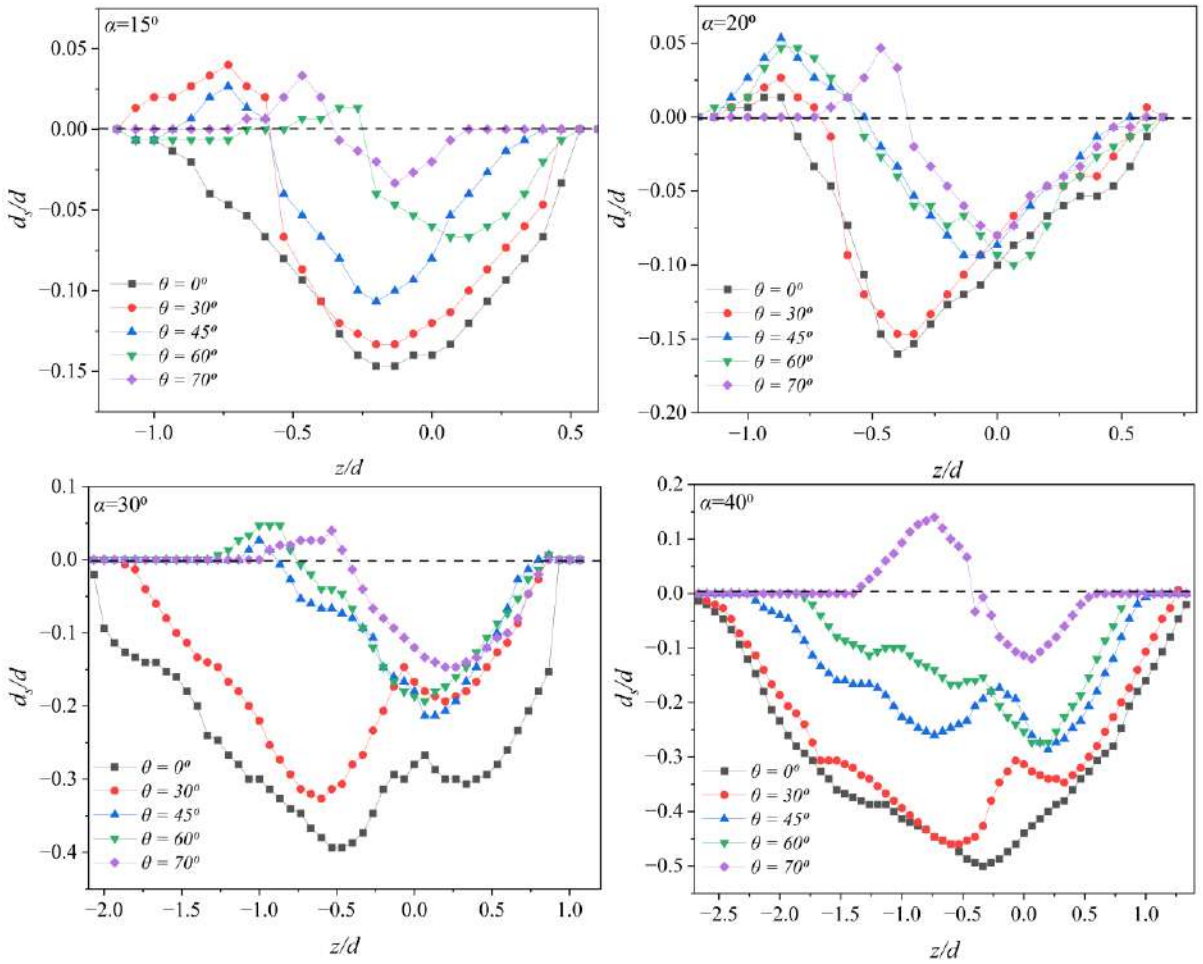

Fig. 5.5c Transverse scour profiles for θ = 0º, 30º, 45º, 60º and 70º at downstream, with different angles of attack for Q = 0.082 m^3/s, H = 0.075 m. The dashed line denotes the initial bed level

5.2.3 Scour Reduction Measurements

Figures 5.6 and 5.7 shows the percentage scour reduction due to increasing the bevel angle compare to rectangular vane (θ = 0º) corresponding to three vane heights (H = 0.045 m, 0.06 m, and 0.075 m), and four angles of attack (α = 15º, 20º, 30º and 40º) under Q=0.082 m^3/s. The percentage reduction in scour depth is computed using the following equation:

$$\% \text{ Scour Reduction} = \left(1 - \frac{\text{Scour depth due to bevel vane}}{\text{Scour depth due to rectangular vane}}\right) \times 100 \qquad (5.1)$$

The maximum scour depth around the vane was significantly reduced by cutting the leading edge at various bevel angles. However, the percentage reduction in scour

downstream of the vane was less compared to the local scour reduction around the vane as the bevel angles increased, apparent from Figs. 5.6 and 5.7. Also, the scour reduction downstream was less compared to the local scour up to the 45º bevel angle. This may be due to the vane's efficiency in generating vorticity not diminishing up to a 45º bevel angle, but instead shifting from the local area to downstream of the vane. Table 5.1 provides the percentage reduction in scour depth relative to the maximum scour depth observed for various parameters at both local and downstream scour holes. The efficiency of reducing scour compared to a rectangular vane increased by increasing the bevel angle for all other conditions.

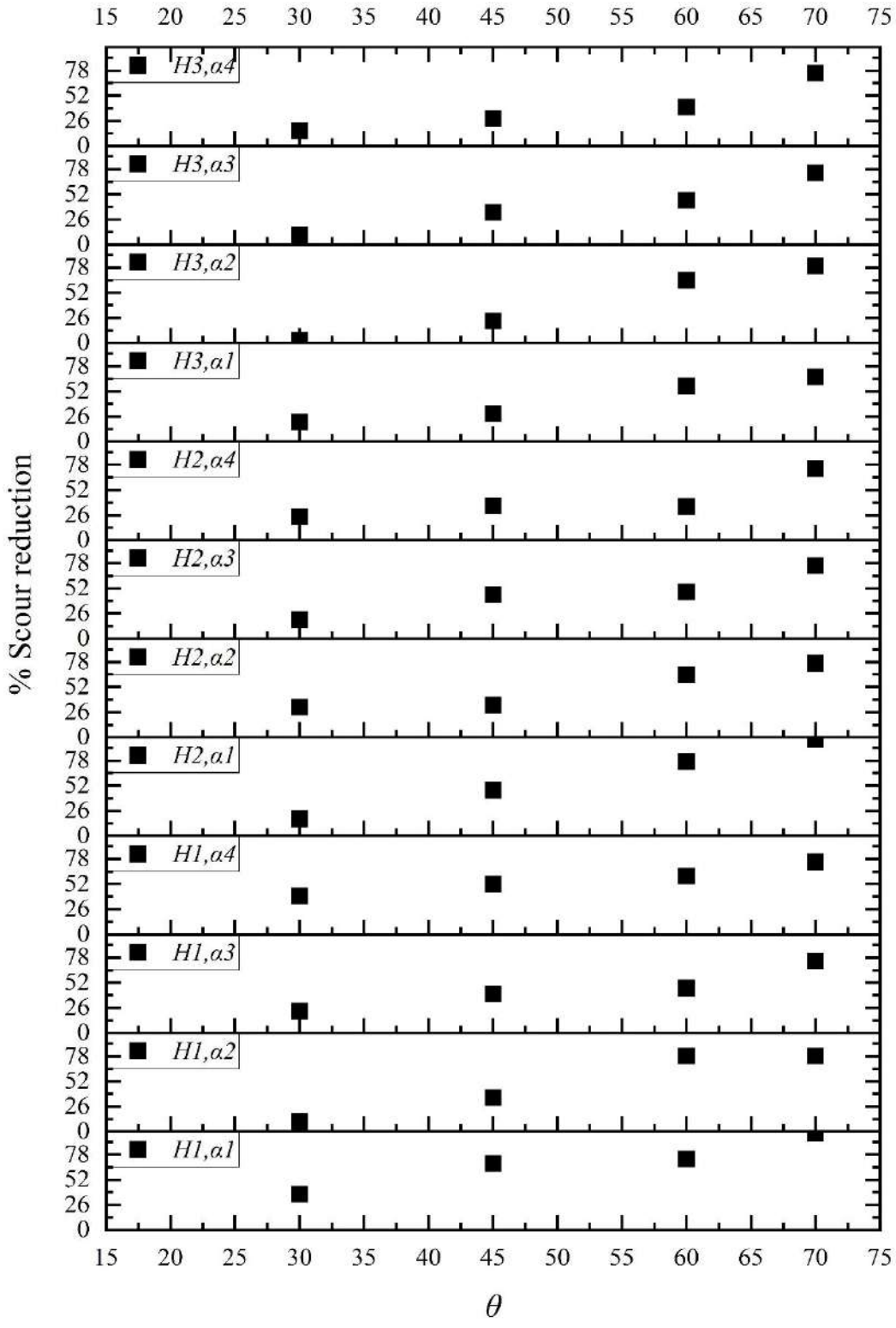

Fig. 5.6 Efficiency of bevel angle in % reducing of scouring near the vane for bevel angles (θ = 0º, 30º, 45º, 60º, 70º) with different vane heights and angle of attacks under Q = 0.082 m^3/s

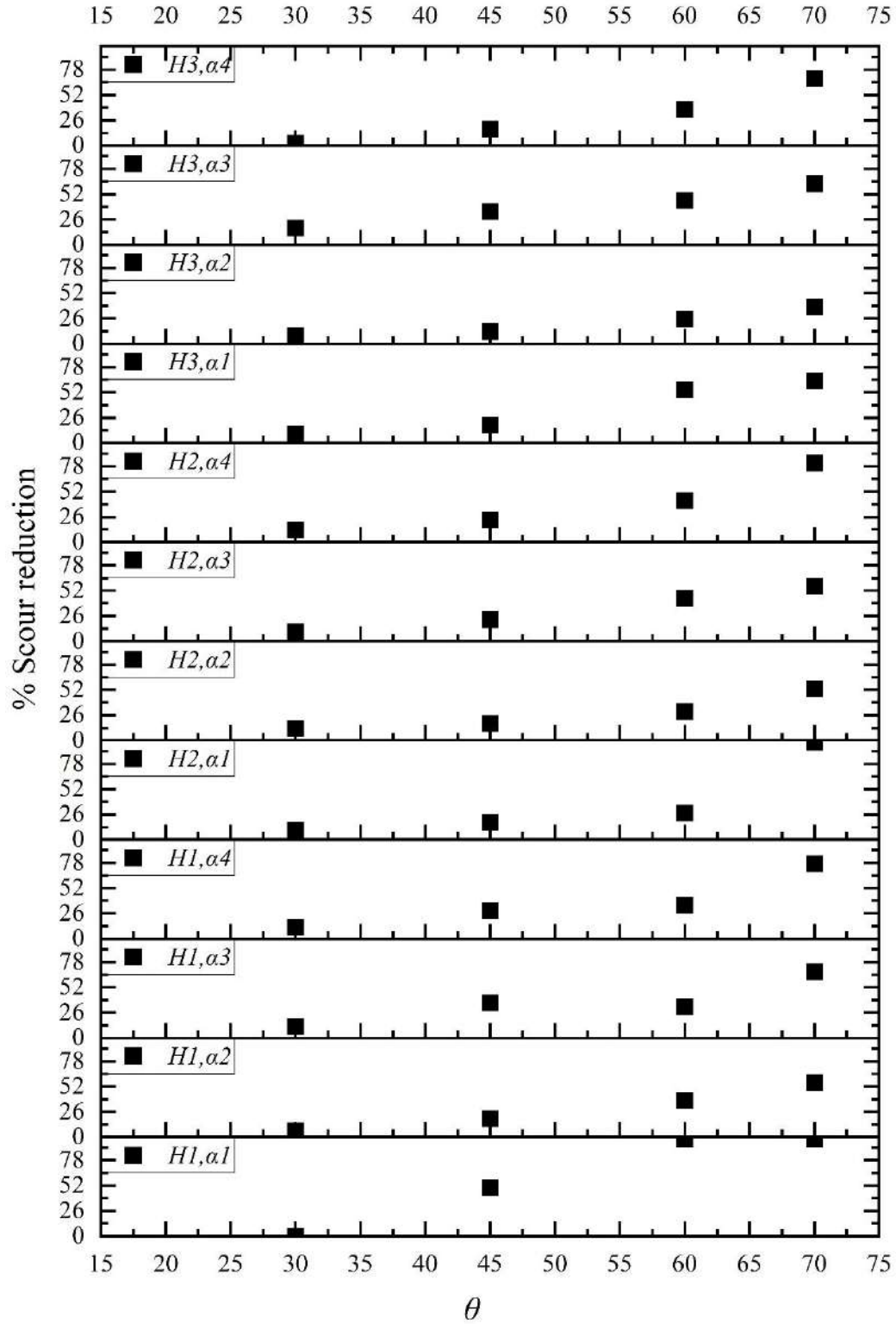

Fig. 5.7 Efficiency of bevel angle in % reducing of scouring downstream of the vane for bevel angles (θ = 0º, 30º, 45º, 60º, 70º) with different vane heights and angle of attacks under Q = 0.082 m^3/s

Table 5.1 Summary of d_{sm} and d_{sd} for bevel angles (θ = 0º, 30º, 45º, 60º, 70º) with different vane heights (H = 0.045, 0.06, 0.075 m) and angle of attacks (α = 15º, 20º, 30º and 40º), under Q=0.082 m^3/s

α º	Scour	θº	H = 0.045 m		H = 0.06 m		H = 0.075 m	
			Scour depth (10^{-2} m)	% reduction	Scour depth (10^{-2} m)	% reduction	Scour depth (10^{-2} m)	% reduction
15	d_{sm}	0	1.9	-	3.4	-	4.5	-
		30	1.2	36.84	2.8	17.65	3.6	20
		45	0.6	68.42	1.8	47.06	3.2	28.89
		60	0.5	73.68	0.8	76.47	1.9	57.78
		70	0	100.00	0	100.00	1.5	66.67
	d_{sd}	0	1	-	1.1	-	2.2	-
		30	1	0	1	9.09	2	9.09
		45	0.5	50	0.9	18.18	1.8	18.18
		60	0	100	0.8	27.27	1	54.55
		70	0	100	0	100.00	0.5	63.64
20	d_{sm}	0	3.7	-	5.1	-	7.4	-
		30	3.3	10.81	3.5	31.37	7.2	2.70
		45	2.4	35.14	3.4	33.33	5.7	22.97
		60	0.8	78.38	1.8	64.71	2.6	64.86
		70	0.8	78.38	1.2	76.47	1.5	79.73
	d_{sd}	0	1.9	-	1.7	-	2.4	-
		30	1.5	6.25	1.5	11.76	2.2	8.33
		45	1.3	18.75	1.4	17.65	2.1	12.5
		60	1	37.5	1.2	29.41	1.8	25
		70	0.7	56.25	0.8	52.94	1.5	37.5
30	d_{sm}	0	7.1	-	10.3	-	14.3	-
		30	5.5	22.54	8.3	19.42	12.9	9.79
		45	4.2	40.85	5.6	45.63	9.5	33.57
		60	3.8	46.48	5.3	48.54	7.8	45.45
		70	1.8	74.65	2.5	75.73	3.7	74.13
	d_{sd}	0	2.5	-	3.2	-	5.9	-
		30	1.8	12	2.9	9.38	4.9	16.95
		45	1.6	36	2.5	21.88	3.9	33.9
		60	1.7	32	1.8	43.75	3.2	45.7
		70	0.8	68	1.4	56.25	2.2	62.7
40	d_{sm}	0	12.1	-	12.7	-	19.5	-
		30	7.3	39.67	9.6	24.41	16.5	15.38

		45	5.8	52.07	8.2	35.43	14	28.21
		60	4.8	60.33	8.3	34.65	11.6	40.51
		70	3	75.21	3.3	74.02	4.8	75.38
	d_{sd}	0	3.5	-	4.9	-	7.8	-
		30	3.1	11.43	4.3	12.24	7.6	2.56
		45	2.5	28.57	3.8	22.45	6.5	16.67
		60	2.3	34.29	2.8	42.86	4.9	37.18
		70	0.8	77.14	0.9	81.63	2.4	69.2

5.2.4 Volume of Local Scour

The scour morphology was measured around the vane by using an ultrasonic bed profiler. Figures 5.8 (a-b) illustrates the variation in scour volume with various bevel angle (θ) for different angles of attack at H = 0.045 m and varying vane heights at α = 20º. The downward pressure gradient induces a downflow along the front face of the submerged vane, leading to the erosion of a groove in front of and along its pressure side. Consequently, flow separation occurs at the upstream edge of the scour hole formed by the downflow, resulting in the development of a horseshoe vortex. For vanes positioned at greater angles of attack, which strengthen the horseshoe vortex to effectively transport sediment away from the scour hole to downstream. Figure 5.8 shows that the volume of scour increases with an increase in both the angle of attack and the vane height, while it decreases with an increasing bevel angle. The rectangular vane generates the strong horseshoe vortex near the vane which create a significant scour hole around the vane. Cutting the leading edge of the vane significantly weakened this vortex strength, resulting in a substantial reduction in local scour volume compared to a rectangular vane (θ = 0°).

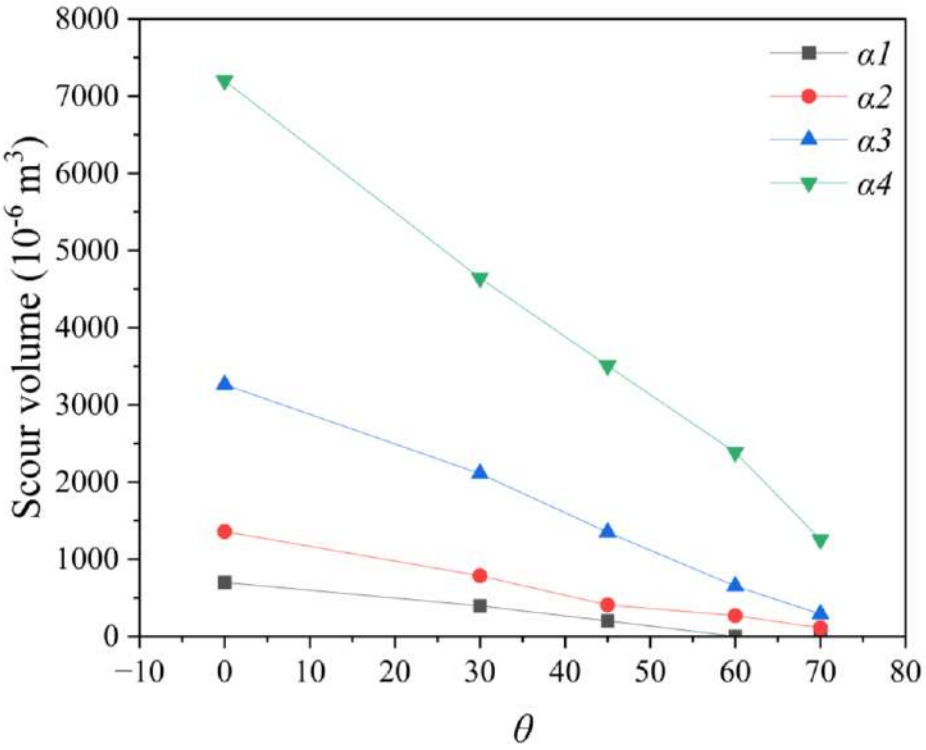

Fig. 5.8a Variation of local scour volume with various bevel angle (θ) for various angle of attack (α) at Q = 0.082 m^3/s, α = 20º

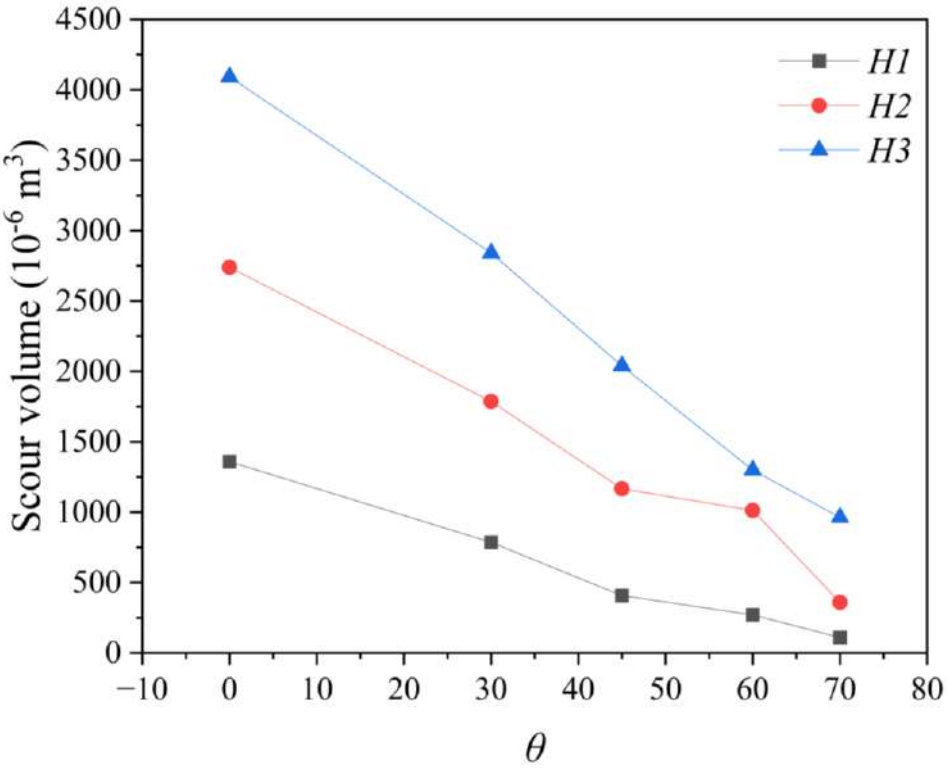

Fig. 5.8b Variation of local scour volume with various bevel angle (θ) for various vane height (H), at Q = 0.082 m^3/s, α = 20º

5.2.5 Dimensional Analysis for Maximum Scour Depth

The maximum scour depth in the local area of the vane and extension of the scour hole downstream of the vane depend on various parameters, namely sediment size (d_{50}), acceleration due to gravity (g), channel width (B), depth of water (d), discharge (Q), average velocity of the flow (V), height of vane (H), length of vane (L), mass density of flowing fluid (ρ), mass density of the sediment (ρ_s), dynamic viscosity of the flowing fluid (μ), bevel angle (θ) and angle of attack (α). Following the method outlined by Ansari and Ahmad (2024), we conducted a dimensional analysis to establish the functional relationship for d_{sm}.

From dimensional analysis, a relation between the previous variables with maximum scour depth can be developed as Eq. (2):

$$d_{sm} = f\,(d_{50}, B, g, \mu, \rho, d, Q, H, L, \theta, \alpha) \tag{5.2}$$

Considering V, ρ, and d as repeating variables and applying the Π Buckingham theorem (1915), the following non-dimensional Π terms were derived:

$$\Pi_1 = \frac{d_{sm}}{d}, \Pi_2 = \frac{d_{50}}{d}, \Pi_3 = \frac{gd}{V^2}, \Pi_4 = \frac{\nu}{Vd}, \Pi_5 = \frac{\rho_s}{\rho}, \Pi_6 = \frac{B}{d}, \Pi_{76} = \frac{L}{d}, \Pi_8 = \frac{H}{d}, \Pi_9 = \theta,$$

$$\Pi_{10} = \alpha$$

The functional relationship may be written as:

$$\frac{d_{sm}}{d} = f\left(\frac{d_{50}}{d}, \frac{gd}{V^2}, \frac{\nu}{Vd}, \frac{\rho_s}{\rho}, \frac{B}{d}, \frac{L}{d}, \frac{H}{d}, \theta, \alpha\right) \tag{5.3}$$

We rearrange the non-dimensional Π_2, Π_5, Π_8 terms as follows:

$$\Psi_1 = \sqrt{\frac{1}{\Pi_2}\frac{1}{\Pi_3}\frac{1}{\Pi_5}} = \sqrt{\frac{V^2 d}{g d d_{50}\frac{\rho_s}{\rho}}} = \frac{V}{\sqrt{g d_{50}\frac{\rho_s}{\rho}}} = F_D \tag{5.4}$$

Here, F_D represents the densimetric Froude number corresponding with different discharges. Since B and L are constant, the effects of Π_6 and Π_7 are negligible. As the

flows is turbulent, the kinematic viscosity (ν) has minimal impact on maximum scour depth so that Π_4 can be ignored (Rajaratnam, 1981).

The functional relationship can now be expressed as:

$$\frac{d_{sm}}{d} = f\left[\frac{H}{d}, \theta, \alpha, F_D = \frac{V}{\sqrt{g\left(\frac{\rho_s}{\rho} - 1\right) d_{50}}}\right] \tag{5.5}$$

Following the same procedure, d_{sd}/d can be expressed as follows:

$$\frac{d_{sd}}{d} = f\left[\frac{H}{d}, \theta, \alpha, F_D = \frac{V}{\sqrt{g\left(\frac{\rho_s}{\rho} - 1\right) d_{50}}}\right] \tag{5.6}$$

5.2.6 Influence of Various Parameters on Maximum Scour Depth

(a) Effect of Angle of Attack

The variations in maximum scour depth with angle of attack for constant H/d, Q, and θ, is shown in Fig. 5.9. It is evident that the scour depth was largest at a 40º angle of attack irrespective of the value of H/d, Q, and θ. As seen in Fig. 5.9, for case H1/θ1/Q1, d_{sm} was 0.01 m for α = 15º, increased to 0.031 m for α = 20º, 0.065 m for α = 30º and reached a maximum value of 0.088 m for α = 40º. A similar trend is observed in all the cases plotted for H, Q, and θ. We infer that the scour depth is maximum when the α is maximum for any constant value of H/d, Q, and θ. Increasing the angle of attack caused the vane to generate stronger vortices, which accelerated the development of scour. Odgaard and Spoljaric (1986) conclude that the optimal angle is approximately 15°, as angles exceeding this value result in significant flow separation and excessive local scour. The intensity of the primary vortex increases non-linearly as the α increases.

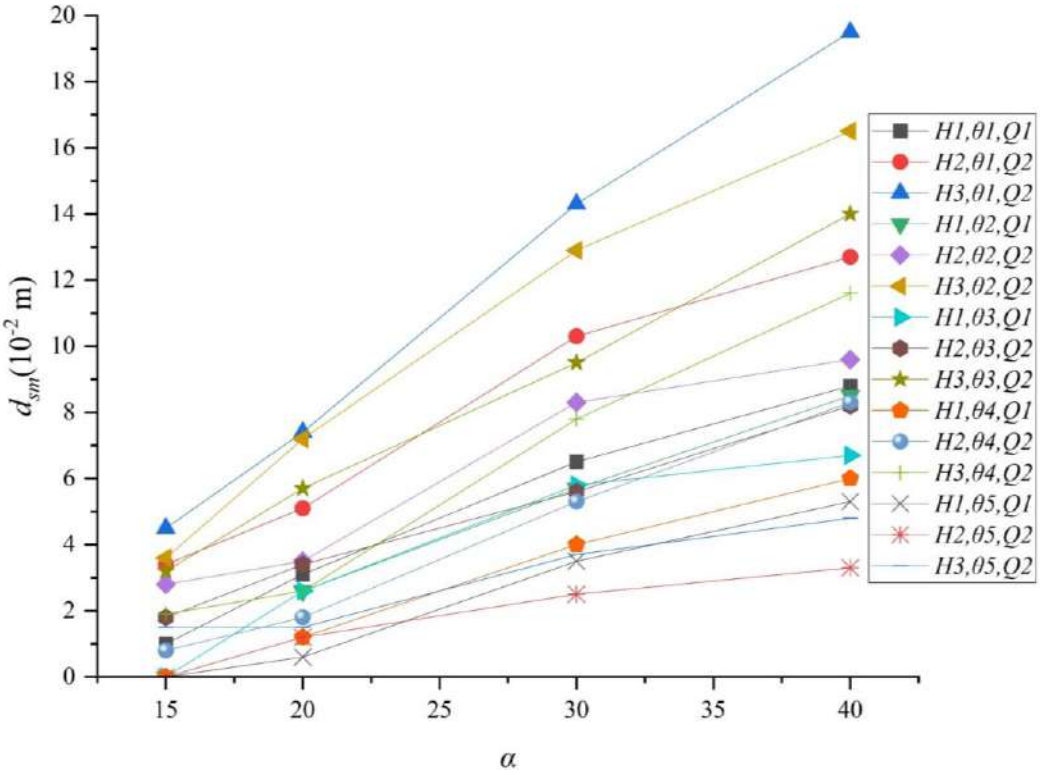

Fig. 5.9 Variation of maximum scour depth with angle of attack (α)

(b) Effect of H/L Ratio

Figure 5.10 illustrates the effects of H/L ratio on the maximum scour depth for constant Q, α, and θ. As seen in Fig. 5.10, for case α1/θ1/Q2, d_{sm} is 0.019 m for H/L = 0.3, and increased to 0.034 and 0.045 m for H/L = 0.4 and 0.5, respectively. A similar trend is observed in all the cases plotted for α, Q and θ. We conclude that the scour depth reaches its maximum when the H/L ratio is at its maximum for any constant value of α, Q, and θ. As the ratio of H/L increases, the lift coefficient also rises, likely because the suppression of the tip vortex by the free surface enhances the pressure difference between the vane surfaces. The pressure difference generates a stronger primary vortex, which leads to the formation of a scour hole. Odgaard and Spoljaric (1986) recommend that the H/L ratio ranges from 0.1 to 0.5 for all scour condition flow stages. The present study uses ranges of H/L between 0.3 to 0.5.

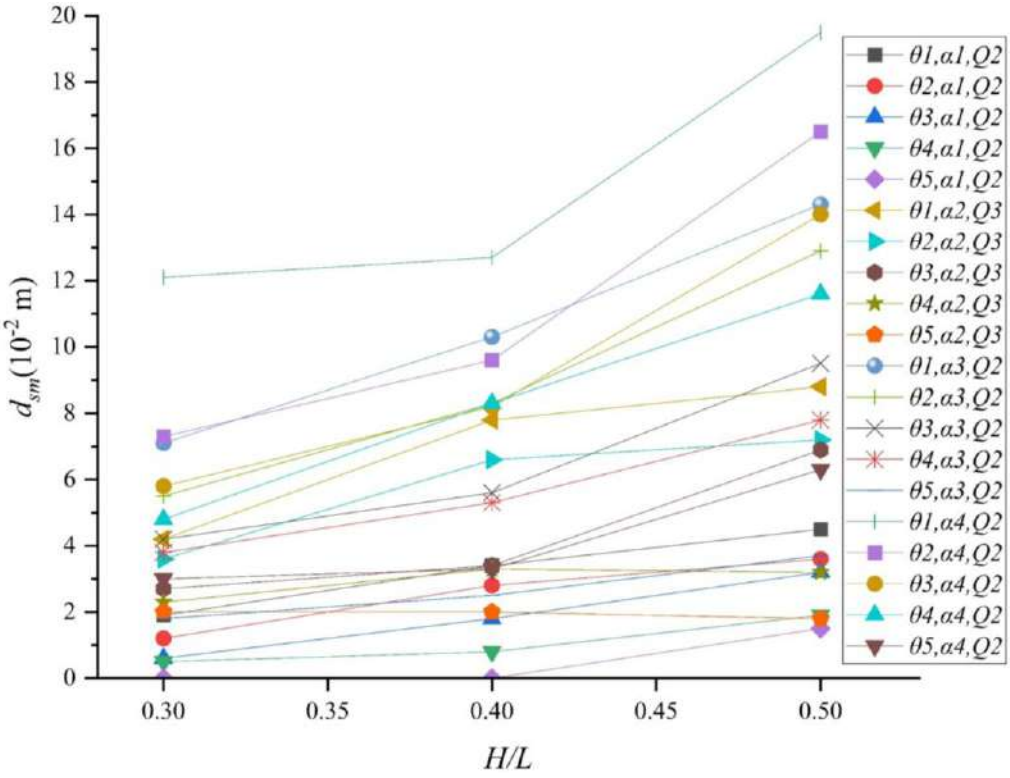

Fig. 5.10 Variation of maximum scour depth with H/L

(c) Effect of Bevel Angle

The effects of the bevel angle on the d_{sm} for constant H, Q, and α are shown in Fig. 5.11. The rectangular vane created maximum scour around the vane for any value of H, Q, and α. In the case of H3/α4/Q2, the d_{sm} is 0.195 cm for θ = 0º, and decreased to 0.165, 0.14, 0.115 and 0.063 cm for θ = 30º, 40º, 60º, and 70º, respectively. A similar trend is observed in all the cases plotted for H, Q, and α. The bevel submerged vane drastically decreased the local scour. The vane's leading edge is the main factor responsible for the formation of the horseshoe vortex, which generates an intense scour depth near the tip and dissipates after a certain distance. So, cutting the leading edge (known as bevel vane) minimized the impact of the horseshoe vortex and reduced the maximum scour around the vane.

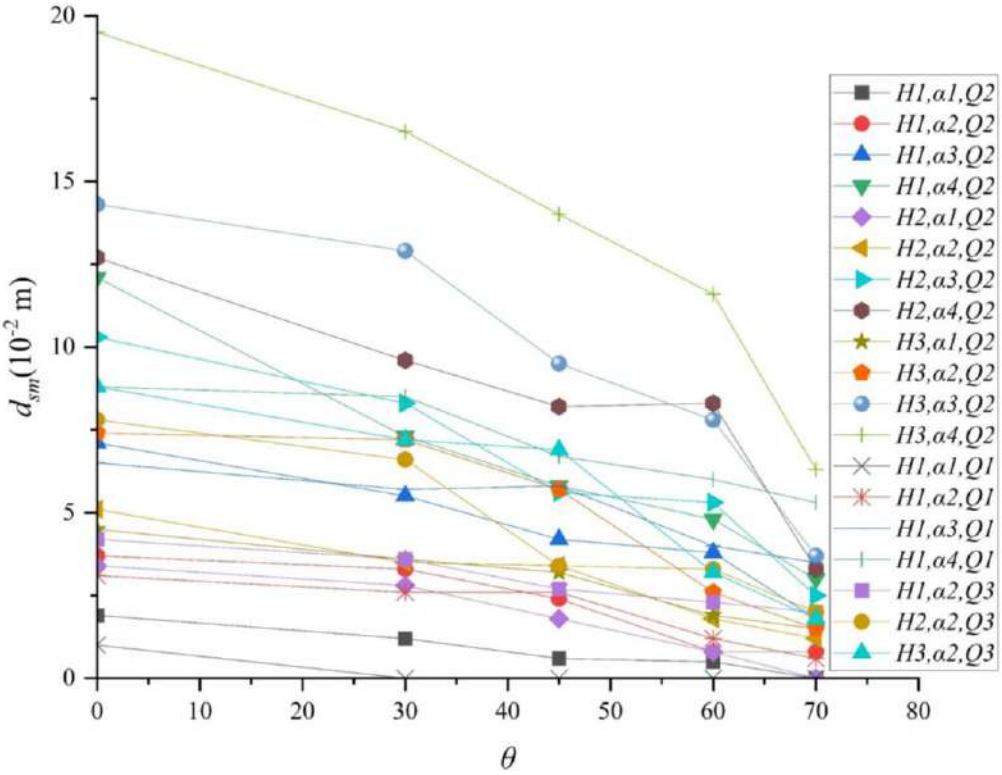

Fig. 5.11 Variation of maximum scour depth with bevel angle (θ)

(d) Effect of Discharge

The effects of discharge on the d_{sm} for constant α, H, and θ are shown in Fig. 5.12. In this study, the Densimetric Froude number (F_D) are 2.66, 2.81 and 3.22 corresponding with discharges of 0.058 m^3/s, 0.082 m^3/s and 0.092 m^3/s respectively. The maximum discharge generated the maximum scour around the vane. As seen in Fig. 5.12, for case H1/α2/θ1, d_{sm} is 0.031 m for Q = 0.058 m^3/s, and increased to 0.037 m for Q = 0.082 m^3/s and 0.042 m for Q = 0.092 m^3/s. A similar trend is observed in all the conditions plotted for H, θ, and α. Discharge is the most critical factor in increasing vortex flow around the vane, leading to greater scour in the local area surrounding the vane.

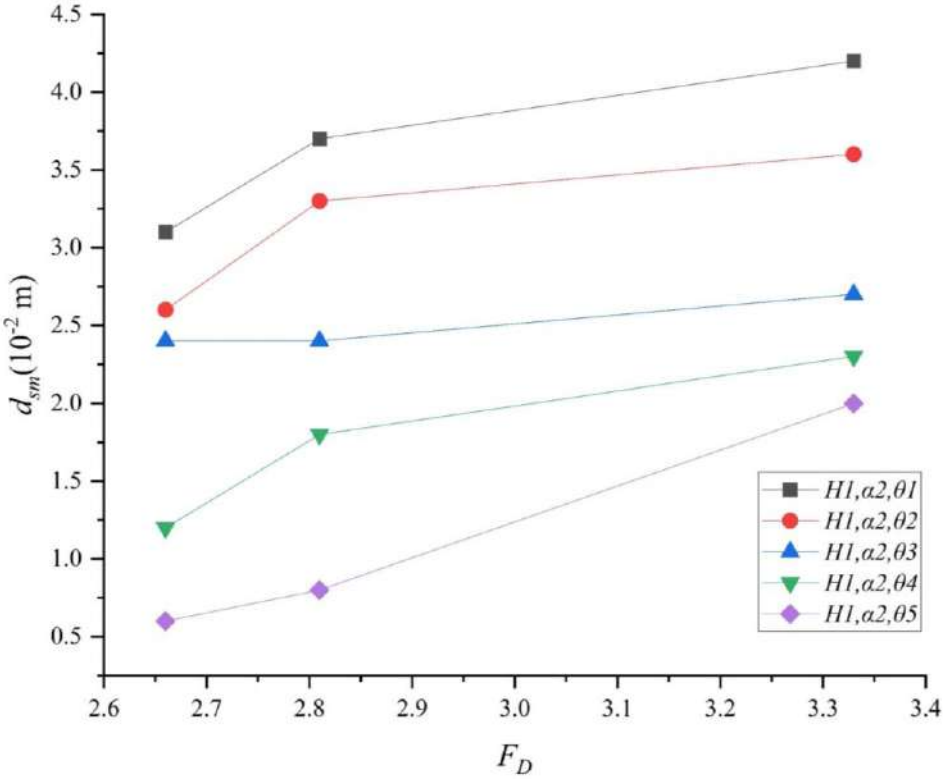

Fig. 5.12 Variation of maximum scour depth with F_D

5.2.7 Estimation of maximum scour depth of local and downstream scour

The effects of the individual parameters on d_{sm}/d and d_{sd}/d were examined using graphical analysis. Figure 5.13 (a – d) demonstrates the effects of H/d, α, θ, and F_D on d_{sm}/d. As evident from Fig. 5.13, the trend line shows that d_{sm}/d increased with an increase in the H/d, F_D, and α. However, d_{sm}/d decreased with an increase in θ. A similar pattern in the downstream scour hole (d_{sd}) is observed in Fig. 5.14 (a – d). Due to increasing the angle of attack, the vane produced strong vortices in the flow field, leading to an acceleration of scour development. The trend line for local scour depth influenced by various parameters is steeper compared to that of downstream scour depth. Therefore, the local scour around the vane is influenced more significantly by H/d, α, θ, and F_D than the downstream scour.

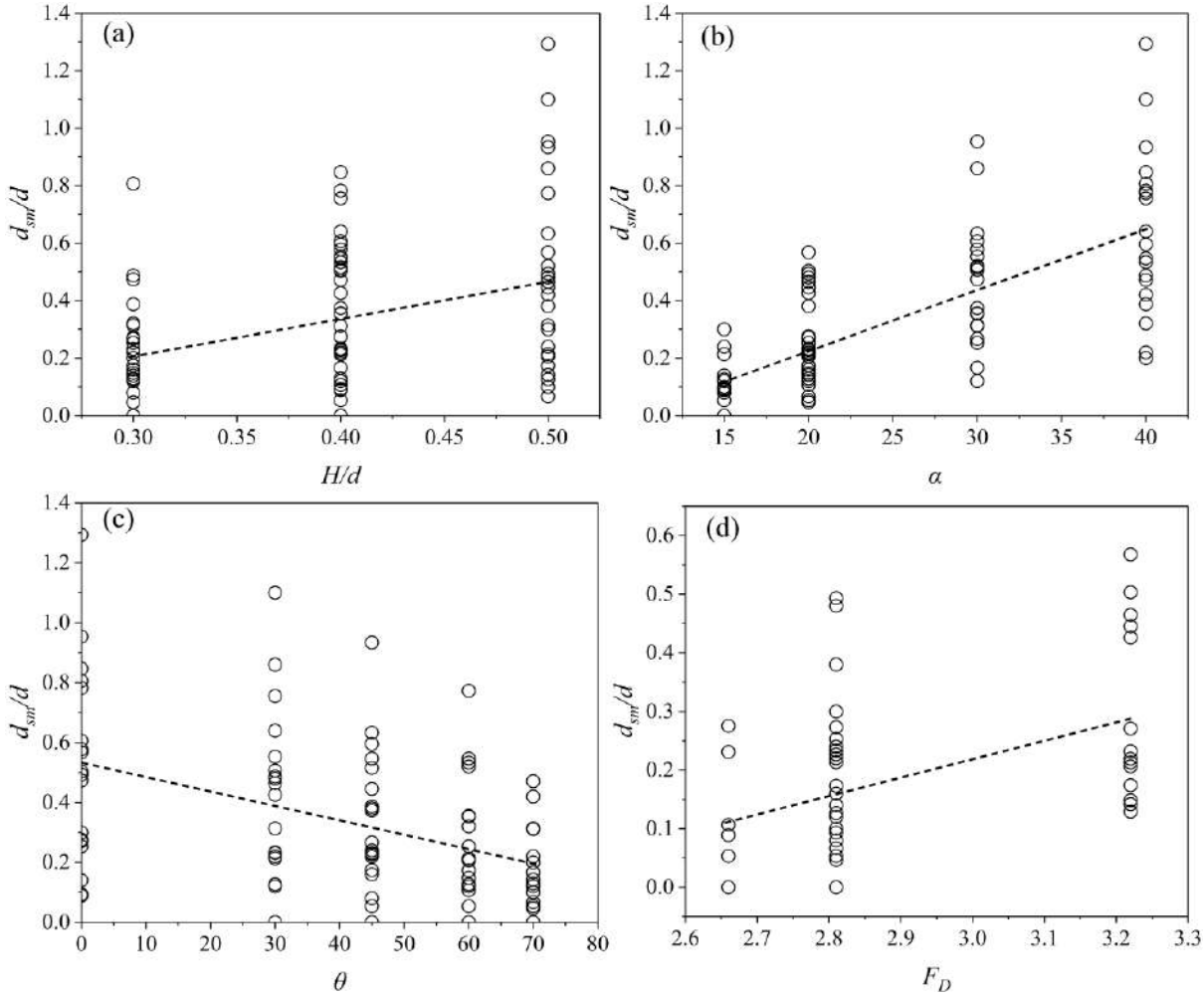

Fig. 5.13 Effect of various parameters on d_{sm}/d: (a) H/d, (b) α, (c) θ and (d) F_D

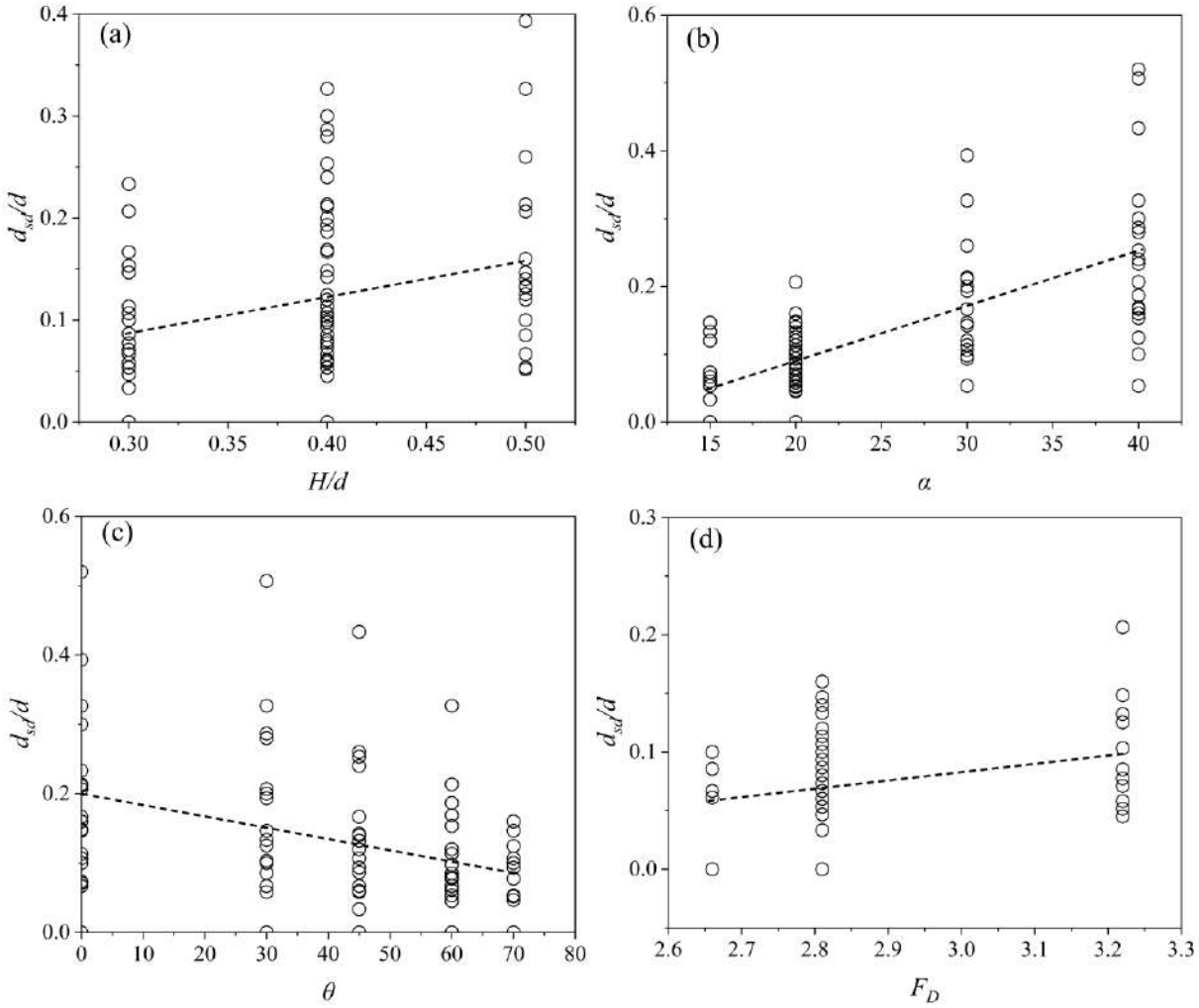

Fig. 5.14 Effect of various parameters on d_{sd}/d: (a) H/d, (b) α, (c) θ, and (d) F_D

The equations derived for d_{sm} and d_{sd} from the experimental data in this study and using least-squares curve fitting methods. A randomly selected 80% of the datasets was utilized to develop the equations, while the remaining 20% was employed to validate them. The proposed equation for the maximum scour depth around the submerged vane is as follows:

$$\frac{d_{sm}}{d} = 1.13\left(\frac{H}{d}\right)^{1.49}(\sin\alpha)^{1.86}(\cos\theta)^{0.99}{F_D}^2 \tag{5.7}$$

The coefficient of correlation (R^2) for Eq. (5.7) was determined to assess the linear relationship between the observed and predicted values, resulting in a value of 0.933, which demonstrates a strong agreement between the observed and computed results. The mean absolute percentage error (MAPE) and the root mean square error (RMSE)

were calculated to evaluate the model's predictive performance. The values of MAPE and RMSE were 22.3% and 0.09, respectively, which represents the good fit for the prediction. Figure 5.15a illustrating least-squares method substrates that the scour depth calculated using Eq. (5.7) falls within ± 25% of the observed values. Equation (5.7) is applicable for the ranges of $0.04 \leq d_{sm}/d \leq 1.4$, $0.3 \leq H/d \leq 0.5$, $15^{o} \leq \alpha \leq 40^{o}$, $2.66 \leq F_D \leq 3.22$, and $0^{o} \leq \theta \leq 70^{o}$.

For the maximum scour depth downstream of the vane, again 80% of the datasets was chosen randomly for training, whereas 20% was used for validation. The resulting equation is:

$$\frac{d_{sd}}{d} = 1.04\left(\frac{H}{d}\right)^{1.57}(\sin\alpha)^{1.66}(\cos\theta)^{0.84}F_D^{1.06} \tag{5.8}$$

The R^2 for Eq. (5.8) is 0.93, which represent good correlation between the observed and computed results. The values of MAPE and RMSE were 18.1% and 0.035, respectively, which represents the good fit for the prediction. Figure 5.15b illustrates that the scour depth calculated using Eq. (5.8) falls within ± 25% of the observed values. Equation (5.8) is valid for the ranges of $0.02 \leq d_{sm}/d \leq 0.51$, $0.3 \leq H/d \leq 0.5$, $15^{o} \leq \alpha \leq 40^{o}$, $2.66 \leq F_D \leq 3.22$, and $0^{o} \leq \theta \leq 70^{o}$. Equations (5.7) and (5.8) were validated for the clear-water condition (meaning that no sediment movement occurred from upstream of the vane) and cohesionless sediment.

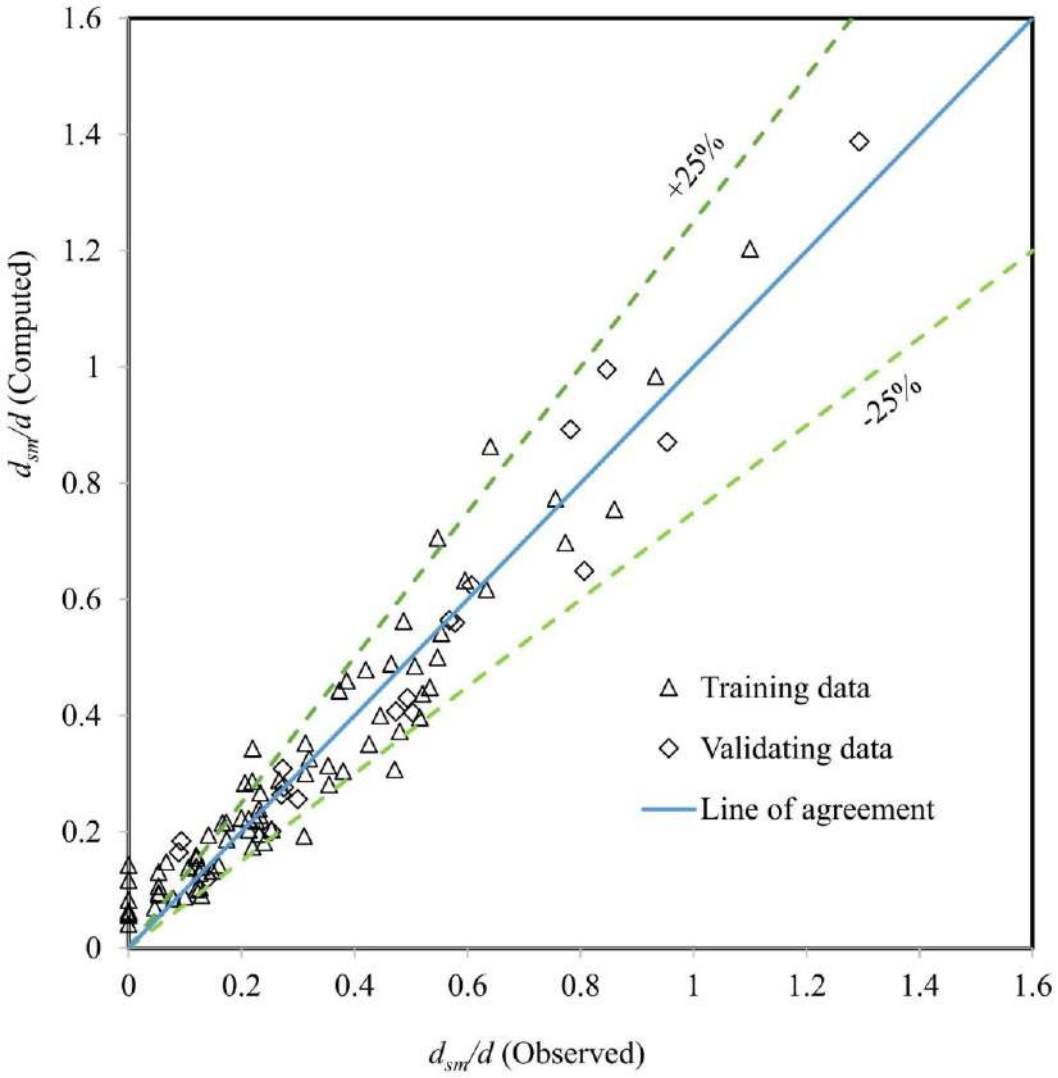

Fig. 5.15a Comparison of calculated d_{sm}/d with observed values

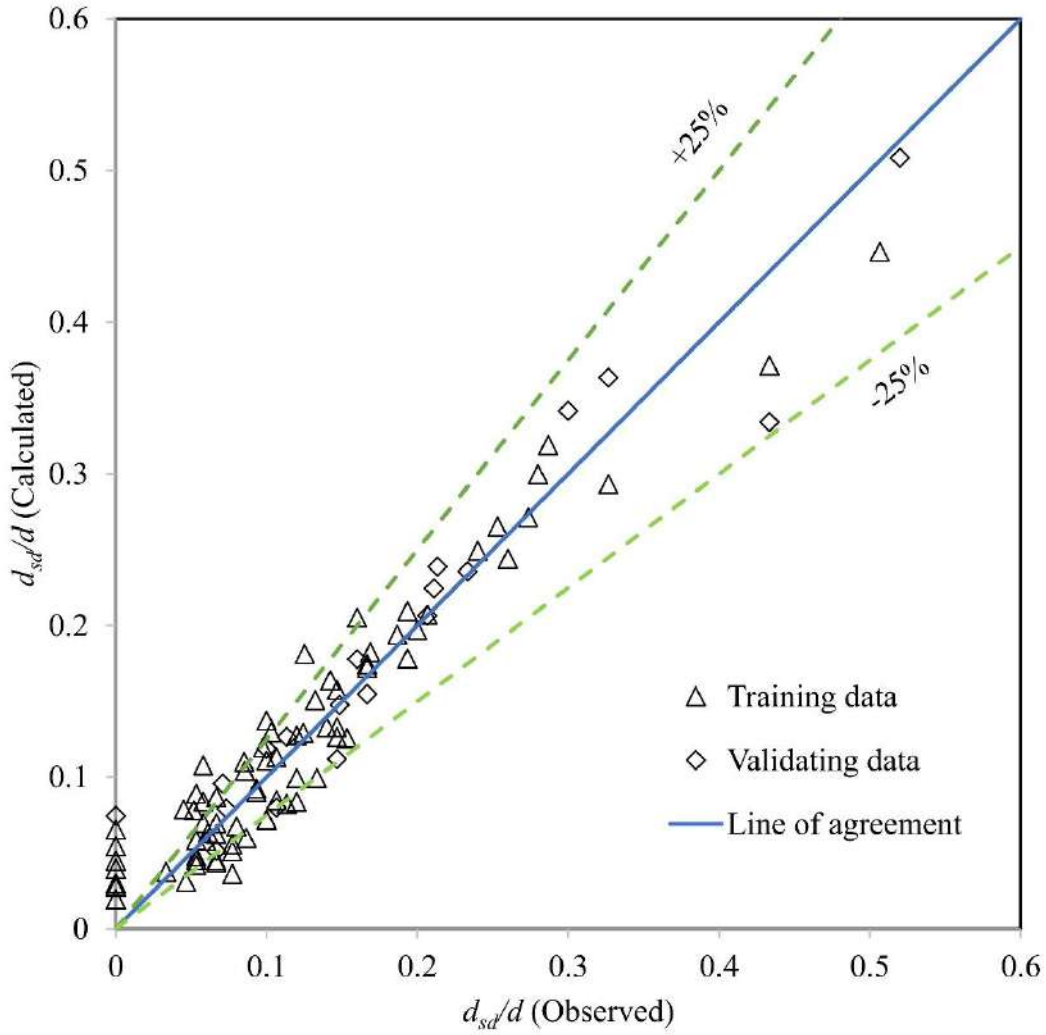

Fig. 5.15b Comparison of calculated d_{sd}/d with observed values

The study compared the maximum scour depths calculated using Eq. (5.7) and Eq. (5.9) with observed values in Fig. 5.16. The results indicate that the equation proposed by Hossain et al. (2004) underestimates compared to the present Eq. 5.7. In contrast, the proposed equation (Eq. (5.7)) predicts values within a ±25% margin of error. Eq. (5.7) incorporates flow conditions, an aspect not included in the equation proposed by Hossain et al. (2004). Using experimental data, Hossain et al. (2004) proposed an equation for the maximum scour depth:

$$d_s = 1.55\left(\frac{HL\sin\alpha}{d}\right)^{0.92} \tag{5.9}$$

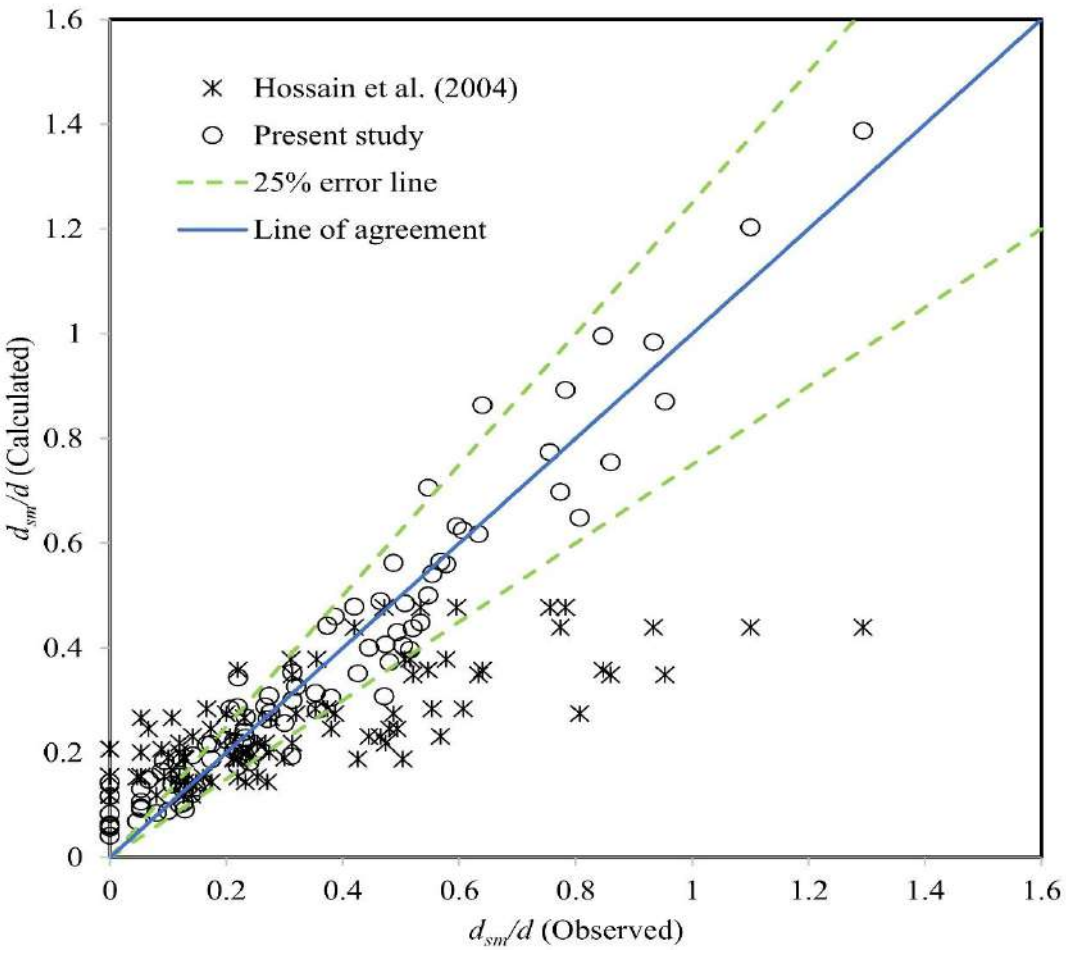

Fig. 5.16 Comparison between the equation of Hossain et al. (2004) and the proposed equation for maximum scour depth

5.2.8 Sensitivity Analysis

Present study assessed the relative significance of the dimensionless independent parameters (H/d, α, θ, F_D) influencing the dependent parameters (d_{sm}, d_{sd}) in Eqns. (5.7 & 5.8) by varying the independent parameters around their mean values in the experiments. These mean values of H/d, α, θ, and F_D were 0.4, 25.26º, 41º, and 2.843, respectively.

For this analysis, the average values (x) of all input variables related to H/d, α, θ, and F_D corresponding to d_{sm}/d and d_{sd}/d, were utilized as recommended by Ahmad (2013). Sensitivity and error analyses were performed by varying the average value of each of the four input parameters by ±10% (defined as Δx), and observing the corresponding changes in the dependent variables (defined as Δy). The error was

evaluated using three indices known as absolute sensitivity (AS) = $\Delta y/\Delta x$, relative sensitivity (RS) = $(x \times \Delta y) / (y \times \Delta x)$, and relative error (RE) = $\Delta y/y$, where Δy represents the error in the output parameter, defined as the difference between the output values predicted for inputs x and $(x + \Delta x)$. The sensitivity analysis for d_{sm}/d is given in Table 5.2, revealing that the d_{sm}/d which is the most sensitive to F_D followed by α and H/d. The relative sensitivity of F_D is about 1.26 times that of α and about 1.3 times that of H/d, for a 10% increment in x. However, for a 10% reduction in x, the relative sensitivity of F_D is about 1.18 times that of α and about 1.5 times that of H/d. The sensitivity analysis for d_{sd}/d is given in Table 5.3, showing that the d_{sd}/d which is the most sensitive to H/d followed by α and F_D. The relative sensitivity of H/d is about 1.02 times that of α and about 1.36 times that of F_D, for a 10% increment in x. However, for a 10% reduction in x, the relative sensitivity of H/d is about 1.01 times that of α and about 1.54 times that of F_D. In both cases, θ is relatively less sensitive compared to other parameters.

Table 5.2 Results of sensitivity analysis for d_{sm}/d

For 10% increment in x						For 10% decrement in x			
x	Δx	Δy	AS	RE	RS	Δy	AS	RE	RS
H/d	0.04	0.072	1.81	0.21	2.096	0.035	0.888	0.103	1.030
α	0.0441	0.082	1.855	0.237	2.37	0.044	0.996	0.127	1.273
θ	0.0716	-0.006	-0.085	-0.018	-0.178	-0.03	-0.419	-0.087	-0.87
F_D	0.284	0.093	0.327	0.27	2.698	0.052	0.182	0.15	1.499

Table 5.3 Results of sensitivity for d_{sd}/d

For 10% increment in x						For 10% increment in x			
x	Δx	Δy	AS	RE	RS	Δy	AS	RE	RS
H/d	0.04	0.0296	0.74	0.216	2.16	0.0154	0.386	0.1127	1.127
α	0.0441	0.0291	0.660	0.2125	2.125	0.0153	0.348	0.112	1.119
θ	0.0716	-0.0014	-0.02	-0.010	-0.102	-0.009	-0.13	-0.066	-0.657
F_D	0.284	0.0217	0.076	0.158	1.583	0.01	0.035	0.073	0.73

5.3 CONCLUDING REMARKS

In river engineering, determining the maximum scour depth is critically important in the design of hydraulic structures as the local scour surrounding the structure impacts its structural stability. A series of experiments was performed in clear-water conditions on various combinations of governing parameters with different flow regimes.

- It is found that the maximum scour hole occurs near the submerged vane and extends downstream of the vane. The maximum scour depth increases with increased *H/d* ratio, angle of attack, and densimetric Froude number. The rectangular shape generates a strong horseshoe vortex at the leading edge of the vane and dissipates quickly, producing a significant local scour on the pressure side of the vane.
- It is observed that cutting the leading-edge w.r.t vertical axis or bevel shape of the submerged vane decreased the horseshoe vortex significantly, which reduced the local scour depth at the leading edge compared to the rectangular vane. The bevel shape of submerged vane is more effective in reducing local scour around the vane than reducing extended downstream scour.
- Present study proposes empirical Equations (5.7) and (5.8) to calculate the maximum scour depth around the vane and the extended scour in the downstream channel based on the data collected in the current investigation. The calculated values of maximum scour depth around the vane and the extension of the scour downstream of the vane offer good correlation with the observed data.
- The densimetric Froude number of the flow and the angle of attack have the largest influence on the maximum depth of the local scour. At the same time, the height of the vane is the most sensitive parameter affecting the extension of the scour in the downstream channel. Although bevel angle exhibits relatively lower sensitivity compared to other parameters, it remains an effective method for reducing local scour around the vane.

- Furthermore, the bevel shape offers a cost-effective alternative, as it requires less material compared to the rectangular vane design. The present study is limited to a single size of cohesionless sediment and it specifically considers clear-water scour conditions, wherein no sediment is transported from the upstream region. In future studies taper, curved, and porous vanes could be used to find the most efficient shape to limit the local scour. A field study could be conducted to minimize scale effects and to validate the findings from the laboratory study.

6. CFD SIMULATION OF FLOW

6.1 INTRODUCTION

Computational Fluid Dynamics (CFD) has emerged as an effective tool for numerical modelling of flow-related problems. This can be attributed to the remarkable progress in high- speed computing technologies, the adoption of innovative approaches in applied mathematics, and advancements in computer programming. The application of available CFD codes allows the three-dimensional simulations of complex flow problems. Flow structures around and downstream of the vane are highly complex and three-dimensional. Through experimentation, gaining insights into the flow structures of such complex flows remains challenging and elusive. The present study simulates the flow vortex around and downstream of the submerged vane. This chapter provides a comprehensive outline of the numerical modeling approach, mesh generation, and boundary conditions used in the simulation. Also, this chapter discusses the results derived from the Computational Fluid Dynamics (CFD) analysis, including a discussion on the validation of these findings with experimental data.

6.2 COMPUTATIONAL FLUID DYNAMICS (CFD) STUDY

6.2.1 Governing Equations

ANSYS-FLUENT is a computational fluid dynamics (CFD) solver capable of simulating intricate fluid flow phenomena using diverse numerical schemes and turbulence models. To compute turbulent flows using the RANS equations, it is essential to develop turbulence models capable of predicting the Reynolds stresses and scalar transport terms. The most commonly used RANS turbulence models are classified according to the number of additional transport equations, beginning with Prandtl's mixing length theory in 1936 and later extending to the Reynolds stress models. However, the standard k–ε model fails to capture flow separation and often overpredicts turbulent shear stress, particularly under adverse pressure gradient conditions, whereas the k–ω model has been demonstrated to be more effective in predicting separation regions (Menter, 1992b; Versteeg and Malalasekera, 1995). Since

the vane generates a strong vortex as a result of flow separation from its surfaces, the k–ω turbulence model was employed in the present study to accurately capture the flow dynamics around the submerged vane. The turbulent kinetic energy (k) and the specific dissipation rate (ω) are required to compute the eddy viscosity (ξ), as defined by the standard k–ω turbulence closure model (Wilcox, 1988). The transport equations for k and ω are expressed as follows:

$$\frac{\partial k}{\partial t} + u_i \frac{\partial k}{\partial x_i} = \frac{\partial}{\partial x_i}\left[\frac{\left(\mu + \frac{\rho\xi}{\sigma_k}\right)}{\rho}\frac{\partial k}{\partial x_i}\right] + \frac{P_k}{\rho} - \beta^* k\omega \tag{6.1}$$

$$\frac{\partial \omega}{\partial t} + u_i \frac{\partial \omega}{\partial x_i} = \frac{\partial}{\partial x_i}\left[\nu + \frac{\xi}{\sigma_\omega}\frac{\partial \omega}{\partial x_i}\right] + \gamma_1\left[2S_{ij}.S_{ij} - \frac{2}{3}\omega\frac{\partial u_i}{\partial x_j}\delta_{ij}\right] - \beta_1\omega^2 \tag{6.2}$$

Here, k represents the turbulence kinetic energy; ω is the specific dissipation rate; u_i is component of velocity in the i^{th} direction, where i = 1, 2, 3, etc.; x_i or x_j are the coordinate of variable x into the i^{th} or j^{th} direction; ρ is the fluid density; μ is dynamic viscosity of fluid; ν is kinematic viscosity of fluid; S_{ij} is Strain tensor $= \frac{1}{2}\left[\frac{\partial u_i}{\partial x_j} + \frac{\partial u_j}{\partial x_i}\right]$; P_k is Production of kinetic energy $= 2\rho\xi S_{ij}.S_{ij} - \frac{2}{3}\rho K\frac{\partial u_i}{\partial x_j}\delta_{ij}$; σ_k and σ_ω are the turbulent Prandtl number for k and ω. β^* and β_1 are coefficient in Wilcox's k-ω turbulence scheme associated with dissipation of turbulent kinetic energy and turbulent frequency, respectively.

6.2.2 Model Development

The geometry and meshing of the computational domain were developed using the ANSYS CAD V15.0 module named Integrated Computer-Aided Engineering and Manufacturing (ICEM) CFD. The geometry with equilibrium scour bed to be created in ICEM CFD was a rectangular channel of 1.0 m width, 5 m length, and 0.15 m depth. Fig. 6.1 shows the geometry of equilibrium scour sediment bed after experimental run at 20 angle of attack which is generated in ICEM CFD. The bevel submerged vane was

placed at the mid-middle of the channel (0.5 m from either of the banks) and 2m downstream from the inlet of the flume. The length of the vane was 0.15 m, height of 0.045 m, and thickness of 0.002 m. In the present study, five shapes of vanes: a simple rectangular vane and four vanes were included which bevelled at the leading edge at 30, 45, 60, and 70 degrees with respect to the base, respectively shown in Fig. 6.2. Once the geometry was made, 3D blocking was initiated. The sides of the vane were split in order to create the block around it. After that, the vertices were connected to the projected points to complete the blocking structure around the vane, and extra vertices points were projected on the surfaces of channel geometry. The block around the vane was assigned as "solid" to make that impermeable to the flow occurring into it. Fig. 6.3 shows ICEM-CFD generated blocking and meshing of submerged vanes.

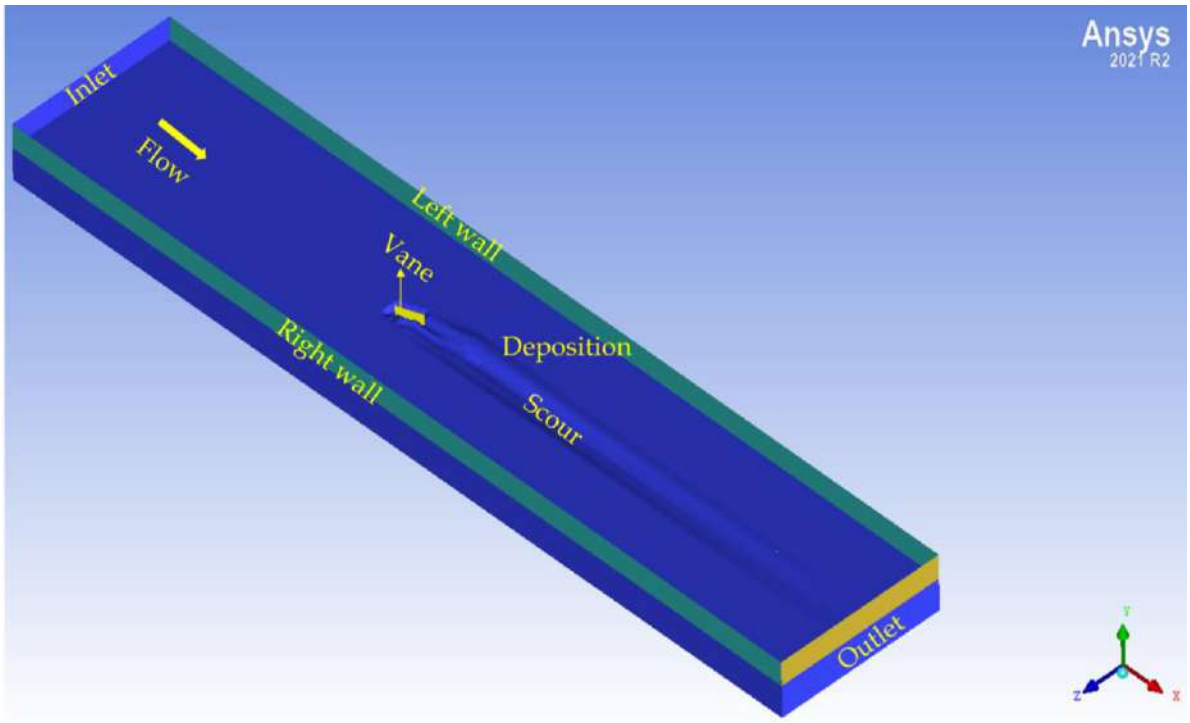

Fig. 6.1 Model of submerged vanes generated by ICEM-CFD

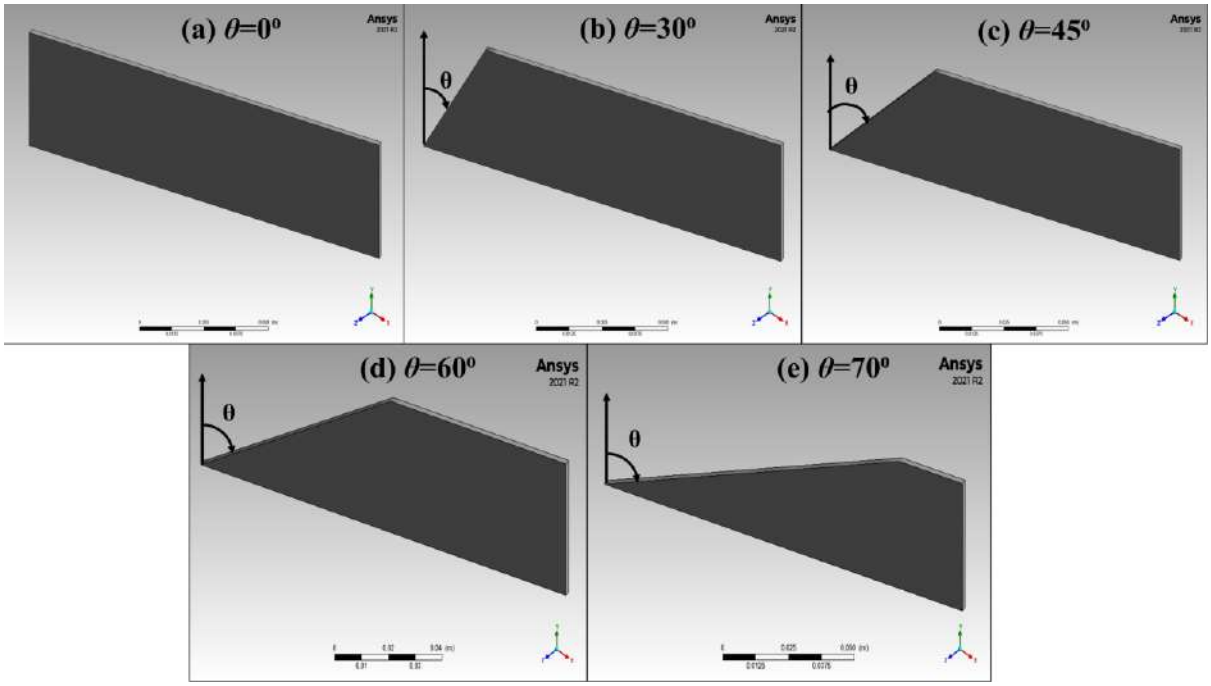

Fig. 6.2 Schematic diagram of vanes of different bevel angles (a) Simple rectangular vane (θ = 0°); (b) θ = 30°; (c) θ = 45°; (d) θ = 60°; and (e) θ = 70°

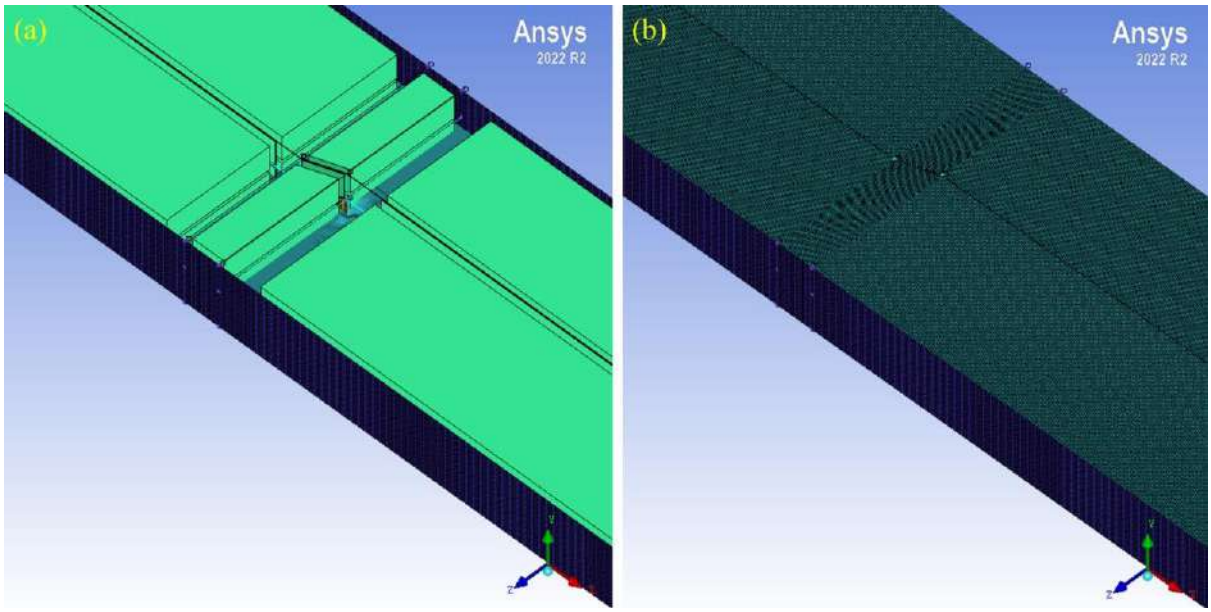

Fig. 6.3 ICEM-CFD generated (a) blocking and, (b) meshing of submerged vanes

The fine meshing was created on the blocking structure around the vane, and meshing was converted to unstructured mesh, which was supported by the ANSYS Fluent solver. Several approaches to determining the mesh quality include the aspect ratio of the mesh elements, the Jacobian ratio, the warping factor, the parallel deviation, the maximum corner angle, the skewness, and the orthogonality of the mesh elements.

The mesh quality was checked in the present study, which came out as 0.83. In order to have a good mesh, mesh quality should be greater than 0.3 (ICEM CFD Manual, 2011). After completing the meshing, the meshing file was transferred to the ANSYS Fluent solver. All sides of the geometry were classified with boundary condition. The inlet and outlet of the geometry were considered as velocity inlet and pressure outlet. In the inlet boundary, the average velocity of 0.55 cm/s was given as the initial velocity. The top surface of the computational domain was given a symmetry boundary condition, representing zero-gradient conditions. Wall boundary conditions were assigned on the sides, vane, and bed of the computational domain, which means the flow cannot pass through these surfaces.

6.2.3 Sensitivity Analysis

In this present study, a channel flume model and the computational mesh was generated using the ICEM-CFD platform. The simulation was conducted using the ANSYS-Fluent software using a computer with a 2.1 GHz processor. Different mesh grid sizes were tried to identify the best fit for the simulation of the flow phenomena around bevel submerged vane. In the present study, two coarse (10mm, 8mm) and two fine (6mm, 4mm) mesh grid sizes were used. The sensitivity analyses were done to identify the best fit of the utilized of these four mesh grids. It can be seen that there was no significant difference in mid-stream wise velocity of fine mesh sizes, as shown in Figs. 6.4 (a-c). Thus, the mesh with the least fine size was adopted for the computation of flow around vane without compromising the mesh quality, solution accuracy, and computational time.

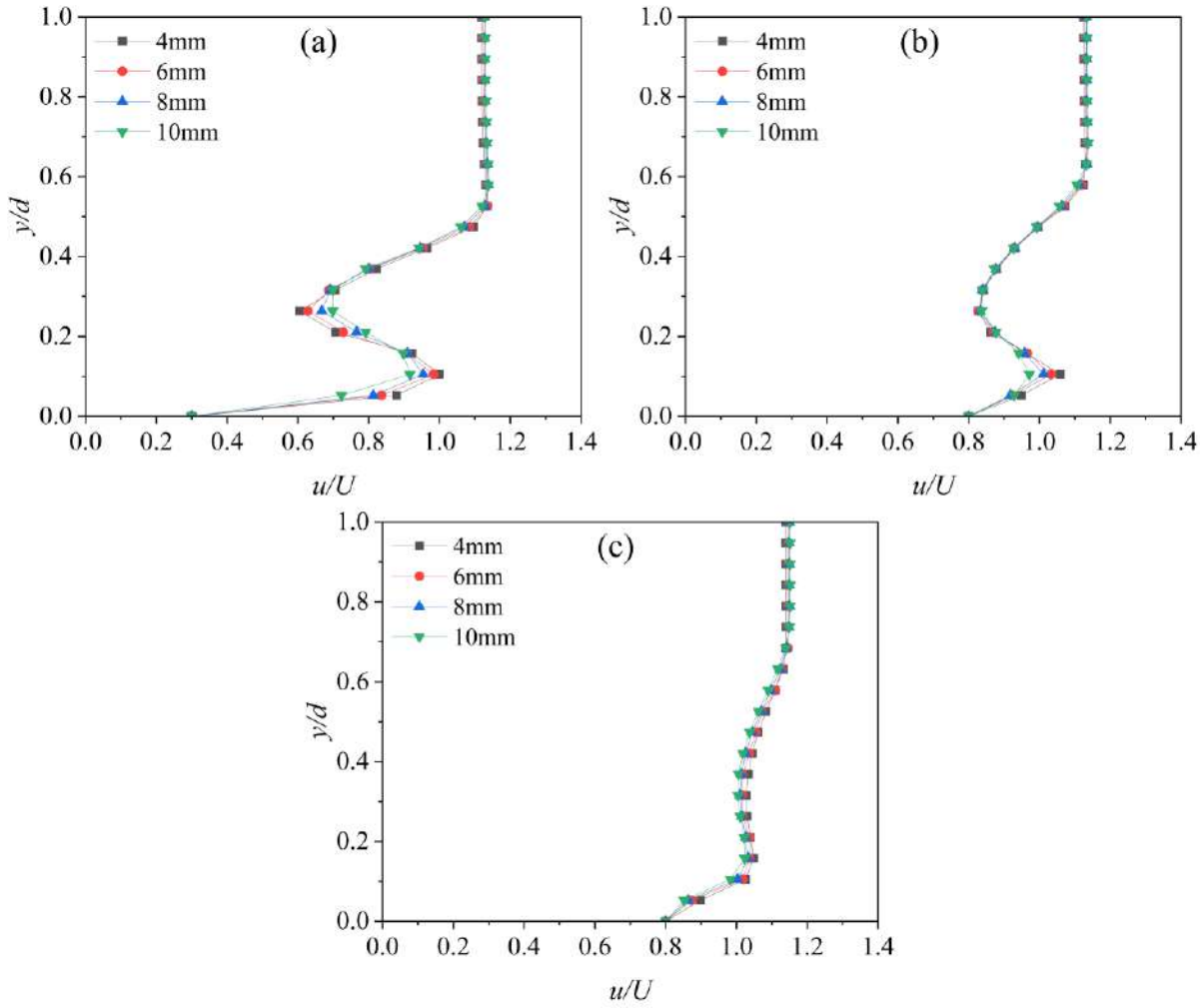

Fig. 6.4 Sensitivity analysis of a model for rectangular vane, (a) x = 2H; (b) x = 8H; (c) x = 20H for Q = 0.082 m^3/s, H = 0.045 m, α = 20º and θ = 0º

6.2.4 Validation of Numerical Model

The three directional velocities were measured in 3H, 8H, and 20H planes downstream of the submerged vane. The distance of the 3H, 8H, and 20H planes from the center of the vane was 0.135 m, 0.36 m, and 0.90 m, respectively. The numerical results were validated with the data observed from the experiments conducted in this study. As evident from Figs. 6.5 (a-e) the CFD results are in good agreement with the experimental data. The observed and simulated streamwise velocity distributions in the vertical direction at 3H, 8H, and 20H plane for five different bevel angles were compared using statistical metrics, including the coefficient of determination (R^2), mean absolute error (MAE), and root mean square error (RMSE), as presented in Table

6.1. All statistical values indicate the extent to which the numerical model accurately represents the observed data in the present study.

$$R^2 = 1 - \frac{\sum_{i=1}^{n} \left(N_i - \widehat{N}_i\right)^2}{\sum_{i=1}^{n} (N_i - \overline{N}_i)^2} \tag{6.3}$$

$$MAE = \frac{1}{n}\sum_{i=1}^{n} |O_i - N_i| \tag{6.4}$$

$$RMSE = \sqrt{\frac{\sum_{i=1}^{n} (O_i - N_i)^2}{n}} \tag{6.5}$$

Where $\widehat{N}_i (= aO_i \pm b)$ is the predicted numerical value, where O_i and N_i are the observed and numerical values. The calculated numerical prediction ($\widehat{N}_i$) is determined by substituting the corresponding observed (O_i) into the regression linear equation, where 'a' represents the slope of the regression line, and 'b' denotes the intercept of N_i when O_i equals zero. The statistical analysis in Table 6.1 indicated that the precision of the numerical simulation results was deemed acceptable. The discernible error between the numerical and observed velocities was primarily associated with the presence of the scour hole around the vane. It can be observed that the precision of statistical parameters was less agreed at the vicinity of the vane as the maximum scour and deposition were observed near the vane to the 8h plane. The scour and deposition decrease with the increase in the bevel angle. At the 20H plane, the statistical analysis indicates that the R^2, MAE, and RMSE results exceeded 99%.

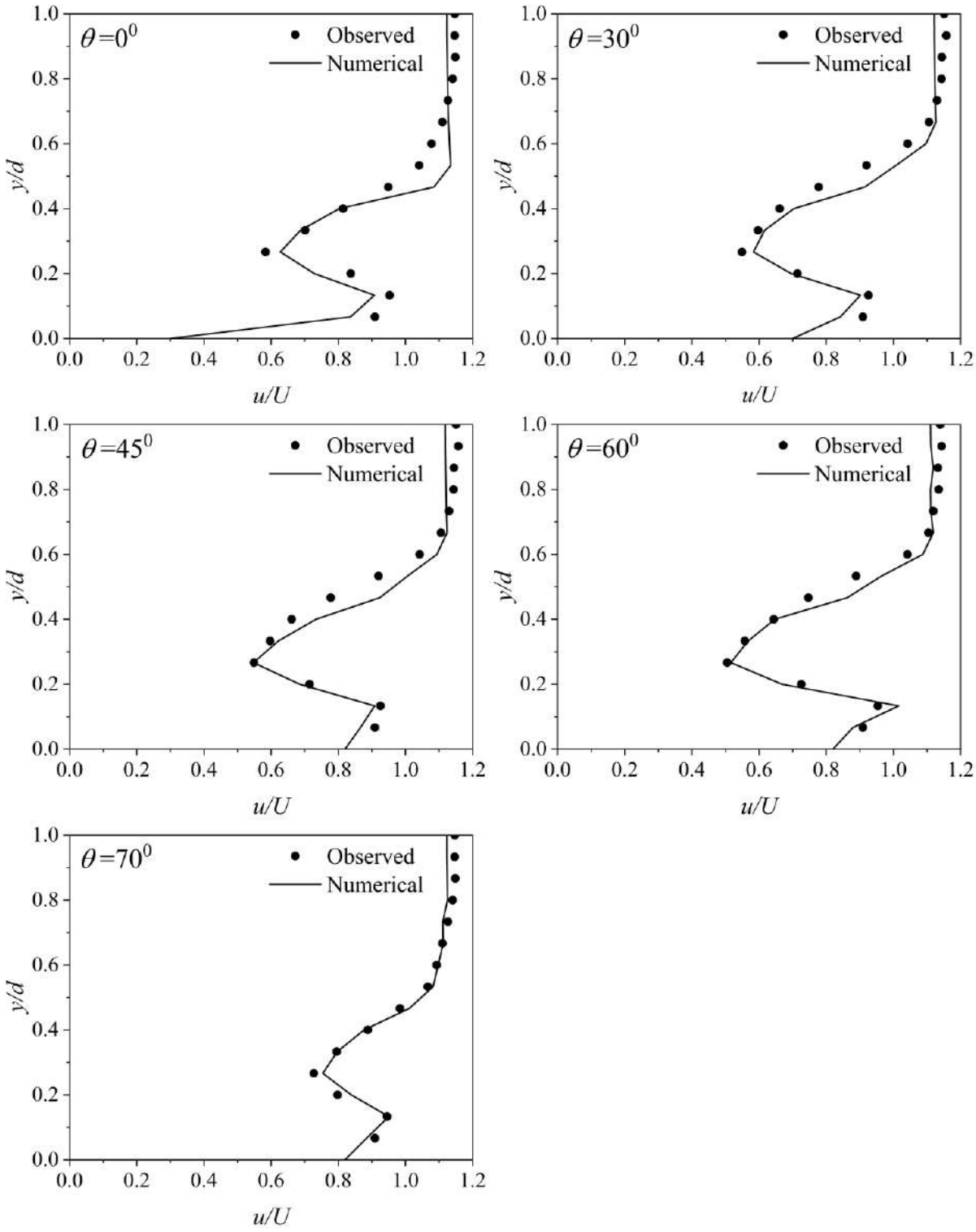

Fig. 6.5a Comparison of stream-wise velocity in vertical direction observed from experiments and numerical simulation for various bevel vane at x = 3H for Q = 0.082 m^3/s, H = 0.045 m, α = 20º

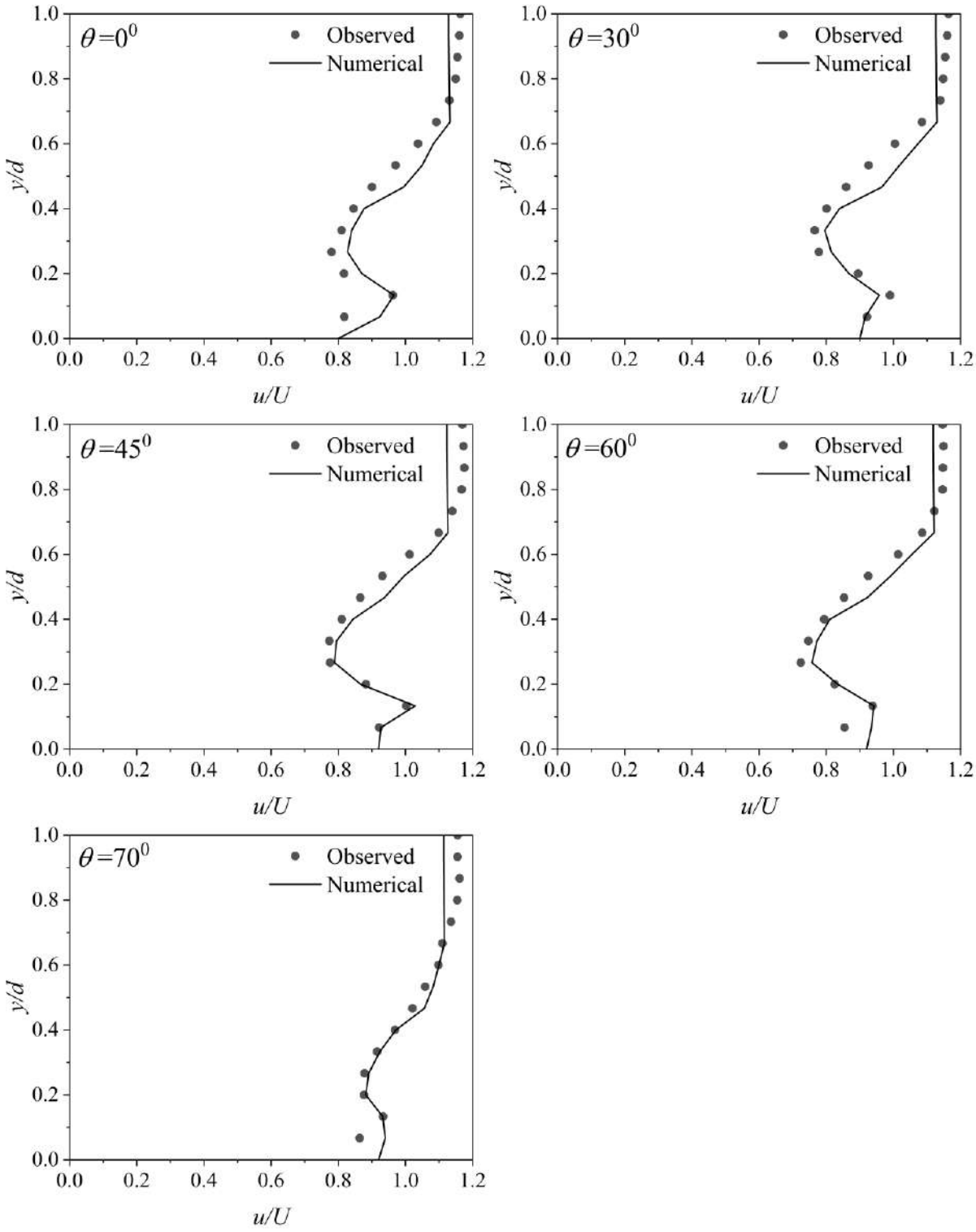

Fig. 6.5a Comparison of stream-wise velocity in vertical direction observed from experiments and numerical simulation for various bevel vane at x = 8H for Q = 0.082 m^3/s, H = 0.045 m, α = 20º

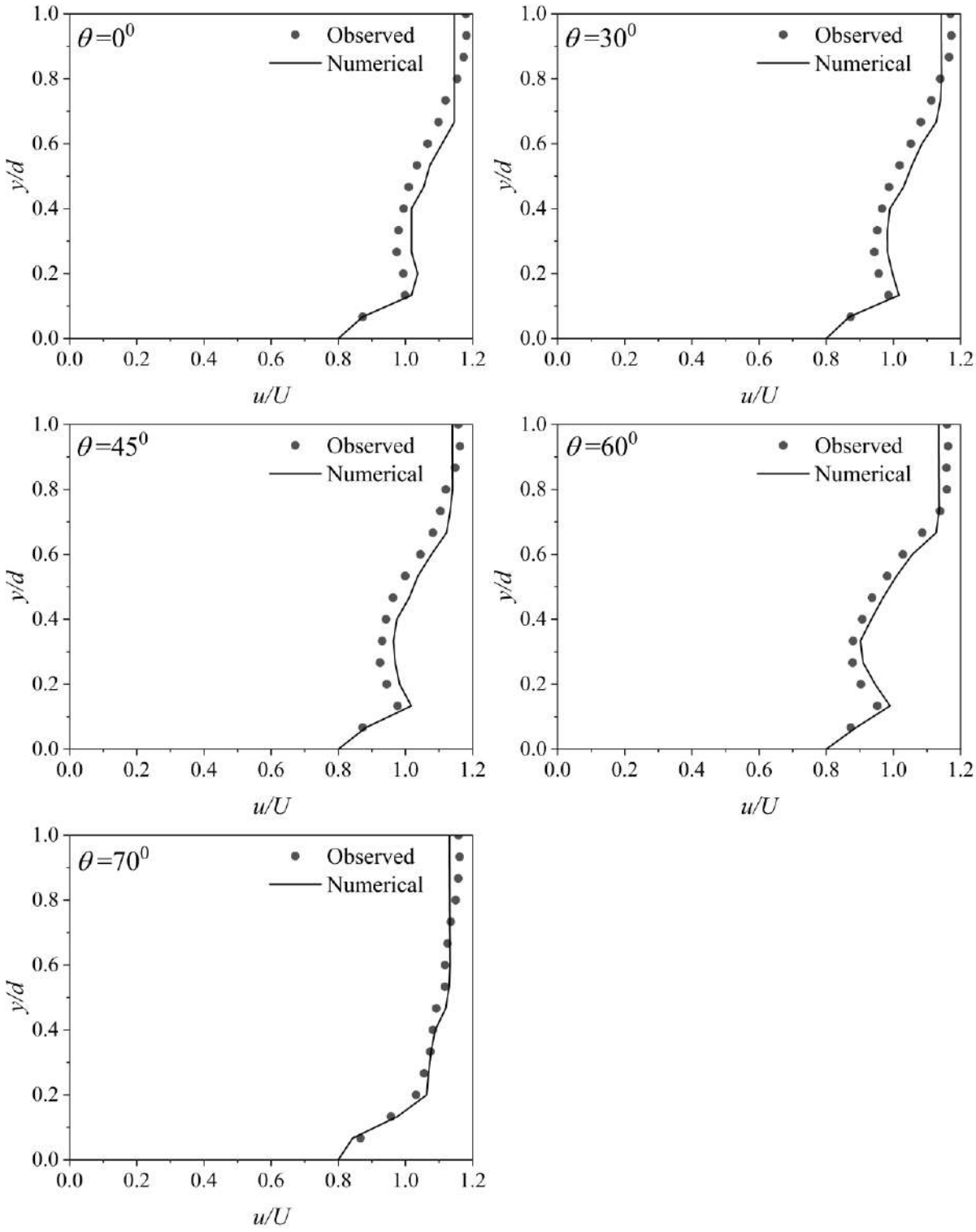

Fig. 6.5a Comparison of stream-wise velocity in vertical direction observed from experiments and numerical simulation for various bevel vane at x = 20H for Q = 0.082 m^3/s, H = 0.045 m, α = 20º

Table 6.1 Comparative error analysis of the numerical and observed streamwise velocity

Bevel angle	Simulated stream-wise velocity								
	3H plane			8H plane			20H plane		
	R^2	MAE	RMSE	R^2	MAE	RMSE	R^2	MAE	RMSE
0º	0.962	0.0235	0.0319	0.976	0.0220	0.0275	0.991	0.012	0.015
30º	0.973	0.0212	0.0281	0.973	0.0210	0.0260	0.991	0.015	0.016
45º	0.971	0.0211	0.0289	0.980	0.0186	0.0220	0.993	0.015	0.017
60º	0.979	0.0182	0.0247	0.984	0.0168	0.0208	0.991	0.014	0.015
70º	0.995	0.0090	0.0109	0.991	0.0109	0.0142	0.995	0.009	0.010

6.3 FLOW PATTERN AROUND SUBMERGED VANE

6.3.1 Flow Field

As per Odgaard & Wang (1991a), the oblique orientation of the vane angle results in a pressure differential between its two sides, inducing an upward flow component on the pressure side and a downward flow component on the suction side. The vane produces a tip vortex that propagates downstream, consequently altering the shear-stress field. From Fig. 6.6, it can be seen that a large spiraling motion was seen downstream of submerged vane. Leading edge was responsible for the generation of vortical structure by accelerating the flow around it, similar observation was observed by Odgaard and Wang (1991). As illustrated in Fig. 6.6, the leading edge of the submerged vane plays a critical role in initiating the formation of vortical structures by accelerating the flow around it. Similar observations were reported by Odgaard and Wang (1991a), and Wang and Odgaard (1993), who noted that this flow acceleration near the leading edge generates a high-velocity zone accompanied by a negative pressure gradient. This pressure differential leads to flow separation at the vane tip, resulting in the formation of vortices, which they referred to as tip vortices. Figure 6.7 illustrates the direction of the circular (helical) flow generated downstream of the submerged vane. The anticlockwise orientation of the vane with respect to the main flow induced a clockwise rotational circulation in the downstream region. Tan et al. (2005) further explained that the flow over a submerged vane behaves similarly

to that over a weir; it plunges over the vane, accelerates the near-bed flow, and subsequently regenerates vortical structures. A comparable phenomenon was observed in the present study, where a streamline was seen plunging over the vane, accelerating as it lifted, and then merging with the vortex sheet originating from the flow separation at the leading edge.

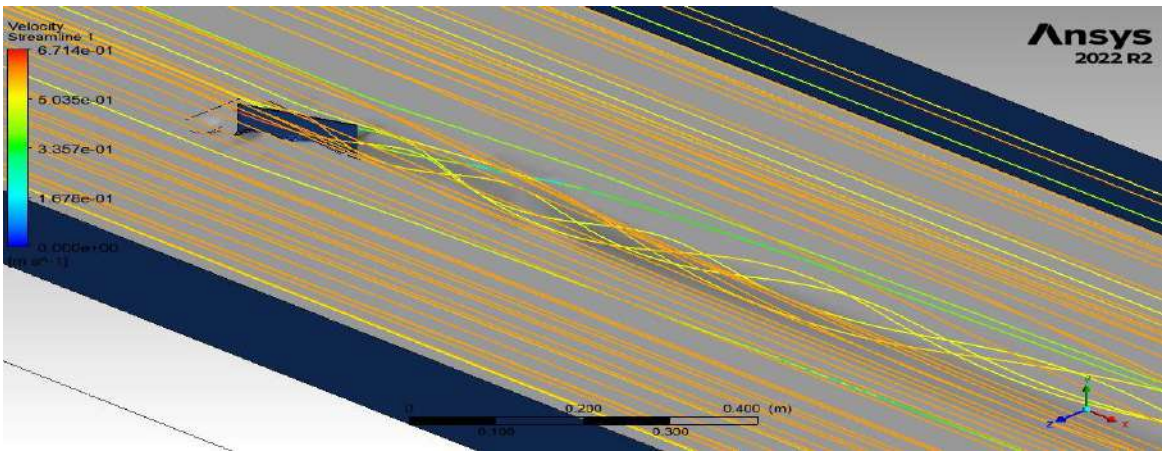

Fig. 6.6 Flow pattern downstream of a submerged vane by using streamline for Q= 0.082 m^3/s, H = 0.045 m, α = 20º and θ = 0°

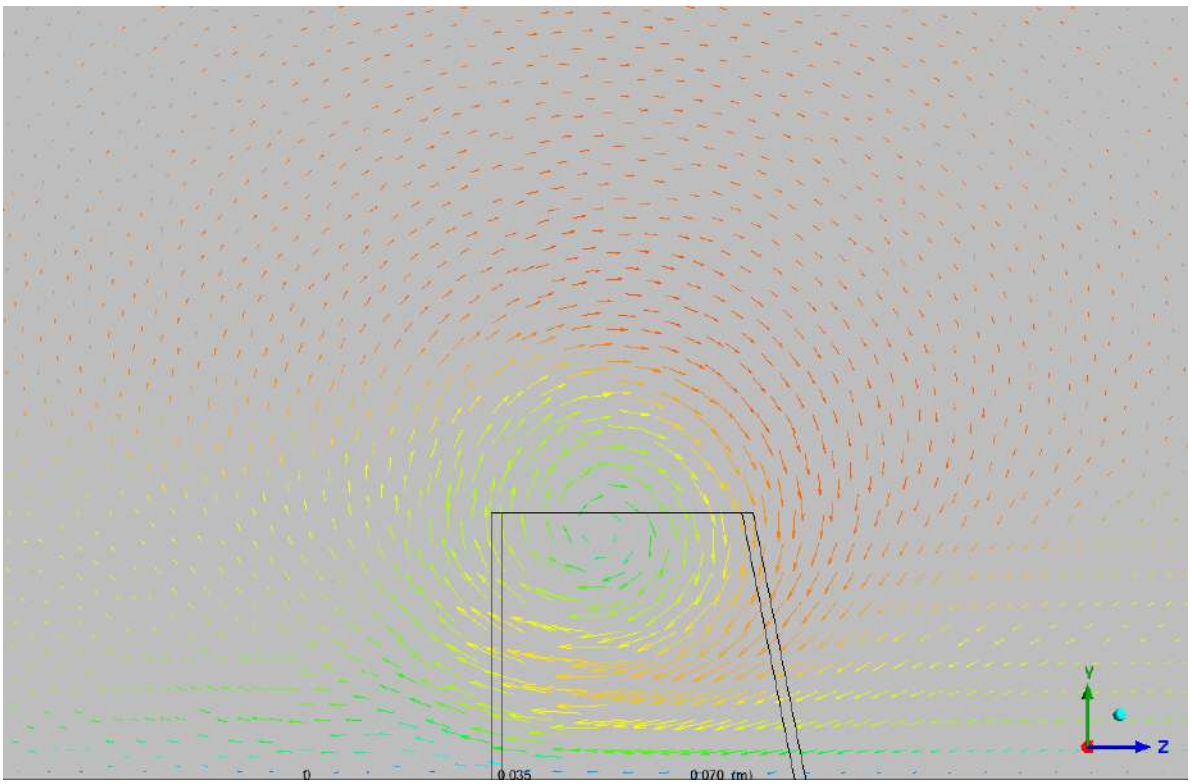

Fig. 6.7 Flow pattern downstream of a submerged vane by using vector for at x = 8H for Q = 0.082 m^3/s, H = 0.045 m, α = 20º and θ = 30°

6.3.2 Pressure Around Vane

Figures 6.8 (a–e) show the pressure field contour around the submerged vane for different bevel angles (a) Simple rectangular vane (θ = 0°); (b) θ = 30°; (c) θ = 45°; (d) θ = 60°; and (e) θ = 70° in the x–z planes at z = 0.02 m, under Q=0.082 m3/s, H = 0.045 m, α = 20º. Due to a small angle of attack with the flow, there arise a vertical pressure gradient on two surfaces of the vane. The front face encountering the incoming flow is referred to as the pressure side, while the opposite face is known as the suction side. Due to this pressure gradient, the pressure increasing from bottom to top on the low-pressure side, decreasing from bottom to top on the high-pressure side which cause an upward velocity component along the pressure side, while on the suction side there is a downward velocity component. It generates the vortex which modify the near-bed flow pattern and redistribute the bed shear stress and sediment transport within the channel. The simulated contour profiles in the x–z plane indicate that positive pressure is observed on the pressure side, while negative pressure appears on the suction side for all bevel shapes. It is also observed that the pressure gradient decreases with increasing bevel angle and gradually shifts from the leading edge toward the trailing edge.

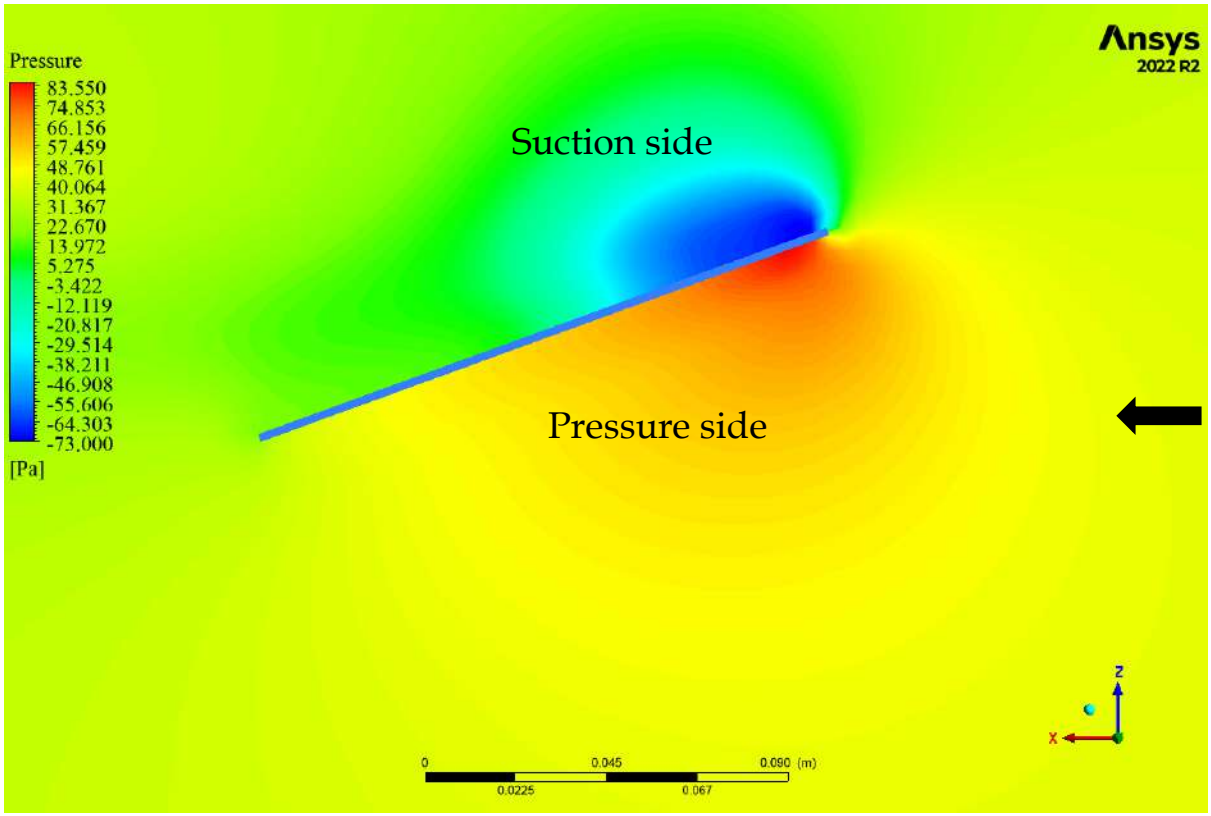

Fig. 6.8a Pressure field around submerged vane in the x–z plane for θ = 0°

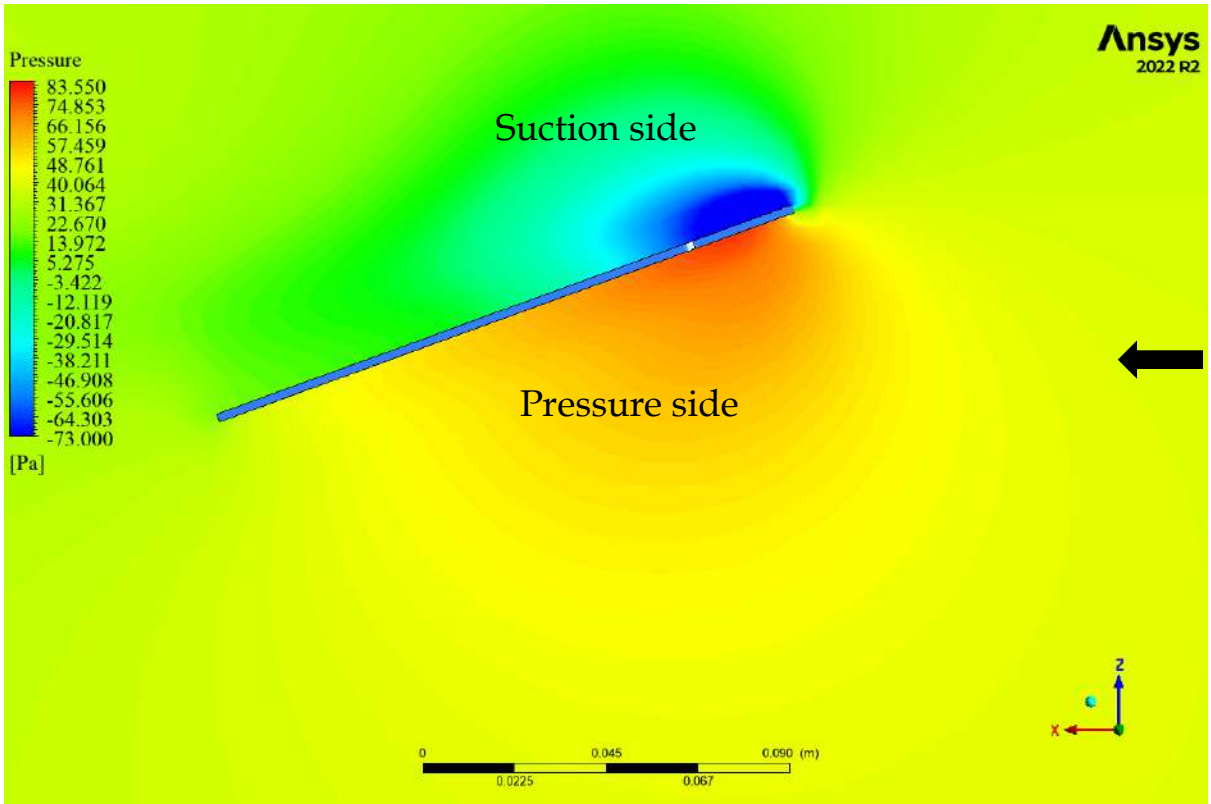

Fig. 6.8b Pressure field around submerged vane in the x–z plane for θ = 30°

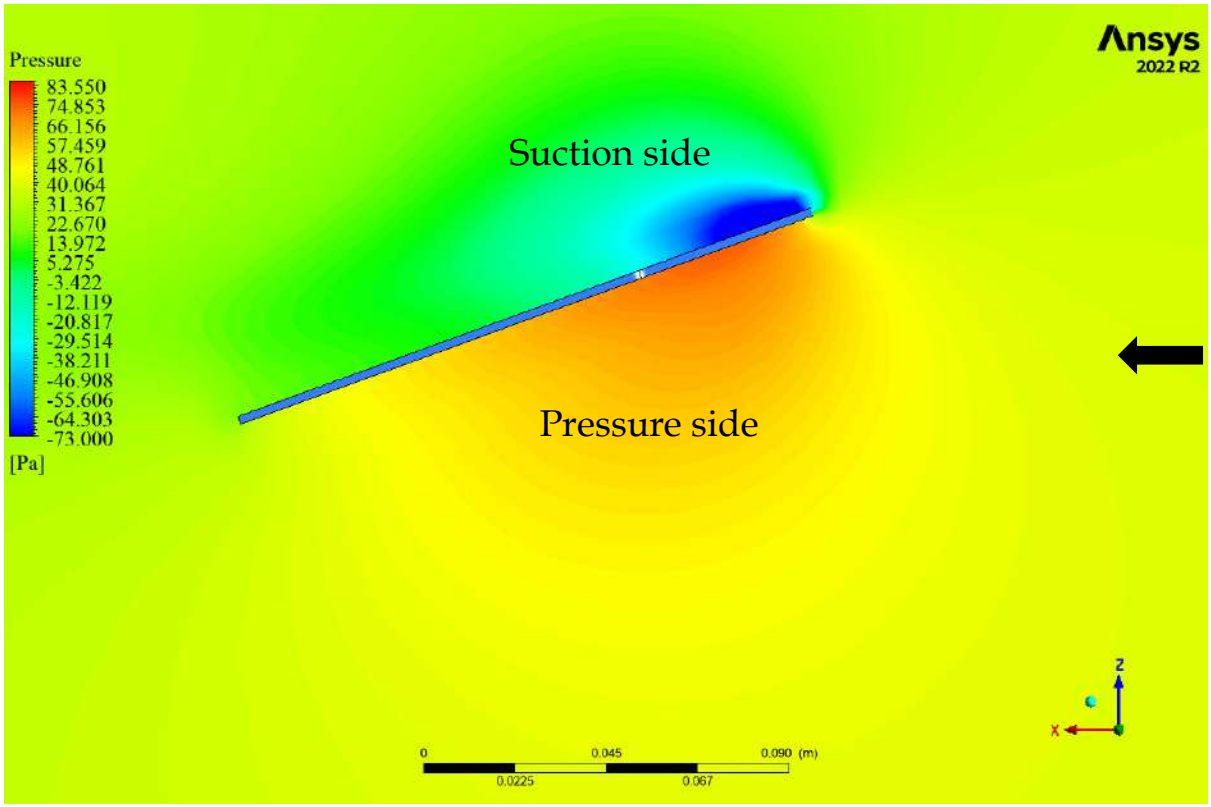

Fig. 6.8c Pressure field around submerged vane in the x–z plane for θ = 45°

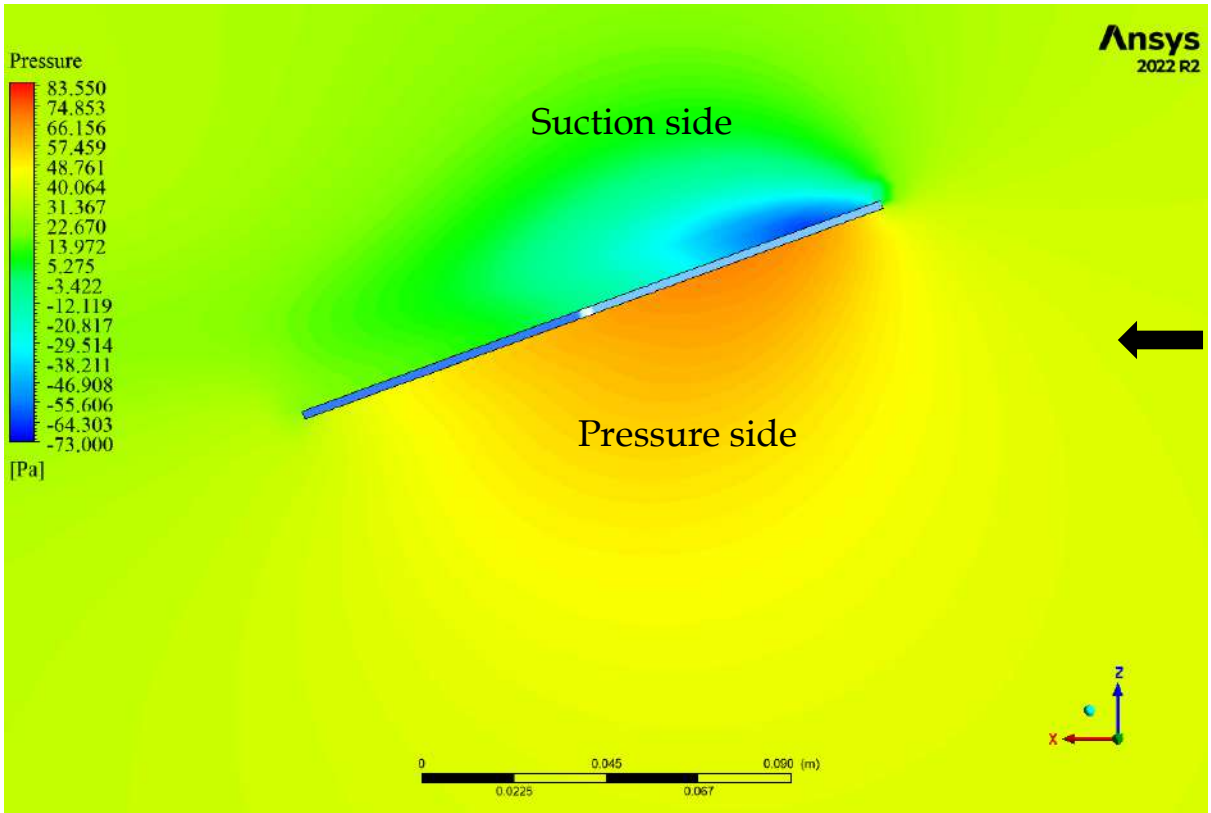

Fig. 6.8d Pressure field around submerged vane in the x–z plane for θ = 60°

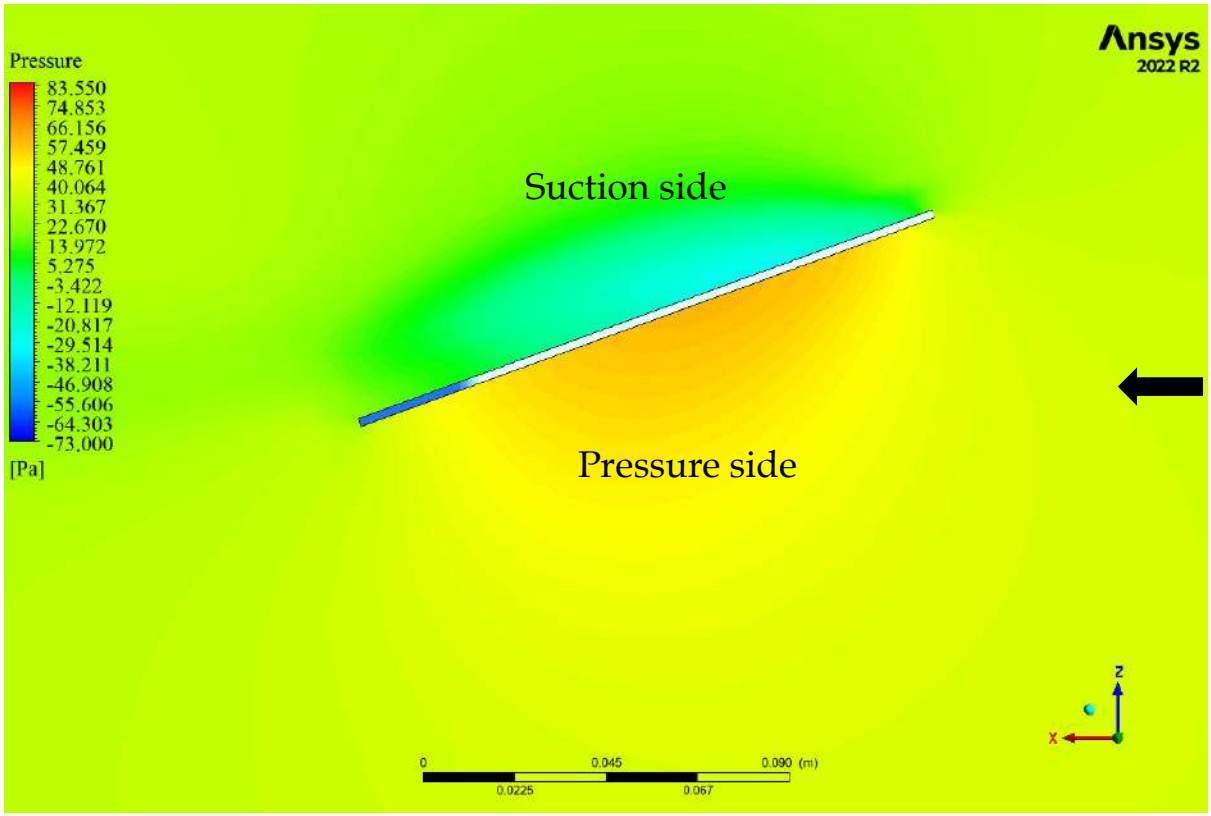

Fig. 6.8e Pressure field around submerged vane in the x–z plane for θ = 70°

6.3.3 Velocity Field

(a) Streamwise Velocity

Figures 6.9 (a-e) shows the observed flow field (u−v) in the x–z plane with velocity magnitude at y=0.02 m under Q=0.082 m3/s, H = 0.045 m, $\alpha = 20^{0}$ for the various shape of bevel submerged vane. Due to the anticlockwise angle of attack, the vane generated the clockwise vortex which travels downstream with the flow and changes the shear-stress field. This vortex induces a high-velocity zone along the right side and a low-velocity zone along the left side of the shear layer. The sediment eroded from the high velocity zone and deposited to the low velocity zone. The reason behind the vane orientation creates a pressure difference, leading to an upward flow on the higher part of the pressure side and a downward flow on the suction side. This interaction generates a primary vortex that propagates downstream of the vane.

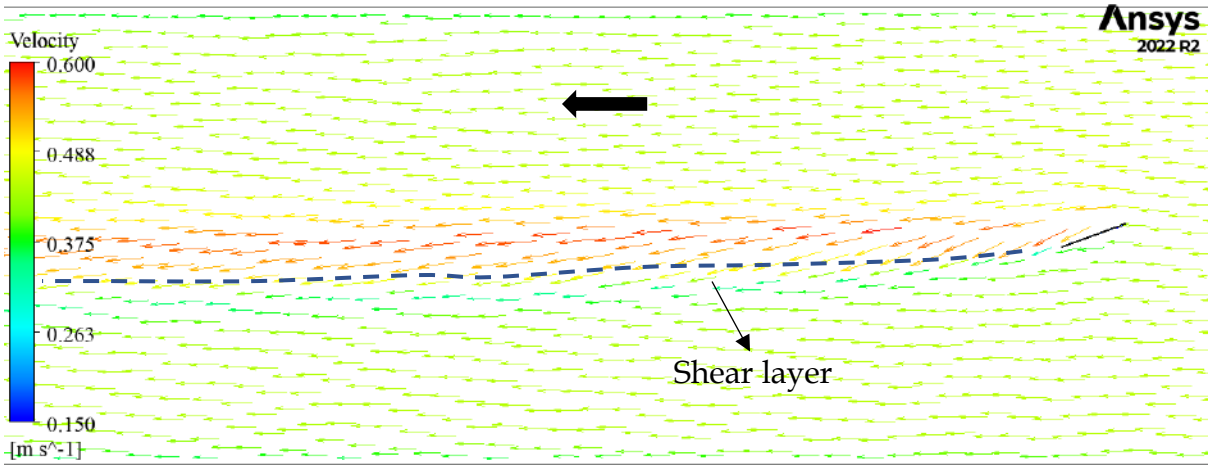

Fig. 6.9a Flow field at x-y plane with velocity colour magnitude for θ = 0°

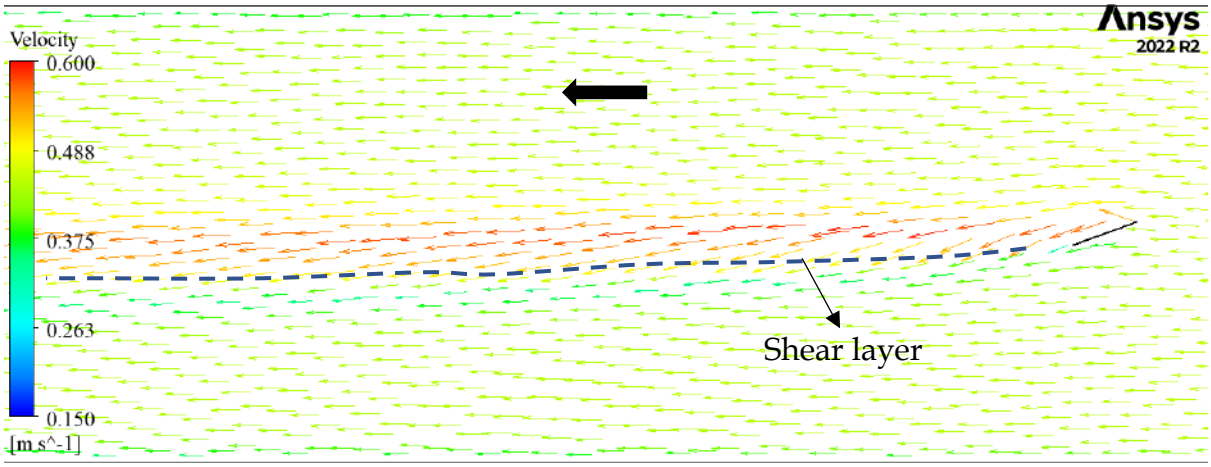

Fig. 6.9b Flow field at x-y plane with velocity colour magnitude for θ = 30°

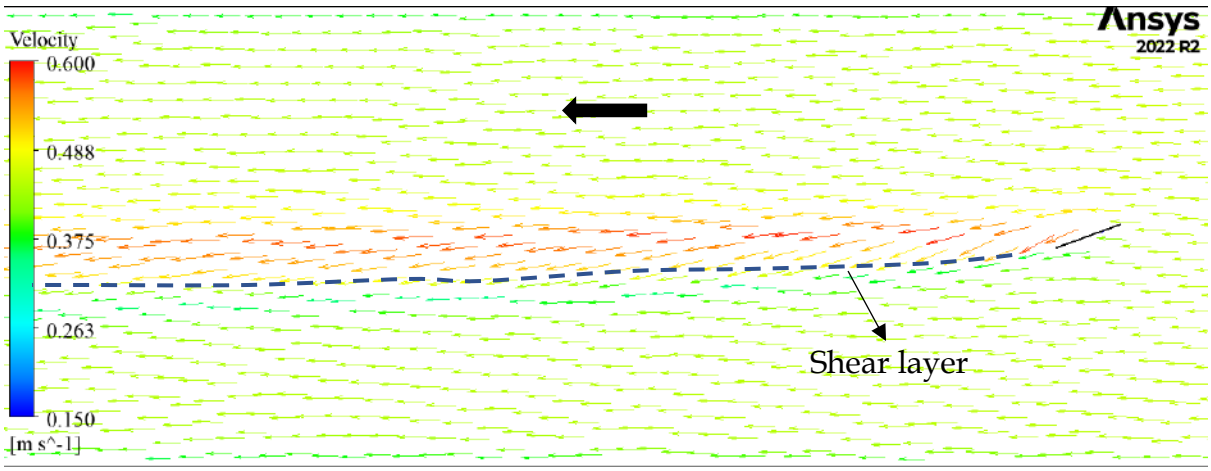

Fig. 6.9c Flow field at x-y plane with velocity colour magnitude for θ = 45°

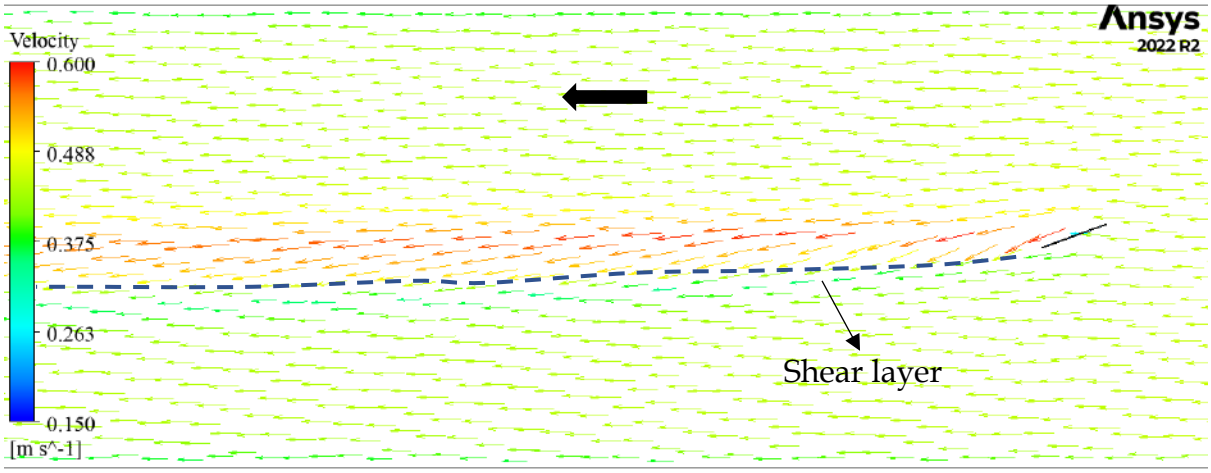

Fig. 6.9d Flow field at x-y plane with velocity colour magnitude for θ = 60°

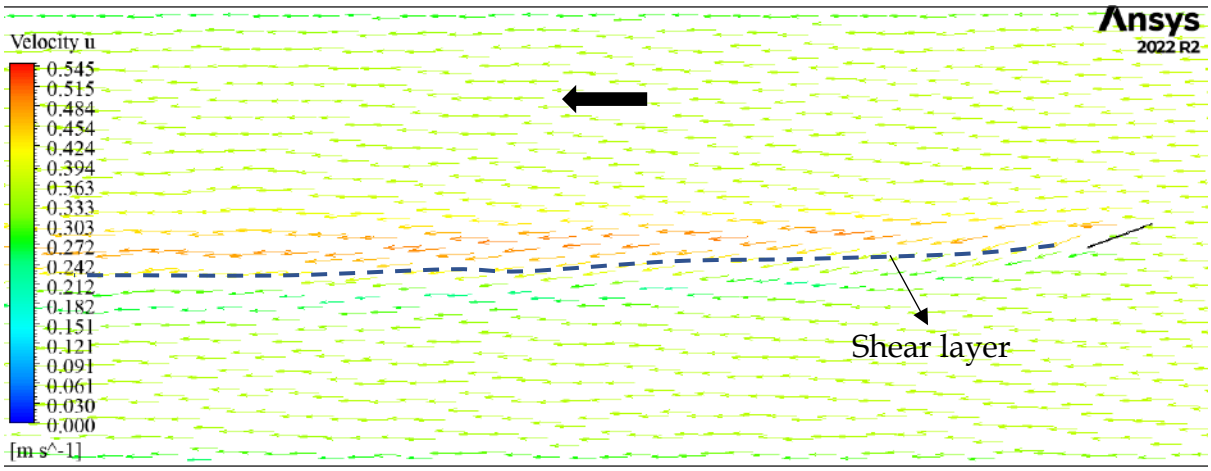

Fig. 6.9e Flow field at x-y plane with velocity colour magnitude for θ = 70°

Figures 6.10 (a-c) presents the velocity field contours downstream of a bevel vane at longitudinal distances of x = 3H, 8H, and 20H. At x = 3H, it is evident that the vane redirects the slower-moving fluid near the bed toward the core flow region on the pressure side. This flow behavior aligns with observations made by Sharma (2016) and Sharma and Ahmad (2019). The upward movement of low-velocity fluid from the bed to the core region leads to a reduction in bed shear stress on pressure side of the vane, which is primarily generated by the near-bed stagnant fluid due to viscous effects (Nezu and Nakagawa, 1993). As more fluid is transported away from the bed, the volume of retarded fluid near the bed decreases, thereby lowering the bed shear stress. This reduction in shear stress subsequently diminishes sediment transport in fluvial systems (Dey, 2016). On suction side, the higher-moving fluid in upper flow

region brought down towards the bed because the vertical velocities are there directed down towards the bed. This phenomenon generates the higher bed shear stress on suction side of the vane. And the large shear stress on the suction side will augment the motion of the sediments in the regions while reduction in sediment movement will occur on the pressure side where bed shear stress is reduced. The observations also indicate that the strength of the circulation diminishes as it travels further downstream from the vane. At the 20H plane, the effects of viscosity have largely dissipated the vortex structure, leaving only a few velocity contours with noticeable curvature. Most regions of the flow appear to have recovered their original undisturbed velocity profile. Fig. 6.10 (a-c) illustrates that for the rectangular vane with bevel angles up to 45°, the circulation remains highly concentrated along the vertical plane at 3H. However, for bevel angles greater than 45°, the circulation begins to spread more significantly in the transverse direction.

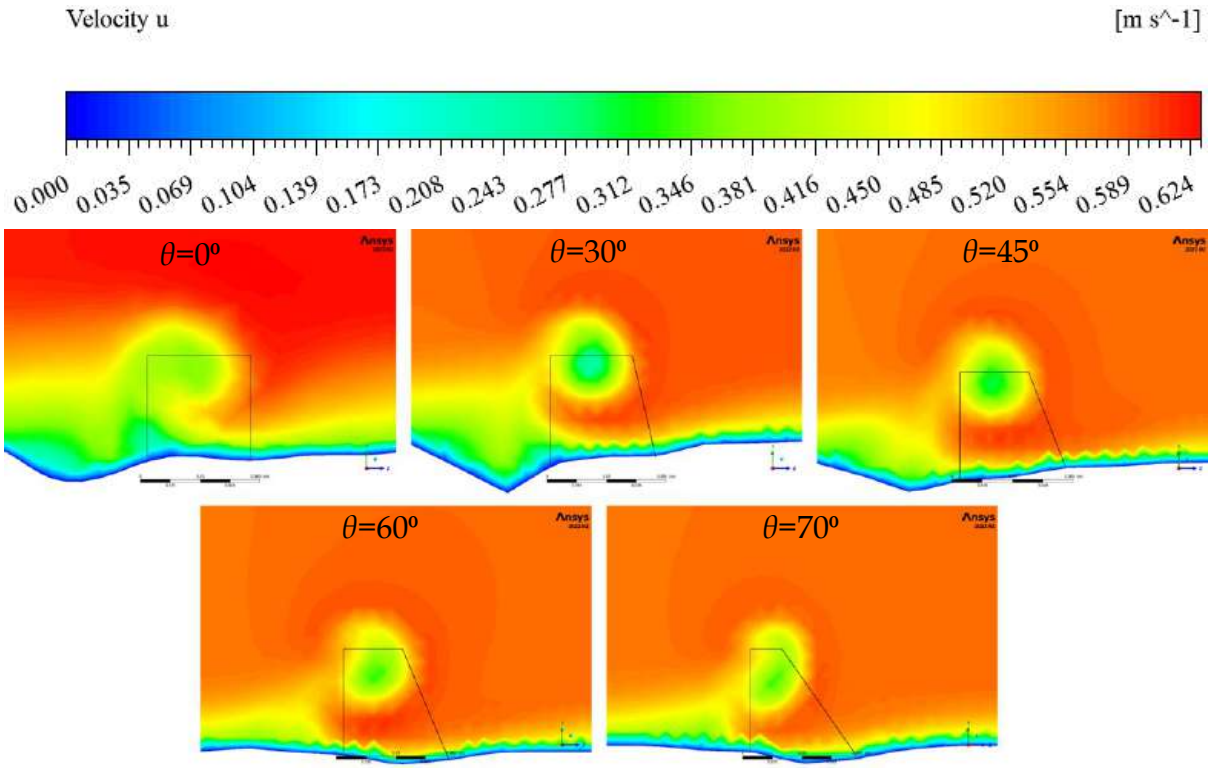

Fig. 6.10a Computed cross-sectional stream-wise velocity contour profile for all vane with different bevel angles at x = 3H for Q = 0.082 m^3/s, H = 0.045 m, α = 20º

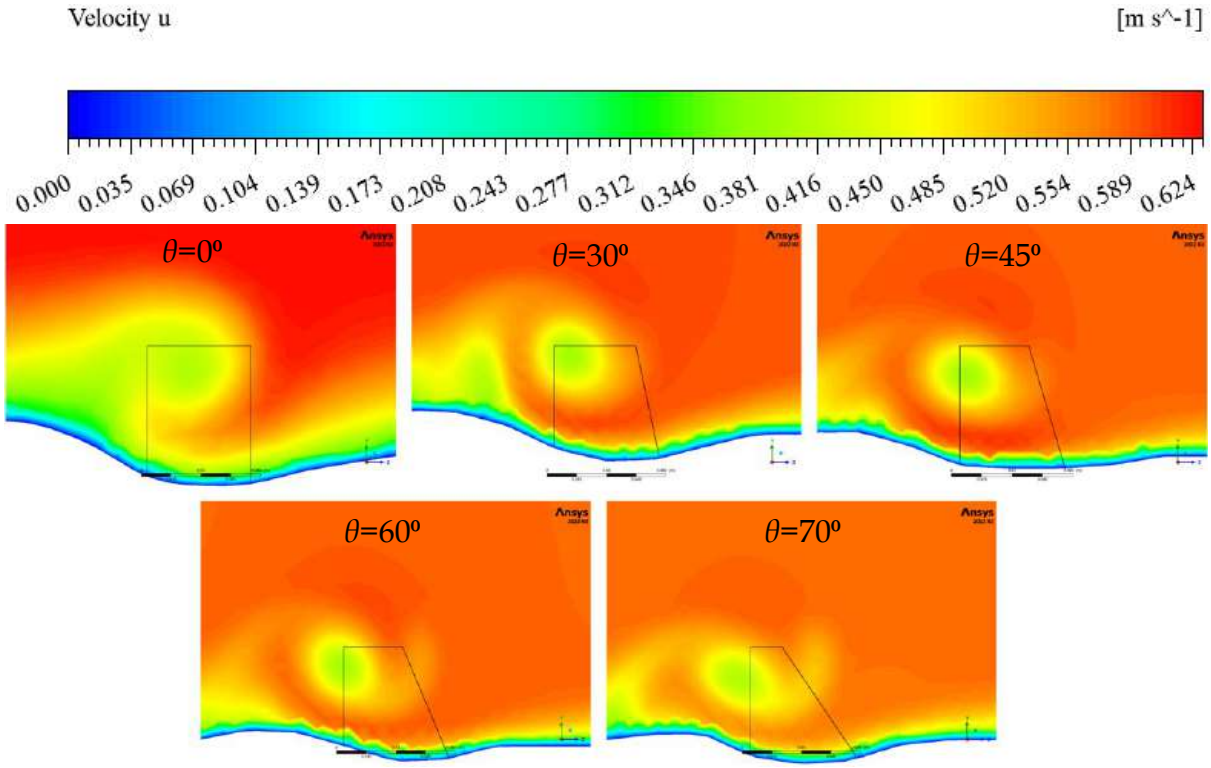

Fig. 6.10b Computed cross-sectional stream-wise velocity contour profile for all vane with different bevel angles at x = 8H for Q = 0.082 m^3/s, H = 0.045 m, α = 20º

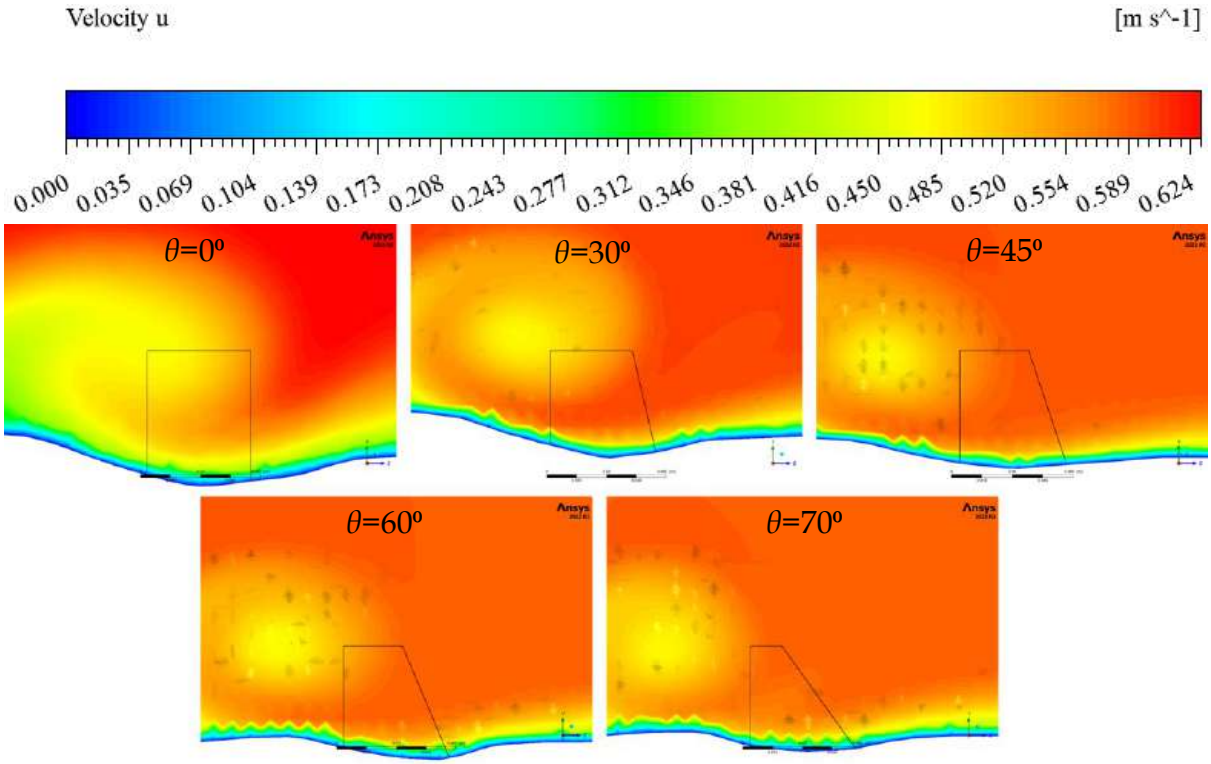

Fig. 6.10c Computed cross-sectional stream-wise velocity contour profile for all vane with different bevel angles at x = 20H for Q = 0.082 m^3/s, H = 0.045 m, α = 20º

(b) Transverse Velocity

Transverse velocity plays a critical role in determining the degree of lateral flow diversion and the strength of secondary currents (Sharma et al., 2016). It is a key factor in the development of transverse bed slopes within river bends, as documented by Zimmermann and Kennedy (1978), Odgaard (1981, 1982), indicating the potential for bed erosion in curved channels. Research by Odgaard and Kennedy (1983) and Odgaard and Mosconi (1987) demonstrated that submerged vanes effectively induce secondary currents with a rotational direction opposite to that generated by the river bend. These vane-induced secondary currents act to counterbalance the bend-induced currents, thereby reducing or preventing erosion. Therefore, it is essential to examine the influence of bevel angle on transverse velocity, as this parameter significantly governs the generation of secondary currents by beveled vanes. Fig. 6.11 (a–e) show the transverse velocity field contour around the submerged vane for different bevel angles (a) Simple rectangular vane ($\theta = 0°$); (b) $\theta = 30°$; (c) $\theta = 45°$; (d) $\theta = 60°$; and (e) $\theta = 70°$ in the x–z planes at z = 0.02 m under Q = 0.082 m^3/s, H = 0.045 m, $\alpha = 20^0$. A strong transverse velocity was observed at the tip of the leading edge of the rectangular submerged vane, while a higher negative transverse velocity was noted along the suction side of the vane. It was also observed that the transverse velocity at the tip of the leading edge decreases with increasing bevel angle of the vane. Beyond a bevel angle of 45°, the transverse velocity component is significantly reduced. The leading edge of the rectangular vane creates the strong horseshoe vortex at leading edge, which generates the intense scour on the pressure side and decay quickly. Due to the higher suction generated at the leading edge and flow coming from front the horizontal velocity component re-attaches itself at the leading edge forming a field of high vorticity and making a strong leading-edge vortex. Figure 6.12 shows that the transverse velocity profile along a vertical line extending from the bed to the water level, corresponding to distances of 3H, 8H, and 20H from the center of the vane under Q = 0.082 m^3/s, H = 0.045 m, $\alpha = 20^0$. It can be seen from Fig. 6.12 that there is a linear decrease in the transverse velocity from the bed to a height of 0.1 times depth of flow (h) where the maximum magnitude transverse velocity was observed. After this maximum, a first inflection point was observed in the profile at mid-depth where the

transverse velocity becomes zero and then it increases again until the water surface is reached, going through a second inflection point at 0.50 y/h. A similar trand of transverse velocity in vertical direction also observed by Solanki et al. (2020). The magnitude of transverse velocity up to 45º bevel angle is showed maximum (Fig. 6.12). Thus, this suggests that upto a bevel angle of 45º, the magnitude of vane generated secondary currents was maximum. Further, it increases the bevel angle, which significant reduce the transverse velocity.

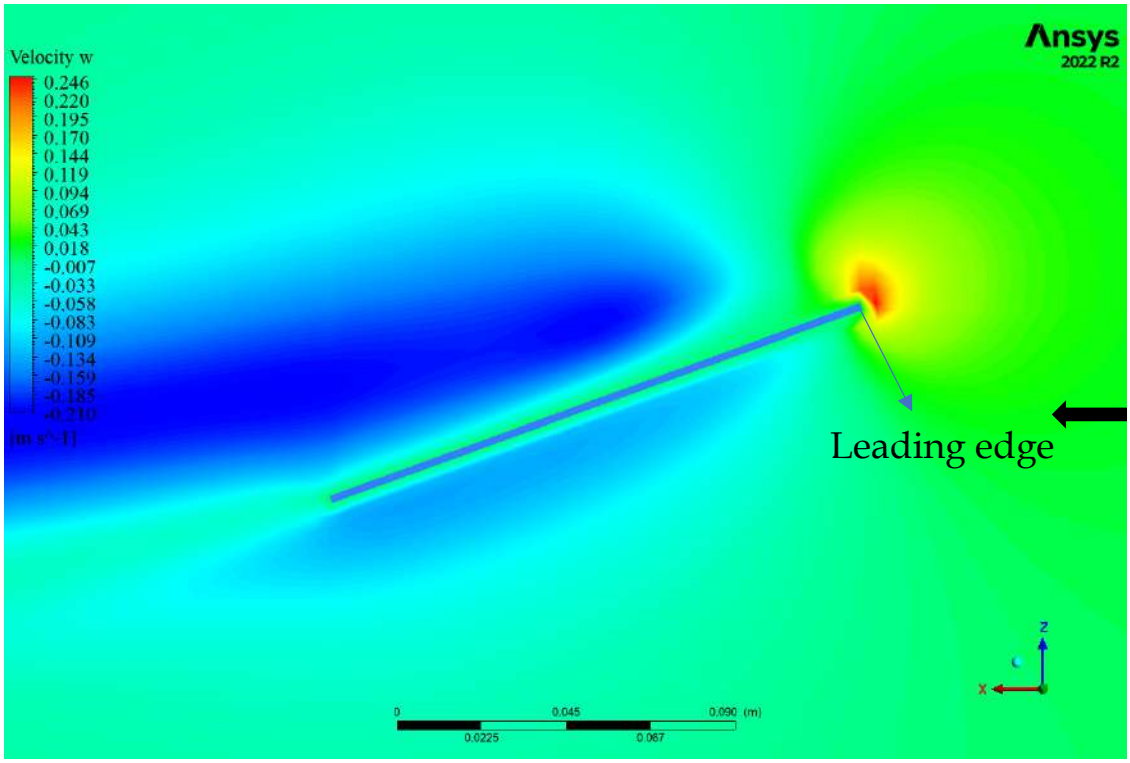

Fig. 6.11a Transvers velocity field at the leading edge of submerged vane in the x–z plane for Q = 0.082 m^3/s, H = 0.045 m, α = 20º, θ = 0º

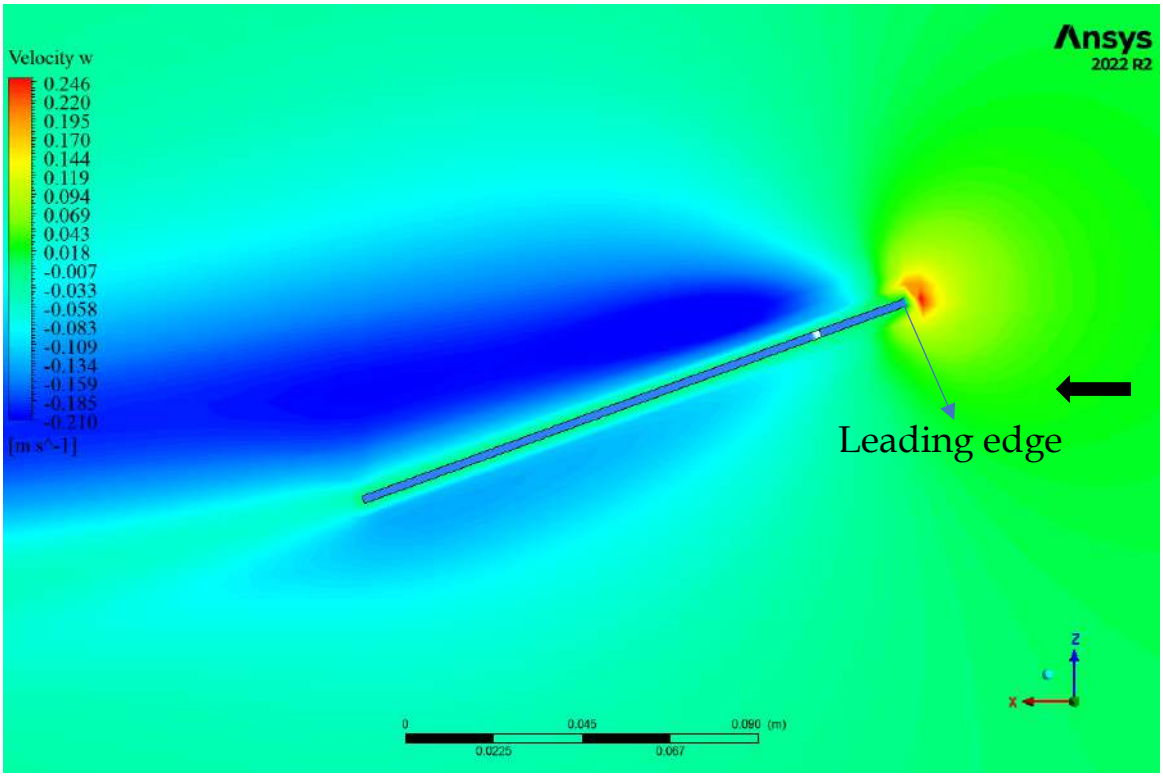

Fig. 6.11b Transvers velocity field at the leading edge of submerged vane in the x–z plane for Q = 0.082 m^3/s, H = 0.045 m, α = 20º, θ = 30º

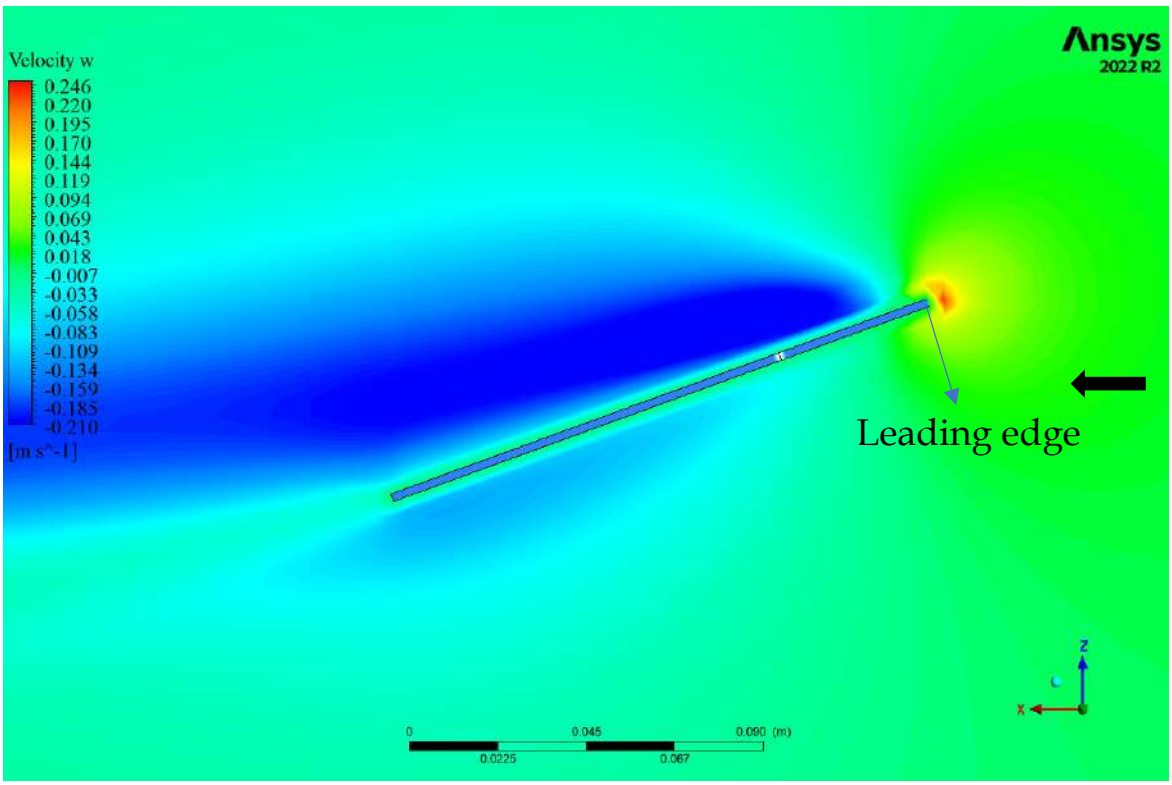

Fig. 6.11c Transvers velocity field at the leading edge of submerged vane in the x–z plane for Q = 0.082 m^3/s, H = 0.045 m, α = 20º, θ = 45º

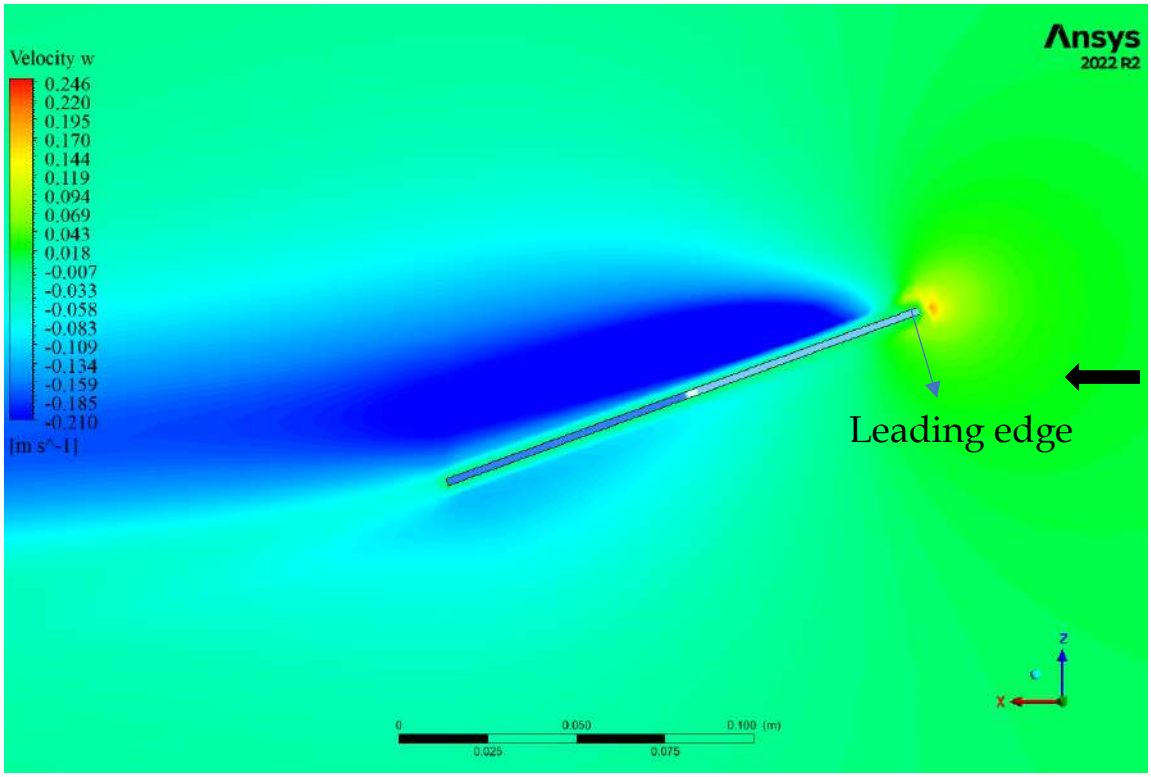

Fig. 6.11d Transvers velocity field at the leading edge of submerged vane in the x–z plane for Q = 0.082 m^3/s, H = 0.045 m, α = 20º, θ = 60º

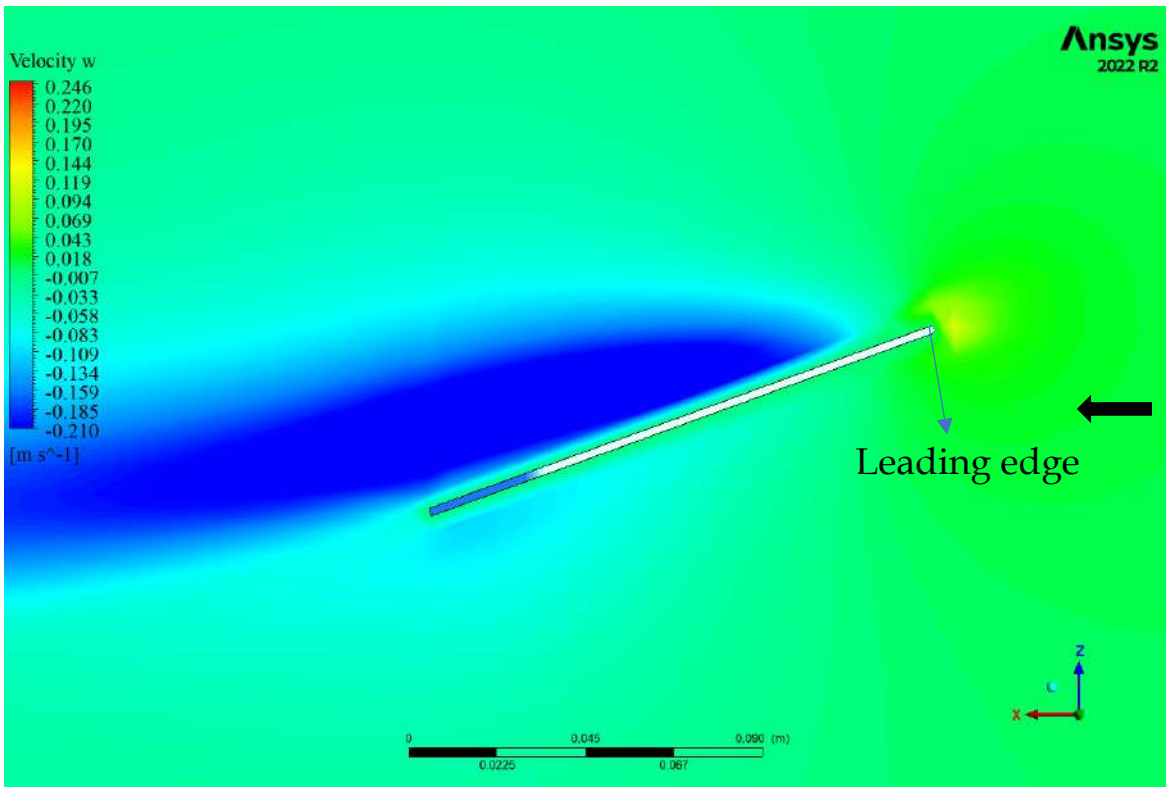

Fig. 6.11e Transvers velocity field at the leading edge of submerged vane in the x–z plane for Q = 0.082 m^3/s, H = 0.045 m, α = 20º, θ = 70º

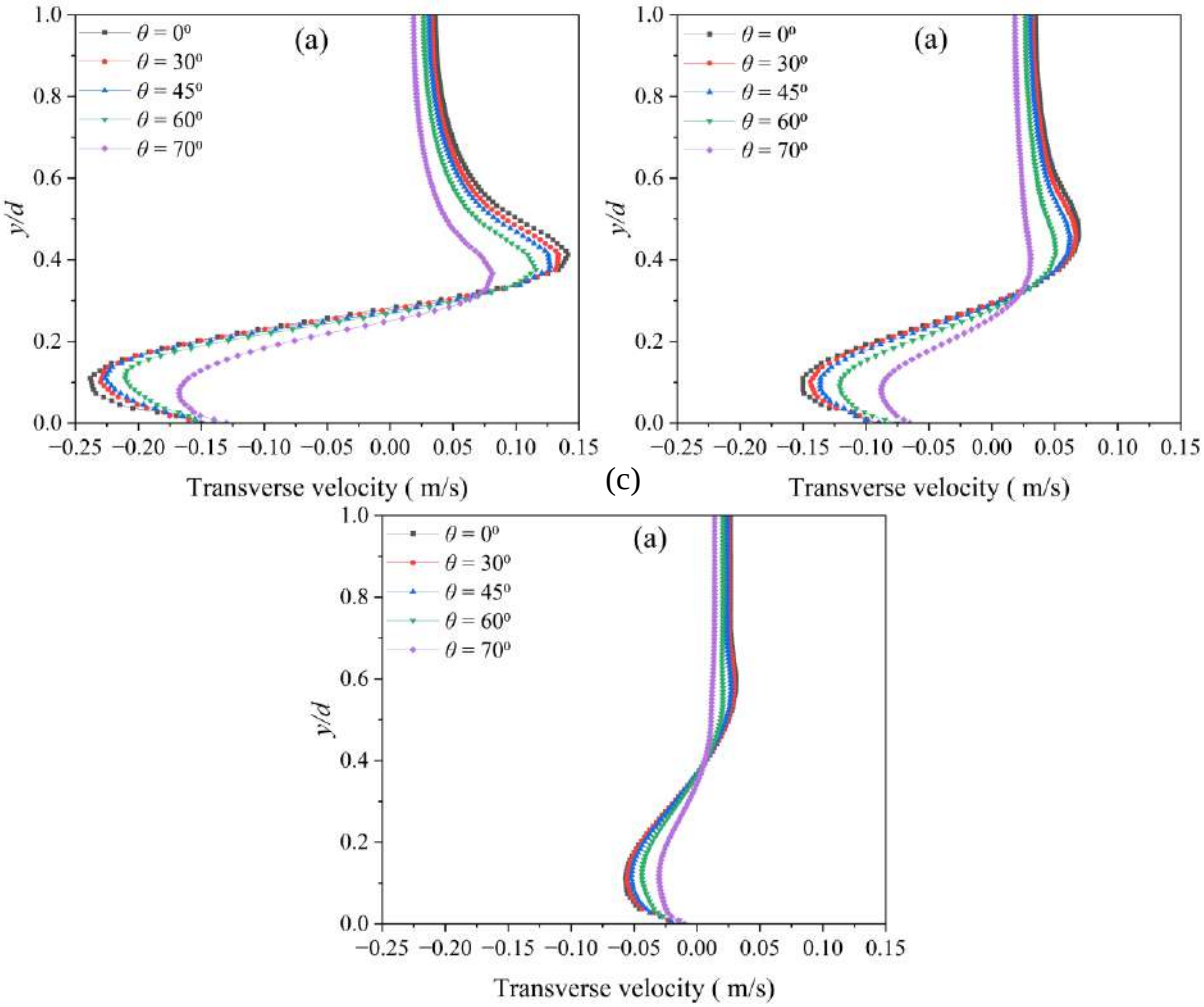

Fig. 6.12 Comparison of transverse velocity for various shape of bevel submerged vane at (a) x = 3H; (b) x = 8H & (c) x = 20H, for Q = 0.082 m^3/s, H = 0.045 m, α = 20°

6.3.4 Vorticity

When a flow passes a submerged vane, the vorticity is generated, which alters the flow direction. The vorticity is generated at the vane's edges and carried downstream with the fluid flow. Vorticity measurements were conducted at the midpoint of the channel domain to abolish the influence of the flow surface and walls on the assessment of vorticity. The lift coefficient (C_L) encompasses both vortex and potential lift generated by flow, where vortex lift relies on flow and potential lift influenced by the form of

the vane (Polhamus, 1966). The potential lift coefficient ($C_{L,P}$) for the condition of zero leading edges can now be determined by (Gupta et al., 2007):

$$C_{L,P} = K_p \sin\alpha\cos^2\alpha \tag{6.6}$$

Also, the derived equation for the vortex lift coefficient ($C_{L,V}$) is

$$C_{L,V} = K_V \cos\alpha \sin^2\alpha \tag{6.7}$$

And,

$$K_V = (K_P - {K_P}^2 K_i)\frac{1}{\cos\theta} \tag{6.8}$$

Here, K_p is the normal force slope, α is the angle of attack, $K_V = (K_P - {K_P}^2 K_i)\frac{1}{\cos\theta}$, $K_i = \frac{\partial C_{Di}}{\partial C_L^2}$, and θ is the bevel angle at the leading edge. Equation 6.8 indicates that with the increase in θ, K_V will increase, and hence C_L will also increase. So, for the increased C_L, the lift force will also increase linearly. For a vane with a consistent shape, the $C_{L,P}$ remains the same, and then the $C_{L,V}$ increases with the increase in the bevel angle. The lift coefficient includes both potential lift and vortex lift components, where the potential lift is affected by the shape of the hydrofoil and adheres to the Kutta-Joukowski law. As per the Kutta-Joukowski theorem, the lift force exerted on a vane is expressed as stated in (Bertin and Smith, 1979; Solanki et al., 2020):

$$F_L = \rho U \Gamma \tag{6.9}$$

Where, F_L represents the lift force per unit length exerted on the vane, ρ is the density of the fluid, U is the average velocity of the fluid, and Γ represents the circulation generated by the vane. In the present study, cutting the leading edge also decreases the surface area and parameters of the vane. The reduction of the vane area causes a decrease in the lift force per unit length and potential lift. Also, the variation in vorticity is attributed to the F_L produced by the vane. The decrease in the F_L can be explained by the observation that the vortex bound to the hydrofoil is influenced by the perimeter of the hydrofoil. The intensity of the vortex will increase with a larger perimeter of the hydrofoil (Solanki et al., 2020). Additionally, Equation 6.9 reveals a

direct relationship between the F_L and Γ induced by the vane. A decrease in F_L also indicates a decrease in circulation, consequently reducing induced vorticity in the flow as it separates from the trailing edge (Solanki et al., 2020). Figure. 6.13 shows the numerical model simulated vorticity_X along a vertical line extending from the bed to the water level, corresponding to distances of 3H, 8H, and 20H from the center of the vane under Q = 0.082 m^3/s, H = 0.045 m, α = 20º for the various shape of bevel submerged vane. It can be observed that the vorticity is almost the same up to 45º bevel angle (Fig. 6.13). Further, it increases the bevel angle, which reduces vorticity. The primary cause for this reduction is the potential lift surpassing the vortex lift beyond a 45º sweep angle. Due to cutting the leading edge at an angle greater than 45°, the surface area and parameter of the vane reduced significantly, which decreases the vortices at the leading edge. A Kutta-type flow condition is present at the leading edge, but the vortex flow impedes the suction at the leading edge (Polhamus, 1966). The leading edge of the submerged vane plays an important role in initiating the primary vortex. As a result of cutting the leading edge, the flow bifurcates horizontally and along the vertical plane on the inclined leading edge. Because of the increased suction created at the leading edge and the flow approaching from the front, the horizontal component of flow re-attaches itself at the leading edge, forming a region with high vorticity and a strong leading-edge vortex. As the bevel angle increases, the horizontal component of flow also increases, increasing the strength of the leading-edge vortex. As the bevel angle increases, the leading and trailing edges come closer together, leading to an interaction between the vorticities of the leading and trailing edges. This interaction significantly reduces the intensity of vorticity at the leading edge. However, the resultant vorticity increases the flow field area downstream after an interaction. At a 70º bevel angle, the proximity between the edges is significantly reduced, leading to a drastic decrease in vorticity. Figures. 6.14 (a-e) presents the Vorticity field (ω_x) contours downstream of a submerged vane at longitudinal distances of x = 3H, 8H, and 20H for Q = 0.082 m^3/s, H = 0.045 m, α = 20º. At the 3H plane downstream of the vane, a concentrated vortex is observed. However, as the flow progresses further downstream, the vortex gradually weakens. Similar findings were also reported by Odgaard and Spoljaric (1989) and Odgaard and Wang (1991),

whose results indicated that the vortex core is located approximately 0.2 times the vane height below the top elevation of the vane. By the time it reaches the 20H plane, the vortex structure has nearly dissipated, and the flow largely returns to its original state. The vorticity field (ω_x) also reduced after increasing the bevel angle more than 45º angle. The upward and downward flow motions induced by the vane generate vortices that alter both the flow pattern and bed shear stress downstream of the structure. The vortex structures formed by beveled vanes with bevel angles greater than 45° differ notably from those generated by rectangular vanes.

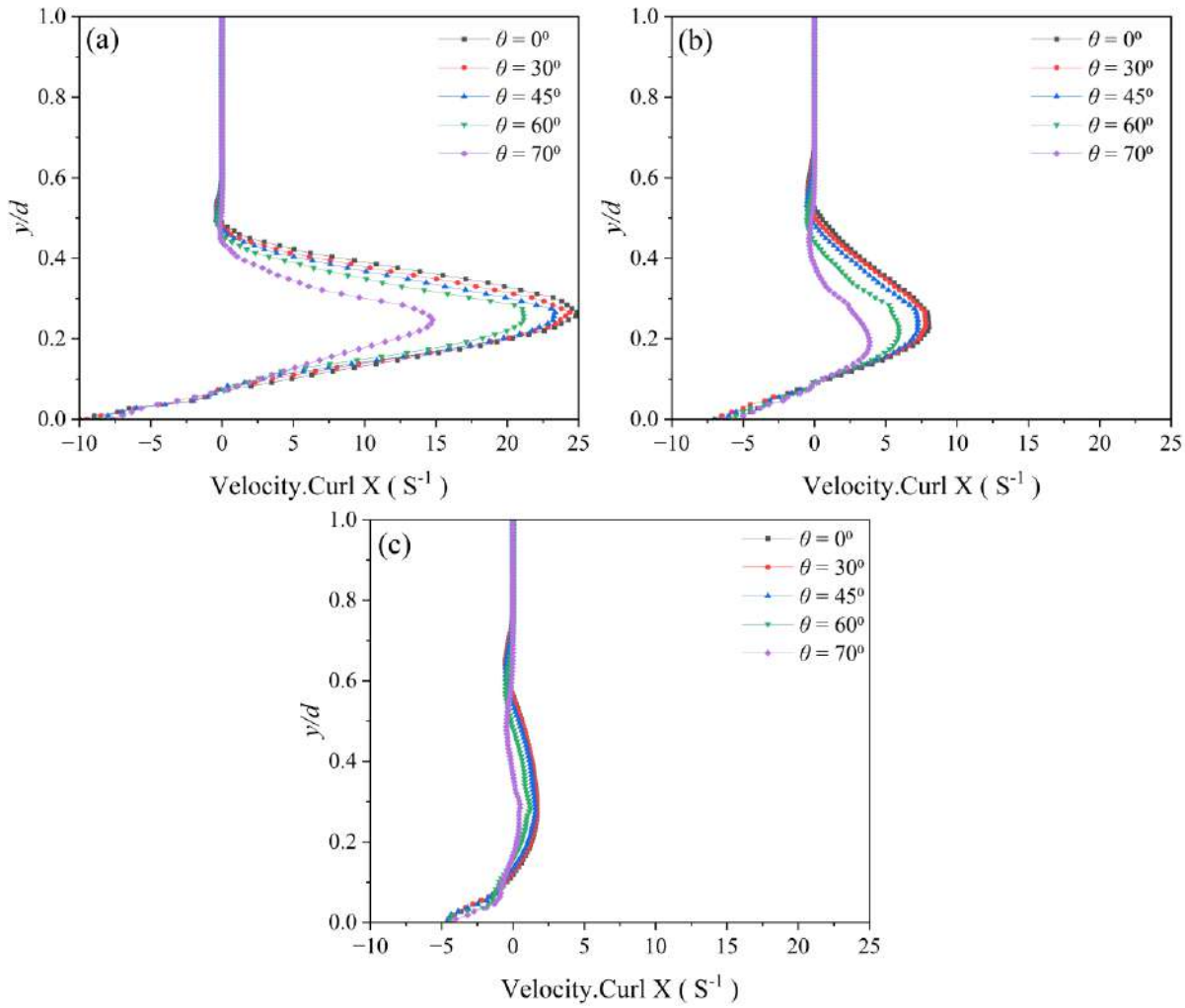

Fig. 6.13 Variation of vorticity_X downstream at vertical direction of the vane

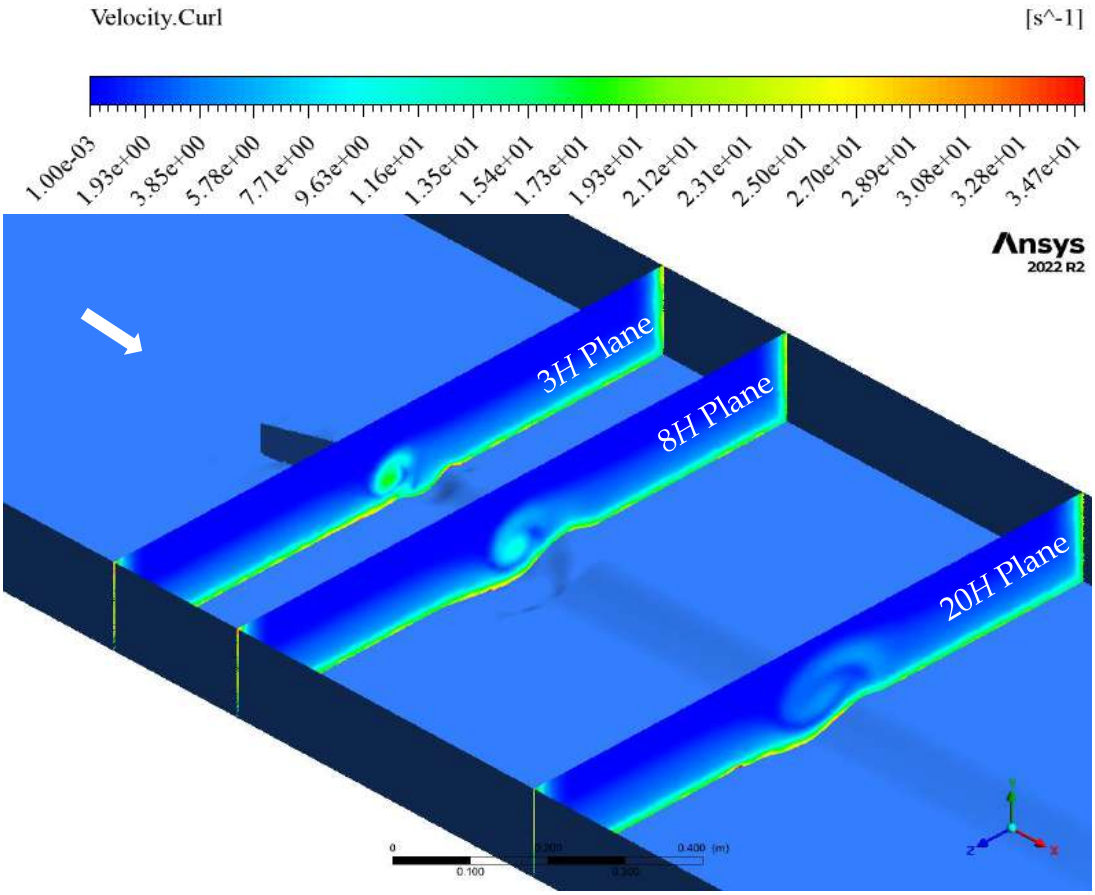

Fig. 6.14a Vorticity field (ω_x) at three planes downstream of vane for $\theta = 0°$

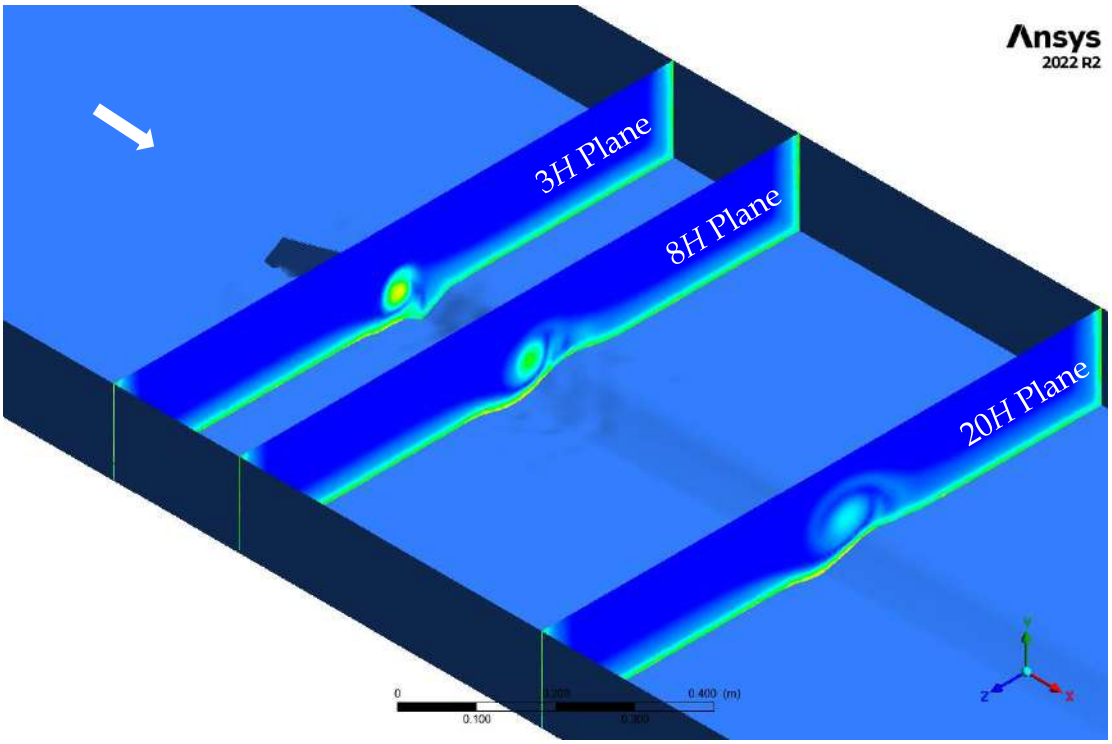

Fig. 6.14b Vorticity field (ω_x) at three planes downstream of vane for $\theta = 30°$

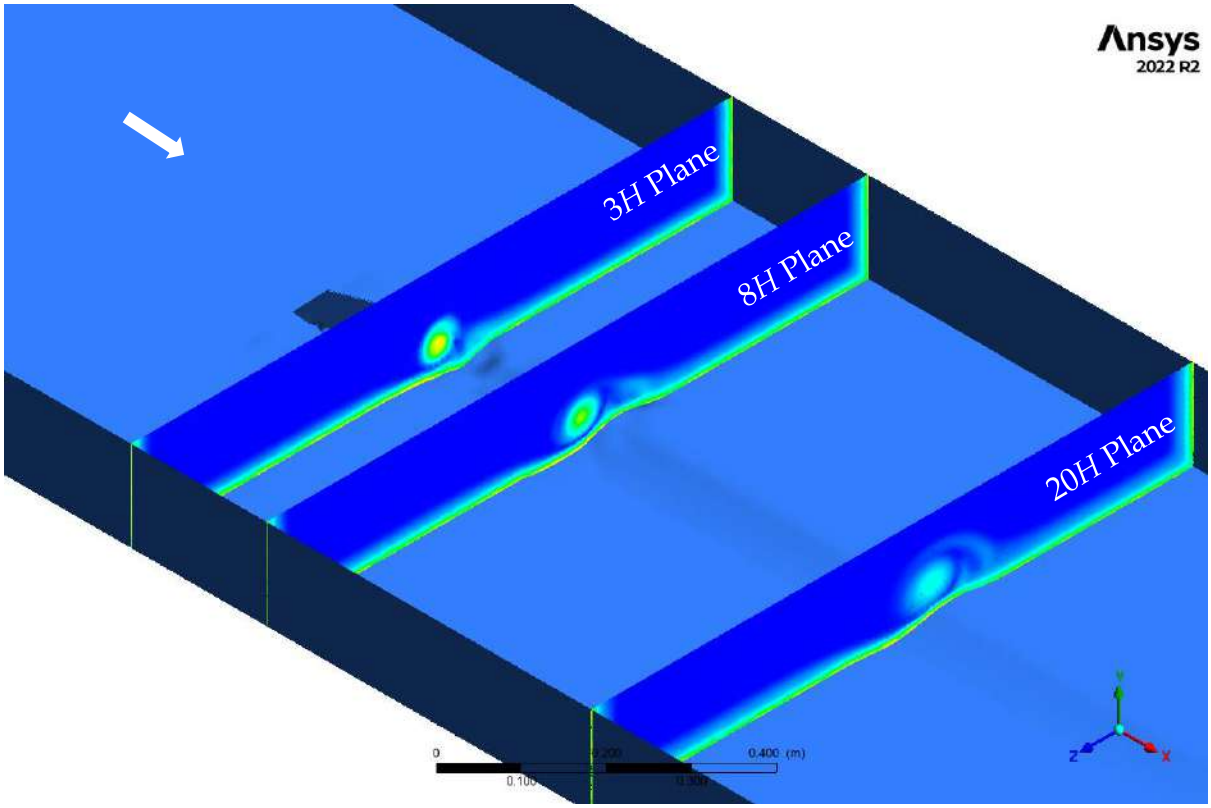

Fig. 6.14c Vorticity field (ω_x) at three planes downstream of vane for $\theta = 45°$

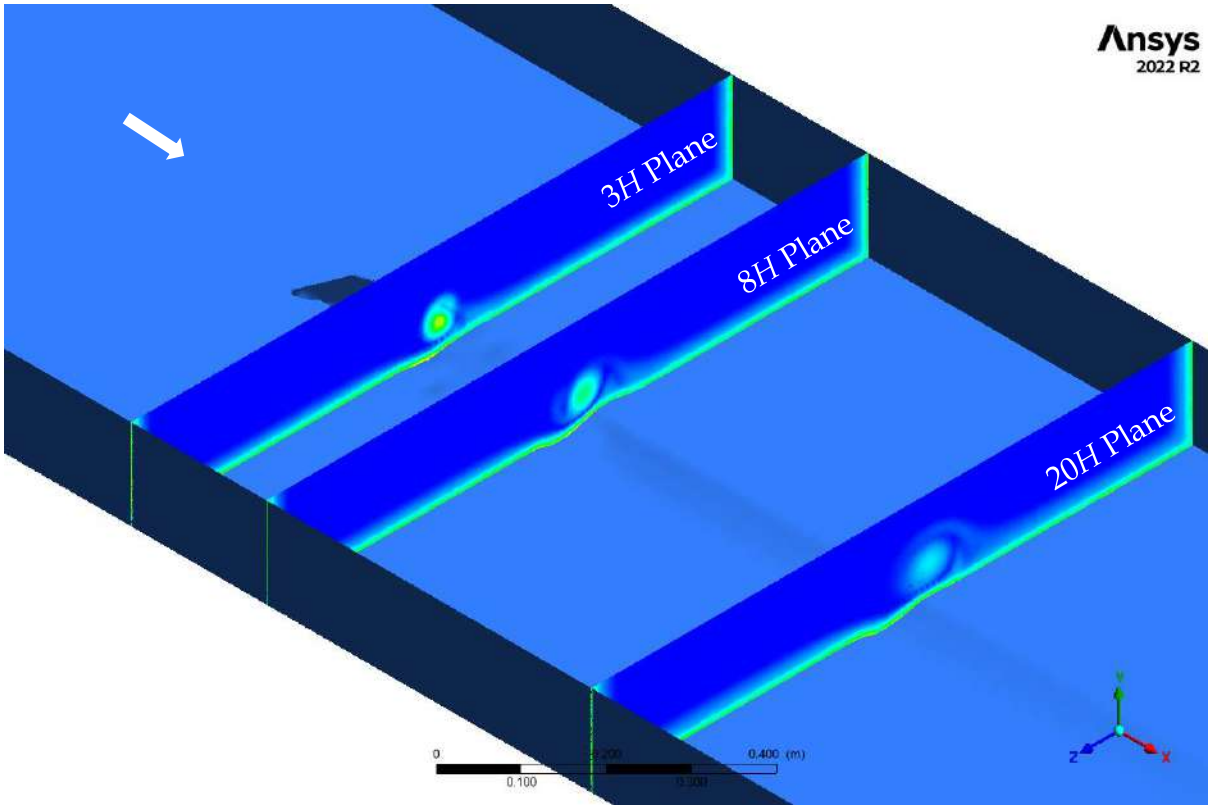

Fig. 6.14d Vorticity field (ω_x) at three planes downstream of vane for $\theta = 60°$

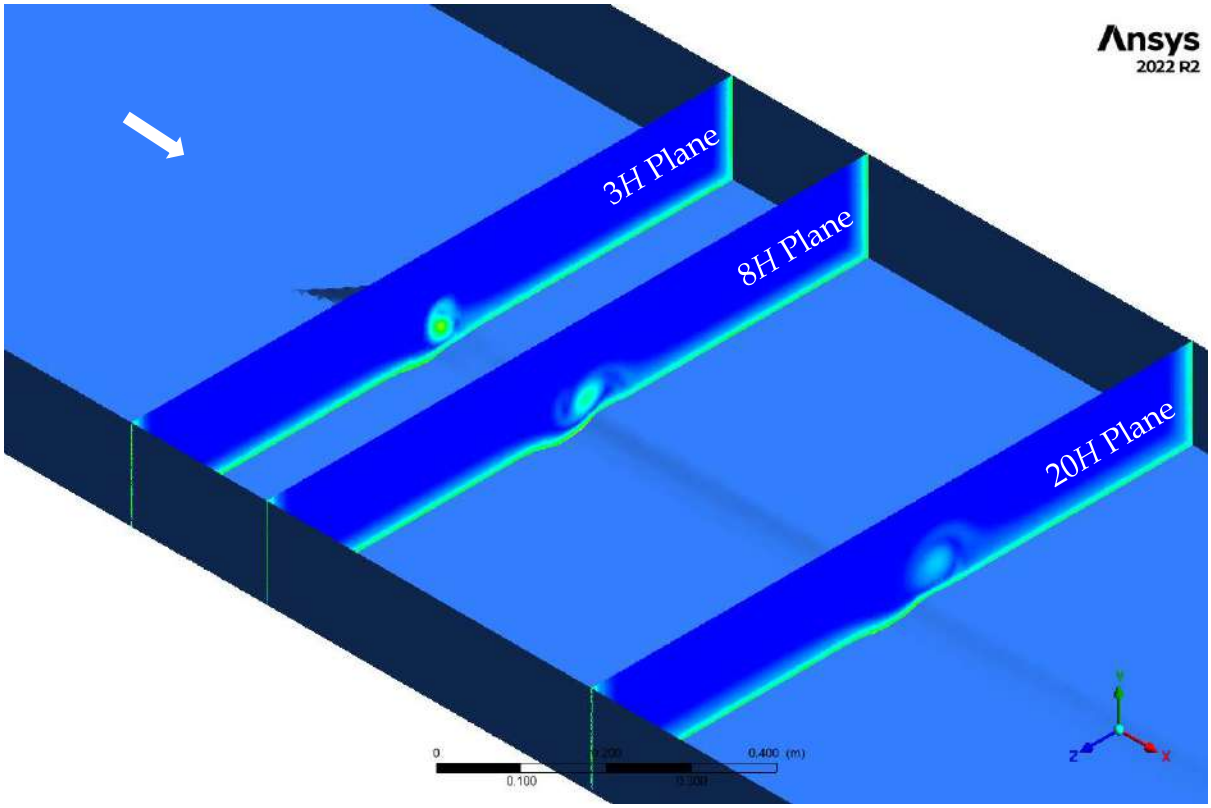

Fig. 6.14e Vorticity field (ω_x) at three planes downstream of vane for $\theta = 70°$

6.3.5 Turbulent Kinetic Energy

Turbulent kinetic energy (TKE) quantifies the kinetic energy associated with turbulent fluctuations as they are transferred across the flow domain through the fluid layers. The mathematical formulations used by FLUENT to compute the turbulent kinetic energy (k) per unit mass, are based on k-ω turbulence scheme proposed by Wilcox (1988). The phenomenon of energy cascading is visualized through contour plots generated along a vertical plane aligned with the center of the vane in the direction of flow. As illustrated in Fig. 15, the spatial distribution of turbulent kinetic energy (TKE) is analyzed within this section, which is specifically chosen to capture the localized turbulence effects induced by the vortex-generating vane. The results reveal that TKE attain peak values in the immediate vicinity of the submerged vane, a similar observation also made by Sharma (2016) and Sharma and Ahmad (2019). These elevated TKE levels are primarily attributed to the intense velocity gradients and fluctuations caused by the vortex generation mechanism. Also, the intensity of TKE is highest for the rectangular vane and decreases with an increase in the bevel angle of

the submerged vane, as shown in Fig. 15, with a significant reduction observed beyond a 45° bevel angle.

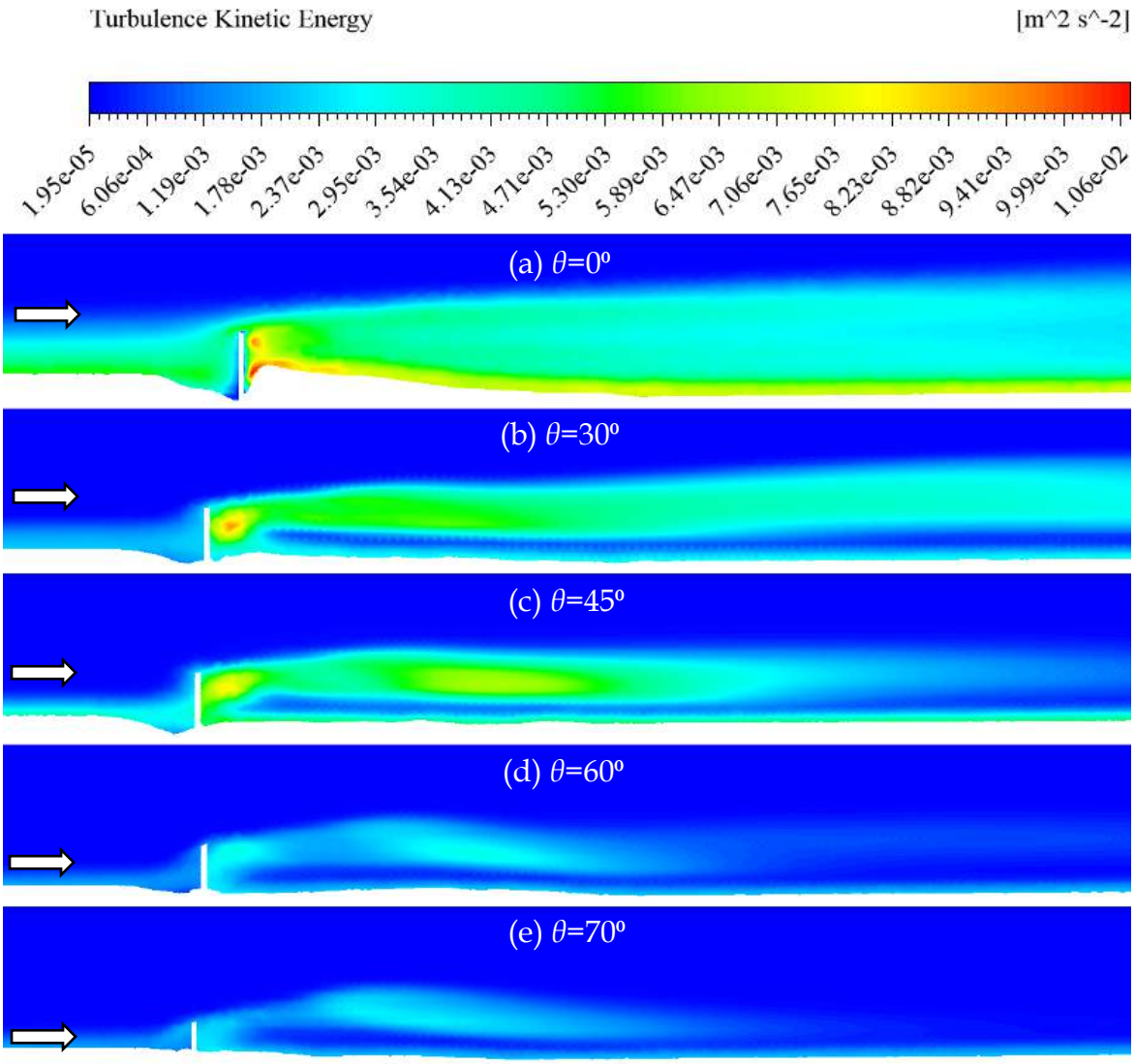

Fig. 6.15 Turbulent kinetic energy contours at vertical x-z plane aligned with the center of the vane in the direction of flow for Q = 0.082 m^3/s, H = 0.045 m, α = 20º for the various shape of bevel submerged vane

Figure 6.16 represents the variation of the TKE along the vertical mid line up to water surface at distances of 3H, 8H, and 20H from the vane center. The submerged vane generates vortices downstream of the vane, which transport the fast-moving upper fluid towards the bed and near bed fluid redirected towards the core flow regions as the vortices propagate through the fluid layers, as earlier discussed. The generation of significant fluctuations within the fluid layers of the core flow region enhances the transport of turbulent kinetic energy (TKE), resulting in a pronounced peak in the

profile. This peak is observed at y/d = 0.21, located very close to the point of vortex inception, as earlier discussed. For 3H plane, the magnitude of TKE profile is maximum for all different shape of bevel submerged vane (Fig. 6.16a) and the rectangular submerged vane creates maximum peak of TKE profile. At 8H plane, the bevel shape up to 45º angle dominance on the TKE fluctuation away from the trailing edge of the vane, shown in Fig. 6.16(b). Figure 6.16(c) shows that at the 20H plane, the TKE profiles of all bevel vanes converging towards each other and the magnitude of the peak is reduced. When the turbulence travel towards downstream of the vane, the viscosity regains its dominance which leads to dissipation of the tip vortices. Furthermore, the TKE generated by the vane remains nearly constant up to a bevel angle of 45°, but decreases significantly beyond this angle.

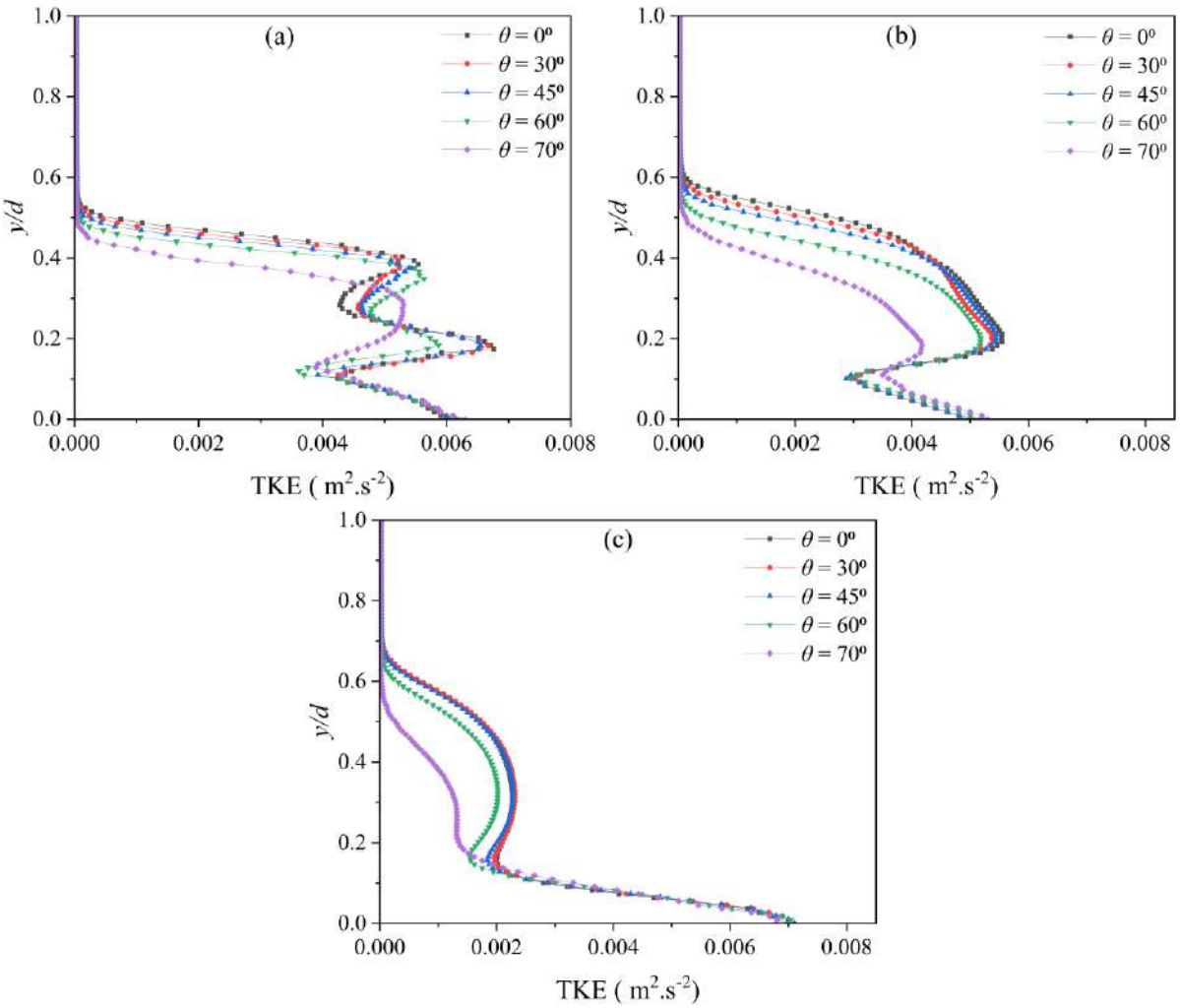

Fig. 6.16 Comparison of TKE for various shape of bevel submerged vane at (a) x = 3H; (b) x = 8H & (c) x = 20H for Q = 0.082 m³/s, H = 0.045 m, α = 20º

6.4 CONCLUDING REMARKS

This chapter presents a CFD-based investigation utilizing the k–ω turbulence model to simulate the flow pattern around submerged vanes and to analyze modifications in the flow field downstream under equilibrium scour conditions. The study includes a comprehensive account of geometry generation, mesh development, boundary condition specification, and physics setup. A numerical approach was employed to optimize the efficiency of various beveled submerged vane configurations in generating vortical structures downstream of the vane. The following conclusion from this chapter can be drawn:

- The analysis of flow field from the CFD simulation were found to be good agreement with the experiment results.
- A large spiraling motion was seen downstream of submerged vane and the leading edge was responsible for the generation of vortical structure by accelerating the flow around it. Also, the orientation of vane anticlockwise along the flow generated the clockwise circulation downstream of the vane.
- The orientation of the vane creates two pressure sides of the vane, a positive pressure is observed on the pressure side, while negative pressure appears on the suction side for all bevel shapes. Observation from simulation study revealed that the pressure gradient decreases with increasing bevel angle and gradually shifts from the leading edge toward the trailing edge.
- A strong transverse velocity was observed at the tip of the leading edge of the rectangular submerged vane, and its significantly decreases with increasing the bevel angle of the vane beyond 45º. The vertical transverse velocity profile revealed that the maximum magnitude transverse velocity was observed from the bed to a height of 0.1 times depth of flow (h).
- Calculation of vorticity downstream of the vane revealed that vorticity is almost the same up to 45º bevel angle, and further increasing the bevel angle significantly reduce the vorticity. The primary cause for this reduction is the potential lift surpassing the vortex lift beyond a 45º sweep angle. Due to cutting the leading edge at an angle greater than 45°, the surface area and parameter of

the vane reduced significantly, which decreases the vortices at the leading edge. Numerical results show that beveled submerged vanes with bevel angles up to 45º do not exhibit a significant reduction in vortex generation efficiency when compared to rectangular vanes.

- Turbulent kinetic energy (k) and its dissipation rate (ε) is attain its peak values in the immediate vicinity of the submerged vane. For rectangular vane, the TKE is maximum and its decrease with increase bevel angle of vane, with a significant reduction observed beyond a 45° bevel angle.

7. APPLICATION OF SUBMERGED VANES: CASE STUDY-1

The optimised shape and size of the submerged vanes have been used to control right bank erosion of the Ganga river downstream of the Bikramshilla bridge at Bhagalpur, Bihar and also to shift the river main course towards left side.

7.1 INTRODUCTION

The Ganga River holds immense cultural, spiritual, and ecological significance in India, serving as a lifeline for millions of people who depend on it for drinking water, agriculture, and livelihoods. The river (or Ganges) originates as Bhagirathi from the Gangotri glaciers in the Himalayas at an elevation 7010 m in Uttarkashi district and flows for a total length of about 2525 km before meeting the Bay of Bengal. The Ganga basin mainly consists of alluvial sediments, which has been collected over most of the Quaternary period building one of the largest alluvial plains in the world. The basin covers 11 States of India, viz., Uttarakhand, Uttar Pradesh, Haryana, Himachal Pradesh, Delhi, Bihar, Jharkhand, Rajasthan, Madhya Pradesh, Chhattisgarh and West Bengal (CWC Report, 2014). The Ganges River system has wide diurnal, seasonal, and annual variations in the sediment load and it varies from 403 to 660 × 106 tonnes/year (Abbas & Subramanian, 1984). Historical satellite imagery over the past 40 years provides a broad idea about the shifting of the river course and changes in its morphology. Earlier,the river exhibited a relatively straight course near the Vikramshila Bridge (extending between Bhagalpur and Ismailpur) until year 1985. Later the river began to meander, leading to significant morphological changes characterized by erosion along the left bank upstream of the Bridge and the right bank downstream of the Bridge. Apparently, the observed changes in the river morphology and courses are influenced by the formation of bends and meanders over the time.

River bends are generally the most unstable segments of the river stretch, where bank erosion is frequently observed. This erosion is primarily influenced by curvature-induced secondary currents induced by centrifugal forces in the bend section. It is also referred to as transverse circulation or helical motion (Kalkwijk & Booij, 1986; Blanckaert & Graf, 2004). These currents arise due to variations in centrifugal

acceleration along the vertical profile of the flow, contributing to the progressive instability of the riverbanks. High-velocity surface currents are driven toward the outer bend of the river, while lower-velocity near-bed currents shift toward the inner bank of the channel (Dey, 2014; Kadia et al., 2024; Stoesser et al., 2010). This dynamic flow pattern leads to increased flow depths and velocities near the outer banks, contributing to channel instability and erosion. Sediment concentration is relatively high in near bed region. This flow pattern transport sediment inward, leading to its deposition near the inner side of the bend. Conversely, the concave bank experiences erosion due to the impact of sediment-deficient fluid originating from the upper layers of the flow (Odgaard & Mosconi, 1987).

A submerged vane can mitigate the secondary flow and its erosive effects on river bends by exerting a torque that counters the centrifugal acceleration induced torque (Odgaard & Mosconi, 1987; Odgaard & Kennedy, 1983). Additionally, the submerged vane structures help in balancing water depths between the inner and outer banks in open-channel flows and in reducing the flow velocity toward the outer bank by redistributing the high- and low-momentum fluids across the channel (Tasar et al., 2023). In recent years, the application of submerged vanes for riverbank protection has significantly increased, primarily due to their cost-effectiveness and ease of installation, thus making them a more effective option than the conventional methods such as dikes and groins. The efficiency and functionality of submerged vanes in sediment management and vorticity generation are largely governed by their shape and dimensions. Previous research has predominantly concentrated on rectangular vanes, as they align with established theoretical frameworks and offer simplicity in fabrication and construction. One significant drawback of using rectangular submerged vanes is the potential risk of structural failure due to local scour occurring near their tips. Significant local scour can lead to the collapse of the outer bank slope in river bends, thereby reducing the effectiveness of submerged vanes as a bank protection measure (Dey et al., 2017). Previous experimental studies have demonstrated that modifying the leading edge of submerged vanes into a beveled shape effectively reduces local scour around the structures (Bejestan & Azizi, 2012;

Mandal & Ahmad, 2024; Mandal et al., 2025). Additionally, incorporating a beveled leading edge on submerged vanes can aid in deflecting floating debris upon contact with the vane and reduced the required construction material which make this cost effective and efficient structure. Beveled submerged vanes have been implemented at a water intake on the Kosi River, Nepal, to minimize sediment entry (Odgaard, 2009).

To the best of our knowledge, the application of bevel-submerged vane for reduction of bank erosion is yet to be investigated thoroughly. Moreover, no prior studies have investigated the effectiveness of submerged vanes for riverbend protection through a scaled physical model study of a major river such as the Ganga. Considering this research gap and the above-discussed challenges at Bhagalpur reach of the Ganga river, the current study aims : 1) to study the morphological changes in the Ganga river at Bhagalpur, Bihar, 2) to conduct physical model study of a reach of Ganga River from 1.0 km (CS-04) downstream to 18 km (CS-18) downstream of the Vikramshila Bridge, and 3) to examine the effectiveness of developed bevelled submerged vanes in reducing the erosion of right bank (outer bank of the bend) and in shifting the main river course toward the left bank.

7.1.1 Study Area & Morphological Changes

The study investigated the morphological changes of a reach of the Ganga River located from Bhagalpur to Ismailpur in Bihar which is stretching from 2 km upstream to 20 km downstream of the Vikramshila Bridge, as shown in Fig. 7.1. Geographical co-ordinates of the area of interest lie between 25°17'16.53" N, 87°0'31.72" E & 25°18'42.99" N, 87°9'40.80" E. Historical satellite images of year 1985, 2010, 2019, and 2024 have been used to study the morphological changes in the Ganga river at Bhagalpur, Bihar. These images and toposheet are shown in Figs. 7.2 (a-d). All river banks of the years 1985, 2010, 2019, and 2024 overlaid on the 1985's Google earth image as shown in Figs. 7.2 (e). Examination of the images reveals that in year 1985, there was a straight channel of the Ganga river from Bhagalpur to Islamabad. In 2010, the right bank of straight channel was eroded and shifted by about 1.5 km towards right side and siltation occurred towards left side of the river. From the year 2010 to 2019,

the river shifted around 3 km towards right bank and then in year 2014, it shifted up to 3.6 km. Historical satellite images reveal that from year 1985 to 2024 the main course of Ganga river between Bhagalpur to Islamabad shifted towards right bank by around 4 km.

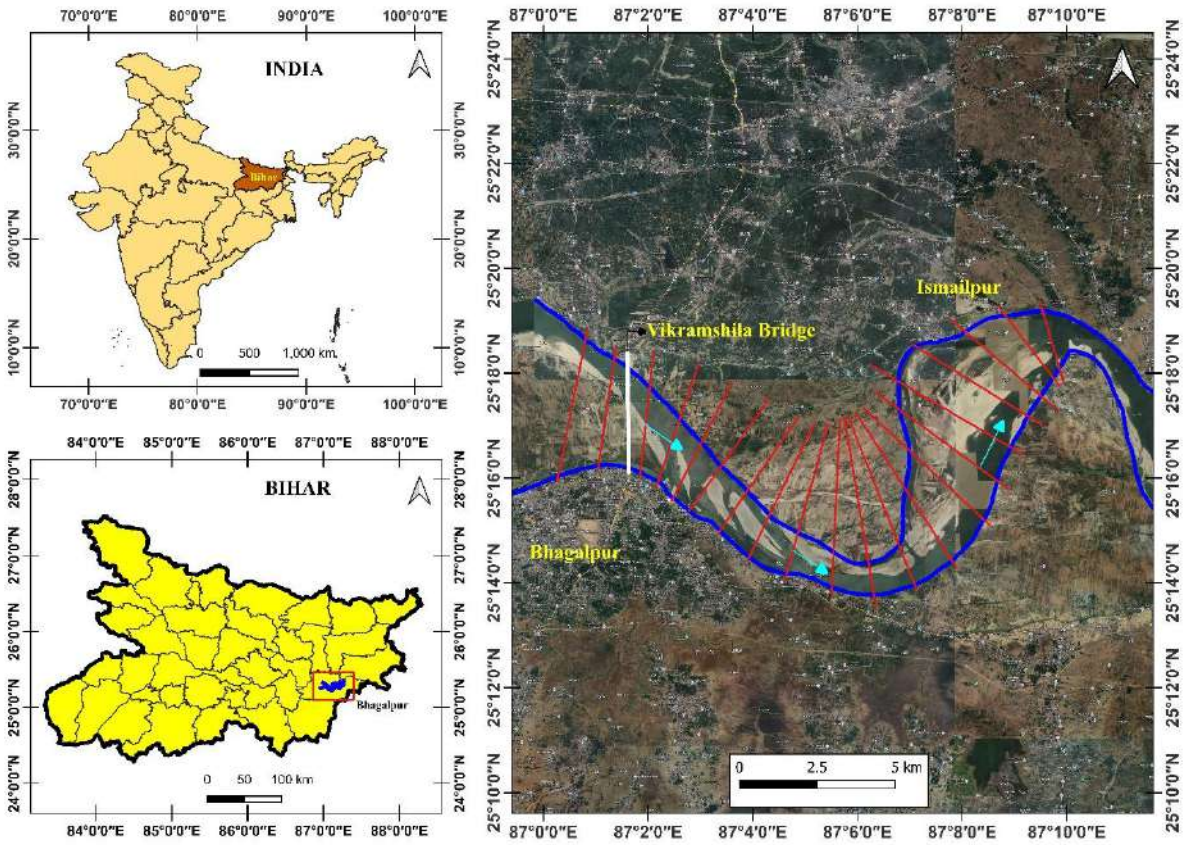

Fig. 7.1 Location of the studied site and the satellite image showing the study area stretching from 2 km upstream to 20 km downstream of the Vikramshila Bridge at Bhagalpur, Bihar [redlines indicate the cross-section line and dark blue lines indicate the river banks]

Fig. 7.2(a) Google earth image of the year 1985

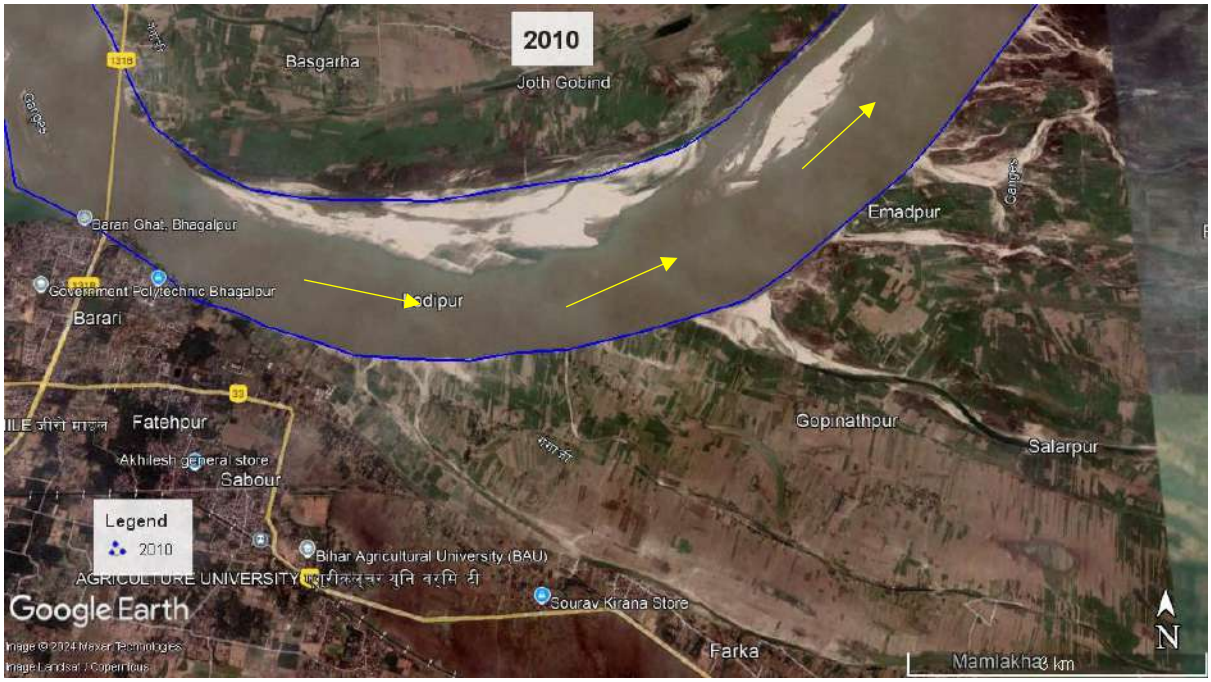

Fig. 7.2(b) Google earth image of the year 2010

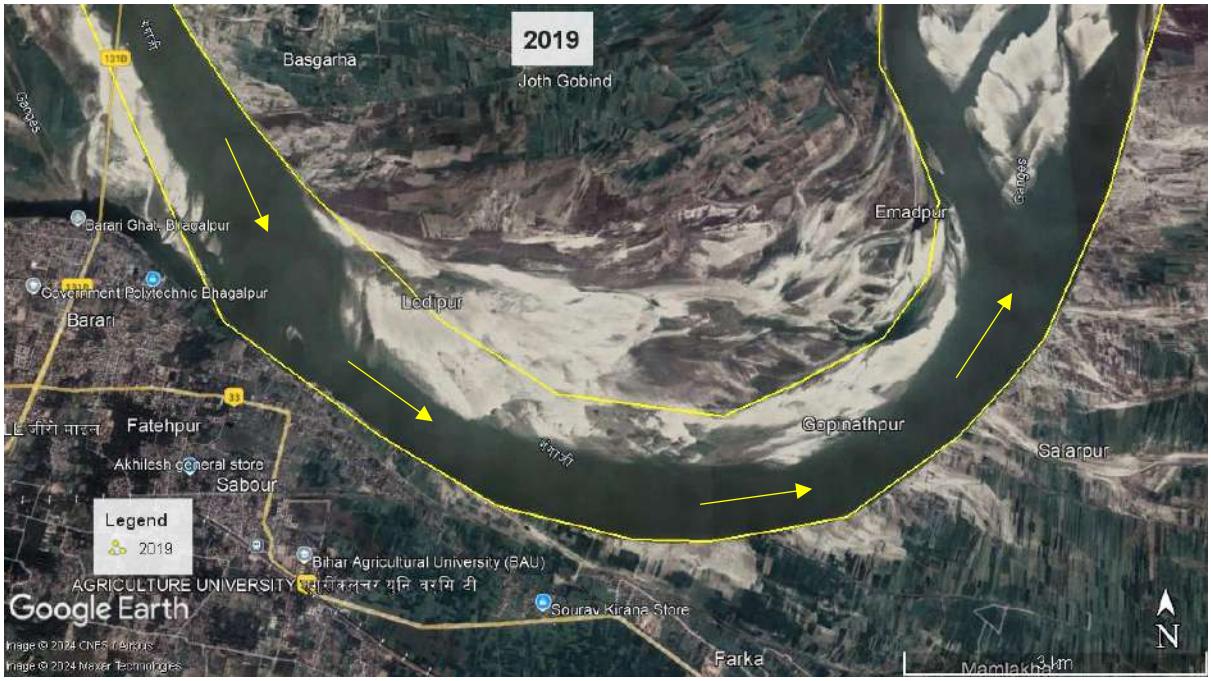

Fig. 7.2(c) Google earth image of the year 2019

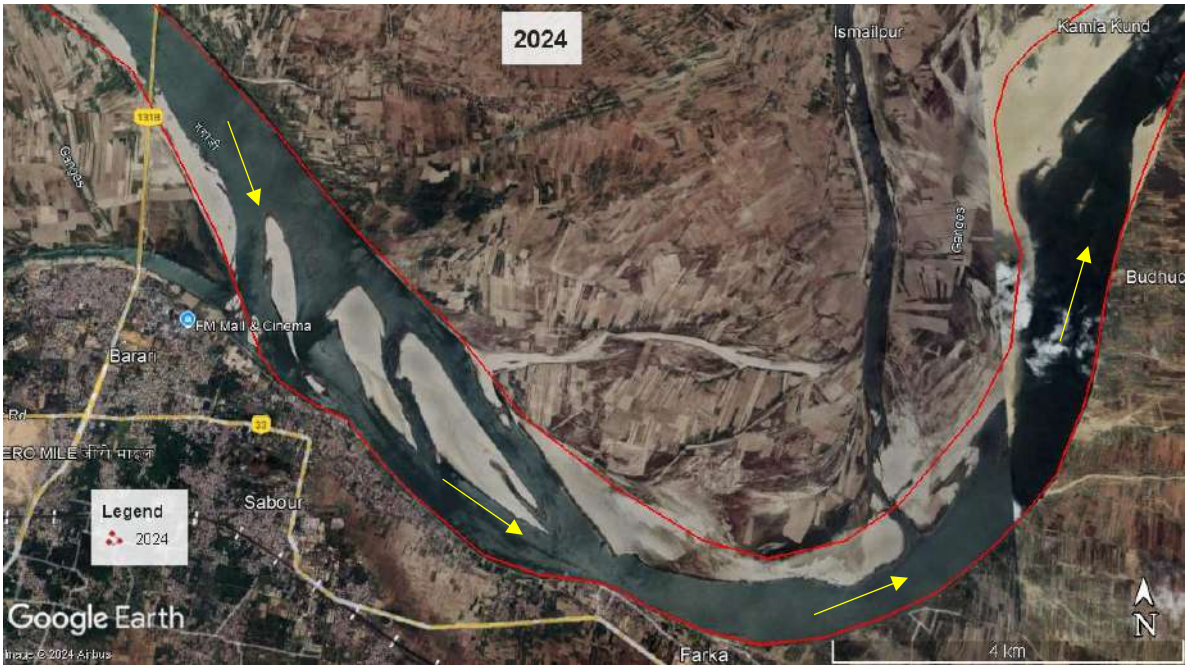

Fig. 7.2(d) Google earth image of the year 2024

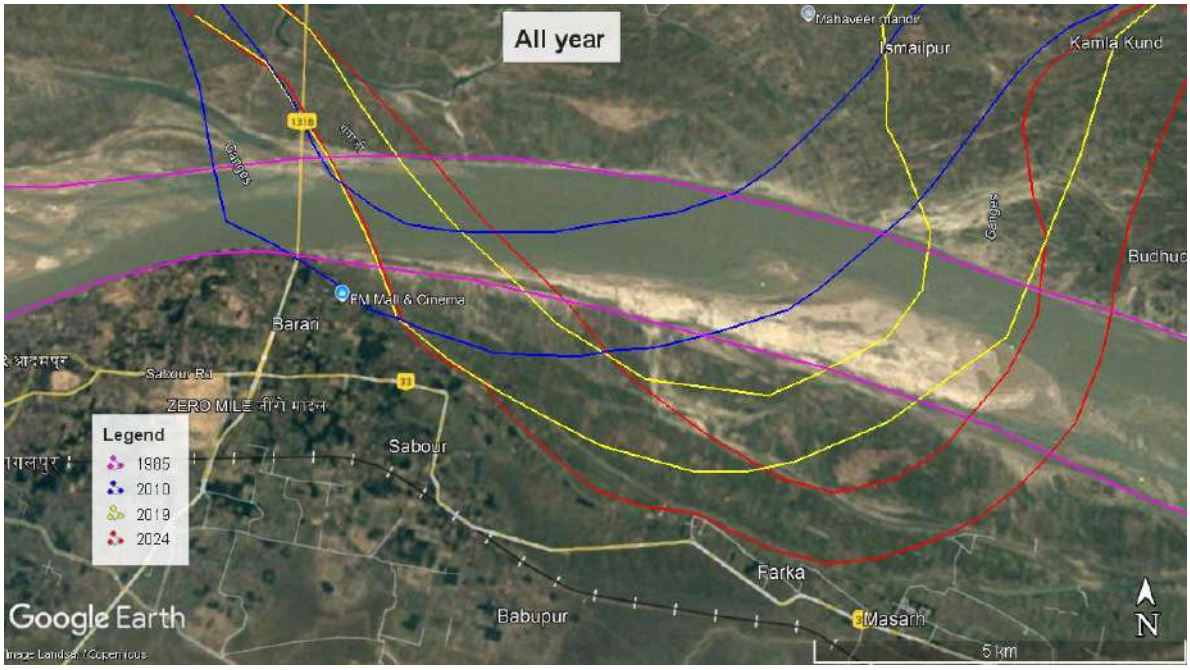

Fig. 7.2(e) Channel lines of the year 1985, 2010, 2019, and 2024 overlay on 1985 Google earth image

7.2 Materials and Methodology

7.2.1 Field Data Collection

Softa Geotechnical Pvt. Ltd was employed to carrying out the survey work of Ganga River at Bhagalpur (2 km upstream to 20 km downstream of the Vikramshila Bridge, Bhagalpur). Geographical co-ordinates of AOI under Ganga river are 25°17'16.53"N, 87°0'31.72"E & 25°18'42.99"N, 87° 9'40.80"E. Topographic and Hydrographic Survey was carried out to Develop Plan & Cross Sections of Ganga river at Bhagalpur. The detailed Topographical survey and Cross Section survey are carried out through the DGPS and Echo-Sounder instrument. Twenty cross section profile were generated. Location map and layout of CS line of hydrographical survey area (AOI) are shown in Figs. 7.3 (a & b). Also, one sample of Cross Section Profile is shown in Fig. 7.3 (c). The chainages for the respective cross-sections are provided in Table 7.1.

Table 7.1 Chainages of the cross-sections are as follows:

S.NO.	Cross-section	Chainage (km)	Remarks
1	CS-1	0	
2	CS-2	1.42	
3	CS-3	2.87	Vikramshilla Bridge
4	CS-4	3.4	Upstream of the model
5	CS-5	4.1	
6	CS-6	4.75	
7	CS-7	5.96	
8	CS-8	7.3	
9	CS-9	8.67	
10	CS-10	10.26	
11	CS-11	11.68	Middle of the model
2	CS-12	13.1	
3	CS-13	14.6	
4	CS-14	16.5	
5	CS-15	17.9	
6	CS-16	19.22	
7	CS-17	20.45	
8	CS-18	21.16	Downstream of the model
9	CS-19	21.9	
10	CS-20	22.12	

Modelled reach is from CS-4 to CS-18.

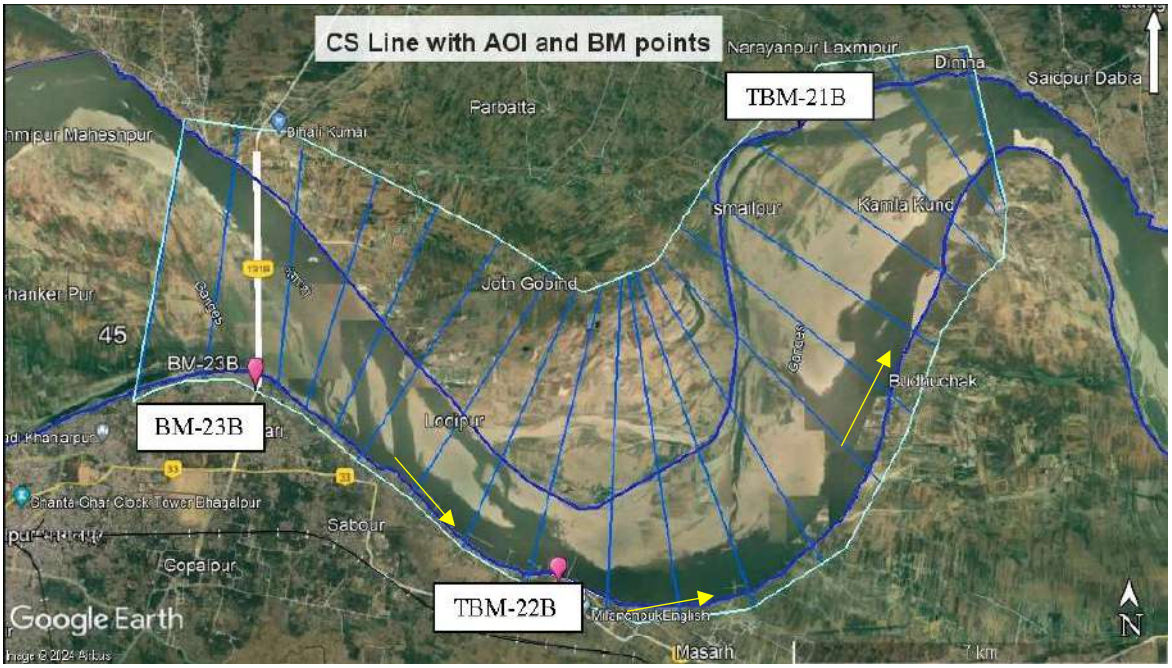

Fig. 7.3(a) Location map and CS line of hydrographical survey area (AOI)

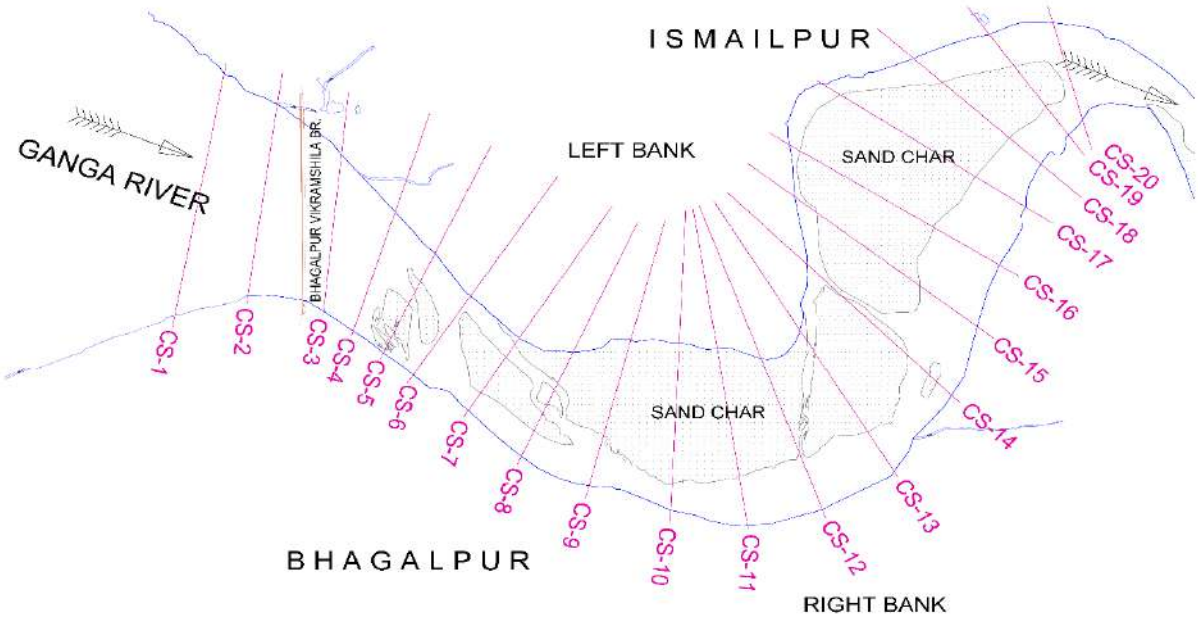

Fig. 7.3(b) Layout of plan and Cross-section

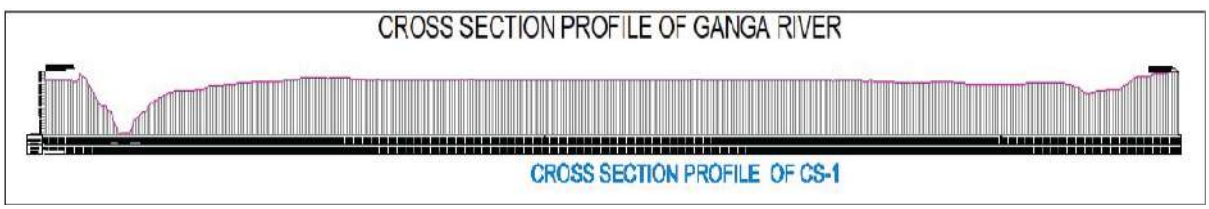

Fig. 7.3(c) Showing the sample Cross Section Profile

Hydrography survey was conducted to measure the water level and deepest bed level of the Ganga river at each cross-section, shown in Table 7.2. Photographs of data collection in Topographical Survey, UAV LiDAR Survey and Hydrographical survey carried out by the agency are shown in Figs. 7.4 (a), (b) and (c).

Table 7.2 Cross Section list and Average river bed level

CS NO.	STARTING COORDINATES		ENDING COORDINATES		Present water level	Present water stream width	Deepest bed level	Highest Elevation on of CS alignment
	NORTHING	EASTING	NORTHING	EASTING	m	m	m	m
CS-1	2799759.98	501418.18	2794323.45	500432.12	25.7	417	-3.96	37.3
CS-2	2799111.79	502337.16	2794715.35	501731.8	25.6	624.2	13.75	34.6
CS-3	2798989.84	503543.95	2794500.97	503090.32	25.6	910.7	11.25	36.7
CS-4	2798539.02	504983.67	2794103.27	503594.71	25.5	1127	19.58	33.9
CS-5	2797894.69	506065.84	2793657.54	504105.03	25.5	1950	19.82	35.2
CS-6	2797285.6	507249.78	2793295.9	504662.76	25.4	980	20.37	34.4
CS-7	2796676.44	508205.49	2792483.32	505572.49	25.4	345	17.01	33.8
CS-8	2796364.77	508661.94	2791556.61	506534.11	25.3	363	18.28	33.6
CS-9	2796407.62	509146.68	2790868.83	507735.8	25.3	763	18.28	33.5
CS-10	2796587.36	509509.92	2790365.31	509237.69	25.2	542	6.05	33.9
CS-11	2796639.98	509637.83	2789918	510673.77	25.2	718.1	9.18	33.3
CS-12	2796687.08	509752.35	2790485.08	511993.38	25.2	551.4	9.27	33.1
CS-13	2796791.02	510001.91	2791291.01	513274.66	25.1	676.1	16.70	32.8
CS-14	2796961.33	510244.19	2792784.79	514361.45	25.1	758.2	15.68	33.2
CS-15	2797528.79	510614.55	2794058.08	514964.09	25.1	614.3	18.34	32.9
CS-16	2798473.35	510464.5	2795300.03	515400.9	25.0	525.3	20.59	32.9
CS-17	2799174.68	511839.88	2796341.58	516014.26	25.0	1015.1	20.72	32.6
CS-18	2800125.4	513000.84	2796852.95	516519.34	25.0	668.8	18.04	34.4
CS-19	2800545.9	514571.92	2797692.76	516572.25	24.9	600.7	17.75	35.7
CS-20	2800705.66	515909.01	2797815.17	516698.72	24.9	446.6	17.32	33.8

Fig. 7.4(a) Showing Topographical Survey Photographs

Fig. 7.4(b) Showing the UAV LiDAR Survey Photographs

Fig. 7.4(c) Showing the Hydrographical survey through Echo-Sounder, Photographs

7.2.2 Available Data

Following data / drawings were used for physical model studies:

1) Plan layout of the Ganga river from 2 km upstream to 20 km downstream of the Bikramshilla bridge, Bhagalpur to Ismailpur.
2) Cross-sections of the river Ganga 2 km upstream to 20 km downstream of the Bhagalpur bridge, Bihar.
3) The peak discharge of Ganga river at Bhagalpur = 1,05,600 m^3/s (Ahmad et al. 2017)
4) HFL value of Bhagalpur = 34.86 m (Ahmad et al. 2017)
5) Water Level at hydrographical survey period 23/01/2024 to 31/01/2024.
6) Average flood slope =1/ 17480 between Bhagalpur & Azmabad sites (Ahmad et al. 2017)

7) Yearly maximum discharge and flood level at Azmabad H.O. Site of CWC (Ahmad et al. 2017)

7.2.3 Design of Vane

The submerged vanes were designed following the outcomes of the present study and guidelines proposed by Odgaard (2009). The design specifications are provided in Table 7.3 and was designed for normal year discharge of 52,800 m^3/s and corresponding water level of 31.56 m.

Table 7.3 Details of submerged vane parameters

Vane parameters	Design specification	Vane dimension
Height of vane (H)	0.2–0.4 times of average flow depth (d)	5 cm
Length of vane (L)	3H	15 cm
Angle of attack (α)	13°–40°	20°
Lateral spacing between vanes	2H to 3H	15 cm
Longitudinal spacing between vanes	15H to 30H	75 cm
Vane to bank distance	3H	15 cm

Previous investigations indicate that the local scour depth increases with an increase in the angle of attack (α). At larger α, the vane is subjected to a relatively larger drag force, with increased flow resistance. The major problem of using of larger α is the occurrence of a greater scour around the vane that may dislodge the vane (Odgaard & Kennedy, 1983; Odgaard & Spoljaric, 1986). Due to these considerations, the installation of a vane with $\alpha > 20^0$ is not feasible for practical applications in the field (Gupta et al., 2010). Therefore, $\alpha \approx 20^0$ was selected for all runs. In the present study, beveled submerged vanes are employed in place of rectangular ones, as they demonstrate effective reduction in local scour without significantly compromising vortex generation efficiency at a bevel angle of 45^0 (Mandal et al., 2025).

7.2.4 Development of a 3D Comprehensive Model

A physical model of river Ganga was constructed on Froudian similarity in the Hydraulics laboratory of Dept. of Civil Eng., IIT Roorkee. Considering the river reach and discharge, the model was constructed to a scale of 1:700 (Length and width scale) and 1:70 (Depth scale). The discharge scale is 1:409963.41. The model represented a reach of the Ganga river from CS-4 to CS-18. The river contours in the model were dressed up with locally available fine sand d_{50} = 0.25 mm as per survey/cross sections provided by our agency (Softa Geotechnical Pvt. Ltd). The physical model of Ganga river with present condition at Bhagalpur is shown in Fig. 7.5 (a) and the proposed submerged vane installed along the right bank of the Ganga river model is shown in Figs. 7.5 (b). The discharge in the model was regulated with a valve provided in the supply pipe and was measured with an electro-magnetic flow meter fitted in the supply pipes. Suitable arrangements in the form of tranquillising tanks and honey comb walls were provided to tranquil the flow before entering the model. Arrangements were also made at the tail of the model to maintain the downstream water level.

Fig. 7.5(a) Physical model of Ganga river at Bhagalpur without vane

Fig. 7.5(b) Installation of vane array at right bank of the physical model

7.2.5 Stage-Discharge Curve at the Study Site

Ahmad et al. (2017) carried out morphological study of the Ganga river and also estimated discharge at various CWC gauging sites for different return periods. The available Stage-Discharge data at Azmabad H.O. station of CWC was transfer to the Chainage of Ganga river at Bhagalpur. Figures 7.6 (a & b) show the Stage-Discharge curve of the Ganga river to u/s and d/s of the study reach.

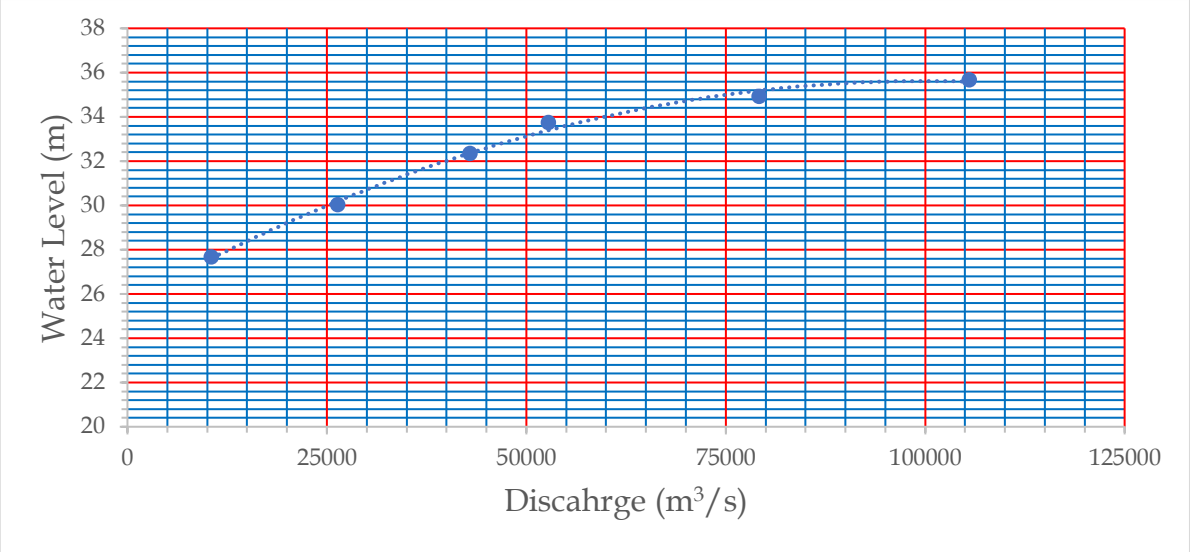

Fig. 7.6(a) Stage-Discharge Curve at Chainage 3.4 Km (CS-04)

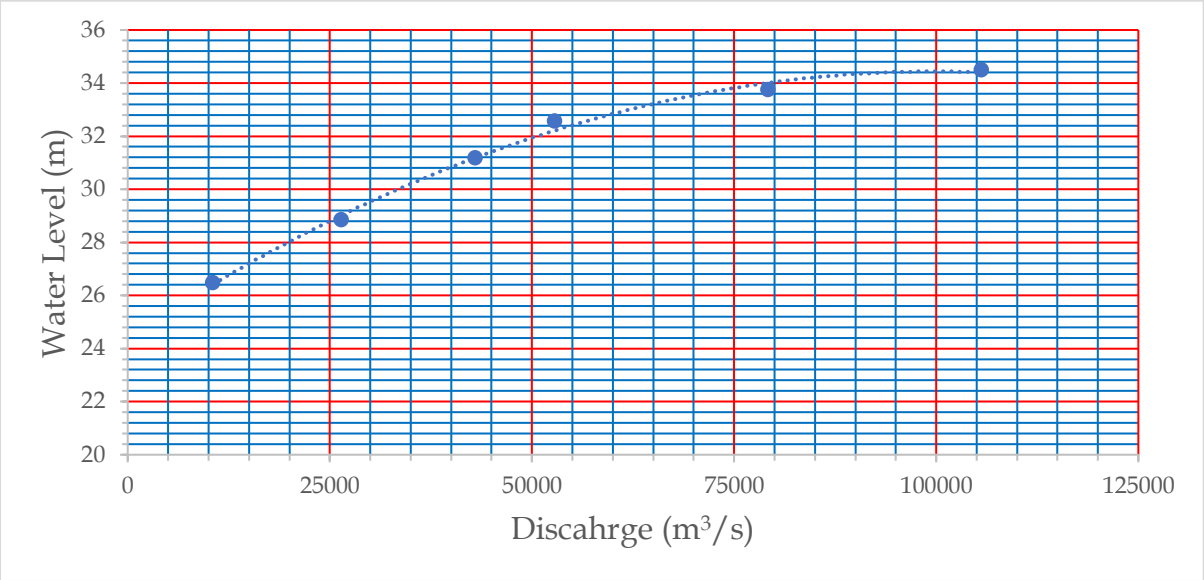

Fig. 7.6(b) Stage-Discharge Curve at Chainage 21.16 Km (CS-18)

7.2.6 Validation of the Physical Model

The model was initially run for validation under virgin conditions (without submerged vane). For validation, discharges varying from 25% to 100 % of the peak discharge were run in the model. For each discharge, the TWL as per Fig. 7.6b was maintained with the help of a tail gate provided in the downstream. After the flow conditions were stabilized, water levels were observed at the upstream and middle of the model. The observed water levels at different locations are plotted against

corresponding computed water levels as shown in Figs. 7.7 (a) & (b), which reveal that measured water levels fairly tally with computed water levels at all discharges run in the model. After the validation, the model was ready for running with different discharges.

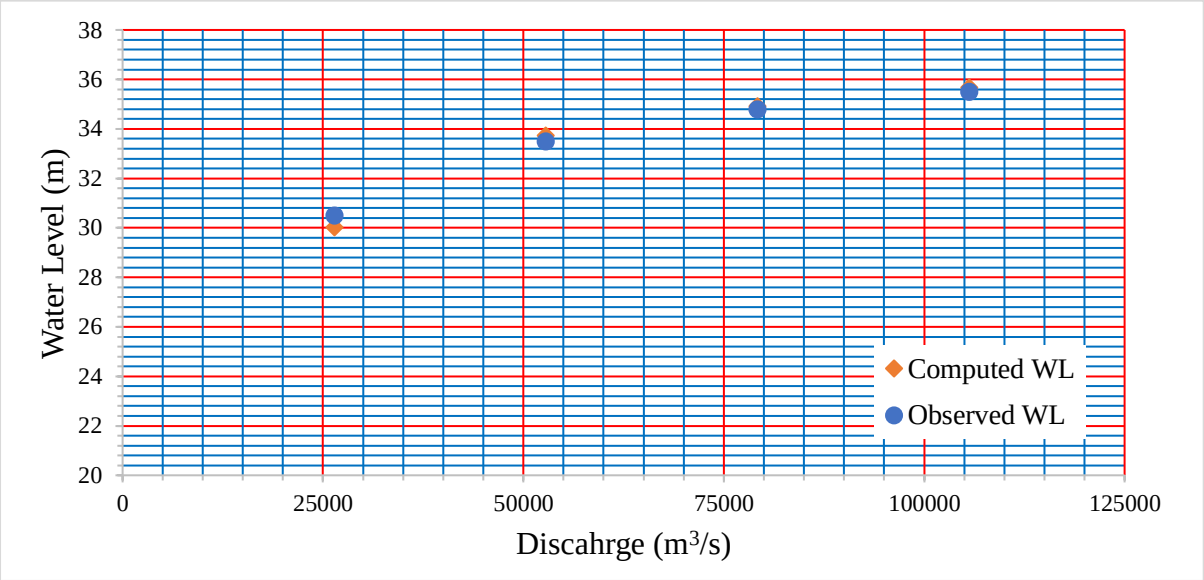

Fig. 7.7(a) Observed and computed water levels at Chainage 3.4 Km (CS-04) of the physical model

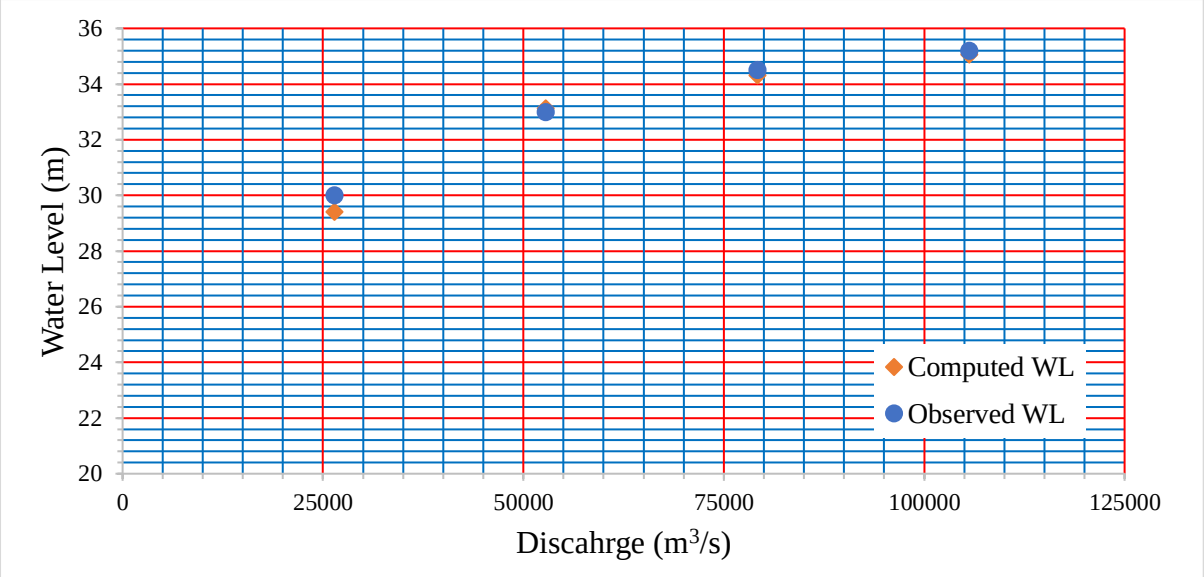

Fig. 7.7(b) Observed and computed water levels at Chainage 11.68 Km (CS-11) of the physical model

7.3 Physical Model Results

7.3.1 General Flow Conditions for different discharges

At 26400 m^3/s, water was entering in the model from central and extreme right channel of the Ganga river, thereafter was taking a sharp turn from CS-07 and the flow was towards right bank and remained on right bank up to the CS-15. When the discharge was increased to 52800 m^3/s, the flow was passing through the whole width of river, however, main flow was passing through the right channel. At 75% of the peak discharge, the flow passed through whole width of the river with more concentration of flow on the right bank. At peak discharge of 105600 m^3/s, the flow conditions were almost similar to that of 79200 m^3/s. Concentrated flow was passing through along the right bank and flow was also seen a channel towards the left side of the river. The flow was deflecting away from the right bank of the river beyond CS-15. Pictorial view of general flow conditions at different discharges is shown in Figs. 7.8 (a-d). In present condition of the site, the main flow passes abutting the right bank of the river as shown in Fig. 7.9. After installation of proposed vane, the main course of the river shifted toward left side away from the right bank as can be seen in Fig. 7.9. This phenomenon was observed at all tested conditions in the physical model. Therefore, the usefulness and effectiveness of the submerged vanes to deflecting the main flow away from the bend section are quite visible.

Fig. 7.8 (a) Flow conditions for 26400 m^3/s discharge

Fig. 7.8 (b) Flow conditions for 52800 m^3/s discharge

Fig. 7.8 (c) Flow conditions for 79200 m^3/s discharge

Fig. 7.8 (d) Flow conditions for 105600 m^3/s discharge

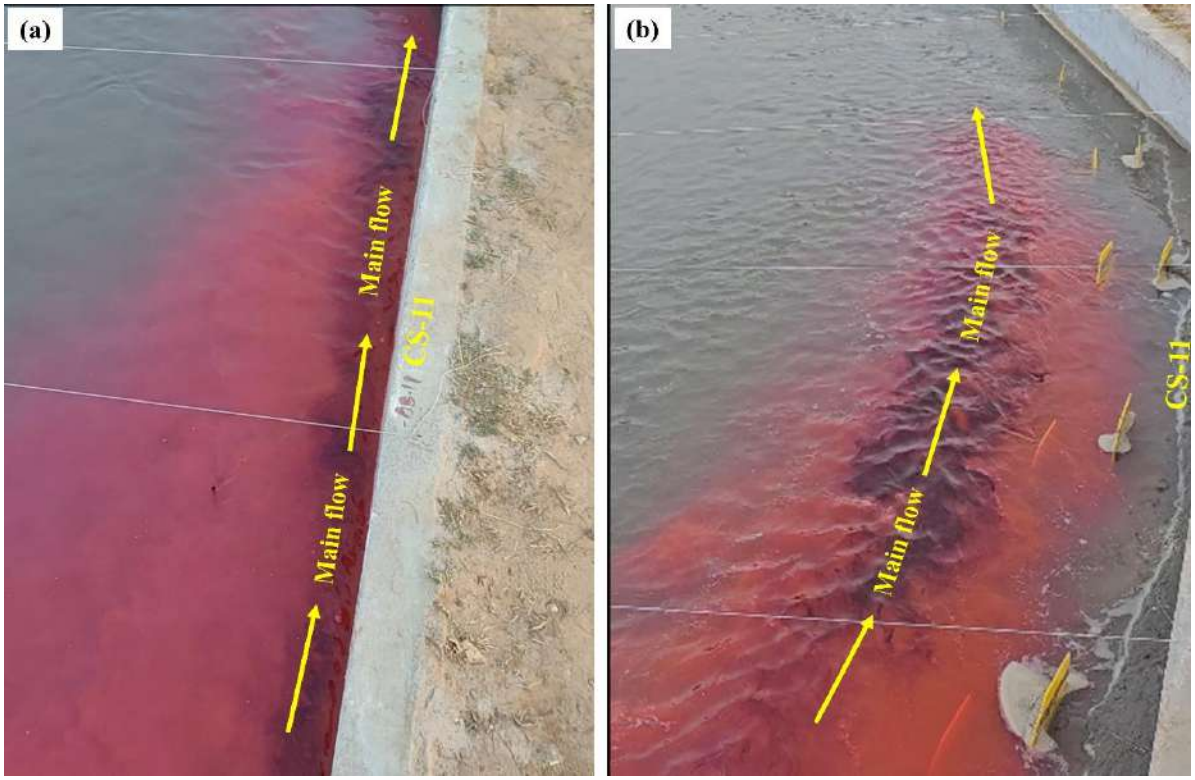

Fig. 7.9 Main course of the Ganga river in the physical model at 52800 m^3/s river discharge (a) flow concentration toward the right bank at the existing site condition (b) shifting of the river main course flow away from the right bank due to installation of proposed vanes

7.3.2 Velocity Observations Without and With Vane Condition

For a better insight of the flow fields and the effectiveness of the vanes, the near free surface flow velocity was measured along 175 m, 350 m, and 525 m offset lines from the right bank between section CS-07 and section CS-14 for all four tested discharges without and with submerged vanes. The observed velocity along these offsets are shown in Figs. 7.10, 7.11, and 7.12 and given in Table 7.4. Fig. 7.10 indicates that vanes reduces the flow velocity along the offset 175 m significantly in the reach between CS-07 and CS-14 for all discharges except at sections CS-07 and CS-08 for discharge of 26400 m^3/s where the reductions are less significant. Quite similar observations are also made for the offset 350 m (Fig. 7.11). However, further away from the right bank, i.e., along the 525 m offset, slight increase in the flow velocity is observed after installing the vanes, particularly for the lower discharges as shown in Fig. 7.12, and these increase in velocity due to shifting of the river main course away from the right

bank. Furthermore, it is interesting to observe that the flow velocity along the selected offsets from the right bank decrease with increasing discharge. Such observations are seemingly influenced by lesser flow concentrations toward the right bank and greater uniform distribution of the flow across the entire river cross-section under higher discharges. In contrast, under lower discharges, the main flow tends to concentrate along the right bank, resulting in comparatively higher velocities in that region. These results obtained from the physical model study show that the installation of proposed submerged vanes at the site would offer a diversion of the main course of the river away from the right bank, thus, protecting the right bank from erosion.

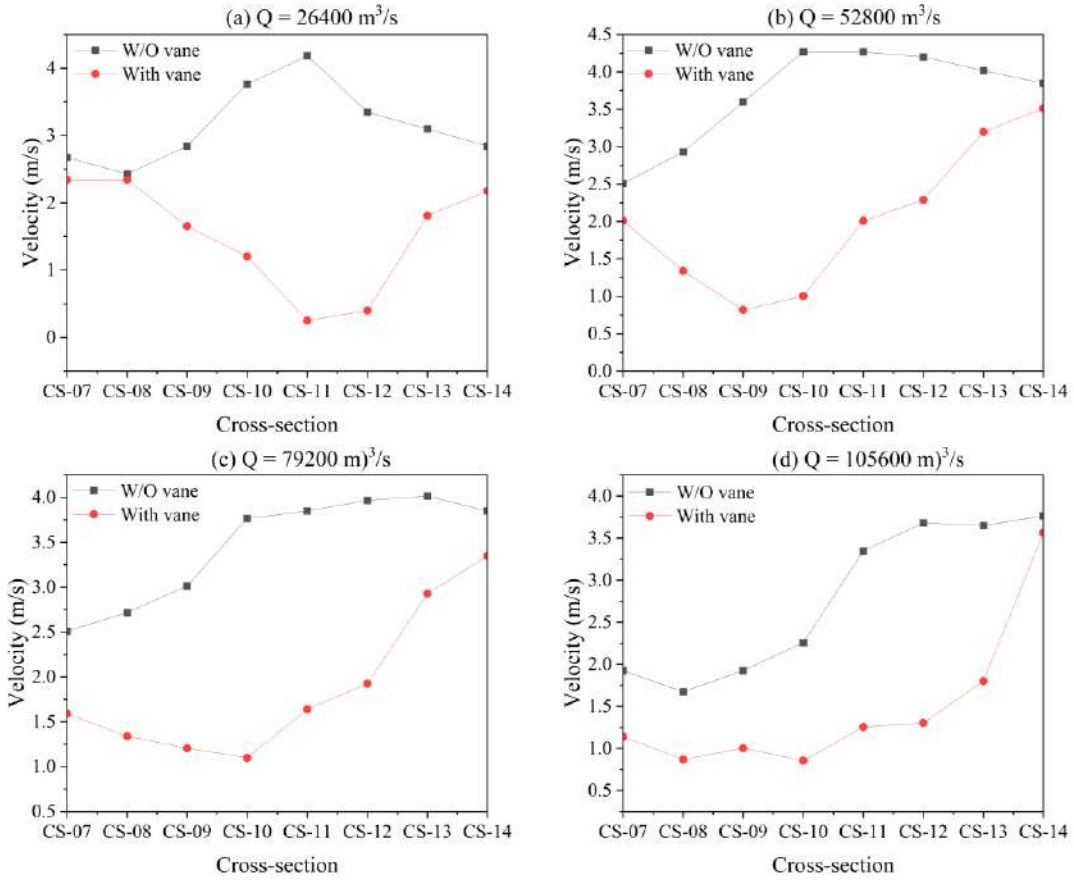

Fig. 7.10 Observed velocity distributions at 175 m offset from the right bank under different discharges without (w/o) and with submerged vane conditions

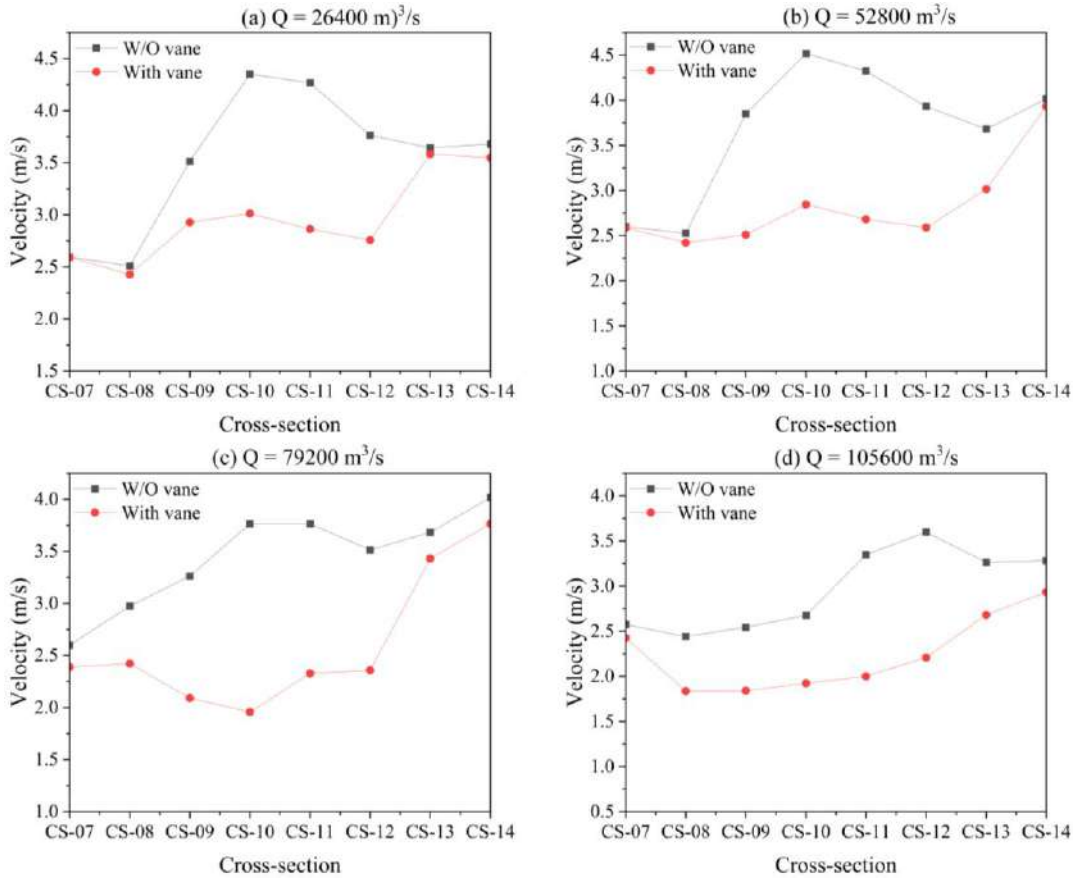

Fig. 7.11 Observed velocity distributions at 350 m offset from the right bank under different discharges without (w/o) and with submerged vane conditions

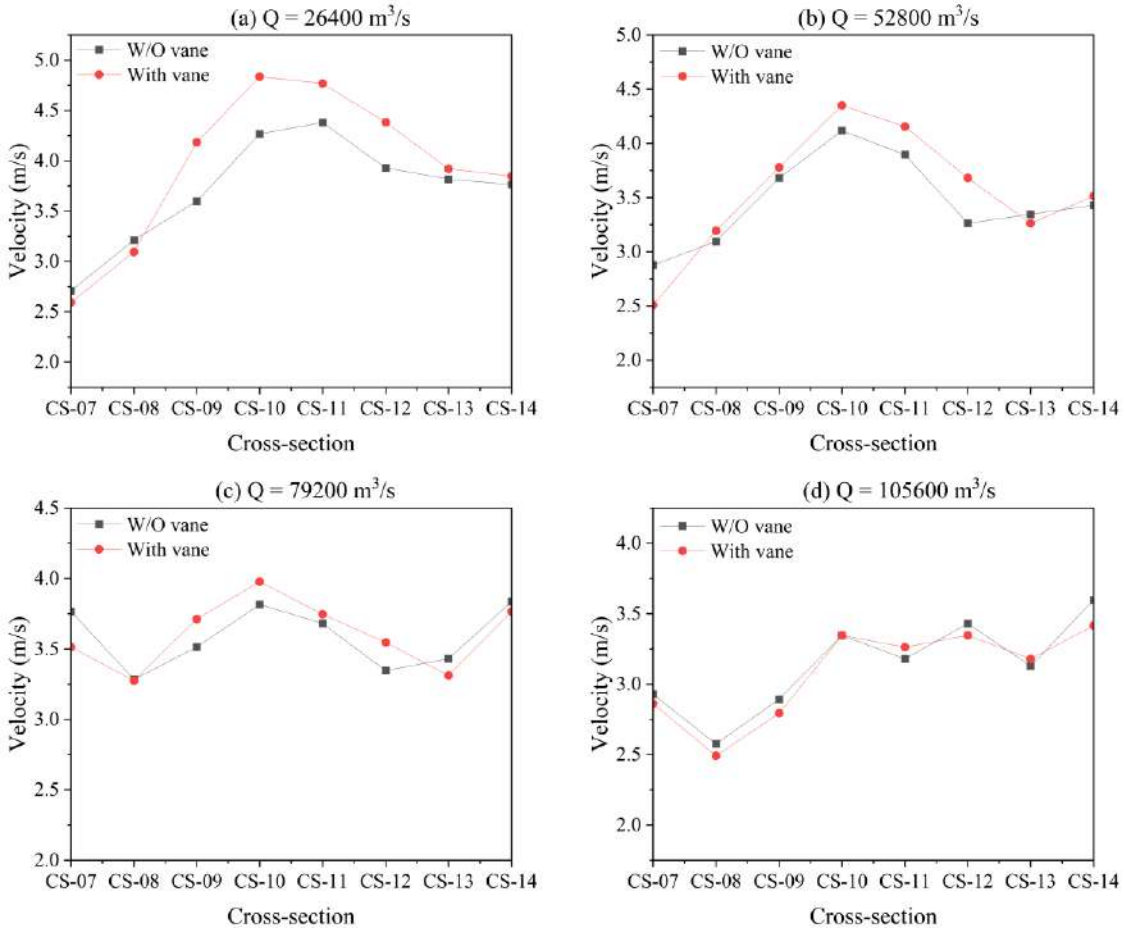

Fig. 7.12 Observed velocity distributions at 525 m offset from the right bank under different discharges for without (w/o) and with submerged vane conditions

Table 7.4 Measured Velocity at three offsets from the right bank in different cross-section for various discharges

Discharge(m^3/s)	Cross-section	Velocity (m/s) from right bank					
		Ch. 175 m		Ch. 350 m		Ch. 525m	
		w/o vane	with vane	w/o vane	With vane	w/o vane	with vane
Q = 26400 m^3/s	CS-07	2.68	2.34	2.59	2.59	2.51	2.59
	CS-08	2.43	2.34	2.51	2.43	3.01	3.10
	CS-09	2.84	1.26	3.51	2.93	3.60	4.18
	CS-10	3.77	1.51	4.35	3.01	4.27	4.94
	CS-11	4.18	0.25	4.27	3.26	3.68	4.77
	CS-12	3.35	0.00	3.77	1.76	3.43	4.18
	CS-13	3.10	2.51	2.34	4.18	2.09	5.02
	CS-14	2.84	2.18	3.18	3.85	3.77	3.85

Q = 58200 m^3/s	CS-07	2.51	2.01	3.18	2.68	2.68	2.01
	CS-08	2.93	1.34	2.43	1.42	3.10	2.59
	CS-09	3.60	0.42	3.85	2.51	3.68	3.18
	CS-10	4.27	1.00	4.52	2.84	4.52	4.35
	CS-11	4.27	2.01	3.93	3.68	3.10	4.69
	CS-12	3.60	2.09	3.93	1.59	3.26	3.68
	CS-13	4.02	3.60	3.68	4.02	3.35	3.26
	CS-14	3.85	3.51	4.02	3.93	3.43	3.51
Q = 79200 m^3/s	CS-07	2.51	1.59	3.18	2.93	3.77	3.51
	CS-08	2.09	1.00	2.18	1.42	2.93	2.18
	CS-09	3.01	1.51	3.26	2.09	3.51	3.01
	CS-10	3.77	0.84	3.77	1.76	4.02	3.60
	CS-11	3.85	1.84	3.77	2.93	3.68	3.35
	CS-12	3.35	1.92	3.51	2.26	3.35	3.35
	CS-13	4.02	2.93	3.68	3.43	3.43	3.01
	CS-14	3.85	3.35	4.02	3.77	4.18	3.77
Q = 105600 m^3/s	CS-07	1.92	1.34	2.18	2.43	2.93	3.26
	CS-08	1.67	0.67	1.84	0.84	2.18	2.09
	CS-09	1.92	1.00	2.34	1.84	2.59	2.59
	CS-10	2.26	0.59	2.68	1.42	3.35	3.35
	CS-11	3.35	1.26	3.35	3.10	3.18	3.26
	CS-12	3.68	1.00	3.60	2.01	3.43	3.35
	CS-13	3.35	3.01	3.26	3.68	2.93	3.18
	CS-14	3.77	3.77	3.68	3.93	3.60	4.02

7.3.3 Post Run Bed Scenario Without and With Vanes

After running the model for 25%, 50 %, 75 % and 100% of the peak discharge, changes in the bed were measured. The maximum discharge was run for about 16-17 hours (prototype time) and change in bed was observed. It was found that degradation has taken place along right bank in the present condition, as shown in Figs. 7.13(a), 7.14(a), 7.15(a), and 7.16(a).

The residual bed with installed vanes after running the model with feeding sediment 256 mg/l concentration are shown in Figs. 7.13(b), 7.14(b), 7.15(b), and 7.16(b). The comparison among the obtained bed profiles across different cross-sections under three conditions, i.e., (i) existing bed profile at site (or bed profile before running the

model), (ii) bed profile after the model run without vanes, and (iii) bed profile after the model run with vanes, are provided in Figs. 7.17 to 7.20. When the flow is entering the bend channel, fast-moving surface currents are compelled to migrate toward the curved bend, while slow-moving near-bed currents are compelled to move toward the center of the river, resulting in large depths and velocities near the outer banks. This high velocity creates a huge erosion towards the right bank along the river for various discharges as shown in Figs. 7.13(a), 7.14(a), 7.15(a), and 7.16(a). It can be observed that bank erosion is less at maximum discharge compared to the 25%, 50%, 75% of the peak discharge, which is related to the less significant flow concentration toward the right bank and grater uniform distribution of the flow across the river cross-section under the higher discharges as compared to that observed for the lower discharges, as discussed earlier. Due to installation of the vanes, the higher velocity is redirecting from the outer bank to the inner bank which is reducing the right bank erosion as shown in Figs. 7.13(b), 7.14(b), 7.15(b), and 7.16(b). The protected area of the right bank by submerged vanes is demarcated by a red dotted line as shown in Figs. 7.13(b), 7.14(b), 7.15(b), and 7.16(b). The residual bed measurements are tabulated in Table 7.5. Observation from physical model study revealed that the submerged vane is effective in protecting the bank erosion. Installation of the submerged vane along the right bank of the river offers favourable results to protect the bank erosion of the bend channels.

Fig. 7.13(a) Residual bed after running the model at 26400 m^3/s discharge w/o vane

Fig. 7.13(b) Residual bed after running the model at 26400 m^3/s discharge with vane

Fig. 7.14(a) Residual bed after running the model at 52800 m^3/s discharge w/o vane

Fig. 7.14(b) Residual bed after running the model at 52800 m^3/s discharge with vane

Fig. 7.15(a) Residual bed after running the model at 79200 m^3/s discharge w/o vane

Fig. 7.15(b) Residual bed after running the model at 79200 m^3/s discharge with vane

Fig. 7.16(a) Residual bed after running model at 105600 m^3/s discharge w/o vane

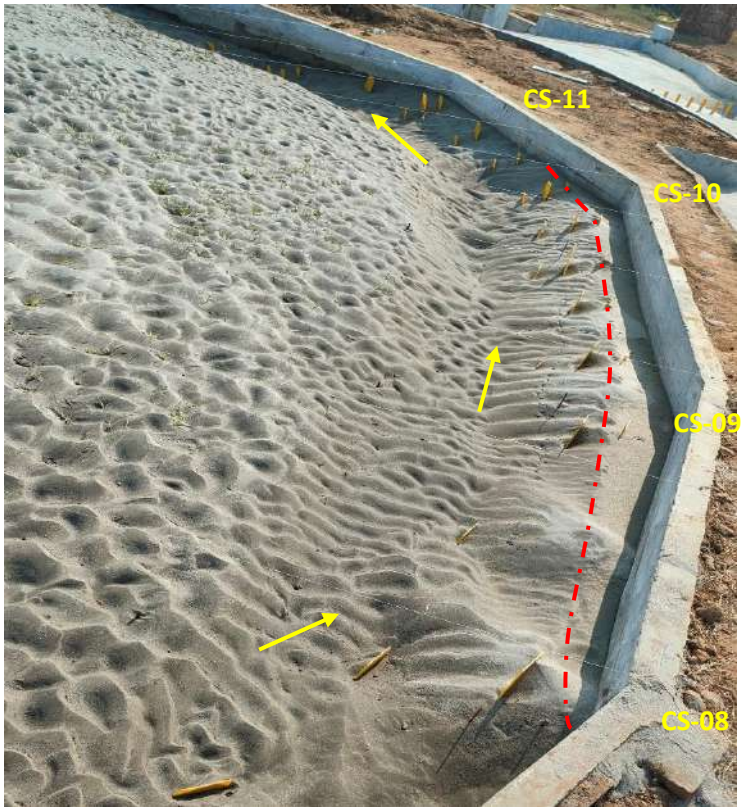

Fig. 7.16(b) Residual bed after running the model at 105600 m^3/s discharge with vane

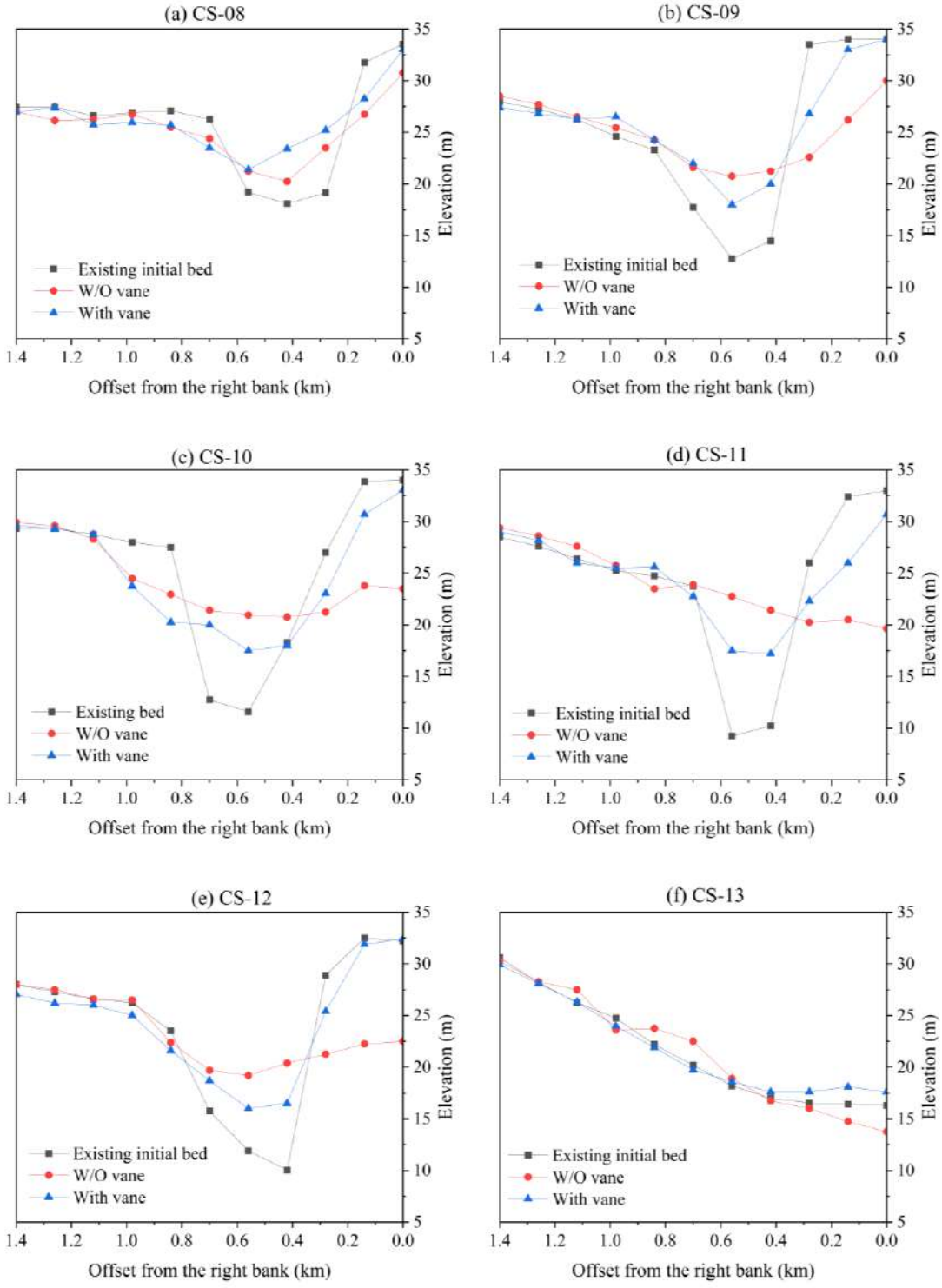

Fig. 7.17 Bed profiles across the physical model for the river discharge of 26400 m^3/s at sections CS-08 to CS-13

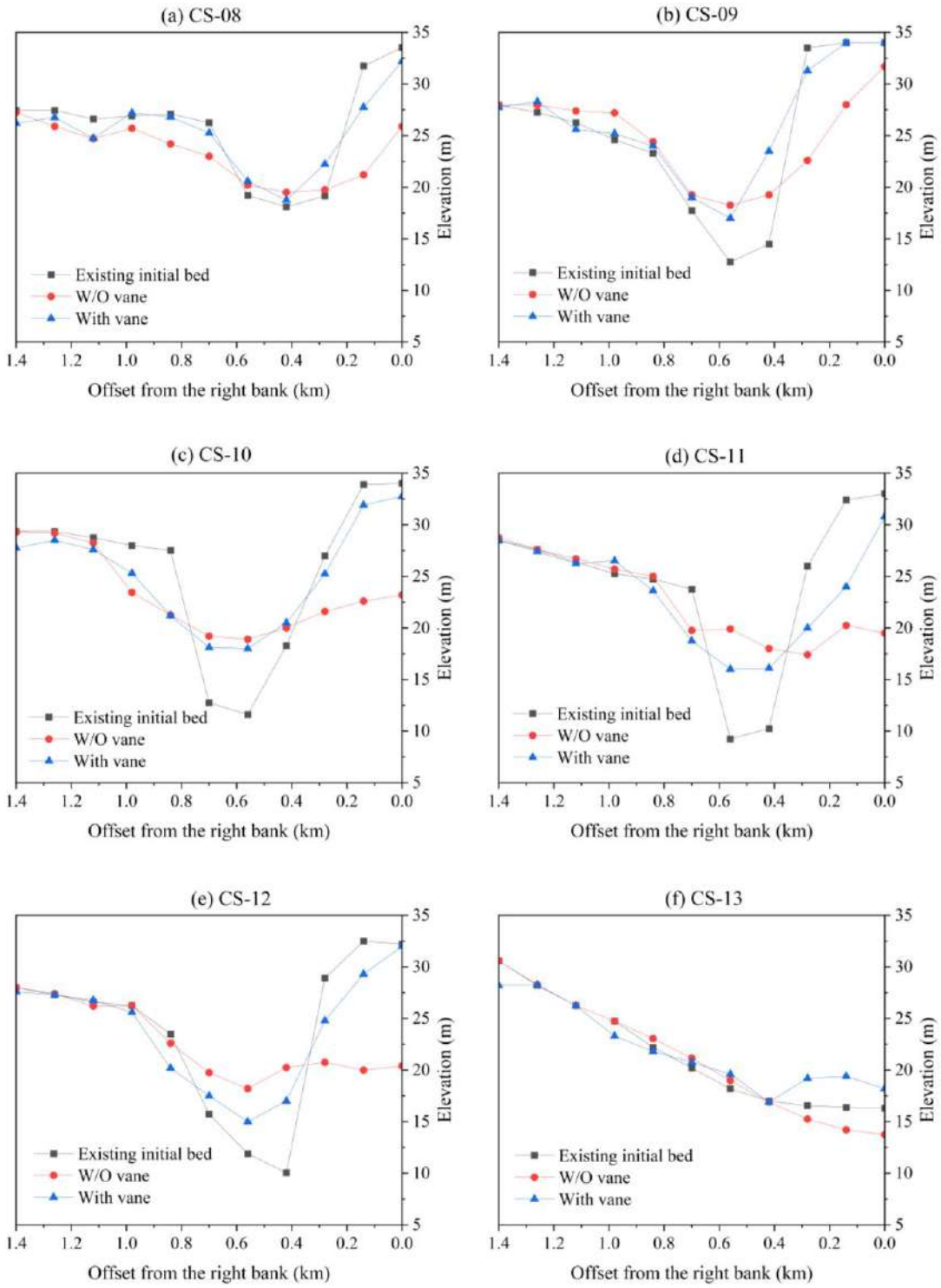

Fig. 7.18 Bed profile across the physical model for the river discharge of 52800 m^3/s at sections CS-08 to CS-13

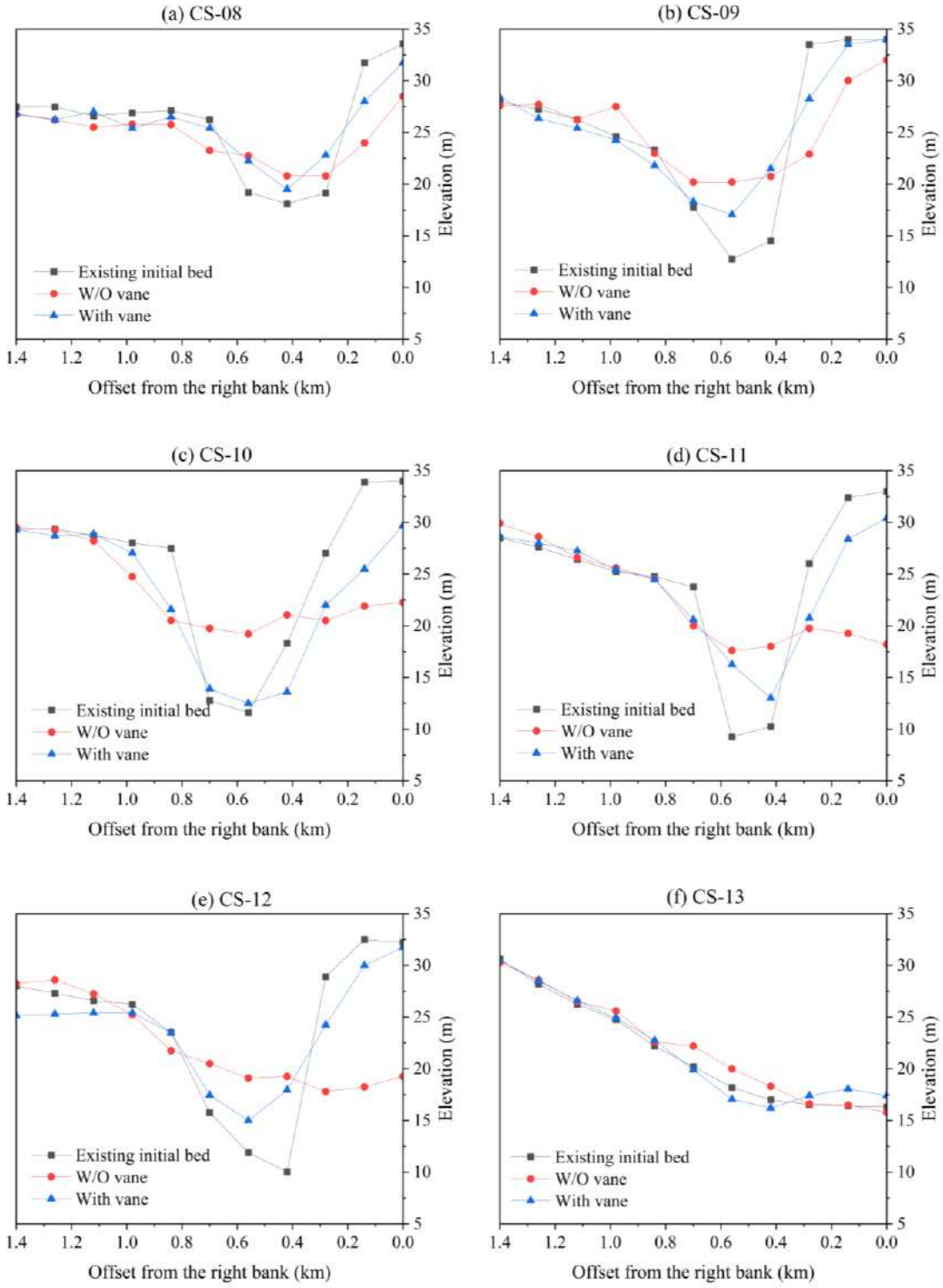

Fig. 7.19 Bed profile across the physical model for the river discharge of 79200 m^3/s at sections CS-08 to CS-13

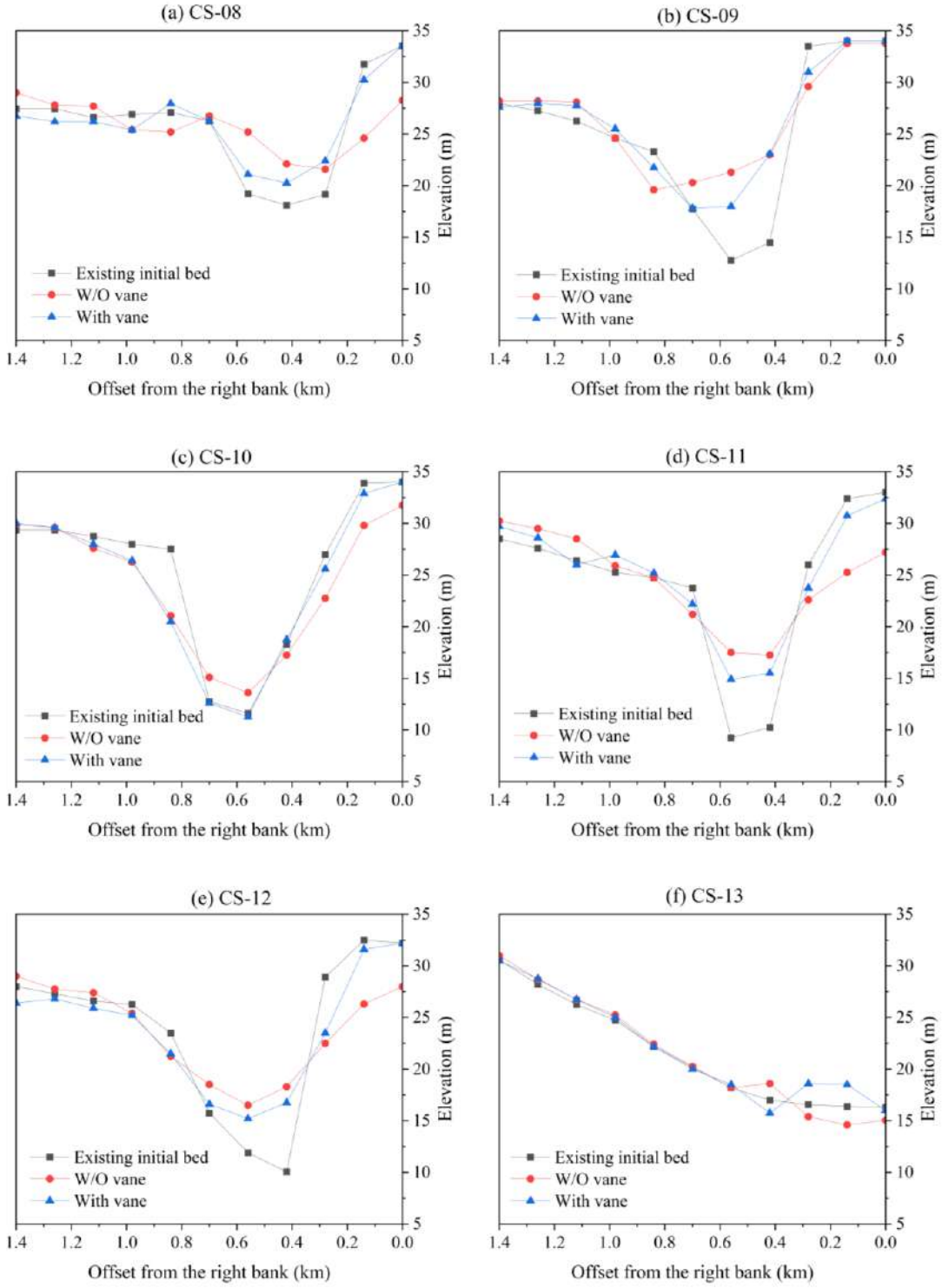

Fig. 7.20 Bed profile across the physical model for the river discharge of 105600 m^3/s at sections CS-08 to CS-13

Table 7.5 Measurement of the residual bed w/o and with vane

Cross-section	Chainage (km)	Q = 26400 m^3/s		Q = 58200 m^3/s		Q = 79200 m^3/s		Q = 105600 m^3/s	
		w/o vane	with vane	w/o vane	with vane	w/o vane	with vane	w/o vane	with vane
CS-08	0	30.75	31	25.9	32.2	19.05	31.75	27.25	33.95
	0.14	26.75	28.25	21.2	27.75	21.05	28	21.6	30.25
	0.28	23.5	25.2	19.75	22.25	20.8	22.8	21.6	22.4
	0.42	20.25	23.4	19.5	18.75	20.8	19.5	22.1	20.25
	0.56	21.25	21.4	20.2	20.6	22.75	22.25	25.2	21.1
	0.7	24.4	23.5	23	25.25	23.25	25.4	26.75	26.25
	0.84	25.5	25.7	24.2	26.8	25.75	26.5	25.2	27.95
	0.98	26.75	25.95	25.7	27.2	25.8	25.4	25.4	25.4
	1.12	26.25	25.75	24.7	24.75	25.5	27	27.7	26.2
	1.26	26.15	27.4	25.9	26.75	26.2	26.25	27.8	26.2
	1.4	27	27	27.25	26.2	26.75	26.8	29	26.75
CS-09	0	27	33.2	33.7	32.75	31.5	31.9	33.75	34.25
	0.14	24.2	33.25	28	33.2	27.7	33.05	33.75	34.6
	0.28	22.6	26.8	22.6	31.3	21.9	28.25	29.6	31
	0.42	21.25	23	19.25	25.2	20.75	21.5	23	23.06
	0.56	20.75	21.25	18.25	20.25	20.2	17.05	21.3	18
	0.7	26.6	22	19.25	23	20.2	18.3	20.3	17.8
	0.84	26.25	24.25	24.4	24	23	21.8	19.6	21.75
	0.98	25.45	26.5	27.2	25.2	27.5	24.25	24.6	25.5
	1.12	26.5	26.3	27.4	25.6	26.25	25.4	28.1	27.75
	1.26	27.7	26.8	27.95	28.3	27.7	26.35	28.2	27.95
	1.4	28.5	27.4	27.95	27.75	27.6	28.4	28.2	27.6
CS-10	0	23.5	30.05	23.2	32.75	22.25	29.7	31.75	31.9
	0.14	23.8	28.7	21.6	31.9	21.9	20.5	29.8	31.75
	0.28	21.25	23.05	21.6	25.25	20.5	24	22.75	25.6
	0.42	20.75	18	20	25.5	21.05	13.6	17.25	18.75
	0.56	20.95	17.5	18.9	18	19.2	11.3	13.6	11.25
	0.7	21.4	21.6	19.2	18.1	19.75	13.9	15.1	12.6
	0.84	22.95	20.25	21.25	21.2	20.5	21.6	21.05	20.5
	0.98	24.5	23.75	23.45	25.3	24.75	27.05	26.25	26.4
	1.12	28.3	28.75	28.25	27.6	28.2	28.85	27.6	28
	1.26	29.6	29.3	29.2	28.5	29.25	28.7	29.6	29.6
	1.4	29.9	29.6	29.3	27.75	29.5	29.3	29.9	30
CS-11	0	19.65	30.7	19.5	30.8	18.2	30.4	27.2	32.38

	0.14	20.5	26	20.25	24	19.25	28.4	25.25	30.75
	0.28	20.25	22.3	17.4	20	19.75	20.75	22.6	23.75
	0.42	21.4	10.2	15	19.1	18	13	17.25	17.5
	0.56	22.75	21.3	19.9	18.5	17.6	16.25	17.5	17.9
	0.7	23.9	22.75	19.75	20.75	20	20.6	21.2	22.2
	0.84	23.5	25.6	25	23.6	24.55	24.5	24.75	25.2
	0.98	25.75	25.5	25.7	26.5	25.6	25.4	25.9	26.95
	1.12	27.6	26	26.7	26.25	26.6	27.25	28.5	26
	1.26	28.6	28.2	27.6	27.4	28.6	28	29.5	28.6
	1.4	29.4	29	28.75	28.5	29.9	28.6	30.25	29.7
CS-12	0	22.5	32.4	20.4	32	19.25	31.75	28	33.95
	0.14	25.05	31.9	20	29.3	18.25	31.5	26.3	31.6
	0.28	23.25	25.4	20.75	24.8	17.8	24.25	25.5	23.5
	0.42	20.4	19.3	20.25	18.9	19.25	17.95	18.3	16.75
	0.56	19.2	18.5	18.2	18	19.1	15	16.5	15.2
	0.7	16.7	18.7	19.75	21.9	20.5	17.45	18.5	16.6
	0.84	20.4	22.6	22.6	22.2	21.75	23.5	21.25	21.5
	0.98	26.5	25	26.25	25.6	25.25	25.4	25.4	25.2
	1.12	26.6	26	26.2	26.75	27.25	25.4	27.4	25.9
	1.26	27.5	26.2	27.4	27.3	28.6	25.3	27.75	26.8
	1.4	28	27.05	28	27.6	28.25	25.15	29	26.4
CS-13	0	13.75	17.6	13.75	18.2	15.8	17.4	15.05	16
	0.14	14.75	18.1	14.2	19.4	16.5	18.05	14.6	18.5
	0.28	16	17.6	15.25	19.2	16.6	17.4	15.4	18.6
	0.42	16.75	17.6	16.9	15.9	18.3	16.2	18.6	15.75
	0.56	18.9	18.6	19	19.6	20	17.05	18.2	18.5
	0.7	22.5	19.75	21.15	20.75	22.2	19.9	20.25	20
	0.84	23.75	21.9	23.05	21.8	22.6	22.75	22.4	22.2
	0.98	23.6	24	24.75	21.3	25.6	24.9	25.25	25
	1.12	27.5	26.3	26.25	26.25	26.5	26.6	26.75	26.75
	1.26	28.25	28.1	28.25	28.25	22.6	28.5	28.7	28.75
	1.4	30.25	29.9	30.6	28.2	30.25	30.5	31	30.5

7.3.4 Efficiency of Erosion Reduction with Submerged Vanes

To better understand and quantify the effectiveness of the submerged vanes in reducing the erosion of the right bank, the change in bed elevations observed for without submerged vane cases are compared with the changes in bed elevations observed for submerged vane cases along three offsets (0 km, 0.14 km, and 0.28 km

from the right bank) within the most critical section of the bend (from CS-09 to CS-12). Figure 7.21 shows the percentage reduction in bank erosion at these offsets under the tested four discharges. The percentage reduction in bank erosion is computed using the following equation:

$$\text{Reduction in bank erosion (\%)} = \left(1 - \frac{\text{Bed elevation change with vanes}}{\text{Bed elevation change without vanes}}\right) \times 100 \quad (7.1)$$

Following Eq. (7.1), a 100% erosion reduction would indicate no future further erosion of the existing outer bank would occur after installing the submerged vanes, whereas a 0% erosion reduction would indicate that changes in bed elevation is same for both conditions. Furthermore, (i) if deposition occurs at the outer bank, then % erosion reduction will exceed 100% and (ii) if the bed erosion with vane is more than without vane, then % erosion reduction will be less than 0%. In this study, the percentage reduction in bank erosion due to the submerged vanes is obtained to be ranging from 63.4% to 100%, from 30% to 100%, and from 15.6% to 79.8% for 0 km, 0.14 km, and 0.28 km offsets from the right bank, respectively as shown in Fig. 7.21. Figure 7.21 also indicates that the percentage reduction in the bank erosion at the right bank (offset = 0 km) is about or equal to 100% and the percentage reduction decreases with the distance from the right bank for all discharges. Furthermore, the observed erosion reduction varies from 35.9% to 100%, from 23.1% to 100%, from 16% to 89.3%, and from 15.6% to 100% for cross-section CS-09, CS-10, CS-11, and CS-12 respectively. At CS-11, the percentage reduction in bank erosion at the right bank remains marginally below 100% across all flow conditions, indicating that this area is the most susceptible section to bank erosion within the river bend, even after the installation of the submerged vanes. Overall, it is found that the installation of submerged vanes is useful to bank protection along the river bend for a wide range of discharges, and the designed submerged vanes are recommended to be used at the investigated Ganga river site for river training and bank protection.

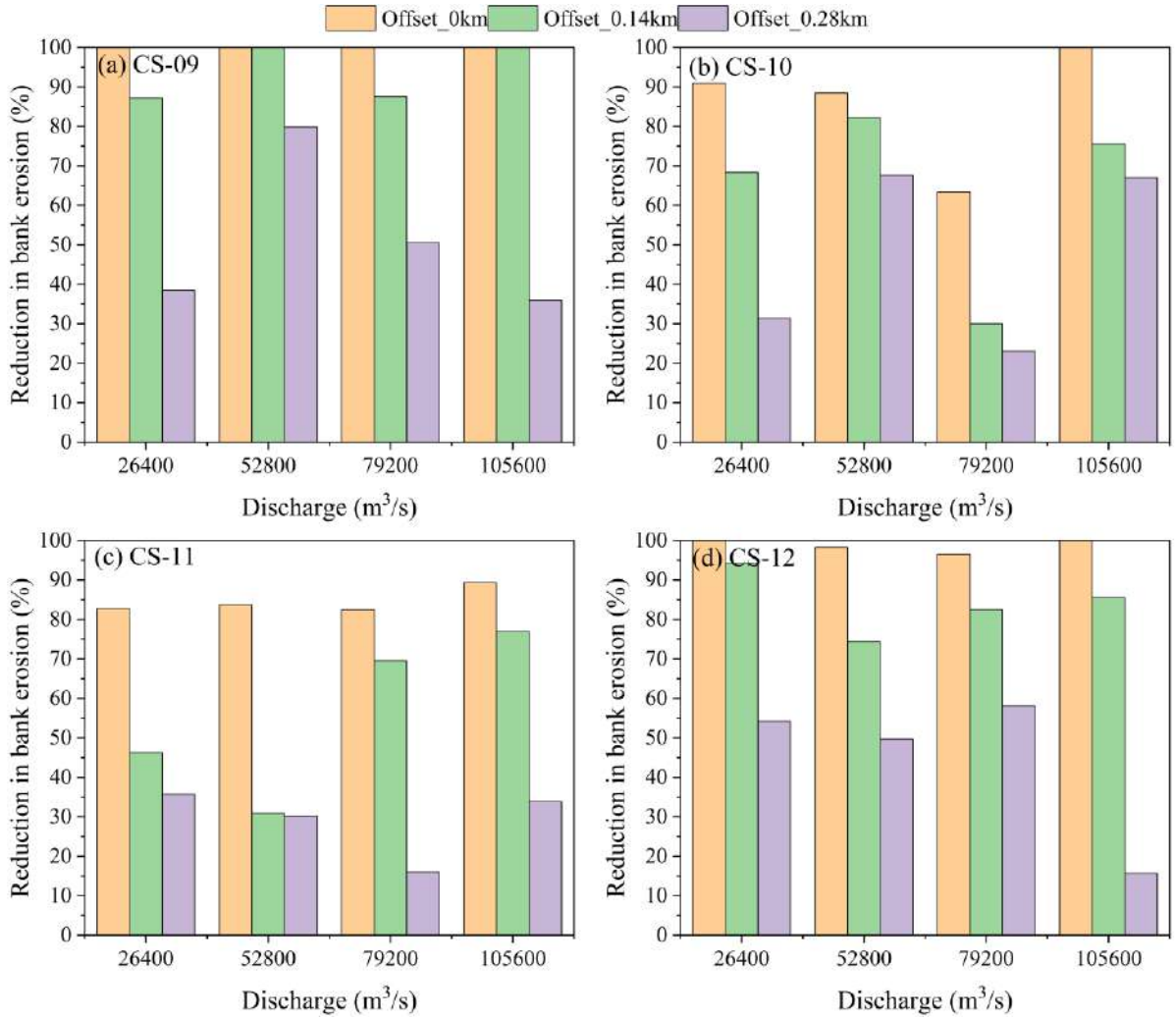

Fig. 7.21 Effectiveness of the submerged vanes in reducing the bank erosion at different cross-sections under four discharges

7.4 CONCLUDING REMARKS

River bend erosion, often driven by secondary currents induced by centrifugal forces, constitutes one of the most difficult challenges in river engineering. In present study, the historical morphological changes in the Ganga river reach from Bhagalpur to Ismailpur in Bihar, India were inspected, and a physical model study of the reach was conducted to investigate the effectiveness of submerged vanes in protecting the river right bank and in shifting the river main course away from the affected right bank. The distorted physical model was built to a horizontal scale of 1/700 and a vertical scale of 1/70 and the experiments were carried out under four discharge conditions and with both without and with submerged vanes situations. The observations made from this study concludes that:

- Historical satellite images of year 1985, 2010, 2019, and 2024 have been used to study the morphological changes in the Ganga river at Bhagalpur, Bihar. Historical satellite images reveal that year 1985 to 2024 the main course of ganga river between Bhagalpur to Ismailpur shifted towards right bank around 4 km.
- The dye test observations indicate that, under the present conditions of the Ganga River, the main flow remains attached to the right bank; however, following the installation of the submerged vanes, the main course of the river sifted leftward away from the right bank.
- The physical model study found that significant bank erosion is occurring along the right bank of the model under the present conditions of ganga river; and the bank erosion is more at lower discharge condition compare to higher discharge.
- The percentage reduction in bank erosion due to the submerged vanes is obtained to be ranging from 63.4% to 100%, from 30% to 100%, and from 15.6% to 79.8% for 0 km, 0.14 km, and 0.28 km offsets from the right bank. Results shows that implementation of submerged vanes can effectively reduce the bend erosion along the outer bank of the river.

8. APPLICATION OF SUBMERGED VANE: CASE STUDY - II

Removal of sediment from the mouth of the spill channel of Padma/Ganga river near Jangipur

8.1 INTRODUCTION

Jangipur Navigation lock in West Bengal links Padma river with Bhagirathi river and its navigational channel joins with a spill channel of the Padma river as shown in Fig. 8.1. For the revival of the Jangipur lock, it is necessary to ensure flow in the spill channel throughout the year. The length of the spill channel is about 30 km, and it originates from a place Suti, as shown in the Fig. 8.1. Over the year, silting has occurred at the mouth of the spill channel which has blocked the flow from the Padma river to the spill channel. In general, water flows in the spill channel in the monsoon period only, as shown in the Figs. 8.2 (a-b). It can be seen in these figures that water is flowing in the channel in the month of November, however, there is no flow in the month of January. To ensure flow throughout the year, it is necessary to desilt the sediment from the mouth of the spill channel. In the present study, the optimised shape and size of the vanes is used at the mouth of the spill channel and its performance shall be studied.

Fig. 8.1 Location of the Jangipur lock and spill channel

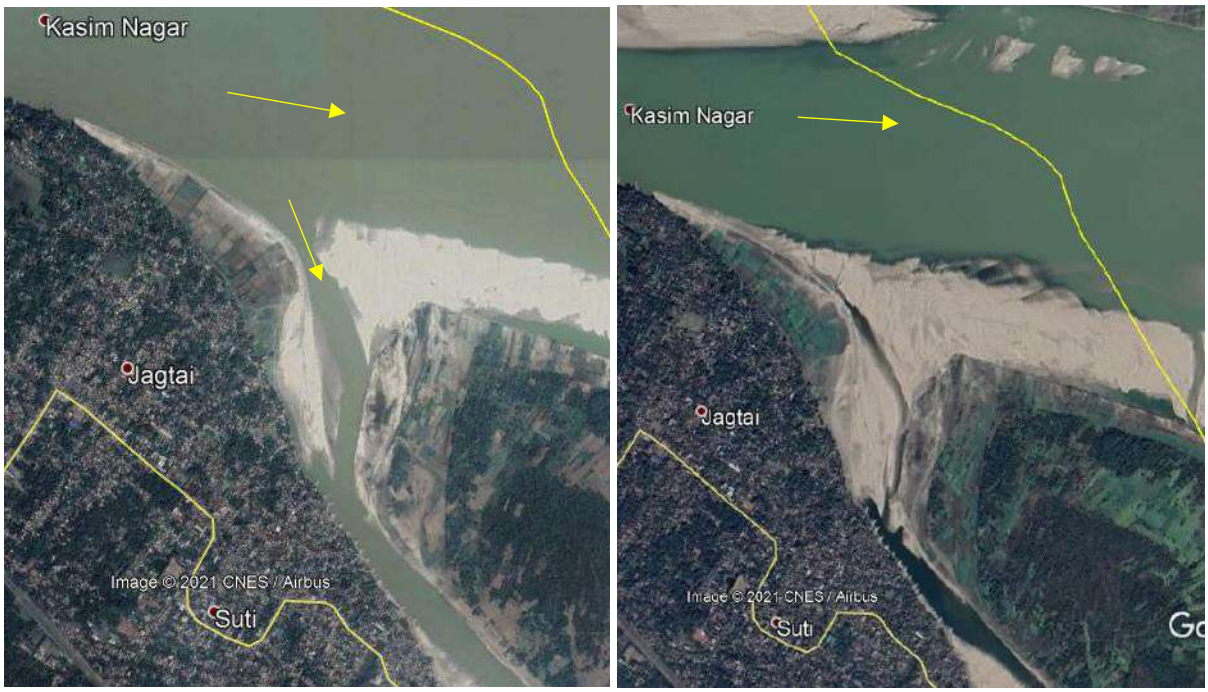

Fig. 8.2 Google images dated (a) 16/11/2019 and (b) 3/1/2020

8.2 MATERIALS AND METHODOLOGY

8.2.1 Physical Model Study

Physical model study a part of the Padma river and spill channel was carried using the survey data carried out by IWAI, Farakka and developed contour map carried out during 22.07.23-23.07.23 as shown in Fig. 8.3.

Normal year discharge in the Ganga river downstream of the Farakka = 41500 m^3/s (Ahmad et al. 2017). This discharge is adopted at the Suti for the model study and corresponding water level = 21.0 m.

The model was conducted on Froude number similarity with horizontal scale of 1:500 and vertical scale of 1:50. A 2000 m length of the Ganga river was reproduced in the model (Fig. 8.4). All the available cross-sections of the Ganga river and Spill Channel were used to produce the profile of the river in the model. A re-circulating system was designed to supply water to the physical model of the Ganga river. The system was consisted of an upstream channel that supplies water to the river model and a downstream channel for collection of the water coming from the model. The downstream channel was extended up to the sump of the pump, from where water was lifted through a pump and discharged into the upstream channel. A valve and an electro-magnetic flowmeter were provided in the delivery pipe of the pump to regulate and measure the discharge, respectively. A perforated wall was provided upstream of the model to break the large eddies of the flow. Loose coarse gravel was provided downstream of the perforated wall to control the bed erosion. A tail gate was provided downstream of the model to maintain desired water level at the downstream cross-section. Available sediment of the median size of 0.25 mm was used to construct the river model. Water level and bed level of the river at various locations of the model were measured by a scale while velocity in the model was measured by a miniature type current meter. Water level and bed elevation were measured by a protype scale. Views of the model under dry condition from different angles are shown in Figs. 8.5 (a-c).

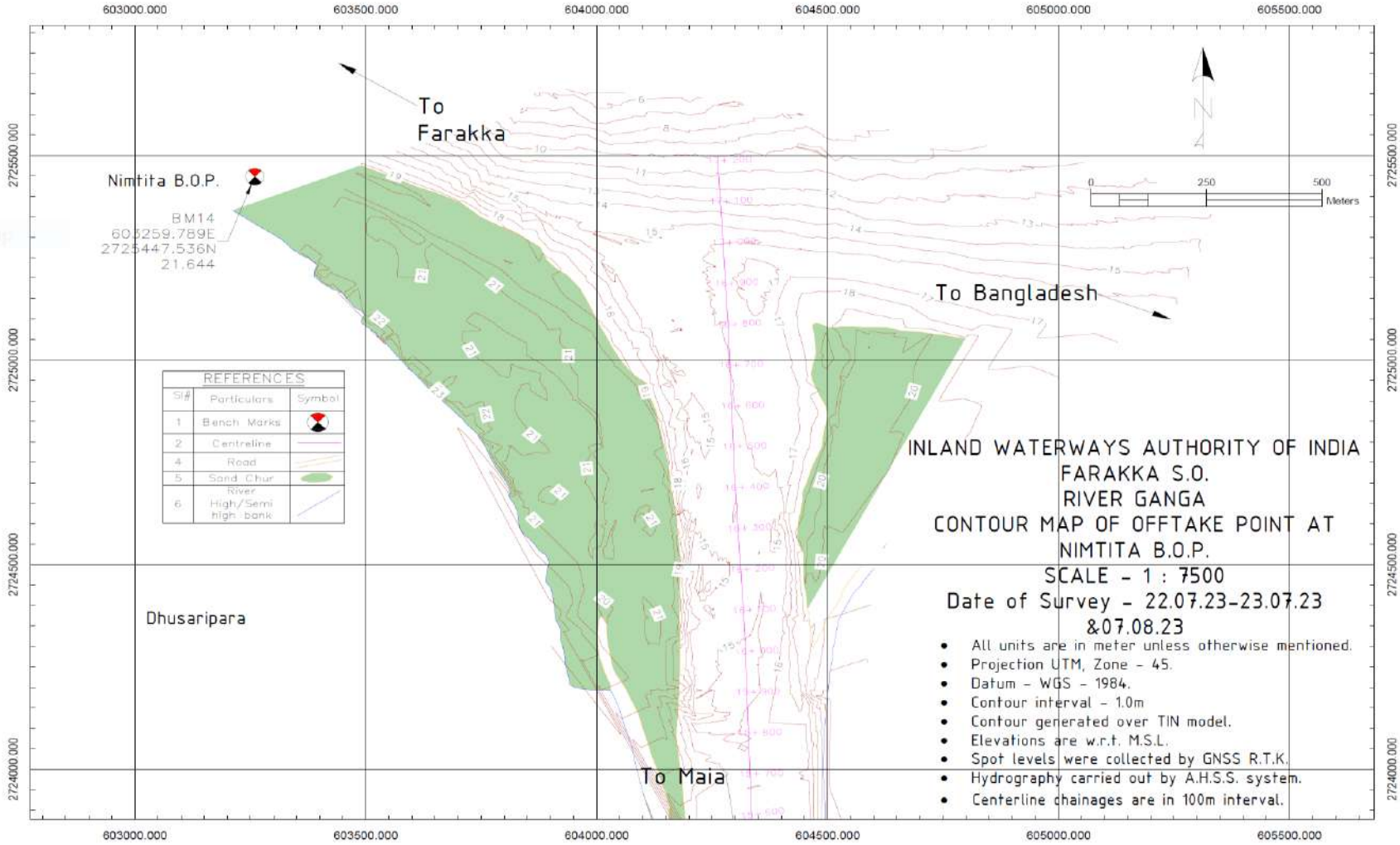

Fig. 8.3 Contour map of offtake point at Namtita, Jangipur

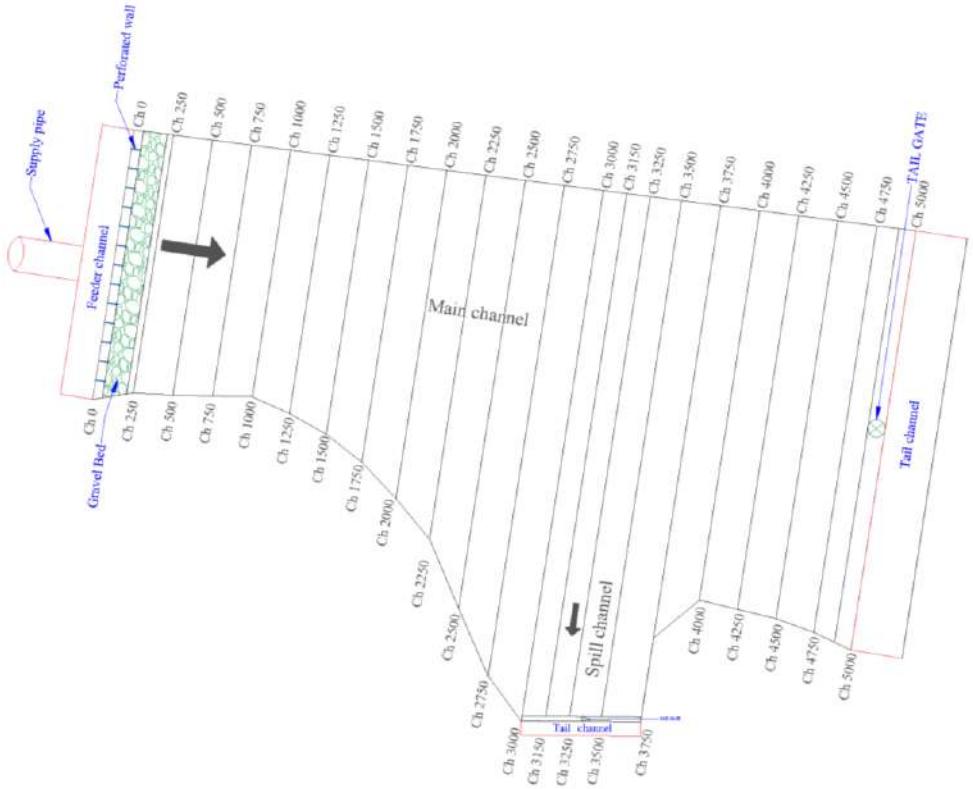

Fig. 8.4 Plan layout of modelled length of the river

Fig. 8.5a Front view of the model under dry conditions

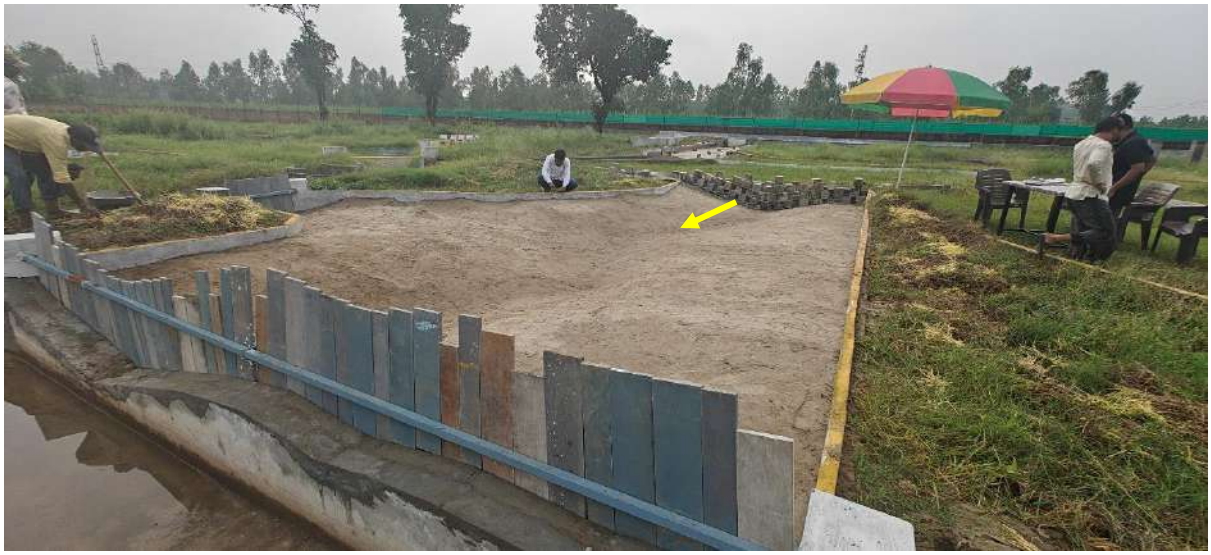

Fig. 8.5b Back view of the model under dry conditions

Fig. 8.5c Side view of the model under dry conditions

8.2.2 Selection of The Physical Model Scale

River models are usually designed with a larger scaling ratio in the horizontal direction than in the vertical direction which lead to distorted models. Flow pattern does not get affected seriously due to distortion and gives good results. A distorted model of rivers is designed with a Froude similitude, where the Froude number scaling ratio is related to the vertical-scale ratio. A classical example of the distorted model is that of the Mississipi river which is constructed with a horizontal scale of 1/2000 and vertical scale of 1/100 i.e., distortion ratio of 20. In general, the distortion

ratio is kept not beyond 10 (Chanson 2004). In practice, river models are scaled with a Froude similitude and viscous scale is minimized. Model scales are selected such that model size is less but at the same time it is ensured that the model Reynolds number is large enough to make the flow turbulent and possibly fully rough at the smallest test flows.

With the consideration of the above points, a mobile bed distorted model based on the model horizontal scale of 1/500 and vertical scale of 1/50 has been proposed herein.

Design discharge $Q = 41500\ m^3/s$

HFL= 70.054 m

Model scale: Horizontal scale $l_r = 1/500$

Vertical scale yr= 1/50

Adopting the Froude number similarity

$$\left.\frac{V}{\sqrt{gy}}\right]_{prototype} = \left.\frac{V}{\sqrt{gy}}\right]_{model}$$

Here V = velocity; y = depth of flow; and g= acceleration due to gravity.

Velocity scale $V_r = \sqrt{y_r} = 0.141$

Discharge scale $Q_r = l_r V_r y_r = \frac{1}{500} \times \left(\frac{1}{50}\right)^{1.5} = 5.66\times10^{-6}$

Discharge in model $Q_m = 41500 \times 5.66\times10^{-6}\ m^3/s$

$= 0.235\ m^3/s$

8.2.3 Design of Vane

In the present study, the submerged vanes were designed following the guidelines proposed by Odgaard (2009). The design specifications are provided in Table 8.1.

Table 8.1 Details of submerged vane parameters

Vane parameters	Design specifications following Odgaard (2009)	Vane dimensions in the model
Height of vane (H)	0.2–0.4 times of average flow depth (d)	3.2 cm
Length of vane (L)	3H	9.6 cm
Angle of attack (α)	13°–40°	20°
Lateral spacing between vanes	2H to 3H	9.6 cm
Longitudinal spacing between vanes	15H to 30H	33 cm

Previous investigations indicate that the local scour depth increases with an increase in the angle of attack (α). At larger α, the vane is subjected to a relatively larger drag force, with increased flow resistance. The major problem of using of larger α is the occurrence of a greater scour around the vane that may dislodge the vane (Odgaard & Kennedy, 1983; Odgaard & Spoljaric, 1986). Due to these considerations, the installation of a vane with $\alpha > 20^0$ is not feasible for practical applications in the field (Gupta et al., 2010). Therefore, $\alpha \approx 20^0$ was selected for all runs. In the present study, beveled submerged vanes are employed in place of rectangular ones, as they demonstrate effective reduction in local scour without significantly compromising vortex generation efficiency at a bevel angle of 45º (Mandal et al., 2025). The designed submerged vanes were placed in the model with specific position as shown in the Fig. 8.6.

Fig. 8.6 Position of the installed submerged vanes in the model. The yellow-shaded area represents the region where bed elevation measurements were taken.

8.3 PHYSICAL MODEL RESULTS

8.3.1 Running the Model Under Existing Conditions

The model was first run under the existing conditions for the discharges of 8,839 m^3/s, 14,142 m^3/s, 19,445 m^3/s, 24,218 m^3/s, 30,052 m^3/s, 35,355 m^3/s, and 41,500 m^3/s, as shown in Figs. 8.7 (a-g). At discharges of 8,839 m^3/s and 14,142 m^3/s, flow was confined entirely within the main channel, with no entry into the spill channel, as shown in Figs. 8.7a & 8.7b. At a discharge of 19,445 m^3/s, flow was just started entering into the spill channel as apparent from Fig. 8.7c. With further increase in discharge, flow into the spill channel increased progressively, as can be seen in Figs. 8.7 (d-g). Discharge passing through spill channels for 30052 m^3/s, 35355 m^3/s, and 41500 m^3/s in the river were 886 m^3/s, 2092 m^3/s, and 3036 m^3/s, respectively under existing condition. The water levels were measured at each cross-section for different discharges. Such water levels are given in Table 8.2 and depicted in Fig. 8.8.

Fig. 8.7a Flow pattern for 8839 m^3/s discharge under existing condition

Fig. 8.7b Flow pattern for 14142 m^3/s discharge under existing condition

Fig. 8.7c Flow pattern for 19445 m^3/s discharge under existing condition

Fig. 8.7d Flow pattern for 24218 m^3/s discharge under existing condition

Fig. 8.7e Flow pattern for 30,052 m^3/s discharge under existing condition

Fig. 8.7f Flow pattern for 35355 m^3/s discharge under existing condition

Fig. 8.7g Flow pattern for 41500 m^3/s discharge under existing condition

Table 8.2 Measure water level at different sections and discharges under existing condition

X-section (m)	Water level (m)						
Discharge (m^3/s) →	8839	14142	19445	24218	30052	35355	41500
750	15	15.75	16.75	18.5	19	20	21
1000	15.1	15.5	16.5	18	19	20.2	20.75
1500	15.2	15.75	16.8	18.2	19.2	19.8	20.5
2000	15.25	15.75	17	18.4	19.5	20.5	21
2250	15.25	15.6	17	18.5	19.65	20.6	21.25
2500	14.75	15.75	16.9	18.25	19.25	20.3	21.1
2750	15.2	15.5	16.85	18.3	19.5	20.3	21.2
3000	15.2	15.9	17.2	18.4	19.25	20.5	21
3500	15.4	15.75	17.1	18.75	19.75	20.75	21.4
4000	15.25	15.6	17.1	18.6	19.5	20.6	21.5
4500	15.2	15.6	17.1	18.25	19.25	20.5	21.25
4700	15.2	15.6	17.1	18.5	19.4	20.5	21.2

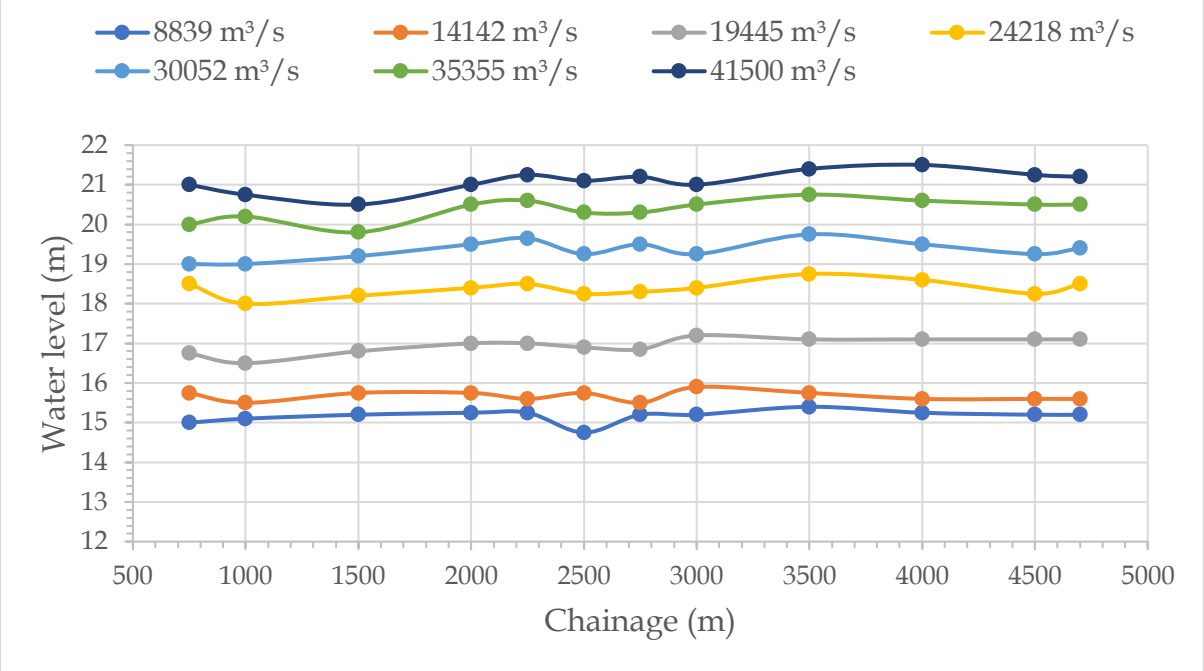

Fig. 8.8 Water surface profile for different discharges under existing condition

8.3.2 Running the Model with Submerged Vanes

The proposed submerged vanes were placed at the mouth of the spill channel in the physical model as shown in Figs. 8.9 (a-b). After the installation of the proposed submerged vanes, the physical model was operated under the same seven discharges, starting from the highest discharge of 41,500 m³/s. Flow pattern for different discharges are shown in Figs. 8.10 (a-g). It was observed that flow begins to enter into the spill channel at a lower discharge of 14,142 m³/s. With further increases in river discharge, flow into the spill channel increased progressively. The water levels at different sections and discharges with submerged vane conditions were measured and shown in Fig. 8.11, and given in Table 8.3. Discharge passing through the spill channel were 441.5 m³/s, 1193.2 m³/s, 2654.3 m³/s, 3699.1 m³/s, and 6185.6 m³/s for river discharge of 19,445 m³/s, 24,218 m³/s, 30,052 m³/s, 35,355 m³/s, and 41,500 m³/s, respectively. Such values of the diverted charges are given in Table 8.3 and are also shown in Fig. 8.12a.

Figs. 8.9a-b View of the model under dry conditions with submerged vanes

Fig. 8.10a Flow pattern for 8839 m^3/s discharge with submerged vanes

Fig. 8.10b Flow pattern for 14142 m^3/s discharge with submerged vanes

Fig. 8.10c Flow pattern for 19445 m^3/s discharge with submerged vanes

Fig. 8.10d Flow pattern for 24218 m^3/s discharge with submerged vanes

Fig. 8.10e Flow pattern for 30,052 m^3/s discharge with submerged vanes

Fig. 8.10f Flow pattern for 35355 m^3/s discharge with submerged vanes

Fig. 8.10g Flow pattern for 41500 m3/s discharge with submerged vanes

Table 8.3 Measure water level at different sections and discharges with submerged vanes

X-section (m)	Water level (m)						
Discharge (m^3/s) →	8839	14142	19445	24218	30052	35355	41500
750	15.75	17.1	18	18.7	19.25	20.4	21.1
1000	15.5	17.1	18	18.6	19.25	20.25	21.1
1500	15.75	16.9	17.5	18.7	19.25	20.5	21
2000	15.75	17	17.75	18.75	19.5	20.75	21.5
2250	15.75	17.1	17.75	18.8	19.7	20.75	21.6
2500	15.75	17.1	17.8	18.8	19.75	20.75	21.25
2750	15.75	17.2	17.9	18.75	19.75	20.7	21.25
3000	15.6	17.1	17.75	18.75	19.75	20.5	21.1
3500	15.7	17.1	17.9	19	20	21	21.5
4000	15.5	17.1	17.9	18.8	19.9	20.9	21.75
4500	15.25	17	17.75	18.85	19.75	20.9	21.5
4700	15.3	16.6	17.4	18.5	19.5	20.5	21.3

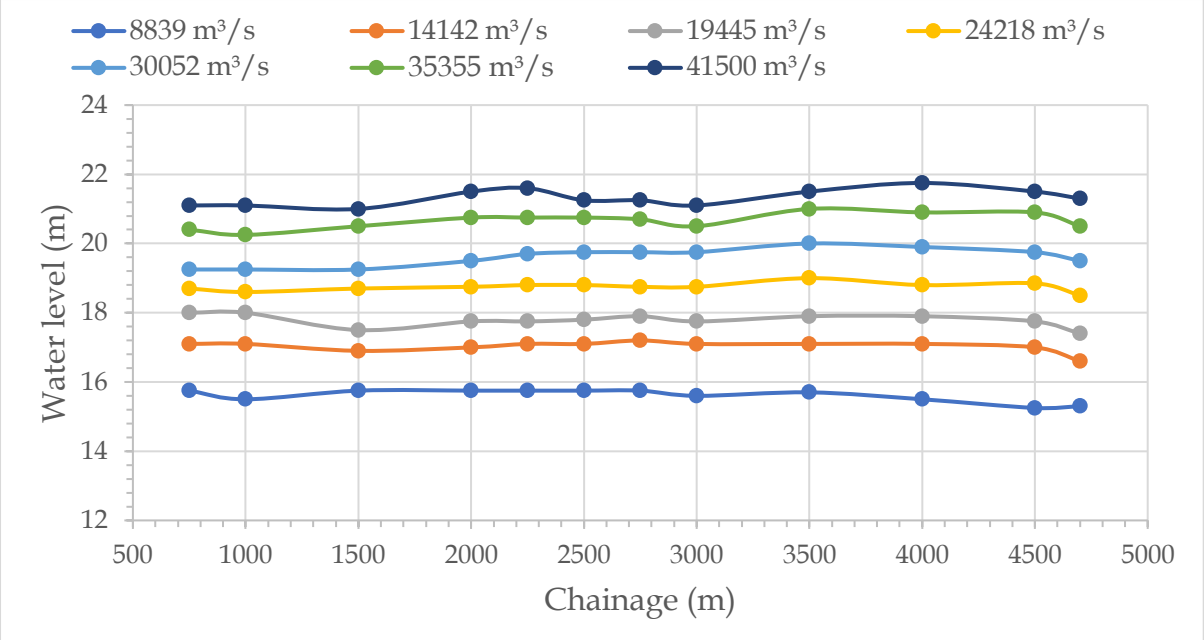

Fig. 8.11 Water surface profile for different discharges with submerged vanes

The percentage flow passing through the spill channel under without and with submerged vane for different inflow discharges are shown in Fig. 8.12a and the calculated values are given in Table 8.4. It is evident that percentage discharge passing through the spill channel are higher under the installed submerged vanes compare to the existing river conditions, as shown in Fig. 8.12b. The increment in percentage discharges due to installation of submerged vane with respect to existing conditions are 2.27%, 4.93%, 5.88%, 4.54% and 7.6% respectively. The overall findings from the physical model study indicate that installation of the proposed submerged vanes at the mouth of the spill channel facilitates the flow in the spill channel.

Table 8.4 Discharge passing through spill channel under existing and submerged vanes conditions

Total incoming discharge in the river (m^3/s)	Existing condition		With submerged vanes	
	Discharge in Spill Ch. (m^3/s)	% age discharge in Spill Ch. (m^3/s)	Discharge in Spill Ch. (m^3/s)	% age discharge in Spill Ch. (m^3/s)
19445	0	0	441	2.27
24218	0	0	1193	4.93
30052	886	2.95	2654	8.83
35355	2092	5.92	3699	10.46
41500	3036	7.31	6186	14.91

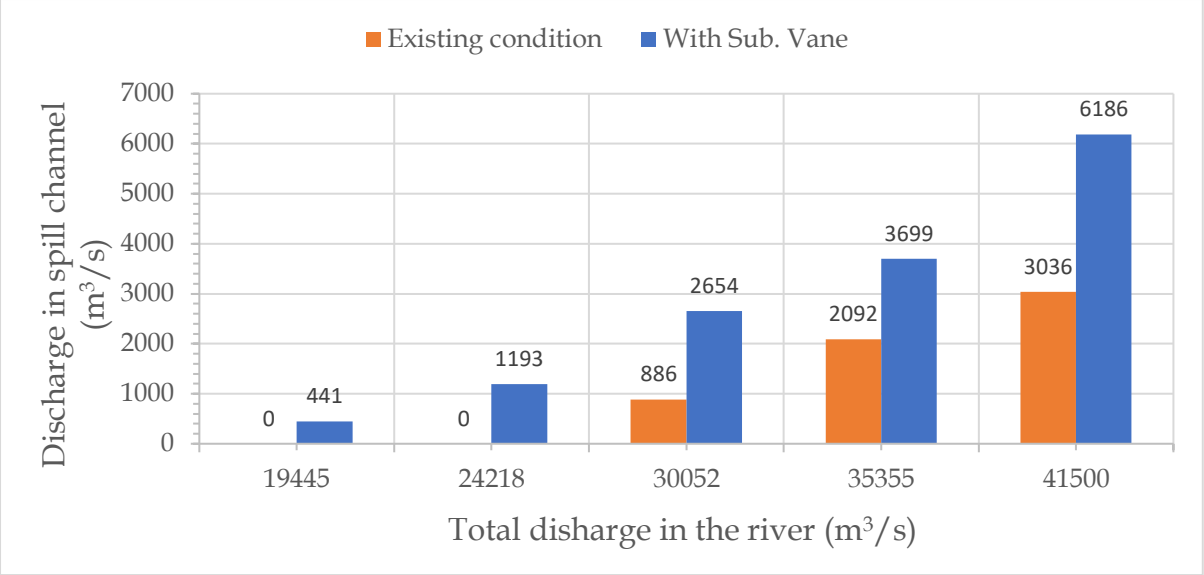

Fig. 8.12a Discharge passing through spill channel under existing and submerged vanes conditions

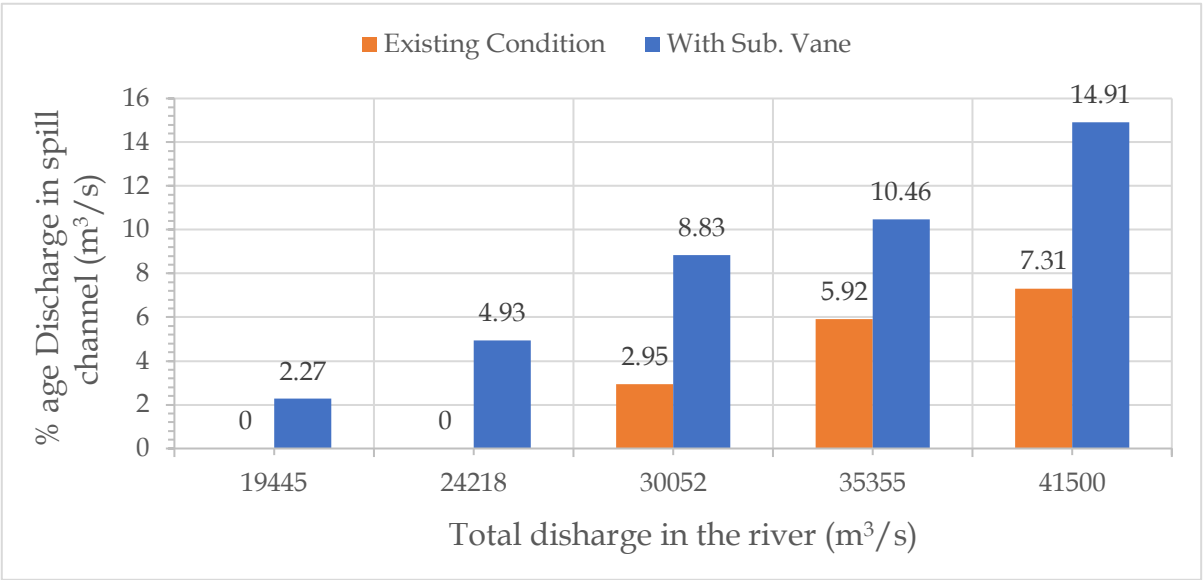

Fig. 8.12b Percentage discharge passing through spill channel under existing and submerged vanes conditions

8.3.3 Comparison of Residual Beds in Spill Channel

After running the model for discharge of 41500 m3/s under the existing condition (i.e., in the absence of submerged vanes) and submerged vane condition, the residual bed of the river and spill channel were measured. Pics of the residual bed under the existing and submerged conditions are shown in Figs. 8.13a & 8.13b, respectively. Whereas the contour bed profiles across the spill channel in study area under without and with submerged vane conditions, are shown in Figs. 8.14 & 8.15. The bed elevation readings were taken between the CS 3150 to CS 2250 in the study area of the model towards the spill channel. The x-axis is located at 1875 m to 3750 m from left bank of the model. The observations indicate that bed degradation occurred within the spill channel under the submerged vane installation. The comparison of deepest bed level under two conditions, i.e., (i) bed profile after the model run without vanes, and (ii) bed profile after the model run with vanes, are provided in Fig. 8.16. The results indicate that the proposed submerged vanes effectively contribute to deepen the bed both near the mouth and throughout the spill channel.

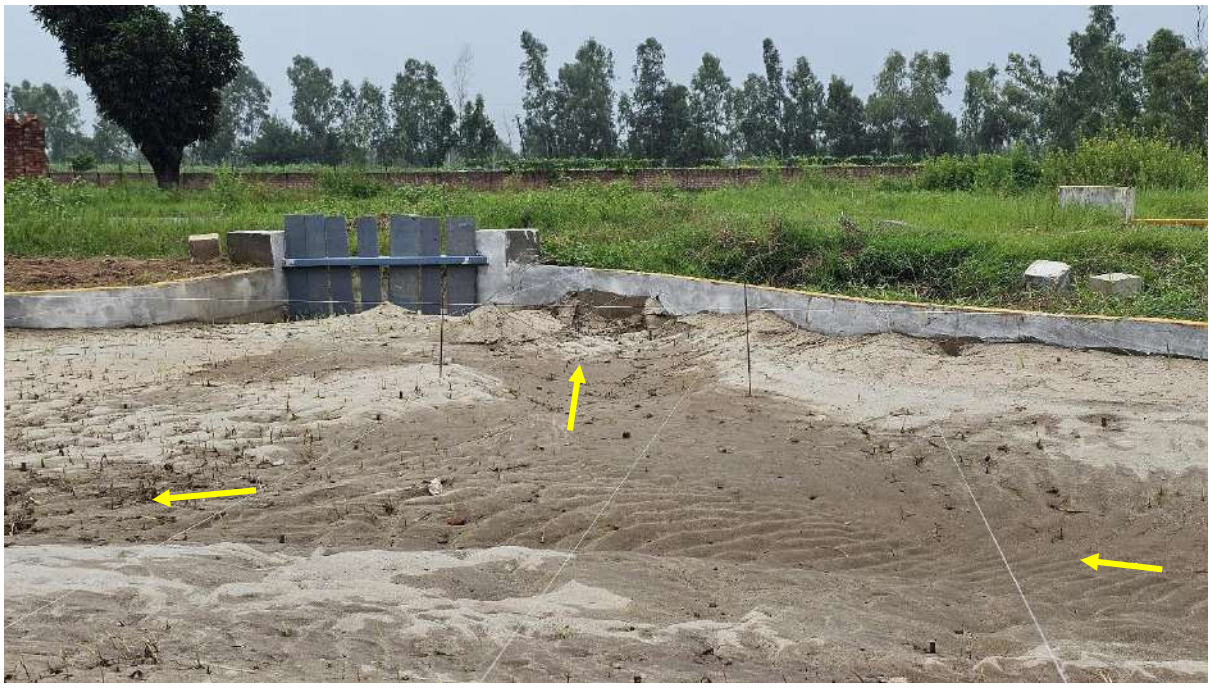

Fig. 8.13a Residual bed after running the model under existing condition

Fig. 8.13b Residual bed after running the model under submerged vane condition

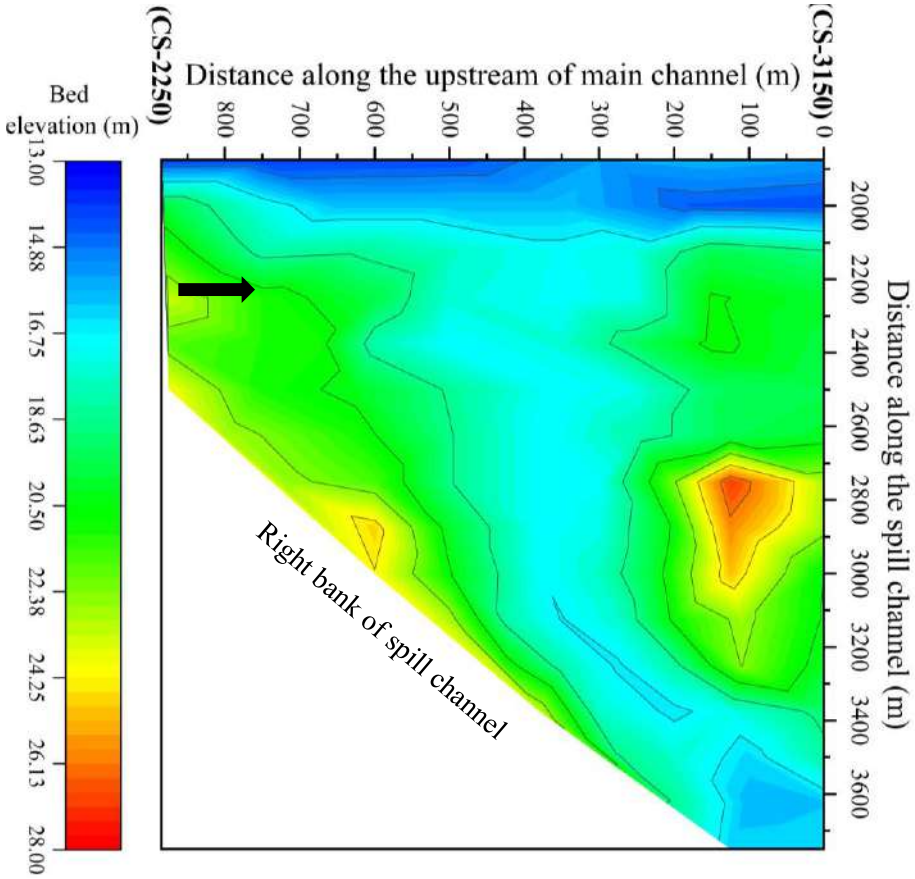

Fig. 8.14 Bed elevation profile of study area in existing condition

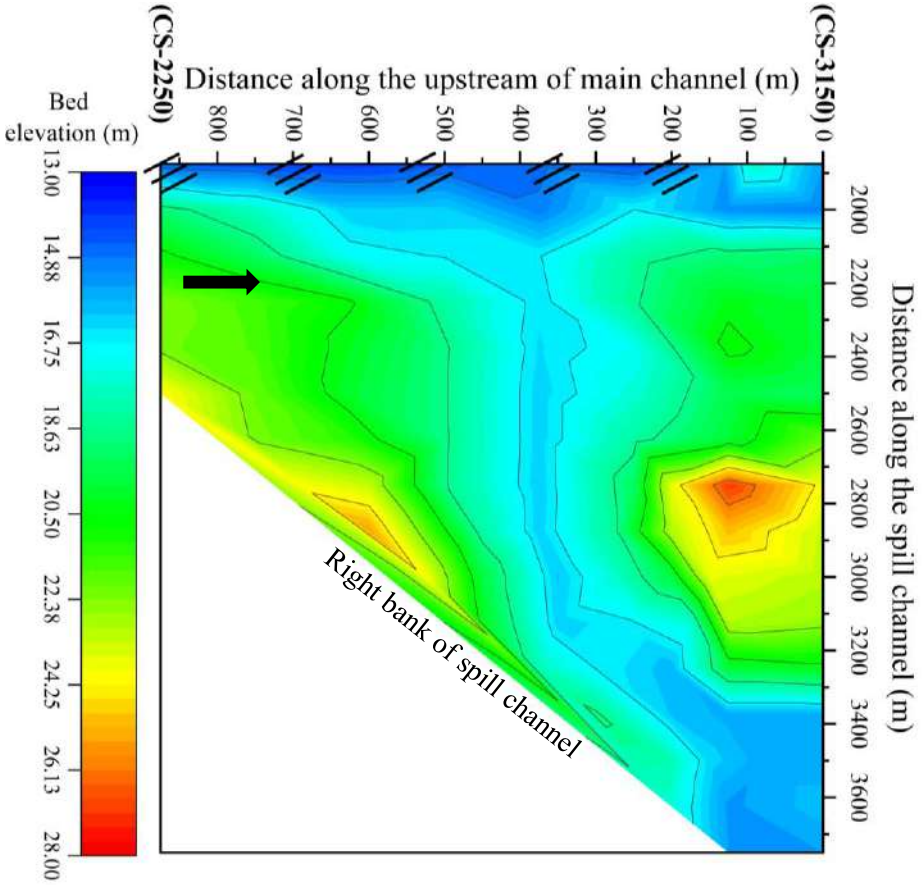

Fig. 8.15 Bed elevation profile of study area in submerged vane condition

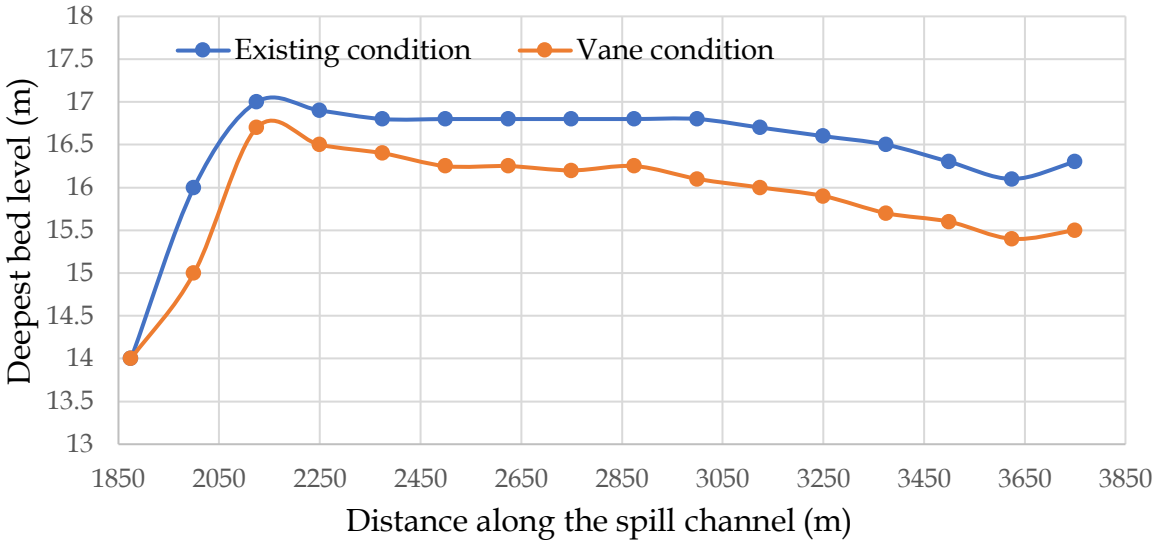

Fig. 8.16 Comparison of deepest bed level under both conditions

8.4 CONCLUDING REMARKS

In the present study, the historical morphological changes in the Jangipur Navigation lock located in West Bengal, India were inspected, and a physical model study of the reach was conducted to revival of the Jangipur lock, to ensure flow in the spill channel throughout the year. The distorted physical model was built to a horizontal scale of 1/500 and a vertical scale of 1/50 and the experiments were carried out under different discharge conditions and with both without and with submerged vanes situations. Following conclusions are derived from this case study:

- With the installation of the submerged vanes at the mouth of the spill channel, the discharge passing through it has increased. The percentage increases in discharge in the spill channel with the installation of submerged vanes compared to existing conditions are 2.27%, 4.93%, 5.88%, 4.54%, and 7.6% for river discharges of 19,445 m^3/s, 24,218 m^3/s, 30,052 m^3/s, 35,355 m^3/s, and 41,500 m^3/s, respectively.
- The measured bed elevation indicates that with the installation of submerged vane, bed has degraded in the spill channel, which has resulted in flow through the spill channel under lean flow season also.
- The comparison of the deepest bed levels indicates that the installed submerged vanes effectively deepen the bed both near the mouth and throughout the spill channel.
- Thus, the bevelled vanes can be used to desilt the mouth of a spill channel or water intake for passing the flow through it.

9. CONCLUSIONS AND RECOMMENDATIONS

In the present study, laboratory experiments and field study both were investigated to study the efficiency of bevel submerged vane. Laboratory experiments were conducted to study the flow characteristics and scour pattern downstream of the submerged vane. Effect of various parameters which considerably affected the scour pattern at the confluence of the channels was studied by collecting data in the present study. The velocity and turbulence characteristics in the equilibrium scoured condition were also investigated. Experiments were carried out for one rectangular and four bevel shape submerged vane, three heights of vane, four angle of attack, and three discharges in open channel flow. A relationship for estimation of maximum scour depth in the scour holes developed near the vane was also obtained. Numerical study was also performed to investigate the flow field the vane and vortex downstream of the vane on equilibrium scoured condition. The *k-w* numerical model effectively replicated the physical behaviour observed in the experimental model. The results of the numerical simulation were validated with the experimental data collected in the present study and found to be in good agreement. The optimal shape of the submerged vane was tested for two field applications.

Following conclusions have drawn from the present study

1) Experimental study was carried out for different bevelled angle, angle of attack and submergence of the vanes along with its curved shape. Characteristics of flow field and bed morphology for all the tested vanes and for different discharges were measured.
2) Curved vanes indicate excessive scour in the vicinity of the vanes. Considering the stability of the curved vanes under severe scour conditions, this shape was not adopted for the further study.
3) Experimental observation indicates that the local scour hole has been observed to increase with increasing angle of attack, vane height, and flow discharge, whereas it decreases with an increase in bevel angle. The horseshoe vortex plays a significant role in generating local scour on the pressure side of the

vane, while the primary vortex originating from the trailing edge persists over a longer distance. Observations indicate that more significant scour occurred on the pressure side of the vane, whereas some deposition is noted on the suction side at low angles of attack. The primary vortex eroded material from the right side and depositing it on the left side along the flow, and changes made to the bed topography gradually diminish as they move downstream.

4) Analysis of the transverse scour profiles indicates that an increase in both the angle of attack and the vane height leads to a more prominent scour hole formation near the leading edge of the vane. Transverse scour profiles also represent the scour and deposition profiles downstream of the vane. The reduction in profile of local scour became more pronounced compared to the downstream scour as the bevel angle of the vane increased.

5) The percentage scour reduction measurement shows that the maximum scour depth around the vane was significantly reduced by cutting the leading edge at various bevel angles. However, the percentage reduction in scour downstream of the vane was less compared to the local scour reduction around the vane as the bevel angles increased.

6) The scour volume was measured around the vane by using an ultrasonic bed profiler. It is found that volume of scour increases with an increase in both the angle of attack and the vane height, while it decreases with an increasing bevel angle.

7) Dimensional analysis was performed for identifying the parameters affecting the maximum scour depth in local scour holes and extension of scour hole in the downstream of the vane. The discharge, angle of attack, densimetric Froude number, vane height and bevel angle were identified as the key parameters affecting the maximum scour depth in scour holes and extension of scour hole in the secondary channel.

8) Effect of different parameters on maximum scour depth in the local scour hole (d_{sm}), and extension of scour hole in downstream of the vane (d_{sd}) was analysed using the experimental data obtained from present study. d_{sm} and d_{sd} were found to increase with increase in densimetric Froude number and vane height

and angle attack. However, d_{sm} and d_{sd} were decreased with the bevel angle of submerged vane.

9) We derived empirical equations from the present experimental data to calculate d_{sm} and d_{sd} by using least-squares curve fitting methods. The calculated values of maximum scour depth around the vane and the extension of the scour downstream of the vane offer good correlation with the observed data.

10) Sensitivity analysis indicated that the densimetric Froude number of the flow and the angle of attack have the largest influence on the maximum depth of the local scour. At the same time, the height of the vane is the most sensitive parameter affecting the extension of the scour in the downstream channel. Although bevel angle exhibits relatively lower sensitivity compared to other parameters, it remains an effective method for reducing local scour around the vane.

11) Three-dimensional velocity components were obtained using an Acoustic Doppler Velocimeter (ADV) to facilitate a detailed analysis of the flow characteristics downstream of the submerged vane based on experimental observations.

12) Three-dimensional velocity was observed along the vertical line extending from the bed to the water level, corresponding to distances of 3H, 8H, and 20H from the center of the vane through downstream. The streamwise velocity profile loses its logarithmic nature but it shows a S-type variation over the vertical direction for all bevel angle which suggests the presence of point of inflexions in the velocity profiles and it confirms the presence of strong vortices at the transect due to submerged vane up to 8H plane. At x = 20H, the velocity distribution has become nearly logarithmic in comparison with velocity profiles at x = 3H and 8H which suggested the dampening of vortices in the flow by viscosity.

13) Turbulence energy shows lesser values near the bed and then its increase to reach the maximum at the 0.85 times the vane height and then again, they reduce when the water surface is approached. The peak of turbulent energy

significantly reduced with increasing the bevel angle beyond 45º. At 20H plane, the TKE profiles of all bevel vanes converging towards each other and the magnitude of the peak is reduced. When the turbulence travel towards downstream of the vane, the viscosity regains its dominance which leads to dissipation of the tip vortices.

14) The analysis of flow field around the submerged vane from the CFD simulation were found to be good agreement with the experiment results.

15) The study on flow pattern revealed that a large spiraling motion was seen downstream of submerged vane and the orientation of vane anticlockwise along the flow generated the clockwise circulation downstream of the vane.

16) The simulated pressure contour profiles in the x–z plane demonstrate a consistent pattern of positive pressure on the pressure side and negative pressure on the suction side across all bevel configurations. Furthermore, the results reveal that with an increase in bevel angle, the pressure gradient diminishes and shifted from the leading edge toward the trailing edge.

17) The streamwise velocity distribution in the x–z plane shows a high-velocity region on the right side and a low-velocity region on the left side of the shear layer downstream of the vane. The sediment eroded from the high velocity zone and deposited to the low velocity zone.

18) A strong transverse velocity was observed at the tip of the leading edge of the rectangular submerged vane, and its significantly decreases with increasing the bevel angle of the vane beyond 45º. The vertical transverse velocity profile shows a linear decrease in the transverse velocity from the bed to a height of 0.1 times depth of flow (h) where the maximum magnitude transverse velocity was observed and it becomes zero at mid-depth then it increases again until the water surface is reached, going through a second inflection point at 0.50 y/h. Beyond a bevel angle of 45°, the transverse velocity at vertical direction is significantly reduced.

19) Calculation of vorticity downstream of the vane revealed that vorticity is almost the same up to 45º bevel angle, and further increasing the bevel angle significantly reduce the vorticity. The primary cause for this reduction is the

potential lift surpassing the vortex lift beyond a 45º sweep angle. Due to cutting the leading edge at an angle greater than 45°, the surface area and parameter of the vane reduced significantly, which decreases the vortices at the leading edge.

20) The turbulent kinetic energy (k) and its dissipation rate (ε) exhibit peak values in the immediate vicinity of the submerged vane. These turbulence characteristics are most intense for the rectangular vane configuration and progressively decline with increasing bevel angle.

21) Both experimental and numerical study show that rectangular vane with bevel angle of 45º reduces the local scour in the vicinity of the vanes without compromising the generation of vortex when compared to rectangular vanes without bevel. Based on these findings, rectangular vanes with 45-degree bevel angle vanes are recommended their applications.

22) The optimized bevel submerged vane is examined to reducing bend erosion along the right bank and redirecting the main flow course away from the concave side of the Ganga River located from Bhagalpur to Ismailpur in Bihar.

23) A distorted physical model was built to a horizontal scale of 1/700 and a vertical scale of 1/70 and the experiments were carried out under four discharge conditions and with both without and with submerged vanes situations.

24) Historical satellite images of year 1985, 2010, 2019, and 2024 have been used to study the morphological changes in the Ganga river at Bhagalpur, Bihar. Historical satellite images reveal that year 1985 to 2024 the main course of ganga river between Bhagalpur to Ismailpur shifted towards right bank around 4 km.

25) The dye test observations indicate that, under the present conditions of the Ganga River, the main flow remains attached to the right bank; however, following the installation of the proposed Bevel submerged vanes, the main course of the river sifted leftward away from the right bank.

26) The physical model study found that significant bank erosion is occurring along the right bank of the model under the present conditions of ganga river;

and the bank erosion is more at lower discharge condition compare to higher discharge. Such observations are seemingly influenced by lesser flow concentrations toward the right bank and greater uniform distribution of the flow across the entire river cross-section under higher discharges.

27) Developed bevelled submerged vanes have been used to control right bank erosion of the Ganga river downstream of the Vikramshilla bridge at Bhagalpur through a physical model study to a scale of 1/700 (horizontal) and 1/70 (vertical). With the use of the submerged vanes, the percentage reduction in bank erosion is ranging from 63.4% to 100%, from 30% to 100%, and from 15.6% to 79.8% for 0 km, 0.14 km, and 0.28 km offsets from the right bank. Results shows that submerged vanes can effectively reduce the bend erosion along the outer bank of the river by diverting the main course of the river towards the inner side from the outer side of the bank.

28) Developed bevelled submerged vanes have been used to activate a spill channel by removal of sediment at its mouth of Padma/Ganga river near Jangipur, West Bengal. Results indicate that installation of submerged vanes at the mouth of the spill channel increases discharge passing through it. The percentage increases in discharge in the spill channel with the installation of submerged vanes compared to existing conditions are 2.27%, 4.93%, 5.88%, 4.54%, and 7.6% for river discharges of 19,445 m^3/s, 24,218 m^3/s, 30,052 m^3/s, 35,355 m^3/s, and 41,500 m^3/s, respectively in the river. Thus, the bevelled vanes can be used to desilt the mouth of a spill channel or water intake for passing the flow through it.

29) The measured bed elevation indicates that with the installation of submerged vane, bed has degraded in the spill channel, which has resulted in flow through the spill channel under lean flow season also. Thus, the bevelled vanes can be used to desilt the mouth of a spill channel or water intake for passing the flow through it.

Appendix I

Table 1 Scheme of experimentation

Run no.	Discharge Q (m^3/s)	angle of attack α (degree)	Vane height to depth ratio (H/d)	Bevel angle θ (degree)	d_{sm}/d	d_{sd}/d
R1	0.082	15	0.3	0	0.140	0.067
R2	0.082	15	0.3	30	0.127	0.067
R3	0.082	15	0.3	45	0.080	0.033
R4	0.082	15	0.3	60	0.000	0.000
R5	0.082	15	0.3	70	0.000	0.000
R6	0.082	15	0.4	0	0.093	0.073
R7	0.082	15	0.4	30	0.120	0.067
R8	0.082	15	0.4	45	0.053	0.060
R9	0.082	15	0.4	60	0.053	0.053
R10	0.082	15	0.4	70	0.000	0.000
R11	0.082	15	0.5	0	0.300	0.147
R12	0.082	15	0.5	30	0.213	0.133
R13	0.082	15	0.5	45	0.240	0.120
R14	0.082	15	0.5	60	0.127	0.067
R15	0.082	15	0.5	70	0.100	0.053
R16	0.082	20	0.3	0	0.253	0.107
R17	0.082	20	0.3	30	0.220	0.100
R18	0.082	20	0.3	45	0.160	0.087
R19	0.082	20	0.3	60	0.120	0.067
R20	0.082	20	0.3	70	0.047	0.047
R21	0.082	20	0.4	0	0.273	0.113
R22	0.082	20	0.4	30	0.233	0.100
R23	0.082	20	0.4	45	0.227	0.093
R24	0.082	20	0.4	60	0.120	0.080
R25	0.082	20	0.4	70	0.053	0.053
R26	0.082	20	0.5	0	0.493	0.160
R27	0.082	20	0.5	30	0.480	0.147
R28	0.082	20	0.5	45	0.380	0.140
R29	0.082	20	0.5	60	0.173	0.120
R30	0.082	20	0.5	70	0.067	0.100
R31	0.082	30	0.3	0	0.473	0.167
R32	0.082	30	0.3	30	0.313	0.147

R33	0.082	30	0.3	45	0.267	0.107
R34	0.082	30	0.3	60	0.253	0.113
R35	0.082	30	0.3	70	0.120	0.053
R36	0.082	30	0.4	0	0.607	0.213
R37	0.082	30	0.4	30	0.553	0.193
R38	0.082	30	0.4	45	0.373	0.167
R39	0.082	30	0.4	60	0.353	0.120
R40	0.082	30	0.4	70	0.167	0.093
R41	0.082	30	0.5	0	0.953	0.393
R42	0.082	30	0.5	30	0.860	0.327
R43	0.082	30	0.5	45	0.633	0.260
R44	0.082	30	0.5	60	0.520	0.213
R45	0.082	30	0.5	70	0.313	0.147
R46	0.082	40	0.3	0	0.807	0.233
R47	0.082	40	0.3	30	0.487	0.207
R48	0.082	40	0.3	45	0.387	0.167
R49	0.082	40	0.3	60	0.320	0.153
R50	0.082	40	0.3	70	0.200	0.053
R51	0.082	40	0.4	0	0.847	0.327
R52	0.082	40	0.4	30	0.640	0.287
R53	0.082	40	0.4	45	0.547	0.253
R54	0.082	40	0.4	60	0.547	0.187
R55	0.082	40	0.4	70	0.220	0.100
R56	0.082	40	0.5	0	1.293	0.520
R57	0.082	40	0.5	30	1.100	0.507
R58	0.082	40	0.5	45	0.933	0.433
R59	0.082	40	0.5	60	0.773	0.327
R60	0.082	40	0.5	70	0.420	0.160
R61	0.058	15	0.4	0	0.089	0.000
R62	0.058	15	0.4	30	0.000	0.000
R63	0.058	15	0.4	45	0.000	0.000
R64	0.058	15	0.4	60	0.000	0.000
R65	0.058	15	0.4	70	0.000	0.000
R66	0.058	20	0.4	0	0.276	0.100
R67	0.058	20	0.4	30	0.231	0.086
R68	0.058	20	0.4	45	0.231	0.067
R69	0.058	20	0.4	60	0.107	0.061
R70	0.058	20	0.4	70	0.053	0.000
R71	0.058	30	0.4	0	0.578	0.211

R72	0.058	30	0.4	30	0.507	0.200
R73	0.058	30	0.4	45	0.516	0.142
R74	0.058	30	0.4	60	0.356	0.098
R75	0.058	30	0.4	70	0.311	0.107
R76	0.058	40	0.4	0	0.782	0.300
R77	0.058	40	0.4	30	0.756	0.280
R78	0.058	40	0.4	45	0.596	0.240
R79	0.058	40	0.4	60	0.533	0.169
R80	0.058	40	0.4	70	0.471	0.124
R81	0.092	20	0.3	0	0.271	0.071
R82	0.092	20	0.3	30	0.232	0.058
R83	0.092	20	0.3	45	0.174	0.058
R84	0.092	20	0.3	60	0.148	0.077
R85	0.092	20	0.3	70	0.129	0.077
R86	0.092	20	0.4	0	0.503	0.148
R87	0.092	20	0.4	30	0.426	0.103
R88	0.092	20	0.4	45	0.219	0.058
R89	0.092	20	0.4	60	0.213	0.045
R90	0.092	20	0.4	70	0.129	0.077
R91	0.092	20	0.5	0	0.568	0.206
R92	0.092	20	0.5	30	0.465	0.125
R93	0.092	20	0.5	45	0.445	0.132
R94	0.092	20	0.5	60	0.206	0.085
R95	0.092	20	0.5	70	0.142	0.052

Appendix II

- **International Journals-05**

(1) Mandal, A., Gautam, H., & **Ahmad, Z.** (2024). Sediment control and flow redistribution with submerged vanes: A review. Water Practice and Technology, 19(5), 2197.

(2) Mandal, A., **Ahmad, Z.**, & Mosselman, E. (2025). Experimental study on scour around beveled submerged vanes. International Journal of Sediment Research, In press, https://doi.org/10.1016/j.ijsrc.2025.05.001.

(3) Mandal, A., **Ahmad, Z.** (2025). An Experimental and Numerical Investigation on Efficiency of a Bevel Submerged Vane. Journal of Hydraulic Research, TJHR-2025-0052. (Under review)

(4) Mandal, A., **Ahmad, Z.** & Kadia, S. (2025). Application of submerged vanes for bank erosion control of Ganga river at Bhagalpur – A physical model study. (Draft)

(5) Mandal, A. & **Ahmad, Z.** (2025). Application of submerged vane for activation of silted spill channel at Jangipur lock - A physical model study. (Draft)

- **International Conferences-01**

(1) Mandal, A., & **Ahmad, Z.** (2024). Experimental Study on Local Scour Around Submerged Vanes of Different Bevel Angles. 10th International Symposium on Hydraulic Structures, ISSN 0374-0056, Zurich, Switzerland, https://doi: 10.3929/ethz-b-000675988.

REFERENCES

Abbas, N. and Subramanian, V., (1984). Erosion and Sediment transport in the Ganges river basin (India). J. Hydrol. 69, 173–182.

Ahmad, Z. (2013). Prediction of longitudinal dispersion coefficient using laboratory and field data: relationship comparisons. Hydraulics Resources, 44(2), 362–376.

Annayat, W., Raja, W., Barbhuiya, A.K., (2025). Analysis of flow past a submerged vane using computational fluid dynamics. Int J Energ Water Res 9, 839–852. https://doi.org/10.1007/s42108-024-00292-1.

Ansari, M. F., & Ahmad, Z. (2024). Scour pattern at zero-degree confluent channels. Acta Geophysica, Springer.

Ansys Fluent (2011). Ansys ICEM CFD user's manual. Pune, India: Ansys Inc.

Azizipour, M., Meymani, F. A., & Shooshtari, M. M. (2020) Enhancing scour protection in river bends: a novel slotted bank-attached vane. Water Science & Technology Water Supply, 20.6. https://doi.org/10.2166/ws.2020.116.

Baltazar, J., Alves, E., Bombar, G., & Cardoso, A. H. (2021) Effect of a submerged vane-field on the flow pattern of a movable bed channel with a 90º lateral diversion. Water, 13, 828. https://doi.org/10.3390/w13060828.

Barani, G. A., & Sardo, M. S. (2013). Experimental investigation of submerged vanes shape effect on river-bend stability. Hydraulic Structures, Spring, 1 (1), 35-41.

Barkdoll, B. D., Ettema, R., & Odgaard, A. J. (1999). Sediment control at lateral diversions: limits and enhancements to vane use. Journal of Hydraulic Engineering, ASCE, 125(8), 862–870. https://doi:10.1061/(ASCE)0733-9429(1999)125:8(862).

Bejestan, M. S., & Azizi, R. (2012). Experimental investigation of scour depth at the edge of different submerged vanes shapes. World Environmental and Water Resources Congress, ASCE, Reston, VA, USA,pp. 1376–1385. https://doi.org/10.1061/9780784412312.138.

Bentley flow master connect edition user's guide (2018). Bentley Systems, Inc., Bentley Systems, Inc., Watertown, CT 06795.

Bertin, JJ. & Smith, ML., (1979). Aerodynamics for engineers. 1st ed. New Jersey: Prentice-Hall.

Best, J. & Ashworth, P. (1994). A high-resolution ultrasonic bed profiler for use in laboratory flumes. Journal of Sediment Research, 64(3).

Bhuiyan, F., Hey, R. D., & Wormleaton, P. R. (2010). Bank attached vanes for bank erosion control and restoration of river meanders. Journal of Hydraulic Engineering, ASCE, 136(9), 583–596. https://doi.org/10.1061/(ASCE)HY.1943-7900.0000217.

Blanckaert, K., & de Vriend, H. J. (2004). Secondary flow in sharp open channel bends. Journal of Fluid Mechanics, 498, 353–380. https://doi.org/10.1017/S0022112003006979.

Bor, A. (2022). Experimental investigation of 90° intake flow patterns with and without submerged vanes under sediment feeding conditions. Canadian Journal of Civil Engineer, 49, 452–463. https://doi.org/10.1139/cjce-2020-0616.

Buckingham, E. (1915). Model experiments and the forms of empirical equations. Transactions of the American Society of Mechanical Engineers, 37, 263–292.

Chanson, R. (2004). Hydraulics of Open Channel Flow, 2nd Edition, Butterworth-Heinemann, London, 258, ISBN 978-0-7506-5978-9.

CWC (2014). GANGA BASIN. Ministry of Water Resources, Central Water Commission, New Delhi, India-Water Resources Information System: www.india-wris.nrsc.gov.in.

Dey, L., Barbhuiya, A. K., & Biswas, P. (2017). Experimental study on bank erosion and protection using submerged vane placed at an optimum angle in a 180º laboratory channel Bend. Geomorphology, 283, 32–40. https://doi.org/10.1016/j.geomorph.2017.01.022.

Dey, S., (2014). Fluvial hydrodynamics: Hydrodynamic and Sediment Transport phenomena, GeoPlanet: Earth and Planetary Sciences. Springer, Berlin. https://doi.org/10.1007/978-3-642-19062-9.

Engelund, F. and E. Hansen (1967), A monograph on sediment transport in alluvial streams, Teknisk Forlag, Copenhagen.

Fathi, A., & Zomorodian, S. M. (2018). Effect of Submerged Vanes on Scour Around a Bridge Abutment. KSCE Journal of Civil Engineering, 22(7), 2281-2289. https://doi:10.1007/s12205-017-1453-5

Goring, D. G, & Nikora, VI. (2002). Despiking acoustic doppler velocimeter data. Journal of Hydraulic Engineering, 128(1), 117–126. https:// doi. org/ 10. 1061/(asce) 0733- 9429(2002) 128: 1(117).

Gumgum, F., & Cardoso, A. H. (2022). Optimizing the desilting efficiency of submerged vane fields at lateral diversions. Journal of Hydraulic Engineering, ASCE, 149(1), 04022031. https:// doi: 10.1061/(ASCE)HY.1943-7900.0002030.

Gupta, U. P., Ojha, C. S. P. & Sharma, N. (2010) Enhancing utility of submerged vanes with collar. Journal of Hydraulic Research, 136(9), 651–655. doi:10.1061/(ASCE)HY.1943-7900.0000212.

Gupta, U. P., Ojha, C. S. P., & Sharma, N. (2006). Vorticity with different shapes of submerged vanes. ISH Journal of Hydraulic Engineering, 12(1), 13–26. https://doi:10.1080/09715010.2006.10514813.

Gupta, U. P., Ojha, C. S. P., & Sharma, N. (2010). Enhancing utility of submerged vanes with collar. Journal of Hydraulic Engineering, ASCE, 136(9), 651–655. https://doi:10.1061/(ASCE)HY.1943-7900.0000212.

Gupta, U. P., Sharma, N., & Ojha, C. S. P. (2007). Performance evaluation of tapered vane. Journal of Hydraulic Engineering, 45(4), 472–477. https://doi:10.1080/00221686.2007.9521781.

Hamidi, M., Sadeqlu, M., & Khalili, A. M. (2024). Investigating the design and arrangement of dual submerged vanes as mitigation countermeasure of bridge pier scour depth using a numerical approach. Ocean Engineering 299, 117270. https://doi.org/10.1016/j.oceaneng.2024.117270.

Hossain, M. M., Islam, Md. R., Saha, S., Ferdousi, S., Van Zwol, B., Zijlstra, R., & Mosselman, E. (2004). Laboratory tests on scour around bottom vanes. Proceedings 2nd International Conference on Scour and Erosion, (ICSE-2). November 14.-17., 2004, Singapore.

Kadia, S., Larsson, I. S., Billstein, M., Rüther, N., Lia, L., & Pummer, E. (2024). Investigating supercritical flow characteristics and movement of sediment particles in a narrow channel bend using PTV and video footage. Advances in Water Resources, 193, 104827.

Kalathil, S. T., Wuppukondur, A., Balakrishnan, R. K., & Chandra, V. (2018). Control of sediment inflow into a trapezoidal intake canal using submerged vanes. Journal of Waterway Port Coastal and Ocean Engineering, 144(6), 04018020. https://doi.org/10.1061/(ASCE)WW.1943-5460.0000474.

Kalkwijk, J.P.T., Booij, R., (1986). Adaptation of secondary flow in nearly-horizontal flow. J. Hydraulic Res. 24 (1), 19–37. https://doi.org/10.1080/00221688609499330.

Klovsky, A. V., & Kozlov, D. V. (2019). Generation of artificial transverse circulation in an open channel flow by submerged vanes. Journal on Construction and Architecture, 14(9), 1158-1166. https://doi:10.22227/1997-0935.2019.9.1158-1166.

Mandal, A., & Ahmad, Z. (2024). Experimental Study on Local Scour Around Submerged Vanes of Different Bevel Angles. 10th International Symposium on Hydraulic Structures, ISSN 0374-0056, Zurich, Switzerland, https://doi: 10.3929/ethz-b-000675988.

Mandal, A., Ahmad, Z., & Mosselman, E. (2025). Experimental study on scour around beveled submerged vanes. International Journal of Sediment Research, In press, https://doi.org/10.1016/j.ijsrc.2025.05.001.

Mandal, A., Gautam, H., & Ahmad, Z. (2024). Sediment control and flow redistribution with submerged vanes: A review. Water Practice and Technology, 19(5), 2197.

Marelius, F., & Sinha, S. K. (1998). Experimental investigation of flow past submerged vanes. Journal of Hydraulic Engineering, ASCE, 124(5), 542-545. https://doi:10.1061/(ASCE)0733-9429(1998)124:5(542).

Marsh, N. A., Western, A. W., & Grayson, R. B. (2004). Comparison of methods for predicting incipient motion for sand beds. Journal of Hydraulic Engineering, 130(7), 616-621. https://doi:10.1061/(ASCE)0733-9429(2004)130:7(616).

Menter, F. R. (1992b). Improved Two-equation k–ω Turbulence Models for Aerodynamic Flows, NASA Technical Memorandum TM-103975, NASA Ames, CA.

Nikora, V. I., Goring, D. G., & Biggs, B. J. F. (1998). Silverstream eco-hydraulics flume: Hydraulic design and tests. Journal of Marine and Freshwater Research, 32(4), 607–620.

Odgaard A. J. & Kennedy J. F. (1983). River-Bend Bank Protection by Submerged Vanes. Journal of Hydraulic Engineering, ASCE, Vol. 109, No. 8, I pp. 161-173.

Odgaard A.J. & Mosconi C.E. (1987). Streambank protection by submerged vanes. Journal of Hydraulic Engineering, ASCE, 113(4), 520-536.

Odgaard, A. J. (2009). River training and sediment management with submerged vanes. USA: American Society of Civil Engineers.

Odgaard, A. J. (2015). River channel stabilization with submerged vanes. In: Yang, C. & Wang, L. (eds) Advances in Water Resources Engineering. Springer, Cham, Switzerland, pp. 107–136. https://doi.org/10.1007/978-3-319-11023-3_3.

Odgaard, A. J., & Kennedy, J. F. (1983). River-Bend Bank Protection by Submerged Vanes. Journal of Hydraulic Engineering, ASCE, 109(8), 161-173. https://doi:10.1061/(ASCE)0733-9429(1983)109:8(1161).

Odgaard, A. J., & Mosconi, C. E. (1987). Streambank protection by submerged vanes. Journal of Hydraulic Engineering, ASCE, 113(4), 520-536. https://doi:10.1061/(ASCE)0733-9429(1987) 113:4(520).

Odgaard, A. J., & Spoljaric, A. (1986). Sediment control by submerged vanes. Journal of Hydraulic Engineering, ASCE, 112(12), 1164-1181.

Odgaard, A. J., & Spoljaric, A. (1989). Sediment control by submerged vanes. Design basis. River Meandering, 12, 127–151.

Odgaard, A. J., & Wang, Y. (1991a). Sediment management with submerged vanes. I: Theory. Journal of Hydraulic Engineering, ASCE, 117(3), 267-283. https://doi:10.1061/(ASCE)0733-9429(1991)117:3(267).

Odgaard, A. J., & Wang, Y. (1991b). Sediment management with submerged vanes. II: Applications. Journal of Hydraulic Engineering, ASCE, 117(3), 284-302.

Odgaard, A.J., & Spoljaric, A. (1986). Sediment control by submerged vanes. Journal of Hydraulic Engineering, ASCE, 112(12), 1164-1181.

Ouyang, H. T. (2009). Investigation on the dimensions and shape of a submerged vane for sediment management in alluvial channels. Journal of Hydraulic Engineering, ASCE 135(3), 209–217. https:// doi:10.1061/(ASCE)0733-9429(2009)135:3(209).

Ouyang, H. T., & Lin, C. P. (2016). Characteristics of interactions among a row of submerged vanes in various shapes. Journal of hydro-environment Research, 13, 14–25. https://doi:10.1016/j.jher.2016.05.003.

Ouyang, H. T., Lai, J. S., Yu, H., & Lu, C. H. (2008). Interaction between submerged vanes for sediment management. Journal of Hydraulic Research, 46(5), 620-627. https://doi:10.3826/jhr.2008.3160.

Paphitis, D. (2001). Sediment movement under unidirectional flows: an assessment of empirical threshold curves. Coastal Engineering, 43, 227–245.

Polhamus, E. C. (1966). A Concept of the Vortex Lift of Sharp-Edge Delta-Wings on a Leading-E Suction Analogy. TN D-3767, December, NASA.

Rajaratnam, N. (1981). Erosion by plane turbulent jets. Journal of Hydraulic Research, 19(4), 339–358.

Safaripour, N., Vaghefi, M., & Mahmoudi, A. (2020). Experimental study of the effect of submergence ratio of double submerged vanes on topography alterations and temporal evaluation of the maximum scour in a 180-degree bend with a bridge pier group. International Journal of River Basin Management, 20(4), 427-441. https://doi:10.1080/15715124.2020.1837144.

Sarlak, H., Bejestan, M. S., & Sajjadi, S. M. (2023). Experimental investigation of the effect of permeability and angle of gabion submerged vane on bed topography. Arabian Journal of Geosciences, 16, 288.

Solanki, K., Sharma, H., & Joshi, N. (2020). Flow and parameter optimization of tapered vane. Journal of Ecohydraulics, 1–13. https://doi:10.1080/ 24705357.2020.1771223.

Stoesser, T., Ruether, N., Olsen, N.R.B., (2010). Calculation of primary and secondary flow and boundary shear stresses in a meandering channel. Adv. Water. Resour. 33 (2), 158–170. https://doi.org/10.1016/j.advwatres.2009.11.001.

Tasar, B., Unes, F., Gemici, E., & Zelenakova, M. (2023). Experimental and numerical study on flow control using 3-array submerged vane in laboratory channel bend. Water, 15, 659, https://doi.org/10.3390/w15040659.

Teronpi, J., & Misra, U. K. (2015). Experimental investigation of local scour around submerged vanes. International Journal of Innovative Research in Advanced Engineering, 2 (7), 21–24.

Vaghefi, M., Zarei, E., Ahmadi, G., & Behroozi, A. M. (2023). Experimental analysis of submerged vanes' configuration for mitigating local scour at piers in a sharp bend: Influence of quantity, length, and orientation. Ocean Engineering, 289, 116267, https://doi.org/10.1016/j.oceaneng.2023.116267.

Wahl, T. L. (2000). The WES stream investigation and streambank stabilization handbook. Proceedings, Joint Conference on Water Resources Engineering and Water Resources Planning & Management Minneapolis, 1–10.

Wang, Y., & Odgaard, A. J. (1993). Flow control with vorticity. Journal of Hydraulic Research, 31(4), 549-562. https://doi:10.1080/00221689309498877.

Wilcock, P, & Pitlick, J, Cui, Y. (2009). Sediment transport primer: estimating bed-material transport in gravel-bed rivers. Gen Tech Rep RMRS-GTR-226. Fort Collins, CO U.S. pp 1–78.

Wilcox, D. C. (2009). Formulation of the k-omega Turbulence Model Revisited. AIAA Journal, 46, 2823-2838.

Yarahmadi, M. B., & Bejestan, M. S. (2016). Sediment management and flow patterns at river bend due to triangular vanes attached to the bank. Journal of hydro-environment Research, 10, 64–75. http://dx.doi.org/10.1016/j.jher.2015.10.002.

Zarei, E., Vaghefi, M., & Hashemi, S. S. (2019). Bed topography variations in bend by simultaneous installation of submerged vanes and single bridge pier. Arabian Journal of Geosciences, 12, 178, 1-10. https://doi:10.1007/s12517-019-4342-z.